NTIA Report 88-239

Millimeter-Wave Propagation Characteristics and Channel Performance for Urban-Suburban Environments

Edmond Violette
Richard Espeland
Kenneth C. Allen

U.S. DEPARTMENT OF COMMERCE
C. William Verity, Secretary
Alfred C. Sikes, Assistant Secretary
for Communications and Information

December 1988

PREFACE

Certain commercial equipment, instruments, or materials are identified in this paper to specify adequately the experimental procedure. In no case does such identification imply recommendation or endorsement by the National Telecommunications and Information Administration, nor does it imply that the material or equipment identified is necessarily the best available for the purpose.

CONTENTS

LIST OF FIGURES

LIST OF TABLES

MILLIMETER-WAVE PROPAGATION CHARACTERISTICS and CHANNEL PERFORMANCE for URBAN-SUBURBAN ENVIRONMENTS

Edmond Violette, Richard Espeland, and Kenneth C. Allen*

Measurements were performed in an urban-suburban environment with narrowband and wideband rf probes, which include millimeter-wave frequencies, in order to study propagation characteristics for street level paths. The primary objective of this report is to evaluate the performance of the rf channels in these environments for both line-of-sight and non-line-of-sight paths and to compare a model developed for line-of-sight paths to measurements taken in Denver, CO.

Key words: urban-suburban; millimeter wave; propagation; performance; model

1. INTRODUCTION

Since 1983, the Institute for Telecommunication Sciences has been sponsored by the U. S. Army to study millimeter-wave propagation characteristics for paths between mobile terminals in urban and suburban environments. This report provides a comprehensive review of work performed in this portion of the radio spectrum pertaining to urban-suburban paths and includes the most recent and most informative measurements conducted in downtown Denver, CO. A model to predict channel performance in an urban street setting was developed, tested, and modified as necessary to best represent the channel for the multipath situation where terminal separation and antenna beamwidth are the principal variables.

At street level, one of the major concerns for line-of-sight (LOS) paths is interference created between the direct signal and the reflected signals. Reflected signals, especially from street surfaces and from building walls, vehicles, signs, etc., can cause deep fades. This may cause the received signal level to fall below the receiver's detection threshold or the required signal-to-noise ratio. For wideband links (high-rate digital systems, for example), distortion may result from reflected multipath signals because the added propagation time delay causes information characters to overlap in time, producing the condition known as intersymbol interference. The severity of these problems depends upon such link parameters as path geometry, antenna beamwidths, frequency, data rate (bandwidth), and system fade margin.

* The authors are with the Institute for Telecommunication Sciences, National Telecommunications and Information Administration, U.S. Department of Commerce, Boulder, CO 80303 3328.

A series of three measurement efforts were conducted over about a 3-year period for path lengths up to 1.5 km. Data were recorded for a variety of scenarios using two operating systems. One system used narrowband channels at 9.6, 28.8, and 57.6 GHz and the second used narrowband channels at 11.4 and 28.8 GHz and a wideband channel at 30.3 GHz. Parameters measured in addition to received signal level (RSL) on all channels, were bit-error-rate (BER) at a 500 Mb/s transmission rate and a channel impulse response with resolution of 1 ns or better. These parameters were generally recorded as a function of path length, antenna height, antenna polarization, and antenna beamwidth. Signal distortion associated with multiple reflections and/or scattering components was correlated with a resultant BER using the 30.3 GHz wideband probe (Violette et al. 1983a; Espeland et al., 1984). Some of the measured data provided information at 9.6, 28.8, and 57.6 GHz regarding reflective properties of building and pavement surfaces. Also, for the same frequencies, data were taken with narrow beamwidth scanning antennas on line-of-sight (LOS) paths to separate multipath components and on non-LOS paths to analyze reflected and diffracted components (Violette, et al., 1983b).

During 1984, transmissivity properties of some common building materials were measured using the 9.6, 28.8, and 57.6 GHz probes. Following these tests, these continuous wave (CW) probes were improved to provide sensitivity of detection (received signal level) of approximately -132 dBm over a dynamic range of 80 to 85 dB. With this level of probe performance, it was possible to examine non-LOS links in the suburban environment where the energy reached the receiver by penetration through structures and vegetation and/or by diffraction from building edges or other objects producing scattering components.

A third series of primarily LOS measurements in the urban environment was conducted in Denver, CO. Both transmitting and receiving terminals were again mounted in vans. There was an 11.4 GHz CW probe and a 28.8 GHz narrowband probe that shared an antenna with the 30.3 GHz wideband system by using an appropriate transducer in the feed. This instrumentation allowed the fading characteristics of a very narrow (3 kHz) channel and a very wideband (1 GHz) channel to be compared. More importantly, the wideband channel was used to measure the impulse response at approximately 5-s intervals, which correspond to intervals of about 3 m of travel by the transmitter. This impulse response measurement directly displays signals arriving at the receiver in terms of

amplitude and time delay to a resolution of about 1 ns. The amplitude dynamic range allowed the detection of multipath and scattered components as much as 35 dB below the direct signal. In addition, the performance of the 500 Mb/s channel can be analyzed by comparing the measured impulse response with the corresponding recorded BER value. During the course of these measurements, several locations were chosen along three different street settings, each with varied features. Data were recorded for both narrowbeam and widebeam antennas as well as for both linear polarizations and cross-polarized antenna modes. A preliminary analysis of the wideband probe data has been reported (Violette et al., 1985).

A model was developed to predict link performance in an urban-suburban environment for LOS paths. In the computer model, the urban environment is idealized to consist of flat streets with uniform distance between buildings. The principal propagation paths between transmitting and receiving antennas within a few meters of the ground are described for this environment. The signal amplitude for each path is estimated from propagation losses including free-space loss, clear-air absorption, and loss during reflection from street and/or building surfaces (reflection coefficients). The delay time is computed from each ray path length. The angle-of-arrival at both antennas is computed for each ray path. Antenna gain patterns may be applied to compute the amplitudes of the various rays that comprise the received signal.

From the information computed for each ray path, telecommunication channels may be described in a number of ways. For example, the impulse response or the received signal level (RSL) may be found by adding the various signal components.

In actual urban environments, the relative phases of the various path components cannot be readily predicted because of irregularities in the street and building surfaces. By assuming random, uniformly distributed phases for the path components, a cumulative distribution of RSL is predicted for an ensemble of urban environments. The distribution is modeled as Nakagami-Rice and approximated using the Weibull distribution.

Several model results are presented in this report for a variety of parameters used to define the street geometry and propagation conditions. It is impractical to model the actual value for reflection coefficients as they vary in a complex manner with location and angle. Therefore average or typi-

cal values of reflection loss are used in the model. These values were determined by selecting the best fit of the model output to the measured data. A full treatment of this modeling effort is given in Section 6.

2. EQUIPMENT AND EXPERIMENTAL CONFIGURATIONS

Over the 3-year study period, two measuring systems were available; however, they were not used simultaneously. One system used frequencies at 9.6, 28.8, and 57.6 GHz and the other system operated at frequencies of 11.4, 28.8, and 30.3 GHz, both systems fully coherent. The transmitting and receiving units of these systems were each mounted on a vehicle, thus allowing considerable flexibility in path length and configuration. The 30.3 GHz channel provided a wideband probe, accomplished by upconverting the 28.8 GHz carrier with a 1.5 GHz subcarrier modulated with a pseudorandom code generator operating at 500 Mb/s. The 28.8- and 30.3-GHz channels use a common antenna at both the transmitting and receiving ends of the link. The antennas are equipped with feeds providing dual linear polarization. The isolation between the orthogonal linear modes was better than 38 dB. With the wideband channel, impulse response measurements and bit-error-rate (BER) measurements at 500 Mb/s were compiled to analyze complex propagation paths such as the urban environment presents.

For each of the experimental studies, various link configurations were used to optimize the several propagation factors investigated. The diagrams in Figure 1 show four operating configurations. A description of these configurations and a comment on the data obtained follows:

A. Azimuthal and Elevation Scans
In this configuration, the transmitter and receiver were set at a fixed distance and the receiving antenna was scanned either in azimuth or elevation. The measurements to determine building and material losses on non-LOS paths were conducted in this mode. The transmitter terminal was also equipped for azimuthal and elevation adjustments.

B. Horizontal Position Scan
The receiver was set on a line perpendicular to a reflecting surface and the transmitter was moved on a line parallel to the reflecting surface. This mode of operation was used to determine aspect sensitivity of the reflected signal in a folded path mode.

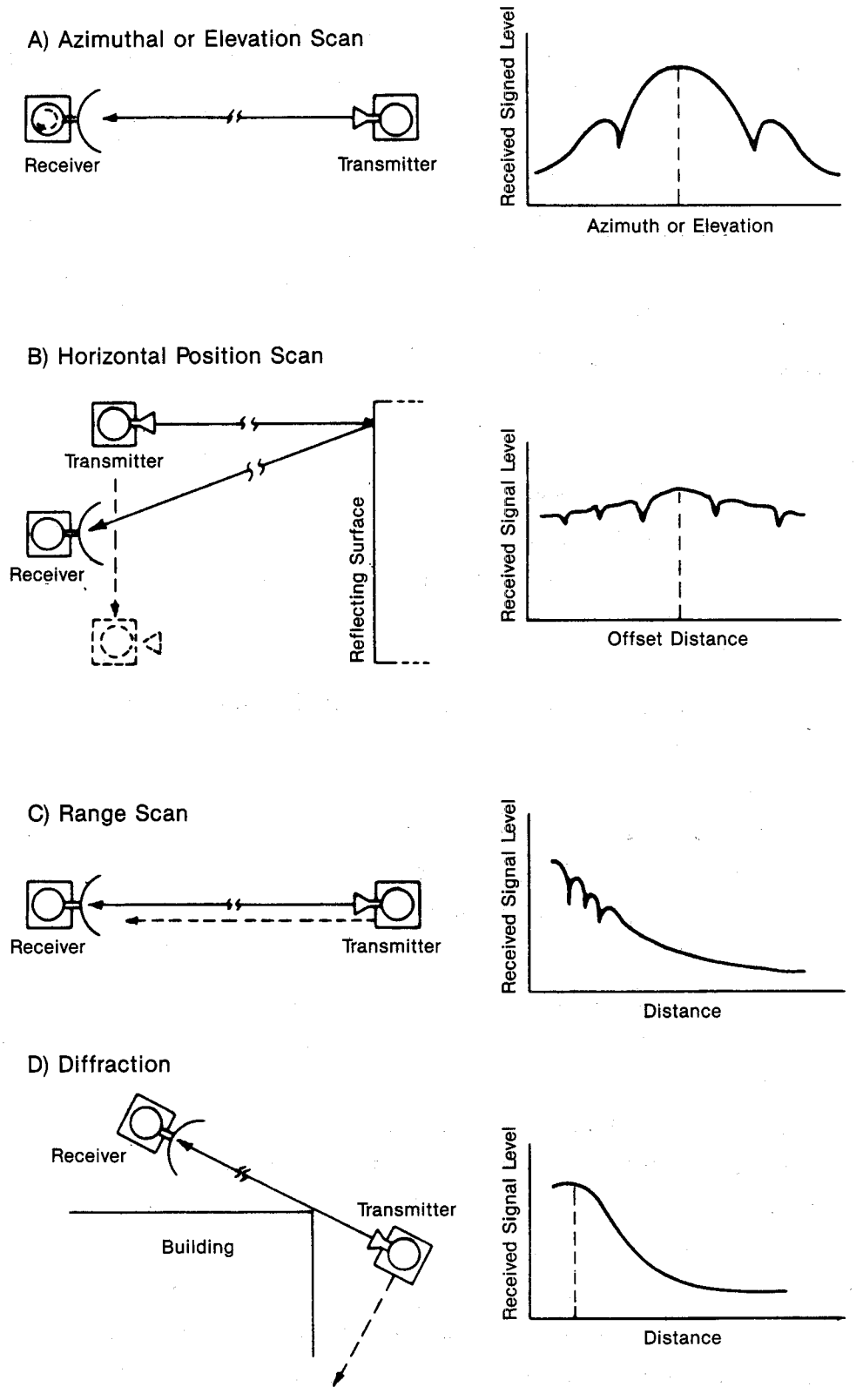

Figure 1. Test link operating configurations.

C. Range Scan
The receiver was stationary and the transmitter was moved along a line toward the receiver. The recorded signal represents a measure of signal amplitude with multipath components as a function of distance for a LOS path. This was also the most frequently used mode for measuring BER and impulse response.

D. Edge Diffraction
The receiver was set with the antenna pointing at an edge of a path obstruction. The transmitter, with the antenna pointing at the same edge, was moved along a constant radius arc from line of sight to several degrees beyond line of sight. The diffraction effects are measured as the transmitter is moved from the exposed region to the shadow region.

Block diagrams of the transmitter and receiver section No. 1 are shown in Figure 2. The receiver was modified after the 1983 tests. The principal result of these modifications was to increase the dynamic range and the receiver sensitivity. These changes are indicated in Table 1.

The block diagram of the transmitter section of operating system No. 2 is shown in Figure 3, which includes the up converter to generate the 30.3-GHz carrier and the high data-rate modulator. Block diagrams of the receiver section of operating system No. 2 are shown in Figures 4 and 5. The receiver section includes the down converter at 30.3 GHz and the demodulator. The BER receiver and impulse response cross-correlator are shown as subsections. The BER receiver and the impulse response cross-correlator were not operated simultaneously. The operating parameters for system No. 2 are listed in Table 2.

The bit-error-rate (BER) interval counter (set for 1 s) has a minimum detectable error rate of 1×10^{-8}. A maximum error rate of 5×10^{-1}, occurs in the nonsynchronous state.

The impulse response cross-correlator has an effective dynamic range of 35 dB and 1-ns delay resolution beyond 2-ns time delay.

A detailed description of the 30.3-GHz diagnostic probe (the instrumentation for measuring BER and channel distortion) is given in a 1983 NTIA report (Violette et al., 1983a), and the results of an impulse measurements laboratory calibration are given in a 1985 NTIA report (Violette et al. 1985). Some of those results are included in Section 5.2 of this report.

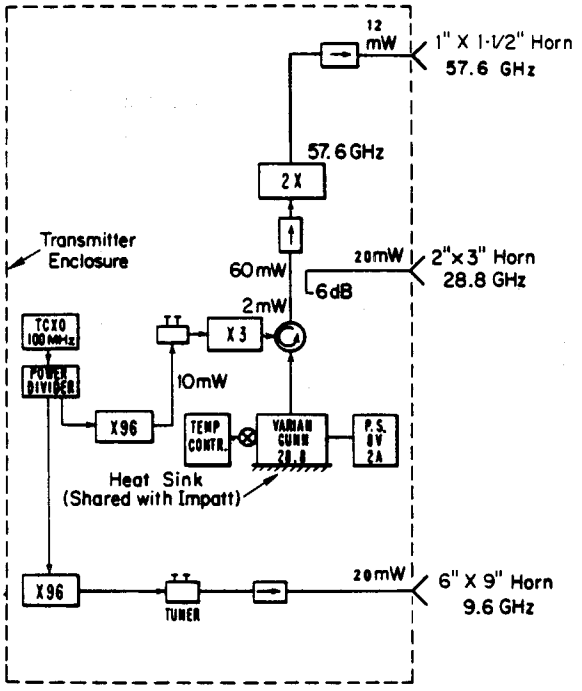

A) Transmitter

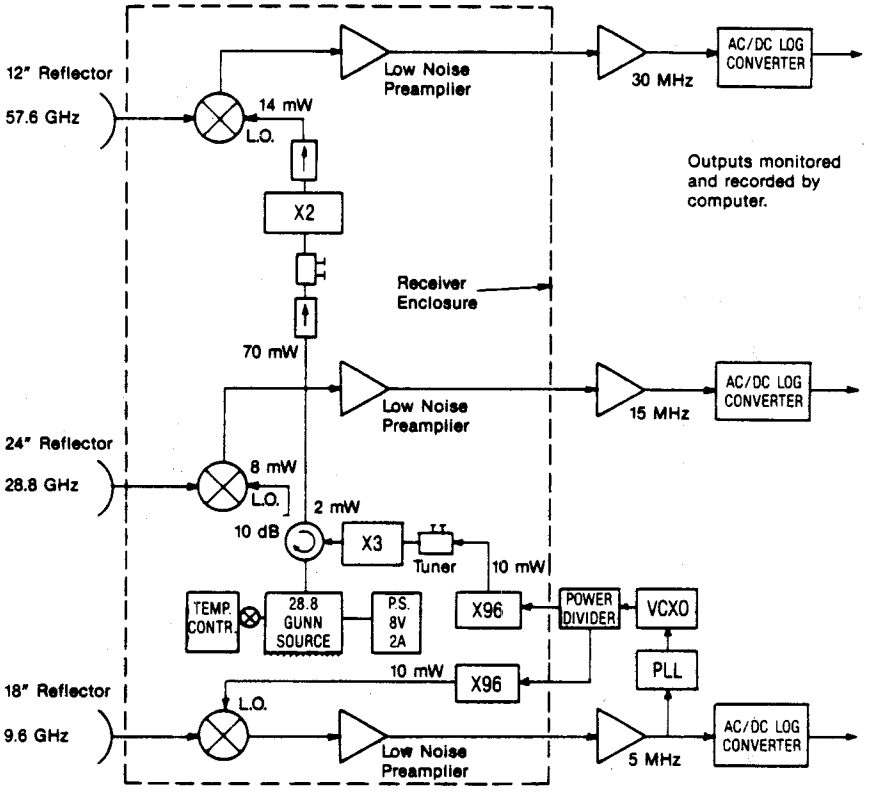

B) Receiver

Figure 2. Block diagrams of the transmitter (A) and the receiver (B) of operating system No. 1.

Table 1.

Operating Parameters for System No. 1

TRANSMITTER

FREQUENCY	OUTPUT (to antenna)	ANTENNA SIZE	ANTENNA GAIN	ANTENNA BEAMWIDTH
9.6 GHz	36 MW	6" x 9" Horn	25 dB	10°
28.8 GHz	20 MW	2" x 3" Horn	25 dB	10°
57.6 GHz	12 MW	1" x 1½" Horn	25 dB	10°

RECEIVER

FREQUENCY	SIZE*	GAIN	ANTENNA BEAMWIDTH	NOISE FIGURE	RECEIVER SENSITIVITY	RECEIVER DYNAMIC RANGE
9.6 GHZ	18"	31.0 dB	4.8°	7.5 dB	-110	60 dB
					**-132	80 dB
28.8 GHz	24"	42.8 dB	1.2°	5.5 dB	-110	60 dB
					**-132	80 dB
57.6 GHz	12"	43.1 dB	1.2°	6.0 dB	-110	60 dB
					**-132	80 dB

* parabolic reflectors
** sensitivity and dynamic range levels achieved with modification (1984)

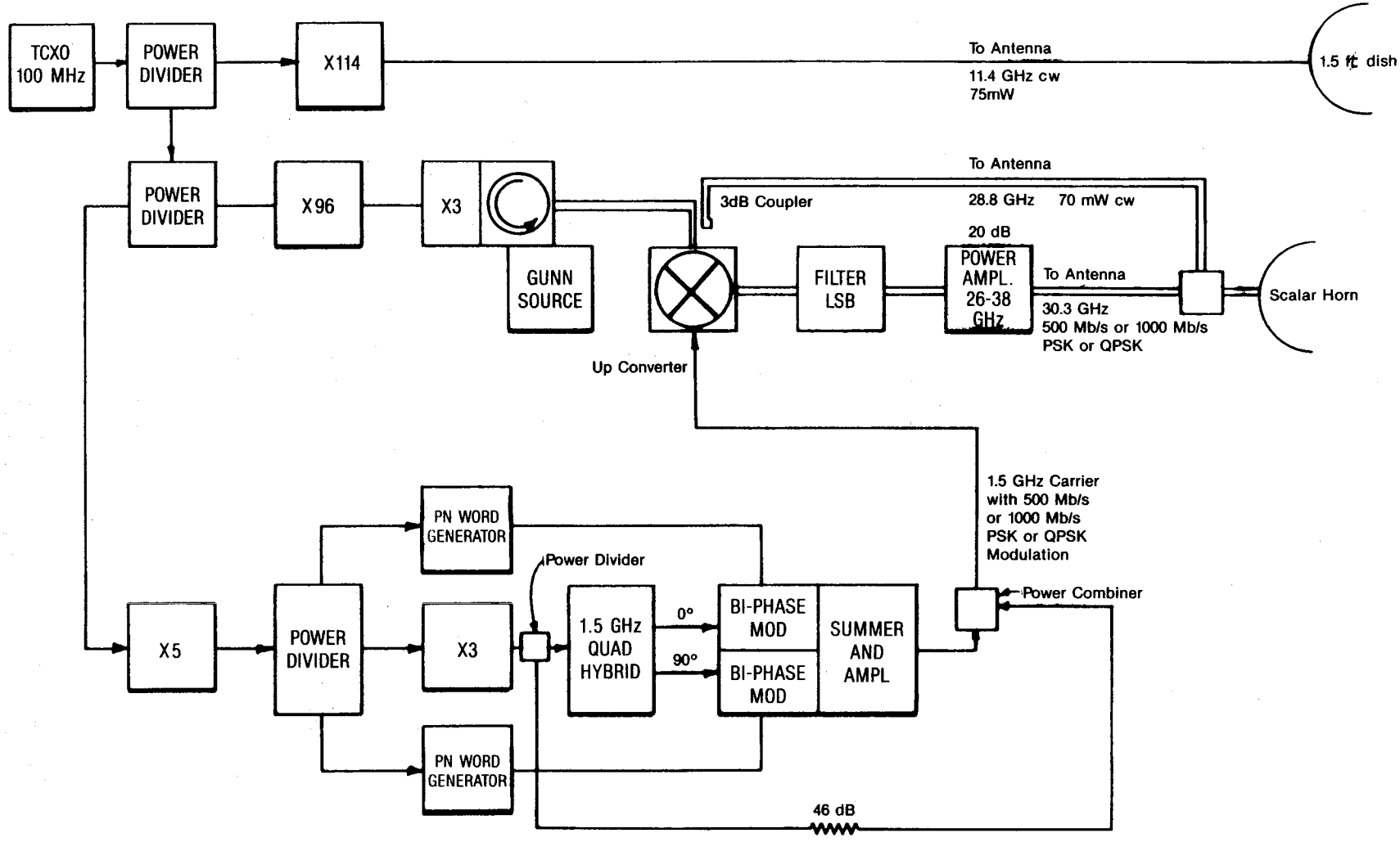

Figure 3. Block diagram of the transmitter terminal for operating system No. 2.

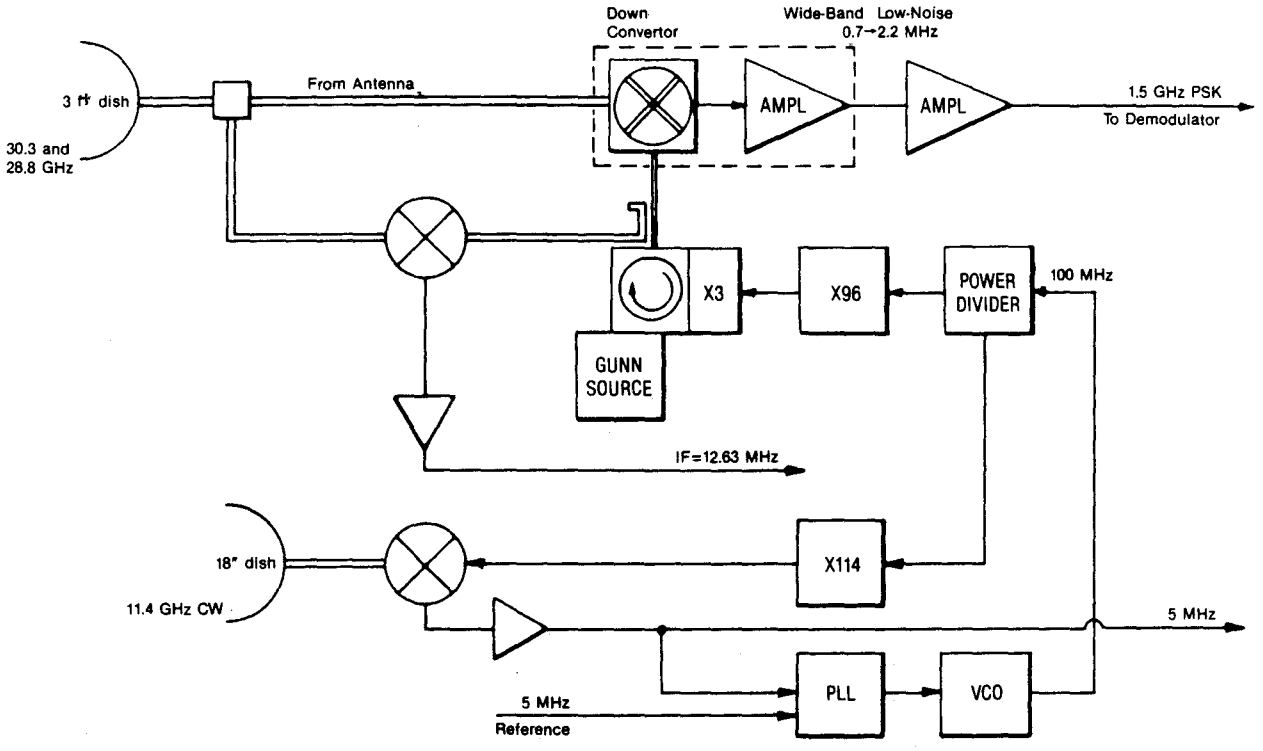

Block diagram of the rf section of the receiver terminal.

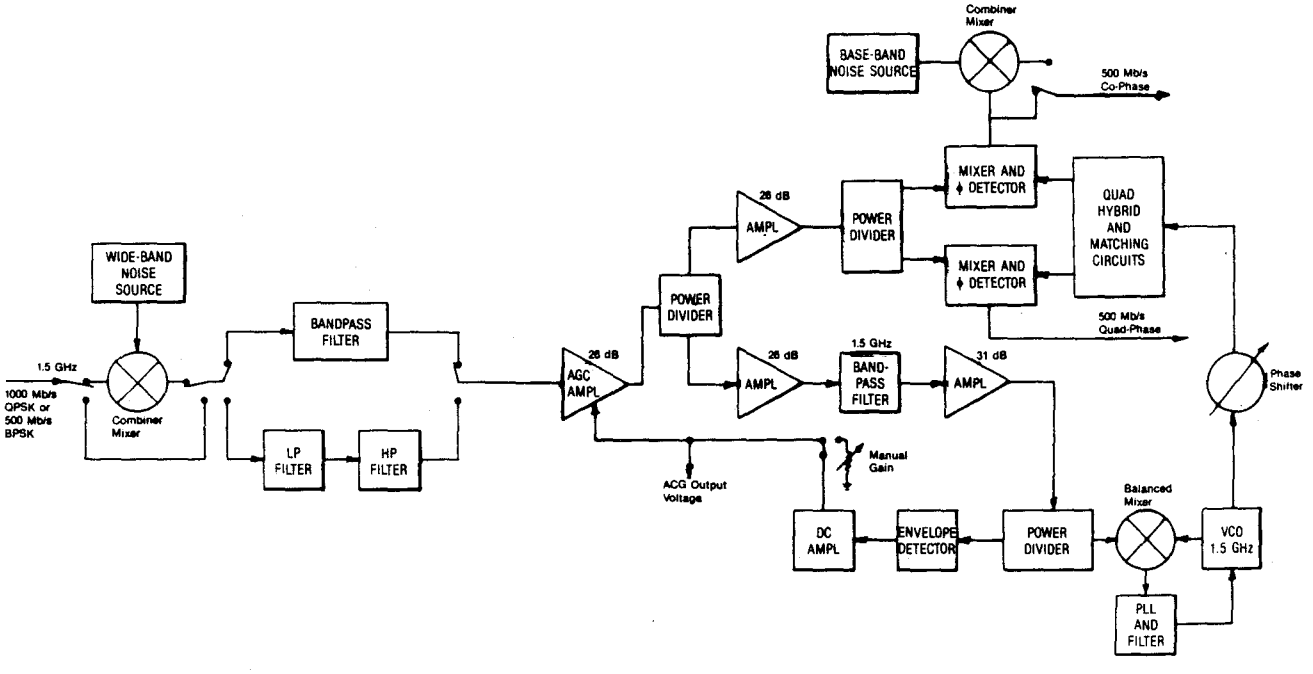

Block diagram of the receiver demodulator.

Figure 4. Block diagrams of the receiver for operating system No. 2, including the receiver demodulator.

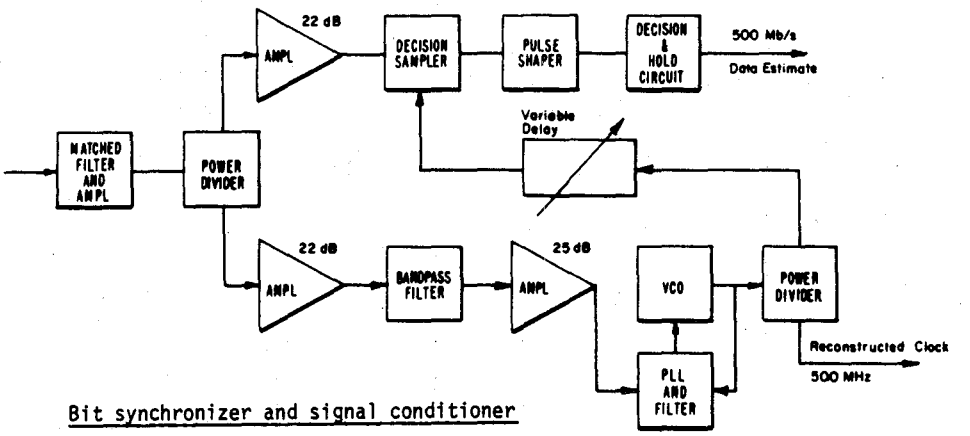

Block diagram of the bit synchronizer, signal conditioner, and bit error receiver.

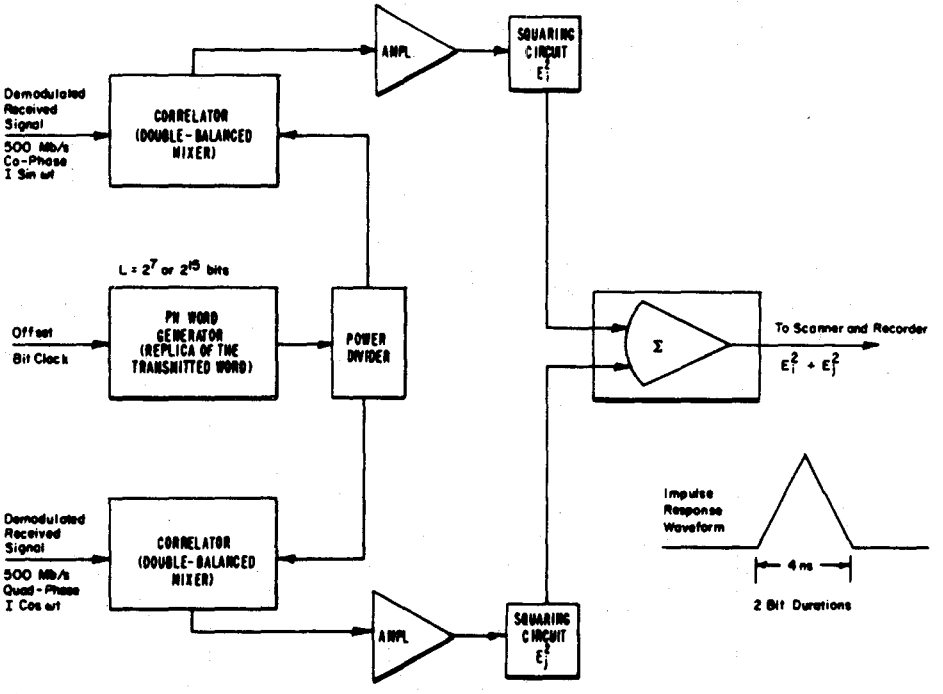

Block diagram of the impulse response cross-correlator.

Figure 5. Block diagrams of the BER receiver components and the impulse response cross-correlator.

Table 2. Operating Parameters for System No. 2

TRANSMITTER

FREQUENCY	OUTPUT (to Antenna)	ANTENNA SIZE	ANTENNA GAIN	ANTENNA BEAMWIDTH
11.4 GHz	75 MW	STANDARD GAIN HORN	16 dB	28°
28.8 GHz	70 MW	*CONICAL HORN	16 dB	30°
30.3 GHz	100 MW	*CONICAL HORN	16 dB	30°

*Conical Scalar Feed Horn shared by beams of orthomode transducer

RECEIVER

FREQUENCY	SIZE	ANTENNA GAIN	BEAMWIDTH	NOISE FIGURE	SENSITIVITY	DYNAMIC RANGE
11.4 GHZ	Rectangular Horn	25 dB	10°	7.5 dB	-132 dBm	80 DB
	Standard Gain Horn	16 dB	28°			
28.8 GHz	12" Scalar Horn Lens	37 dB (narrow-beam)	2.4°	5.5 dB	-132 dBm	80 dB
	1" Scalar* Feed Horn	16 dB (widebeam)	~30.0°	5.5 dB	-132 dBm	80 dB
30.3 GHz	12" Scalar Horn Lens	38 dB (narrow-beam)	2.25°	8.0 dB	-132 dBm	40 dB
	1" Scalar* Feed Horn	16 dB (widebeam)	~30.0°	8.0 dB	-132 dBm	40 dB

3. REFLECTION PROPERTIES

One of the major concerns when operating a millimeter-wave link at street levels is interference between reflected signals and the direct LOS signal. Signal interference produces fades in the received signal level (RSL) and channel distortion which is particularly detrimental to channel performance in high-data-rate or wideband systems.

Some of the early experiments were designed to measure specifically the reflective properties of various building surfaces to determine the characteristics of signals reflected from the ground and buildings along an urban street.

3.1 Reflections from a Reference Surface

To establish a reference with which to compare and evaluate subsequent measurements, a 3 ft (92 cm) square aluminum flat plate was stationed 58 m from the collocated transmitter and receiver. The test site was chosen to be free of reflecting surfaces behind and to the sides of the plate.

The signal amplitude plots shown in Figure 6 are a directional gain plot, using an azimuthal scan (A of Figure 1) on a LOS path with transmitter and receiver terminals separated by 106 m, as compared to a 3-ft square reference reflector over a 116 m folded path with the reflector positioned perpendicular to the path. In all such plots, the free space loss is subtracted so that the RSL is independent of distance. A slight ground multipath fade might be present in the 9.6 GHz reflector plot because the less than 1-m reflector height gave insufficient clearance for the 4.8° antenna beamwidth. At the higher two frequencies, no appreciable ground multipath could occur due to a 1.2° beamwidth for each. Also, the antenna patterns repeated very closely on the reflected and folded path signal plots except for a slight pointing offset.

Using the horizontal position scan configuration (B of Figure 1), reference reflector plots were recorded in Figure 7. Three separate horizontal scans were taken with the transmitter moved by 6 m to either side of the receiver. The heavy trace is the signal plot versus transmitter position offset with the flat reflector oriented at 0° in azimuth angle. The medium

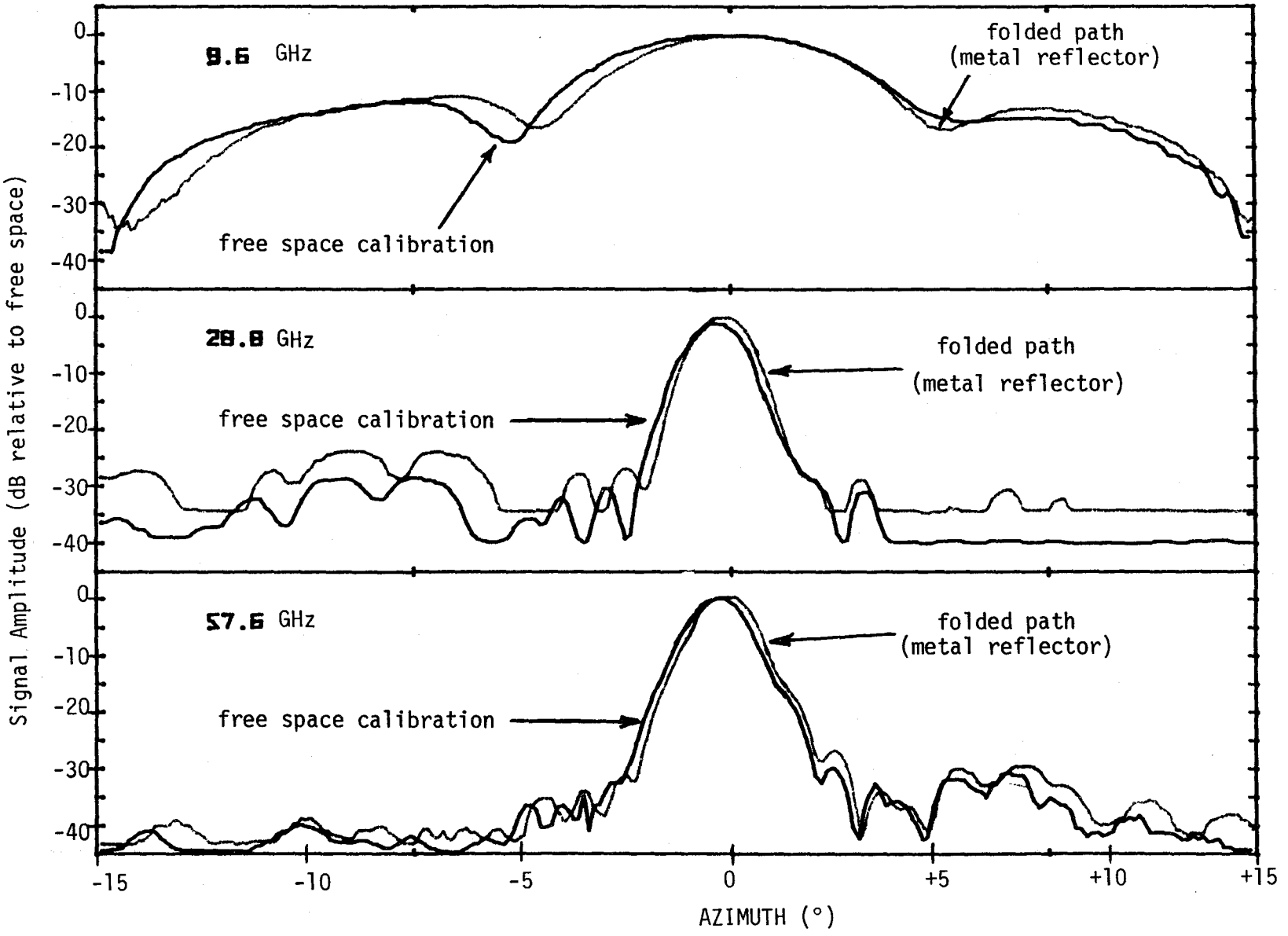

Figure 6. Signal amplitude as a function of azimuthal pointing of the receiving antenna. As indicated the traces are from the free space calibration path with the terminals separated by 106 m and a 3 foot x 3 foot (.914 m x .914 m) metal reflector on the 116-m (round trip) path.

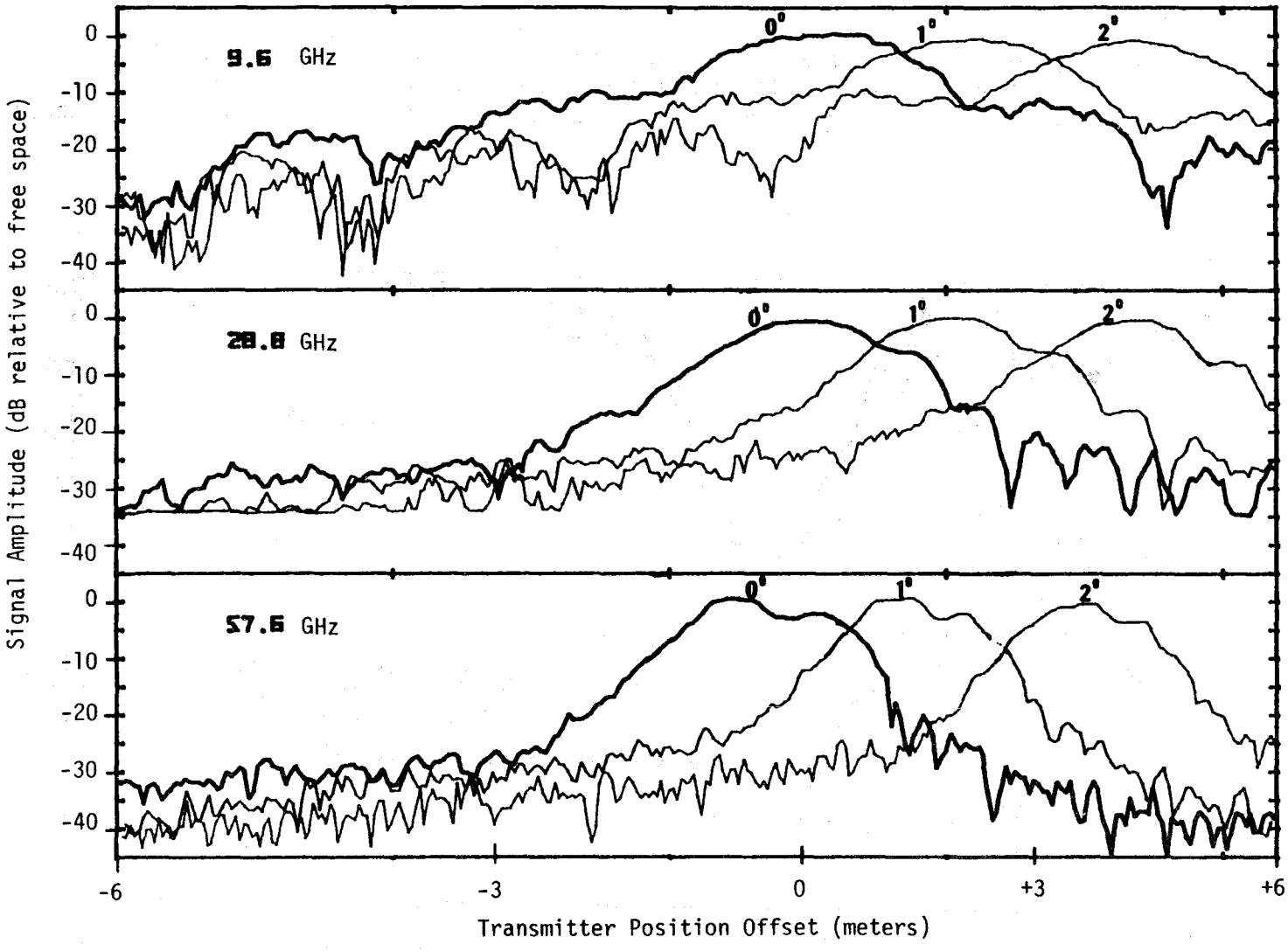

Figure 7. The signal amplitude received from a 3 foot x 3 foot (.914 m x .914 m) reflector at 116 m (round trip). The heavy line trace results from a scan with the transmitter and receiver collocated at the center position and with the reflector perpendicular to the (tansmitter-receiver)-to-(reflector) line. The medium line trace is the result of having the reflector oriented 1° from perpendicular and the light line with the reflector at 2° from perpendicular.

and light traces that peak to the right of center were recorded with the reflector rotated at 1° and 2° counterclockwise about its vertical axis, respectively. These reflected signals produced a very well behaved pattern indicating the high degree of aspect sensitivity of the flat plate, as would be expected.

3.2 Reflections from Building Surfaces

Measurements of reflected and/or scattered signals were made for a variety of surfaces at normal incidence for terminal-to-reflector path lengths of 41 m to 135 m. The exterior building surfaces used as reflectors were metal, brick, concrete, and concrete aggregate. Both the transmitting and receiving terminals were collocated on a line perpendicular to the building, with both sets of antennas pointing at the building. The measurements were made by recording the amplitude of the received signal during an azimuth angle scan (± 15°) and an elevation angle scan (± 10°) of the receiving antennas.

The results for the zero angle of incidence measurements are presented in Table 3. Test numbers, building surface, signal amplitude, path length, and location are given in the table. Reradiated or reflected signal levels were significantly higher for metal than for brick and concrete walls due presumably to the high conductivity of the metal. Values were averaged as shown in the table to indicate the approximate values of reflectivity of the respective surfaces. Note an apparent reduction in signal level with increasing frequency. Most of the variability in the results is believed due to variations in surface roughness and because of the wide beamwidth, some ground multipath may appear in the 9.6 GHz data.

A test to determine if a surface is considered smooth is the Rayleigh criterion (Beckman and Spizzichino, 1963).

$$H < \frac{\lambda}{8 \cos \phi} \qquad (1)$$

where ϕ is the angle of incidence, λ is the rf wavelength, and H is the height of the surface irregularities. This requires that the phase of the waves reflected from the top and bottom of the irregularity differ by less than $\lambda/4$. For a normal reflection the value of H cannot be greater than 4, 1.3, and 0.65 mm for 9.6, 28.8, and 57.6 GHz, respectively, in order to fit the smooth surface criterion. Only the metal and concrete (between the ribs)

TABLE 3

RECORDED AMPLITUDES FROM SEVERAL SURFACES

(ZERO ANGLE OF INCIDENCE)

Test	Surface	SIGNAL AMPLITUDE (dB relative to free space) 9.6 GHz	28.8 GHz	57.6 GHz	Path Length (one way, in meters)	
2-0-18	Metal	0	-1	-1	50	Paint Shop
2-1-28	"	+2	-5	-7	41	North American
2-1-0	"	-2	-3	-1	50	Paint Shop
3-0-14	"	+1	-8	-7	80	Gen. Cable
3-0-22	"	-6	+1	-9	109	Gen. Cable
		-1	-3	-5	(Average)	
3-0-44	Brick (Solid)	-2	-7	-7	95	Joslins
3-1-0	"	-6	-14	-8	47	"
2-0-22	Concrete (ribbed)	-6	-11	-19	64	Neodata
2-1-42	"	-5	-7	-18	65	"
2-0-42	Brick (Windows, doorway)	-9	-14	-18	93	RB3
2-1-22	"	-12	-15	-15	135	"
2-0-10	Concrete Aggregate	-6	-12	-17	75	Cryogenics
3-0-10	"	-12	-10	-20	75	"
		-8.5	-11.25	-15.25	(Average)	

surfaces come close to meeting the Rayleigh criterion at the highest frequency and this applies only for patches that seldom exceed 1-square meter. Beyond an area of 1 square meter, none of the surfaces can be considered smooth for any of the test frequencies used.

The effect of surface roughness is really not apparent from the individual reflection measurements, but a trend as a function of frequency does appear from the averages shown in Table 3. These values are normalized for path length referenced to the 106-m calibration path free of multipath signals. This procedure permits effective reflection coefficient to be calculated from the ratio of the received power that would have occurred if the reflector were perfect, versus the power measured from the reflecting surface in question. For this comparison method, dependence on reflector size and antenna aperture cancel out of the calculation. Consequently, if, for example, a 3-dB power loss was measured in Table 3, the magnitude of the coefficient of reflection of the surface is 0.5.

Table 3 shows a large variation in effective reflection coefficients for identical surfaces when a different path length or spatial position was used in the measurement. The reason for these large variations can best be seen in Figures 8 through 10. Signal amplitude versus transmitter position data were recorded as indicated in configuration B (horizontal position scan) in Figure 1. Figure 8 shows variations in signal amplitude as a function of transmitter position offset (relative to the receiver), using as reflecting surface the solid brick wall, indicated under Test Nos. 3-0-44 and 3-1-0 of Table 3. As seen, the effective reflection coefficient is a highly variable function of position, presumably due to large-scale roughness or unevenness of the surface. Figure 9 shows the variations for a ribbed metal wall with 2.5 x 2.5 cm vertical ridges separated by 50 cm (2 f). This surface is the same as listed for Test Nos. 3-0-14 and 3-0-22 of Table 3.

Two scans were made for Figure 10 as shown by a heavy and a light trace. The reflecting surface was a precast concrete wall with protruding ribs (Test Nos. 2-0-22 and 2-1-42 in Table 3). These vertical ribs are 13 cm wide and protrude 30 cm from the wall at 100-cm intervals. Each of the two scans appears to show a periodicity and a mirror-image character, perhaps a result of the regularity of the protrusions. The reflected signals begin to roll off for the upper two frequencies at about the ± 3-m positions because of the receiving antenna beamwidth limitations.

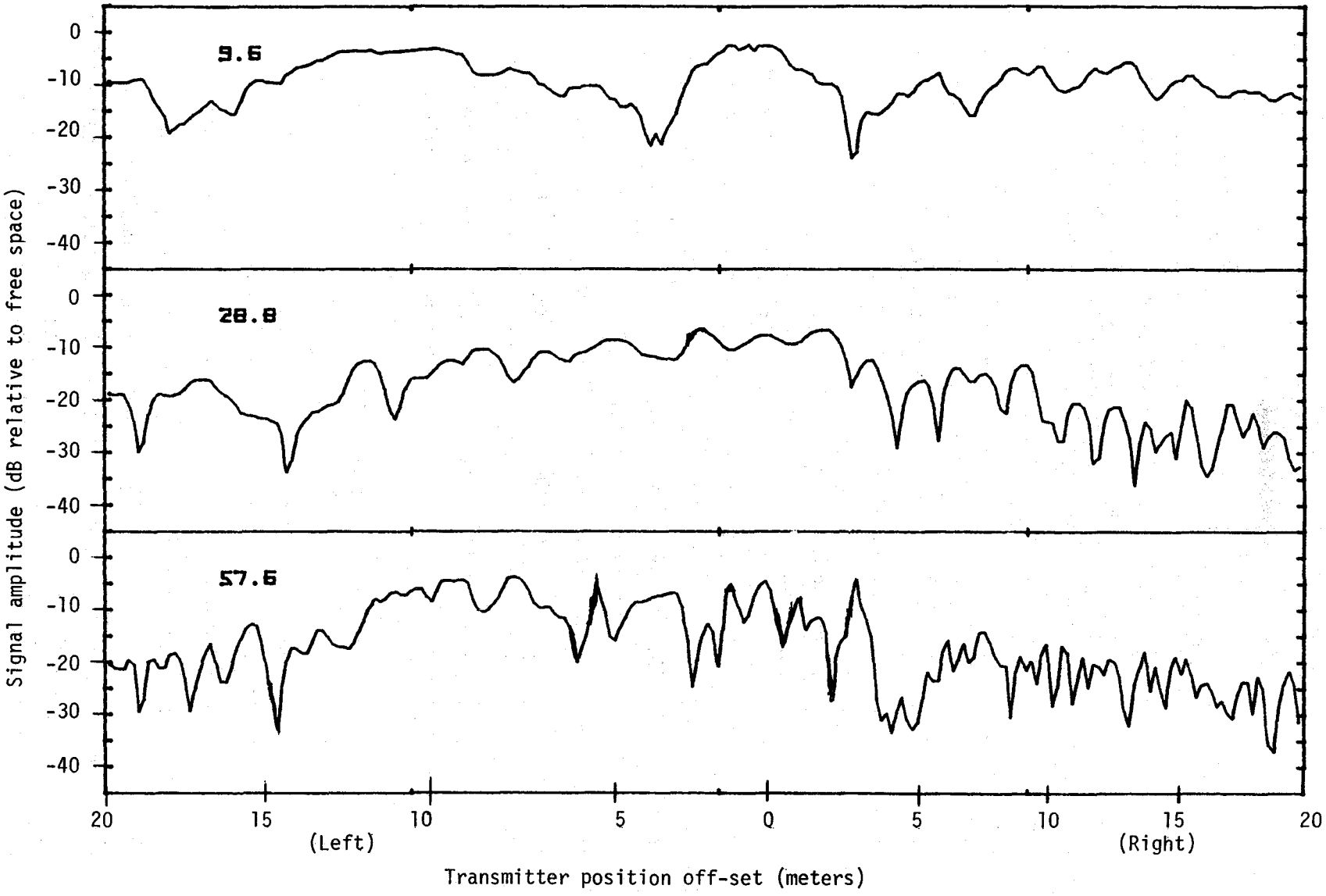

Figure 8. Signal amplitude as a function of transmitter position offset (horizontal position scan) using a solid brick wall as the reflecting surface at a distance of 95 m.

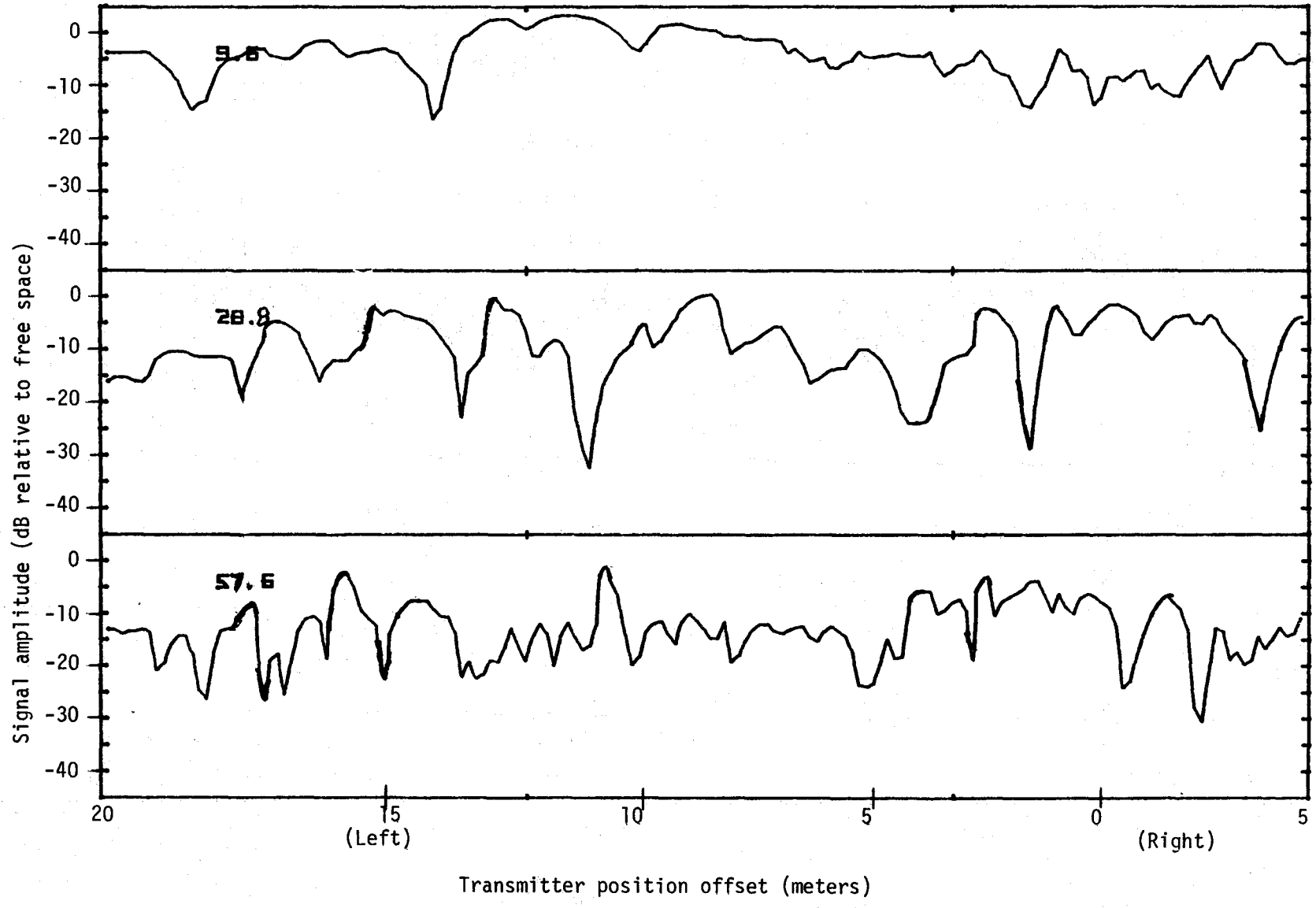

Figure 9. Signal amplitude as a function of transmitter position offset (horizontal scan) using a metal wall as the reflecting surface at a distance of 109 m.

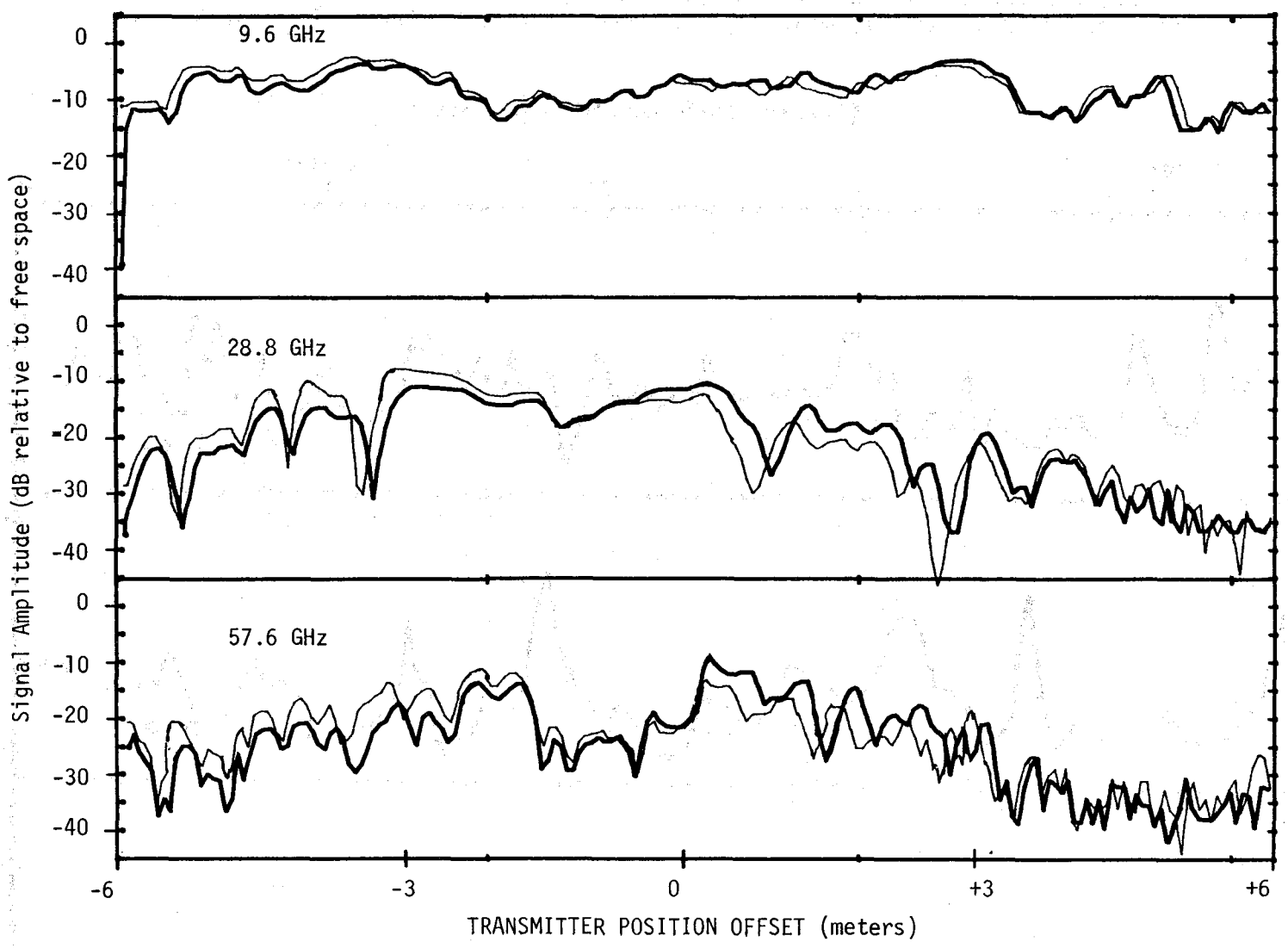

Figure 10. Signal amplitude as a function of transmitter position offset (horizontal scan) using a ribbed concrete wall as the reflecting surface at a distance of 64 m.

These measurements indicate that most building surfaces, being relatively rough and uneven (at millimeter wavelength) exhibit neither the high reflection coefficient nor the high degree of aspect sensitivity as observed from the reference "smooth plate" for reflections at normal incidence.

3.3 Reflections from Roadways

Of primary interest in this report are the measurement and prediction of rf channel performance in an urban-suburban area. Principal reflecting surfaces of this environment are streets and roads; therefore, it is beneficial to learn about the reflection properties of these surfaces. For the application of establishing a LOS communication link between two vehicular mounted terminals, the range scan type of measurement (C of Figure 1) is most appropriate. Several scans were recorded to study the characteristics of the RSL caused by reflections from road surfaces only (i.e., when buildings are not present).

Figure 11 shows a range scan where the RSL is recorded while the transmitter terminal is moved at a nearly constant velocity toward the receiving terminal on an asphalt road in a rural area. The gradual increase in RSL as the transmitter approaches the receiver is the distance squared (R^2) free-space factor. When the street-reflected components are superimposed on the direct signal, a constructive/destructive interference pattern is produced. Also, the 57.6-GHz channel is attenuated at a rate of approximately 10 dB/km due to gaseous absorption of oxygen at the 1500 m (5000 ft) elevation. Between 0.6 and 0.2 km of separation, the interference pattern was strongest because the asphalt surface was well illuminated within the antenna beams. At distances less than 0.2 km, the main beam of the 1.2° receiving antennas, at the upper two frequencies, no longer intercepts the roadway. This becomes true at a closer distance for the 9.6-GHz channel because the receiving beamwidth is 4.8°.

Figure 12 was recorded by moving the transmitter along a gravel road. The ground multipath fades are similar to the data over the asphalt road for the same antenna heights. Because this road was free of traffic, a second run was recorded to observe the repeatability of the measurements. The second run is displaced by 10 dB to make the comparison easier. Even though the gravel road had a very rough surface, up to 3-cm size aggregate, the ground reflection at this low grazing angle appears as strong as from the asphalt road.

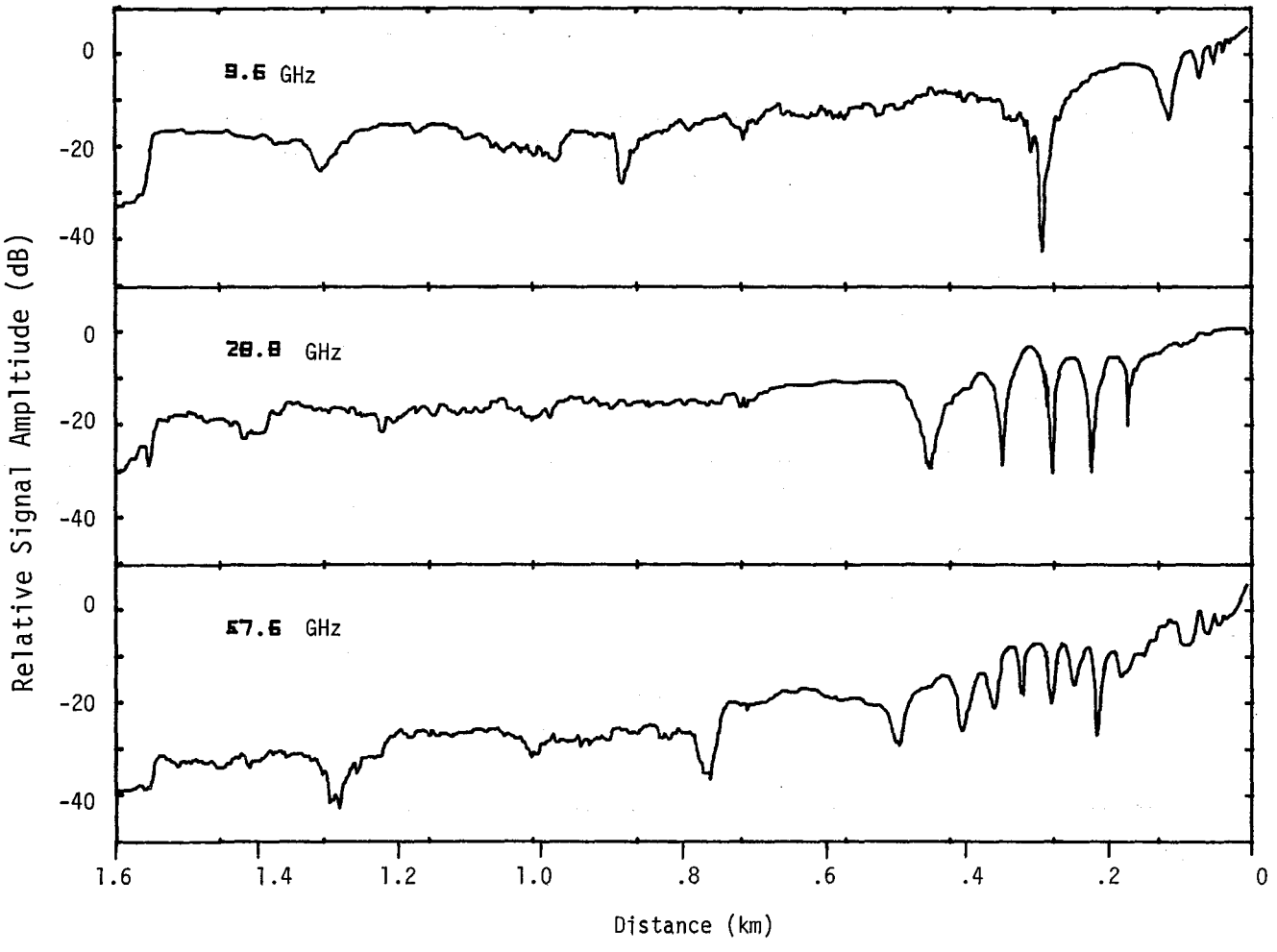

Figure 11. Signal amplitude as a function of range measured along an asphalt road in a rural area. The transmitter is moved at a nearly constant velocity toward the receiver. Vertical antenna polarization. Transmitter height = 2.15 m. Receiver height = 1.8 m.

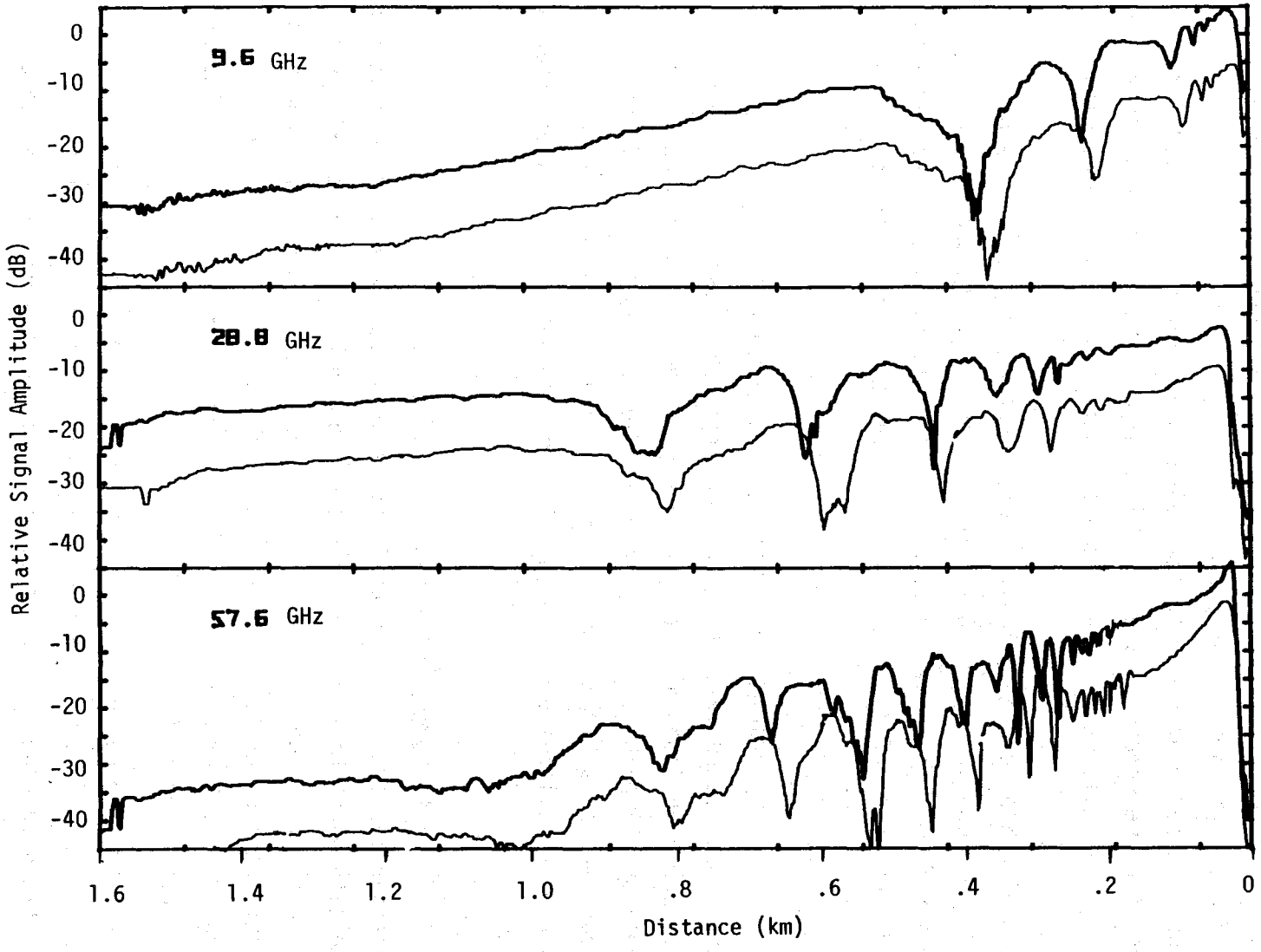

Figure 12. Two separate traces of received signal level as a function of range along a gravel road in a rural area. The transmitter is moved at a nearly constant velocity toward the receiver. Vertical antenna polarization. The transmitter height = 2.15 m. Receiver height = 1 m. The traces are off set by 10 dB.

Not only are the characteristics of RSL fading patterns affected by the antenna beamwidths and antenna heights, but also by curvature or nonflatness of the roadway. A special case of the nonflat surface is shown in Figure 13 where the path profile shielded most of the ground reflections. As the transmitter moved along the path (from 200 m to 350 m), the roadway rose at a rate of 3.8 m for each 100 m of run. At the 350-m point, the road crowned and became level for the remaining 350 m. This nonflat path geometry greatly reduced the ground multipath, even though the path was still line of sight overall.

Additional range scan measurements were recorded for other antenna heights and are shown in Section 6 for comparison to the theoretical model. The conclusion from this roadway data and the prediction model comparisons is that the reflection coefficient for flat surfaces at very low angles is very nearly -1.

4. NON-LINE-OF-SIGHT PATH MEASUREMENTS

To better understand limitations of centimeter/millimeter-wave links in an urban-surburban environment, it is necesary to look at non-line-of-sight paths as well as LOS paths to determine what level of radio system design would be required for a given communication application. Also from an interference potential and possible covert interest, non-LOS path measurements are important.

4.1 Common Materials as Path Obstructions

Comparative measurements of signal levels on an LOS path to signal levels on the same path when obstructed by sheets of common building materials were made on a 370-m path. The 4 ft x 8 ft sheets of material were large enough to cover the antenna cluster at the receiver, which had a maximum height of 2.5 ft and a maximum width of 3.5 ft, and at the transmitter, which had a cluster size of only 0.5 ft by 1 ft.

Table 4 shows the added loss as the materials indicated were placed in front of the antennas. In all but two cases more than one measurement or reading was taken and the average of all readings was entered in the table. Also shown are the maximum and minimum values above and below the average. In every case, the first reading was taken with the material held 4 ft (1.22 m) in front of the receiving antenna. A second reading was taken with the

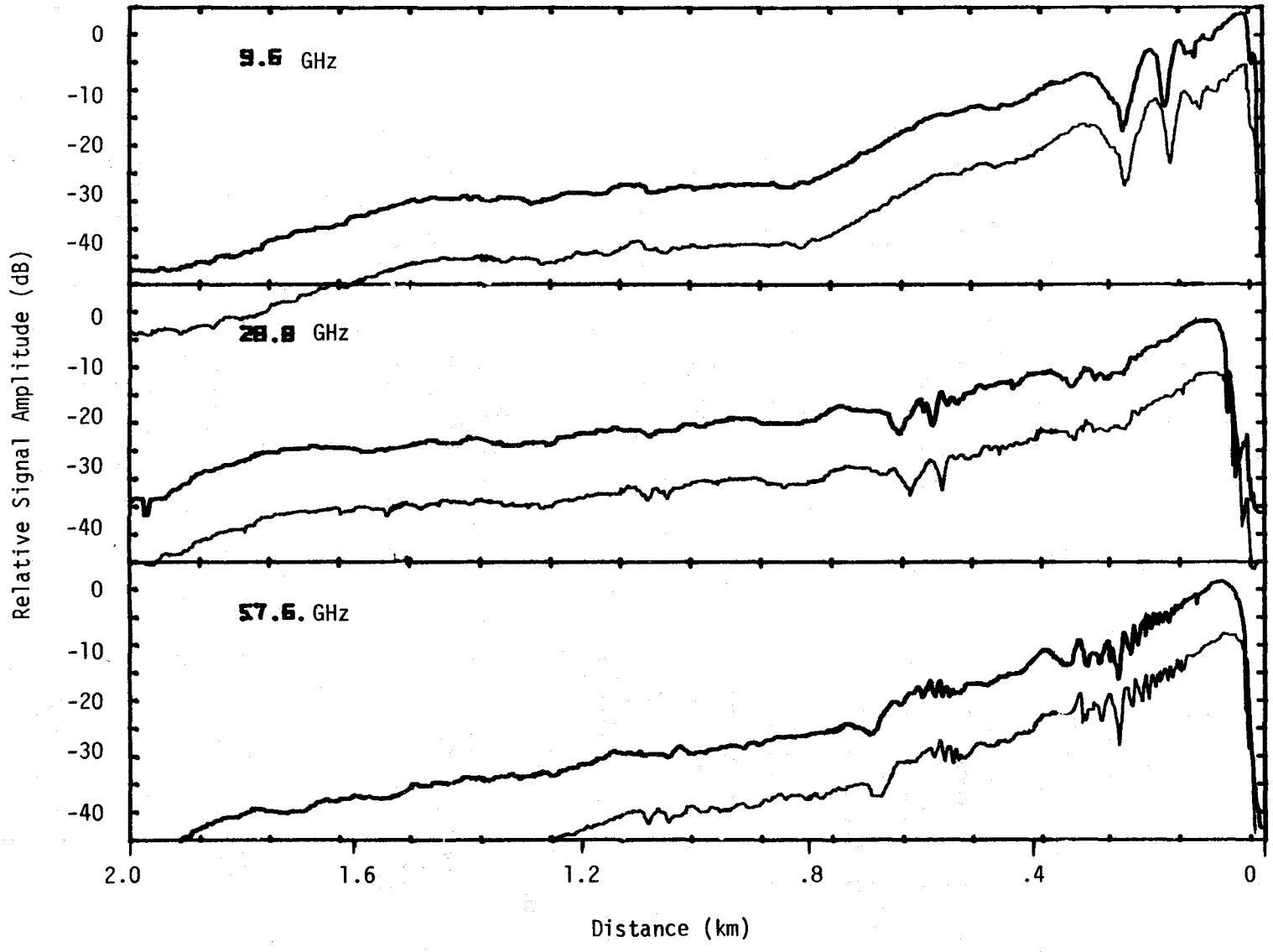

Figure 13. Two separate traces of signal amplitude as a function of range along a gravel road in a rural area. The transmitter is moved at a nearly constant velocity toward the receiver. Vertical antenna polarization. The transmitter height is 2.15 m. Receiver height is 1 m. The traces are off set by 10 dB.

Table 4.

Signal Loss on Path Obstructed With Common Materials

Type of Obstructing Material	Signal Loss (dB) 9.6 GHz Maximum	Minimum	28.8 GHz Maximum	Minimum	57.6 GHz Maximum	Minimum
Commercial Absorber (Ecco Sorb CV-4)(See above) 5 readings	38	+6 -2	51	+3 -5	59	+1 -4
Sheetrock 3/8 in - 2 sheets 5 readings	2	+1 -0	2	+1 -1	5	+1 -1
Plywood 3/4 in (dry) - 1 sheet 4 readings	1	+1 -1	4	+0 -1	8	+2 -3
Plywood 3/4 in (dry) - 2 sheets 1 reading	4		6		14	
Plywood 3/4 in (wet) - 1 sheet 3 readings	19	+8 -13	32	+9 -8	59	+2 -2
Plywood 3/4 in (wet) 2 sheets 3 readings	39	+2 -2	46	+2 -1	57	+2 -3
Aluminum 1/8 in - 1 sheet 1 reading	47		46		53	

material 1.52 m (5 ft) in front of the receiving antennas, and a third was with the material held four feet in front of the transmitting antennas. The fourth and fifth readings were taken with the material 1.52 m (5 ft) in front of the transmitting antennas.

A commercial absorbing material (Echo Sorb CV-4) had a specified loss of >40 dB at 10 GHz, >50 dB at 30 GHz, and >55 dB at 60 GHz, and as seen from the table, the measured values were reasonably near the quoted values. Both sheetrock (plasterboard) and dry fir plywood resulted in small signal losses. Wet plywood sheets, stored outside and with an obviously high moisture content, showed much higher losses and somewhat greater frequency variations. There are indications of edge diffraction components that contribute to the measured signal level. This contribution becomes important only when the signal passing through the obstruction is very small. For example, in the case of an aluminum sheet, no signal should penetrate, but values of only 45 to 50 dB below the LOS path were measured. This signal level is, therefore, assumed to approach the limit of the loss measurement; however, because of edge sharpness of the 1/8-in thick sheet of aluminum, a larger diffraction field would result than for other materials measured.

4.2 Buildings as Path Obstructions

Four buildings were used as path obstructions in these measurements. Each building was different in terms of construction materials, architectural design, and size. In each data set, the measurements were performed as a function of the distance the transmitter and receiver were from the building and of the pointing angles of the transmitting and receiving antennas. Photographs of the four buildings are shown in Figure 14. For each measurement setting, the transmitter and receiver were set on a line perpendicular to the building walls. In the photograph of Building #1, the receiver van is shown on location at the right side of the photograph and in the photograph of Building #4, the transmitter mounted in the pickup truck is shown in front of the building.

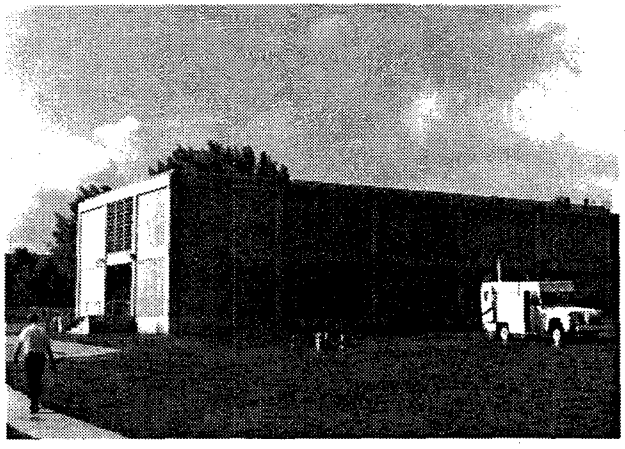

Building #1 Solid cement-block walls
(width=15 m, height=9 m)

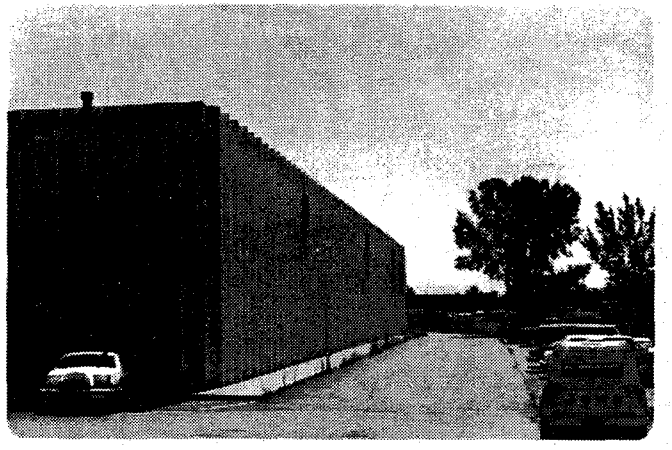

Building #2 Precast concrete walls
(width=100 m, height=8 m)

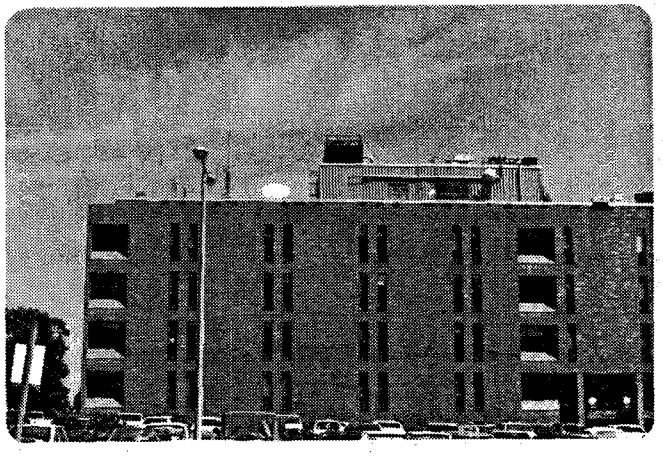

Building #3 Brick exterior
(width=53 m, height=14 m)

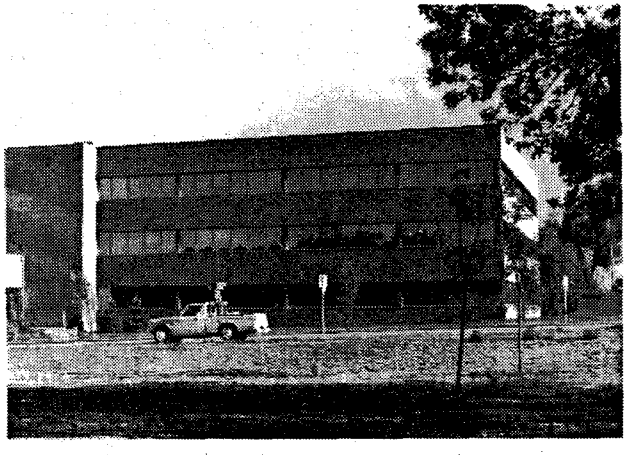

Building #4 Chromatic coated glass
(width=26 m, height=12 m)

Figure 14. Photographs of the four test buildings.

The drawing in Figure 15 shows the test geometry for Test A at Building #1. This setup is typical for each of the buildings, with only changes in the total path length and antenna orientation (pointing to include building edges) being different for the various tests. In Table 5 the measured received signal levels (in dBm) are given as a function of frequency, construction type (width of building at path intersection), and total path length.

The results for Building #1, Test A, show no detectable signal above the noise threshold (-132 dBm) on the 28.8 and 57.6 GHz channels. If the 42-m long path were line of sight, the RSL would be -23, -20, and -38 dBm for the 9.6, 28.8, and 57.6 GHz channels, respectively. The loss through the cement-block structure was about 84 dB at 9.6 GHz and greater than 100 dB at 28.8 and 57.6 GHz. Tests B and C are RSL with the antennas still pointed directly between terminals but at greater distances away from the building walls. These three tests indicated that this flat-roofed structure supported a lower loss diffraction mode of signal propagation because as the path-to-building lengths are increased, the antenna illumination of the exterior edges of the building also increases. The conclusion is clearly demonstrated by performing an elevation scan with the receiving and transmitting antennas and noting that a peak signal occurs when both antennas point directly to the roof edge as in Test D. In effect, the peak signals to the receivers are transported by a double-edge diffraction mode.

Tests 1D, 2B, 2C, and 3B show the higher values of RSL when both the transmitting and receiving antennas were pointed directly at the roof edges. More details of these measurements are contained in NTIA Report 85-184, pages 14-19 (Violette et al., 1985).

In test 4A, an office building with predominantly glass walls was the path obstruction. These walls (windows) are a chromatic coated glass and appear as mirrors (in the visible spectrum) from outside but were transparent from the inside. With only the two exterior walls in the path (the building was empty), surprisingly high losses of 60, 65, and 64 dB for the 9.6, 28.8 and 57.6 GHz channels, respectively, were observed when compared to an equivalent 72-m LOS path. By comparison, these values were as much as 50 dB higher than attenuation through tinted glass doors.

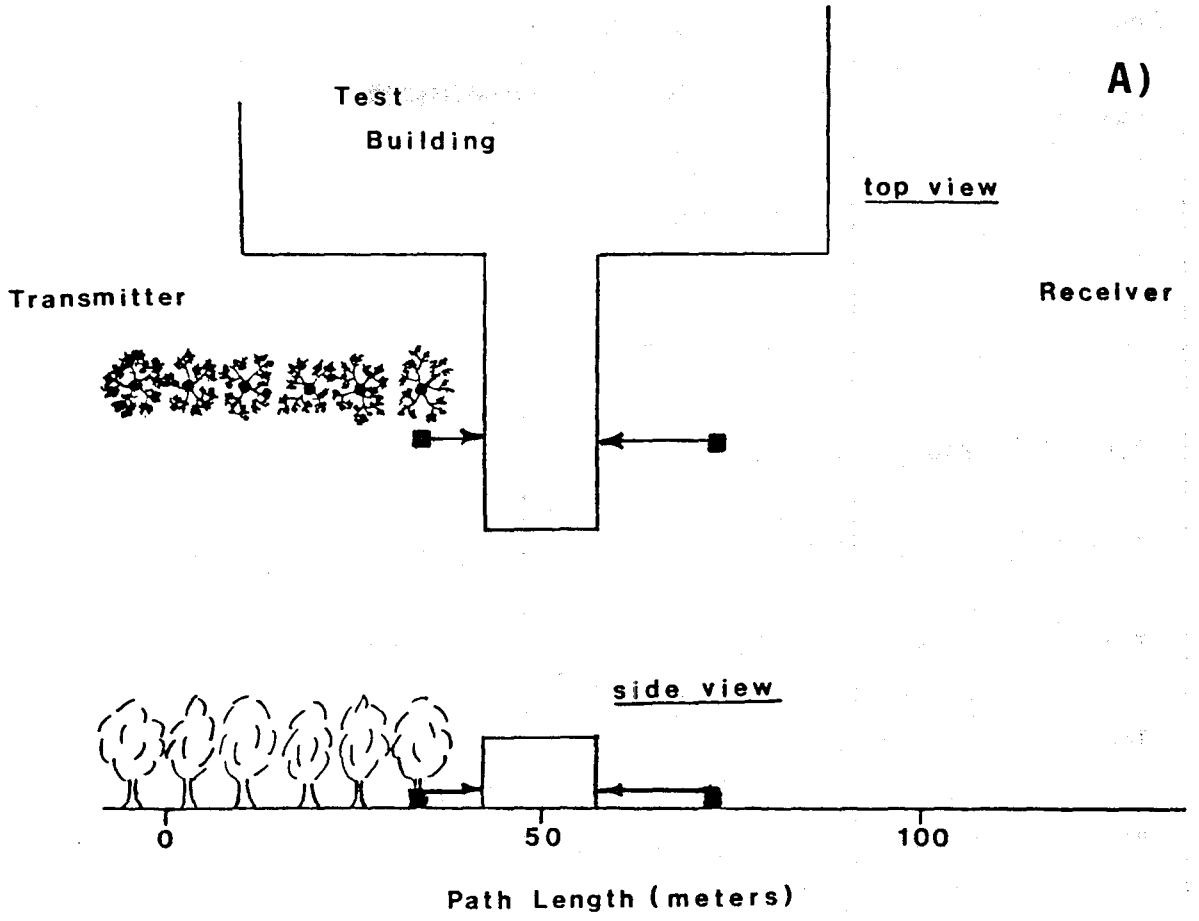

Figure 15. Typical test geometry.

Table 5.

Received Signal Levels with Buildings as Path Obstructors

Building/Test Numbers	Construction Type	Antenna Pointing	Building Width/Height (Meters)	Path Length (Meters)	Received Signal (Level of dBm) Frequency (GHz) 9.6	28.8	57.6
1 A	Solid Cement-Block Walls	Direct	17/6	42	-107	<-132	<-132
1 B	"	"	"	→ 53	- 87	-130	<-132
1 C	"	"	"	→ 90	- 92	- 98	-113
1 D	"	Toward Roof Edge	"	→ 53	- 80	- 80	- 93
2 A	Solid Pre-Cast Concrete	Direct	100/7	200	<-132	<-132	<-132
2 B	"	Toward Roof Edge	"	"	-113	-117	-132
2 C	"	"	"	→ 260	-104	-104	-130
3 A	Brick w/ Windows	Direct	40/16	120	-113	-130	<-132
3 B	"	Toward Roof Edge	"	"	-104	-114	-127
4A	Chromatic Glass	Direct	53/9	72	- 88	- 90	-107

*

4.3 Residential Areas

The measurements in the residential areas were of three types: dense residential, sparse residential, and sparse residential with one terminal elevated. The houses in the dense residential area were mainly one-family, one-story, frame dwellings. The pictures in Figure 16 show typical residential area houses and yards from the three test settings.

The results from these tests are given in Table 6. The received signal levels in dBm on the obstructed paths and the loss in dB due to the obstructions are listed for 9.6, 28.8, and 57.6 GHz. The loss is found by taking the non-LOS RSL given in the table minus what the RSL would have been if the path had been LOS. For each measurement, the antennas were pointed for maximum signal at near on-line pointing, except for path 1B. For the paths that were non-line-of-sight, there was no easy way of determining exact on-line pointing.

Test path 1A was a one-block-long (~ 100 m) path with two one-family dwellings and many trees on-path. The path losses, due to these obstructions, for the higher two frequencies were 69 dB at 28.8 GHz and 70 dB at 57.6 GHz. In test path #1B this path loss was reduced by about 30 dB by elevating the antenna pointing 10°, roughly toward treetop level.

A 950-m LOS path, down a suburban street, was chosen for test 2A. Very little ground clearance was available, so surface multiple components were present along with the direct ray, as was evidenced by a substantial signal variation when either terminal was moved by only a few meters toward or away from the other. Test Paths 2B, 2C, and 2D had houses and trees in the foreground looking out from either terminal, and in addition there was a several-meter rise in the terrain between terminals. In the path selected for tests 3A, 3B, and 3C, the receiver was positioned on the crest of a hill 30 to 40 m above the surrounding terrain. However, the transmitting antennas were looking toward trees and houses which obstructed the path.

For all but the LOS test, it is likely that propagation by diffraction from roof edges and especially treetops accounted for most of the received signal, as noted by test path 1B. In test 1B the path geometry was such that the treetops appeared in the common volume of the antenna beams of each terminal. A similar situation existed with the elevated receiver terminal in test paths 3A, 3B, and 3C. When the wind was blowing, large signal fluctuations in signal levels occurred, which were directly correlated with tree motion.

Path #1 Dense residential

Path #2 Sparse residential

Path #3 Sparse residential (receiver on hill)

Figure 16. Photographs of residential areas.

Table 6.

Received Signal Levels in Residential Areas

Path #/ Test #	Area	Path Length (Meters)	Frequency (GHz) 9.6 RSL dBm	9.6 LOS dB*	28.8 RSL dBm	28.8 LOS dB*	57.6 RSL dBm	57.6 LOS dB*
1 A non-LOS	dense	100	- 73	44	- 95	69	-114	70
1 B non-LOS	residential	Antenna Elevated 10°	- 60	33	- 66	40	- 81	37
2 A LOS	sparse residential	950	- 48		- 37		- 67	
2 B non-LOS	"	1200	<-132	?	<-132	?	<-132	?
2 C non-LOS	"	1000	-106	57	-114	68	<-132	?
2 D non-LOS	"	900	-104	56	-112	67	<-132	?
3 A non-LOS	sparse residential	650	- 90	45	-106	64	-113	53
3 B non-LOS	"	800	- 51	4	- 68	24	- 81	19
3 C non-LOS	"	1450	- 84	52	- 82	33	- 91	24

*Loss due to obstruction (non-LOS RSL-RSL if path were LOS)

In test paths 2B, 2C, and 2D, no trees or buildings were in the common volume illumination because of the high terrain near midpath. The RSL was small or not detected in each of these tests and the propagation mode when signals were seen probably occurred by multiple diffraction/scatter from trees.

If, as suspected, the majority of the received signals are by diffraction/scatter modes, the coherent bandwidth of the propagated and detected signal would be limited by time-delay spread on the rf signal components. Calculations using the antenna beamwidths and the geometry of scattering components from treetops or roof edges for paths in this section indicate the total delay spread should not exceed 5 ns, which would allow usable bandwidths of 50 to 100 MHz depending on the type of modulation.

4.4 Diffraction from a Vertical Edge

A potential propagation mode, when buildings obscure the LOS path, is diffraction from edges or corners. The transmission loss over a diffraction path depends on the shape and electrical characteristics of the diffracting edge. A corner of a building formed from poured and finished concrete was used to make diffraction loss measurements at the three operating frequencies. The path lengths and geometries are shown in Figure 17. Three sets of data are presented in Figures 18, 19, and 20. These data were measured using, respectively, locations T_1 and R_1, a 62-m path; T_1 and R_2, a 106-m path; and T_2 and R_2, a 146.5-m path. The solid line traces in these figures show the measured signal amplitudes for each frequency as indicated for horizontal-horizontal and vertical-vertical polarizations and the broken line traces show predicted diffraction losses due to a "knife-edge."

The predicted values shown in the figures were generated from equations based on the Geometrical Theory of Diffraction (Keller, 1962), which assumes the incident field at the edge to be a plane wave. The gain of the diffracted ray is assumed to fall off as $1/\sqrt{r_d}$, i.e., a cylindrical wave, where r_d is the distance from the edge. When the electrical field vector is polarized parallel to the edge (VV polarization for vertical edge), the field intensity is expected to be less in the shadow region than when the electric field vector is polarized perpendicular to the edge. The measured data of Figures 18 through 20 show this dependence. However, the measured values gave

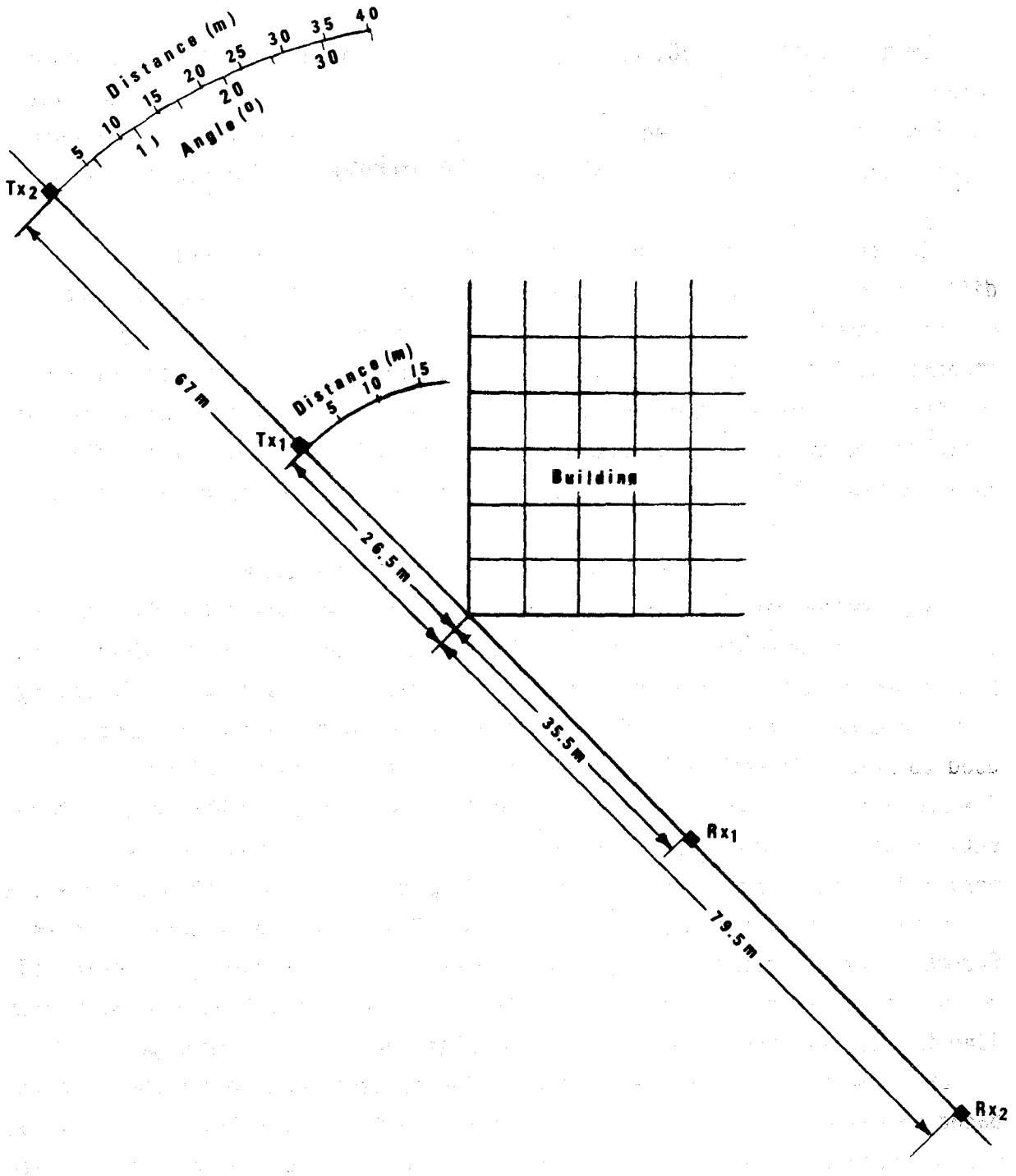

Figure 17. A drawing showing the transmitter and receiver locations for the data in Figures 18, 19, and 20.

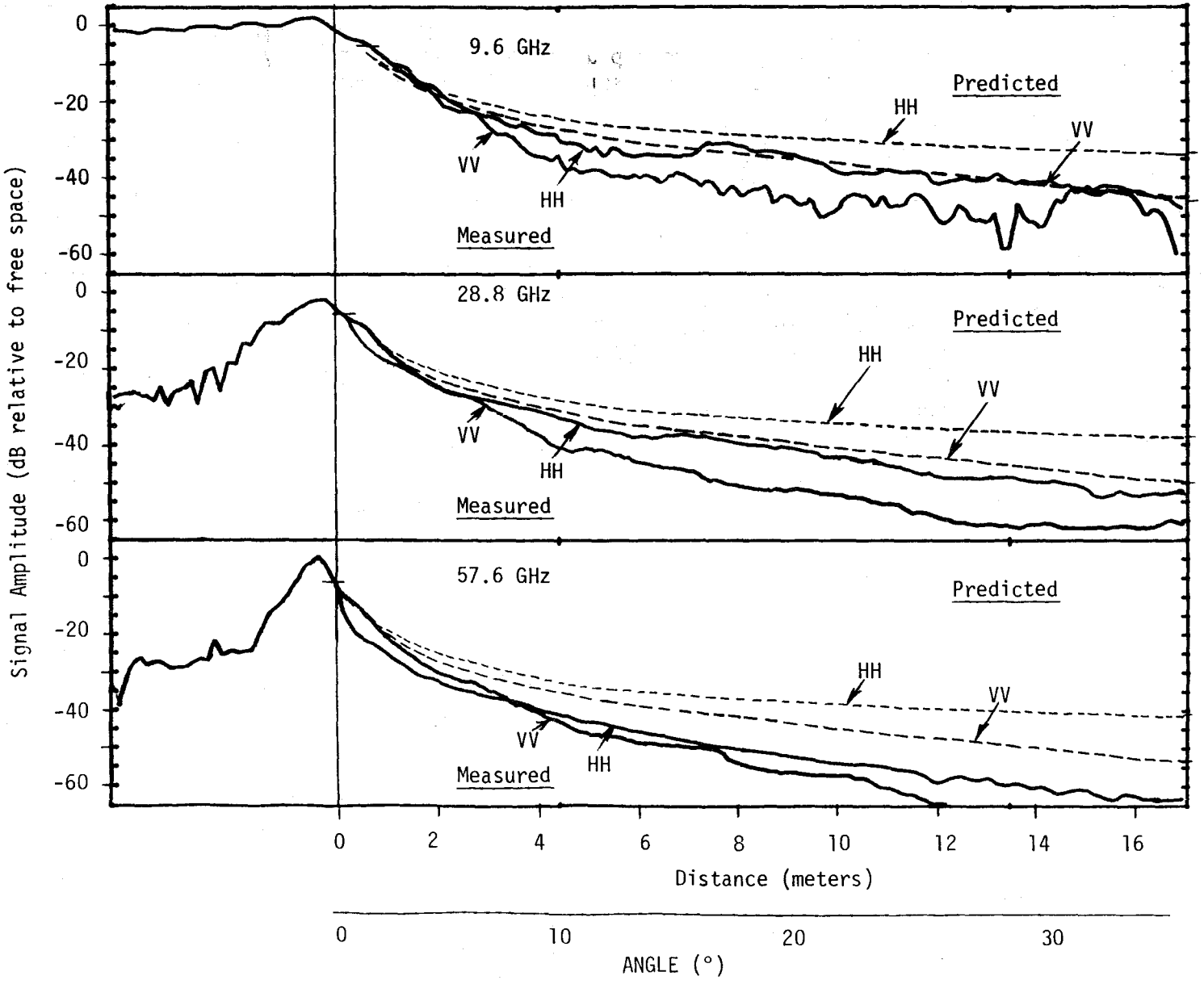

Figure 18. Signal amplitude measurements from an edge diffraction for 9.6, 28.8, and 57.6 GHz. Edge to receiver distance = 35.5 m and the edge to transmitter distance = 26.5 m.

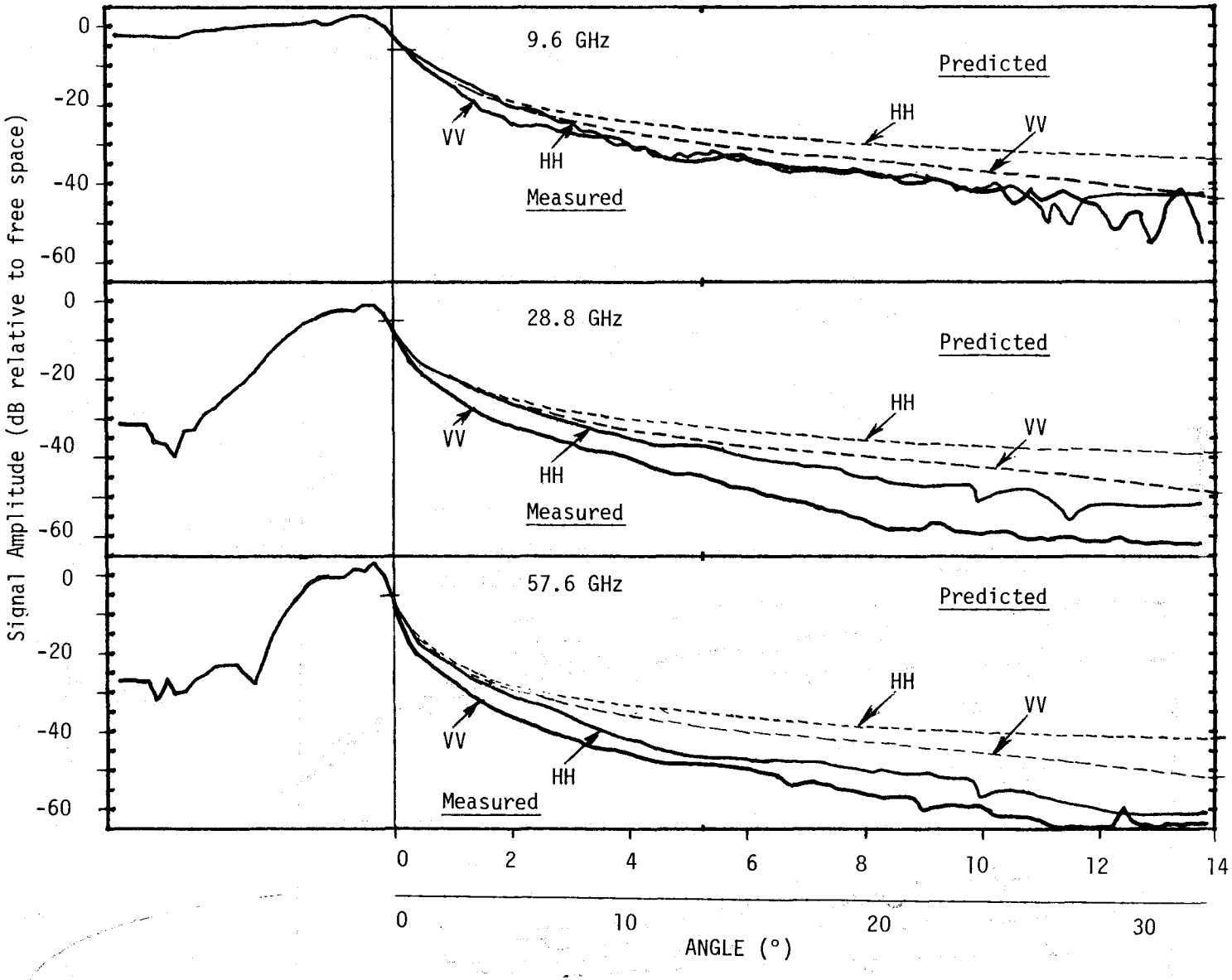

Figure 19. Signal amplitude measurements from an edge diffraction for 9.6, 28.8, and 57.6 GHz. Edge to receiver distance = 79.5 m and the edge to transmitter distance = 26.5 m.

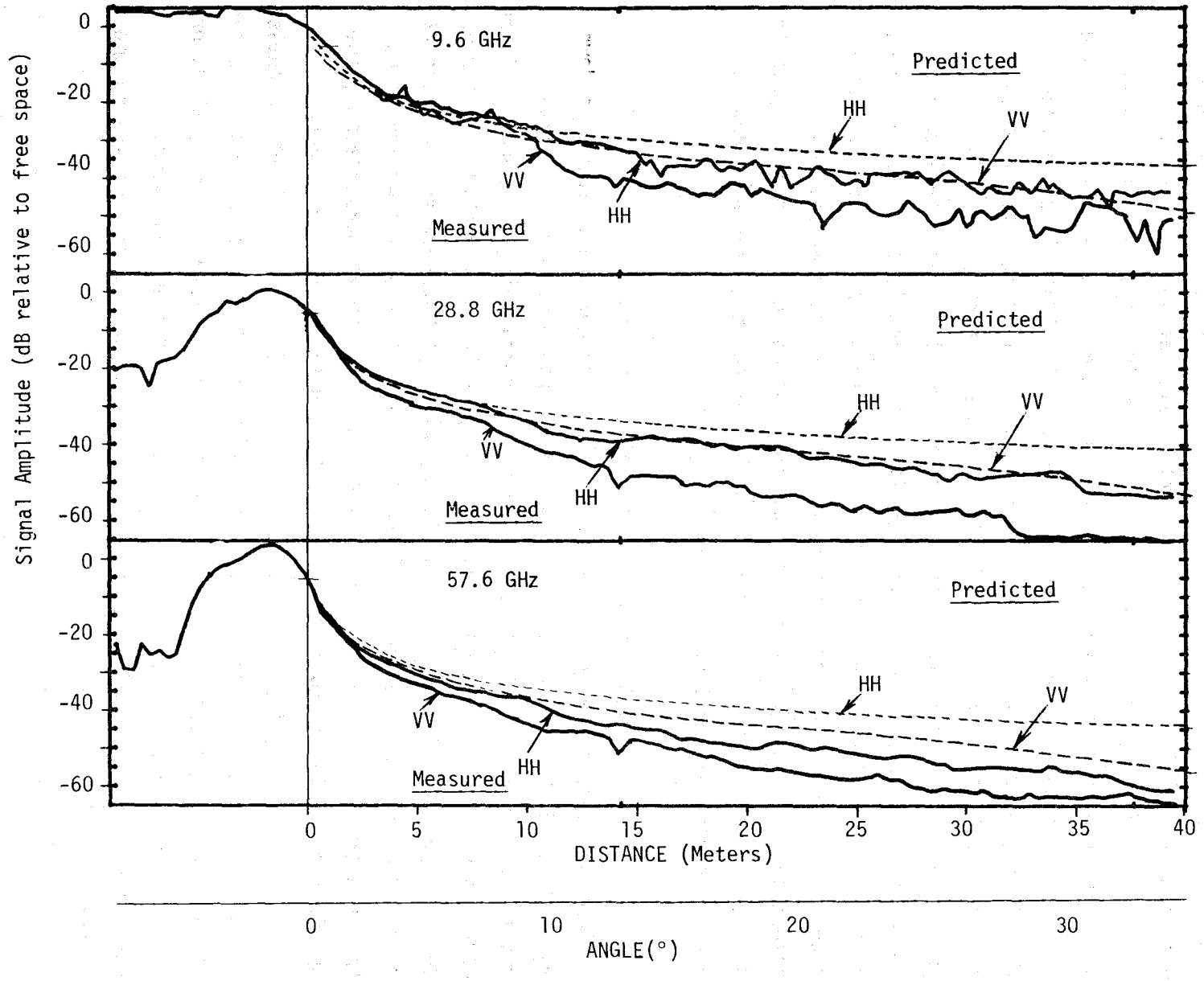

Figure 20. Signal amplitude measurements from an edge diffraction for 9.6, 28.8, and 57.6 GHz. Edge to receiver distance = 79.5 m and the edge to transmitter distance = 67 m.

diffraction losses greater than the predicted values, particularly, as the terminal moves further into the shadow region. This increase in loss compared to predicted values may occur because the corner is not a "knife-edge" as assumed in calculating the predicted values. In fact, the concrete corners are formed such that they have a 1.5-cm flat bevel at 45° to each side.

A different path length was used for Figure 18 compared to Figure 19 by positioning the receiver terminal 35.5 m from the edge in the first case and 79.5 m from the edge in the second case, keeping the transmitter terminal 26.5 m from the edge for both cases. As seen by comparing these figures, there is little difference in diffraction loss as expected. The data in Figure 20 were taken with the transmitter distance from the edge increased to 67 m and show no appreciable difference in diffraction loss for equal angles from the grazing line. These measurements, and those in Section 4.2, demonstrate that when a link using directive antennas is operated with an "unpenetrable" building as a path obstruction, it may be possible to establish a usable non-line-of-sight communication link by pointing the antennas to enhance the edge diffraction mode of propagation.

4.5 Urban Non-Line-of-Sight Paths

Some propagation measurements on non-LOS paths were performed in a downtown Denver, CO, area. In this area most buildings were more than five stories and some were up to 30 stories high. Approximately 15 percent of the space within each block is open and used for off-street automobile parking or pedestrian parks. The street map in Figure 21 shows the receiver location at the corner of 17th and California Streets and several transmitter locations with the approximate antenna pointing for each. For these measurements, the transmitting antenna beamwidths were all 10° and the receiving antenna beamwidths were 4.8°, 1.2°, and 1.2° for the 9.6, 28.8, and 57.6 GHz channels, respectively. In general the pointing of the transmitter antennas was selected to be either in a direction where the receiver was believed to be located, or in a direction where open areas existed but toward distant buildings to enhance the chances of multiple reflections producing a signal return to the receiver.

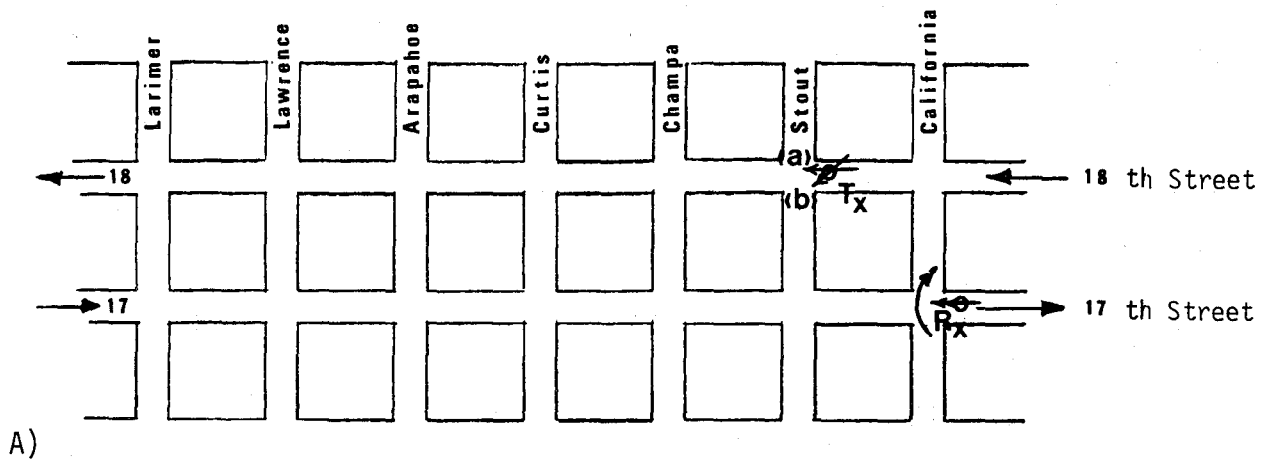

A)

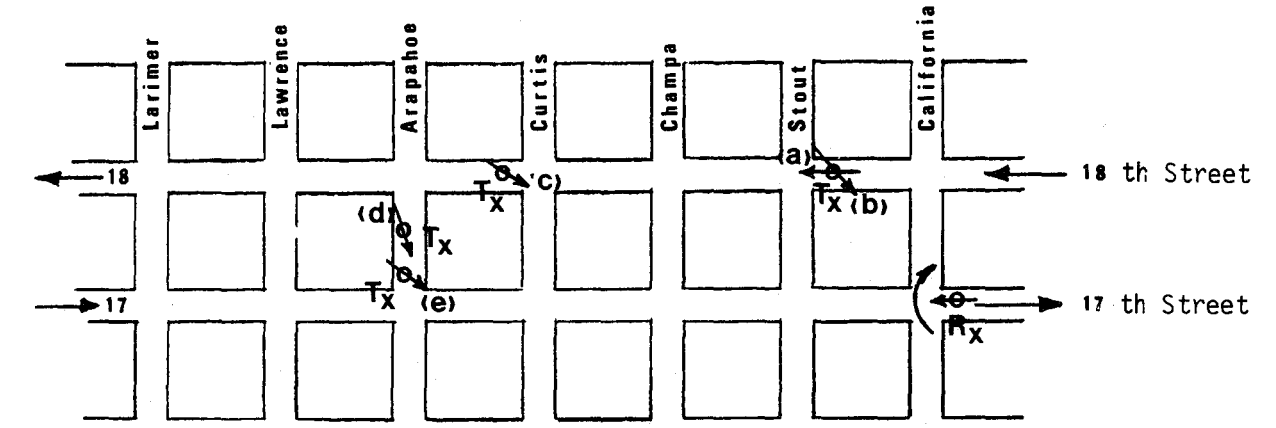

B)

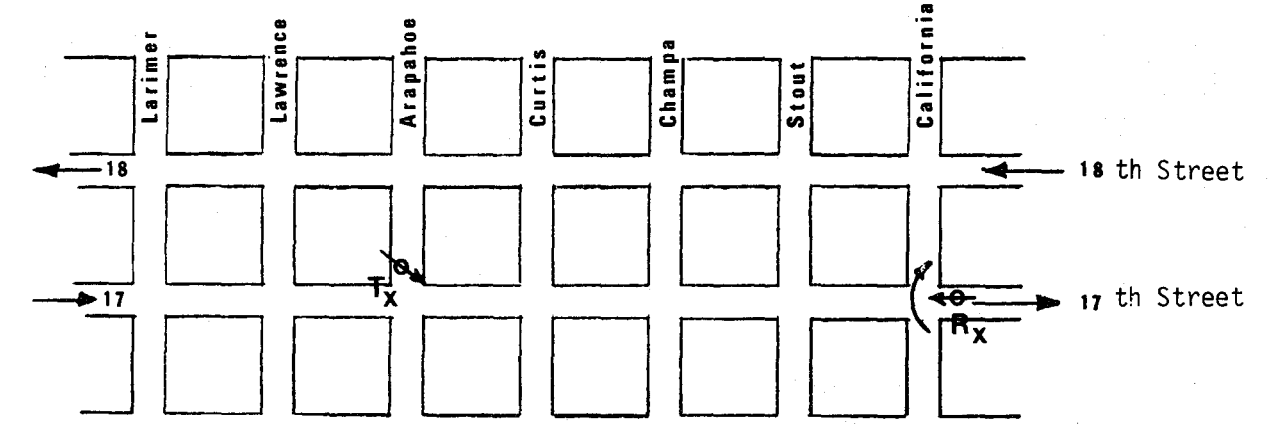

C)

Figure 21. Test locations using the 9.6, 28.8, and 57.6 GHz millimeter-wave test system in downtown Denver for non-line-of-sight measurements.

Table 7 indicates, for each frequency, the amount that the non-LOS received signal level was reduced from the level that would have been present had the path been free space over the actual terminal separation as shown in Column 3 of the table. The recorded values for signal-to-noise ratios account for differences in receiver noise figures and noise temperatures at the antennas. Note that for some measurements the receiving antennas were fixed, pointing directly down 17th Street (270°) and for others, where the word "search" appears, the receiving antennas were scanned in azimuth for greatest RSL. It was found that in most cases, the peak signals for the upper two frequencies (narrow beamwidth) occurred at antenna positions from 12° to 15° from the 270° down the street pointing, which suggests that these signals arrived from reflections off nearby buildings.

Also note that no elevation scans were attempted because, with the positioner used at that time, it was both difficult and time consuming to obtain the necessary precision. The antennas were aligned for 0° elevation (parallel to the ground). Had elevation scanning been tried, it is possible that increased received levels would have resulted.

5. LINE-OF-SIGHT MEASUREMENTS

A large number of the measurements conducted to study millimeter-wave propagation characteristics in urban-suburban environments were made on line-of-sight paths on various streets in Denver, CO. The data collected during these urban line-of-sight tests included received signal levels at all operating frequencies, impulse response measurements, and bit-error-rate measurements. In addition to the two operating systems discussed in Section 2, which provided two sets of narrowband frequency channels and a wideband channel, measurements were made using narrowbeam and widebeam antennas. Both vertical-vertical and horizontal-horizontal antenna polarization were used in the measurements.

The results from these measurements are presented in three categories: received signal amplitudes, impulse response measurements, and system bit-error-rate measurements. Some special calibration and evaluation data are included in the impulse response and bit-error-rate categories.

Table 7.

Measurement Results for Non-line-of-sight Tests in Downtown Denver

Receiver Locations	Transmitter Locations	Distance between Terminals (m)	Pointing Angle RX	Pointing Angle TX	Received Signal 9.6 GHz	(dB relative to free space) 28.8 GHz	(dB relative to free space) 57.6 GHz	Location in Figure 21
Corner of California & 17th	18th & Stout	125	270°	270°	-65 25 dB(S/N)	-82 5 dB(S/N)	Below noise threshold	(a)
"	"	125	search	240°	-59 31 dB(S/N)	-66 21 dB(S/N)	-47 -1 dB(S/N)	A (b)
"	"	125	270°	275°	-61 29 dB(S/N)	-85 2 dB(S/N)	Below noise threshold	A (a)
"	"	125	search	135°	-54 36 dB(S/N)	-63 22 dB(S/N)	-47 -1 dB(S/N)	B (b)
"	18th & Curtis	370	search	135°	-39 36 dB(S/N)	-46 30 dB(S/N)	-42 4 dB(S/N)	B (c)
"	Arapahoe 150' back from 17th	430	270°	170°	-35 43 dB(S/N)	-47 30 dB(S/N)	-42 3 dB(S/N)	B (d)
"	Arapahoe 20' back from 17th	425	270°	125°	-23 55 dB(S/N)	-41 35 dB(S/N)	-32 13 dB(S/N)	B (e)
"	"	425	search	125°	-15 67 dB(S/N)	-19 59 dB(S/N)	-11 35 dB(S/N)	C

5.1 Received Signal Amplitudes

A signal amplitude plot for vertical antenna polarization is shown in Figure 22 as a function of transmitter terminal position as it traveled at a nearly constant velocity (approximately 10 km/h), along a 0.9-km section of 17th Street in downtown Denver, CO, toward a stationary receiver terminal. Comparative data are shown in Figure 22 for a rural asphalt road where the transmitter terminal traveled toward the receiver terminal over a somewhat longer span of 1.6 km. In Figure 22A the fading is caused by multipath components reflected from the building walls, signs, cars, trees, etc., in addition to the street surface. The fading seen in Figure 22B is due to the destructive signal interference of reflections from the road surface only, as discussed in Section 3. In both of these examples the signals were recorded using the narrowband receivers at 9.6, 28.8, and 57.6 GHz with narrowbeam receiving antennas of 4.8°, 1.2°, and 1.2°, respectively. The transmitting antennas' beamwidths were all 10°.

Overall, the plots for the urban street in Figure 22 show less deep fades between 0.1 and 0.5 km than the same range on the rural road. This is due primarily to the fact that the more numerous multipath components reduce the probability of deep nulls as compared to when only a street-reflected component and a direct ray are present. Also, even though the tests were conducted during the early morning hours, an occasional vehicle along the downtown route may interrupt the ground reflection for some fraction of the travel. Generally, the antenna heights were sufficient to allow the direct ray to pass over vehicles, but at times trucks or buses may have obstructed the path. When the direct ray is obstructed, the signature is usually recognizable because all channels fade simultaneously. Another difference in Figure 22 is that between 0.5 and 0.9 km on the downtown street there are much deeper and more numerous fades than in the rural road plot. This occurs because the further the terminals are separated the more the building wall surfaces are illuminated by the main lobe of the antenna beams.

Further insight of the complex geometry of the 17th Street path is gained from a review of Figure 23, a street profile, and from Figure 24(A), (B), and (C), which are photographs of the street fronts along 17th Street in Denver, CO.

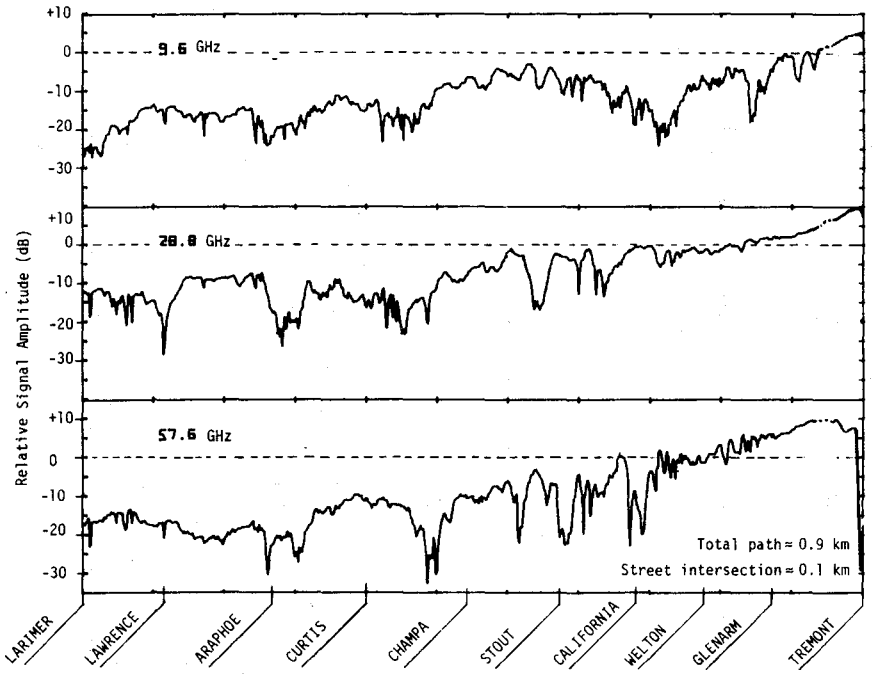

A) Measured along 17th Street in downtown Denver, CO.

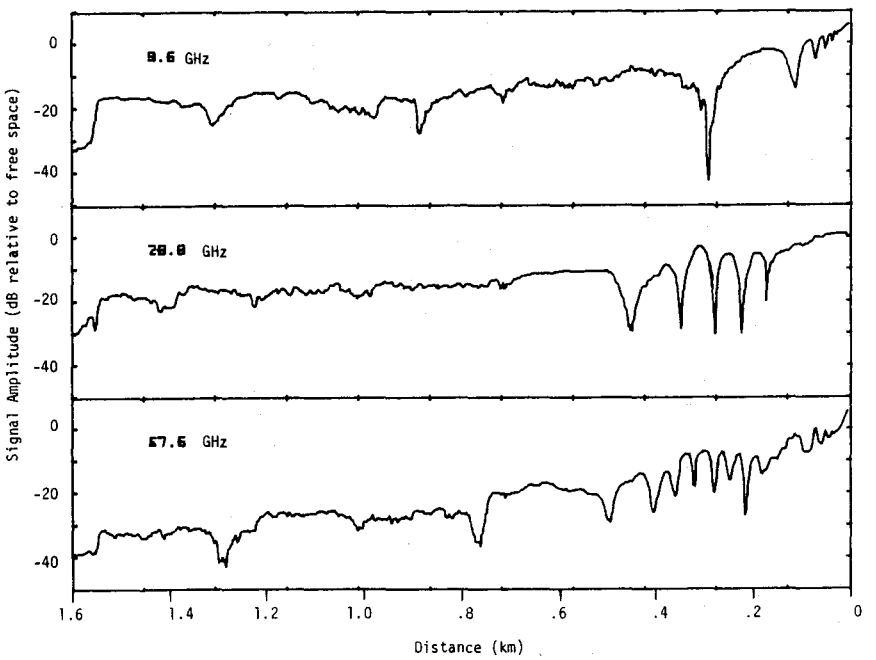

B) Measured along an asphalt road in a rural area. Transmitter height= 2.15m. Receiver height= 1.8m.

Figure 22. Signal amplitude as a function of range measured along select test paths. The transmitter is moved at a nearly constant velocity toward the receiver. Vertical antenna polarization.

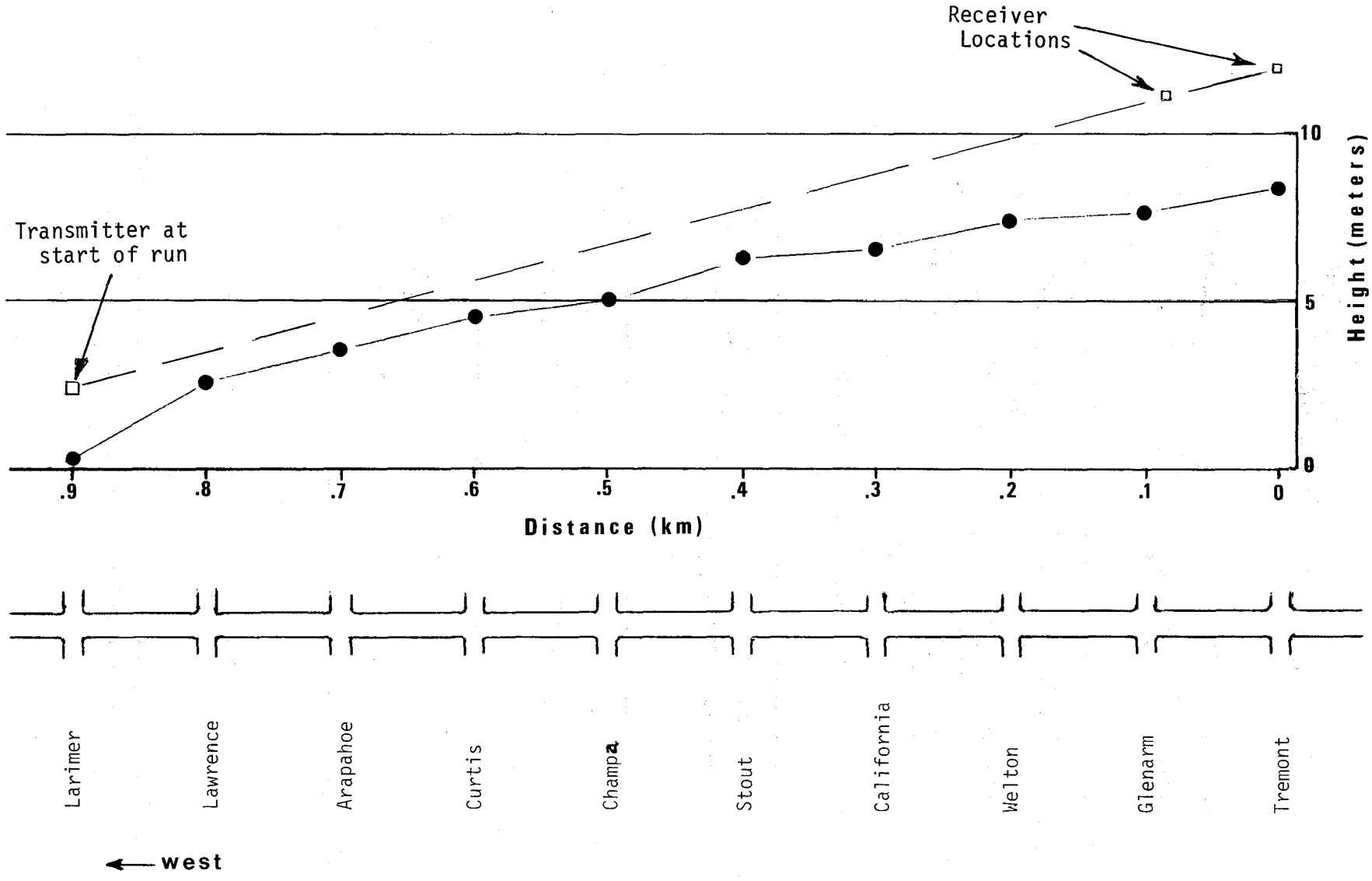

Figure 23. A drawing showing the street intersection elevation profile and using the LOS path for the portion of 17th Street in Denver, CO, used to measure signal amplitude as a function of distance.

A)

B)

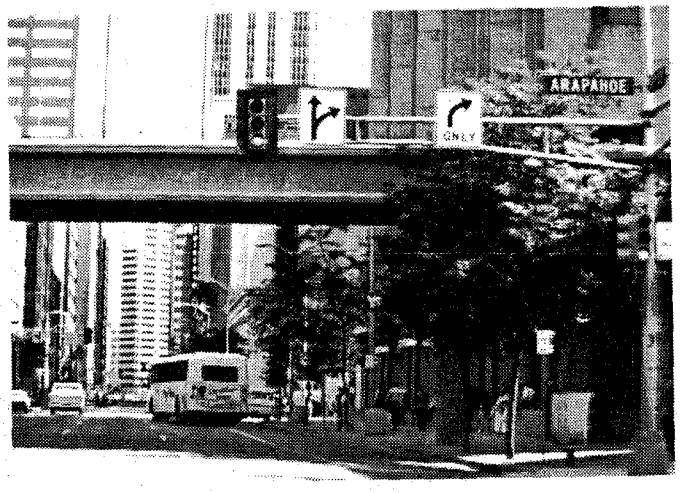

C)

Figure 24. Photographs of street fronts along 17th Street in Denver, CO.

5.2 Receiver Off-Angle Pointing

A set of three runs was made along the 0.9-km path from Larimer to Tremont to assess the impact on the received signal level by off-angle receiver antenna pointing. For the first run, the receiving antennas were at 0° pointing (along the transmitter-receiver line). For the second and third runs, the receiving antennas were pointed off-angle 2° and 4°, respectively. The resultant signal amplitudes from these three runs are shown in Figures 25, 26, and 27, in the order of increasing frequency (9.6, 28.8, and 57.6 GHz).

The traces in these three figures are offset to more clearly display the characteristics of each run. All traces are plotted to the same amplitude scale and a 10-dB signal scale is indicated in each figure.

At all frequencies, more numerous amplitude variations occurred in the RX = -2° and RX = -4° plots compared to the direct pointing (RX = 0°) as a result of more and larger reflections from the buildings along the street. A succession of deep multipath fades (as a function of distance) occurred at 9.6 GHz between Curtis and Stout Streets for the RX = -4° pointing, probably because the wider 4.8° receiving antenna beamwidth allows the building reflections and the direct ray to be more nearly equal. The higher two frequencies (1.2° beamwidth) produced interesting fading patterns and indicate the effectiveness of buildings as reflectors as they are the main received signal source for the off-pointing runs. Information about signal characteristics in these street scenarios may be important for narrowbeam mobile communication systems, as good antenna alignment may not always be maintained. In addition to signal fading, channel distortion can become a problem, if bandwidths are extended, due to the time delay spread of the multipath signals.

5.3 Transmitter Off-Angle Pointing

In order to enhance the reflections from building walls relative to the direct ray, the transmitter antennas were off-pointed in 10° steps. This provided a variety of reflections that were identifiable as to number of wall reflections that occurred by the angle-of-arrival at the receiving antennas. These data were recorded with the terminals stationary and separated by 485 m. For each transmitter antenna setting (0°, 10°, 20°, 30°), the

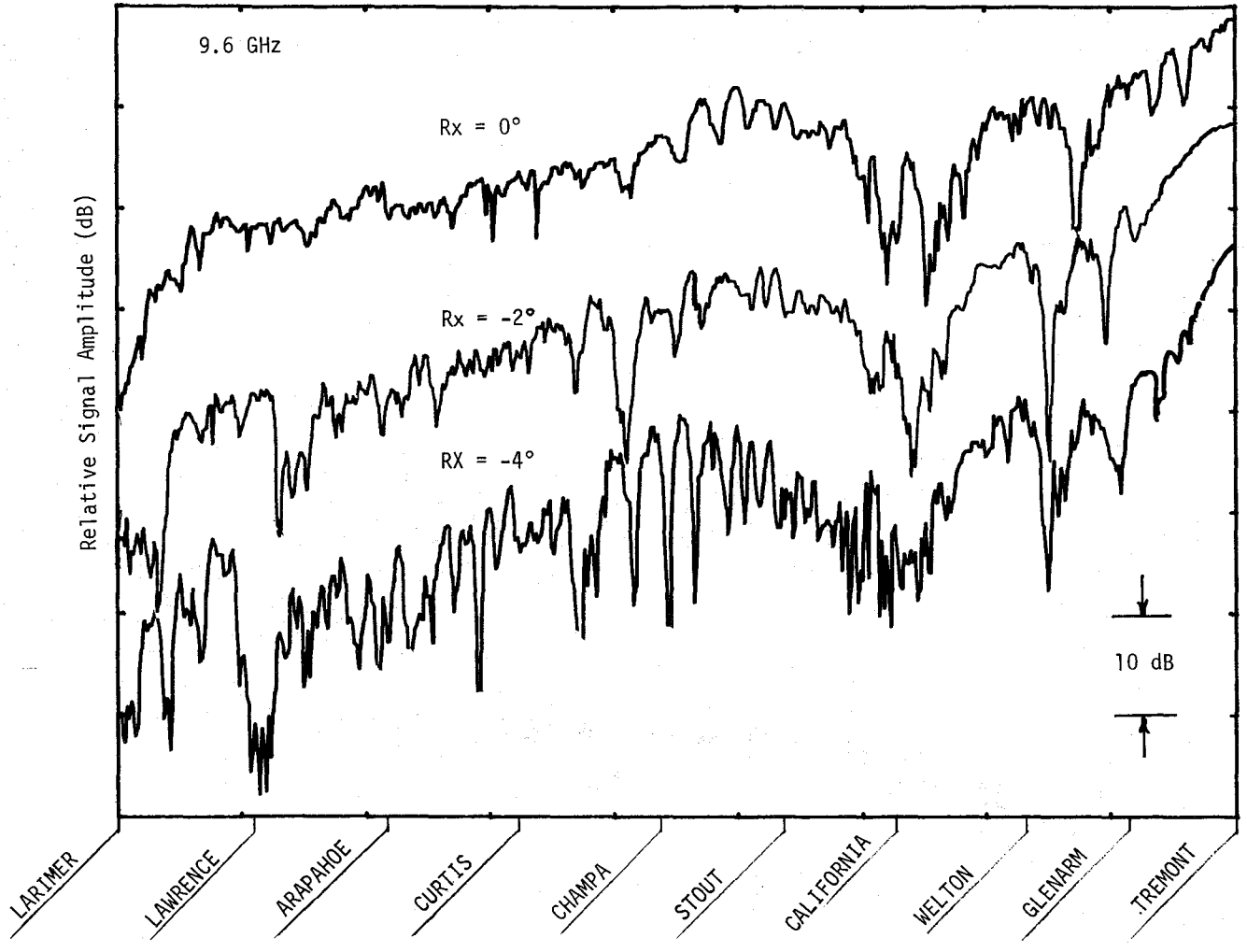

Figure 25. Signal amplitude at 9.6 GHz as a function of range measured along 17th Street in downtown Denver, CO. The transmitter is moved at a nearly constant velocity toward the receiver. Vertical antenna polarization. The receiving antenna is aligned as indicated for each run.

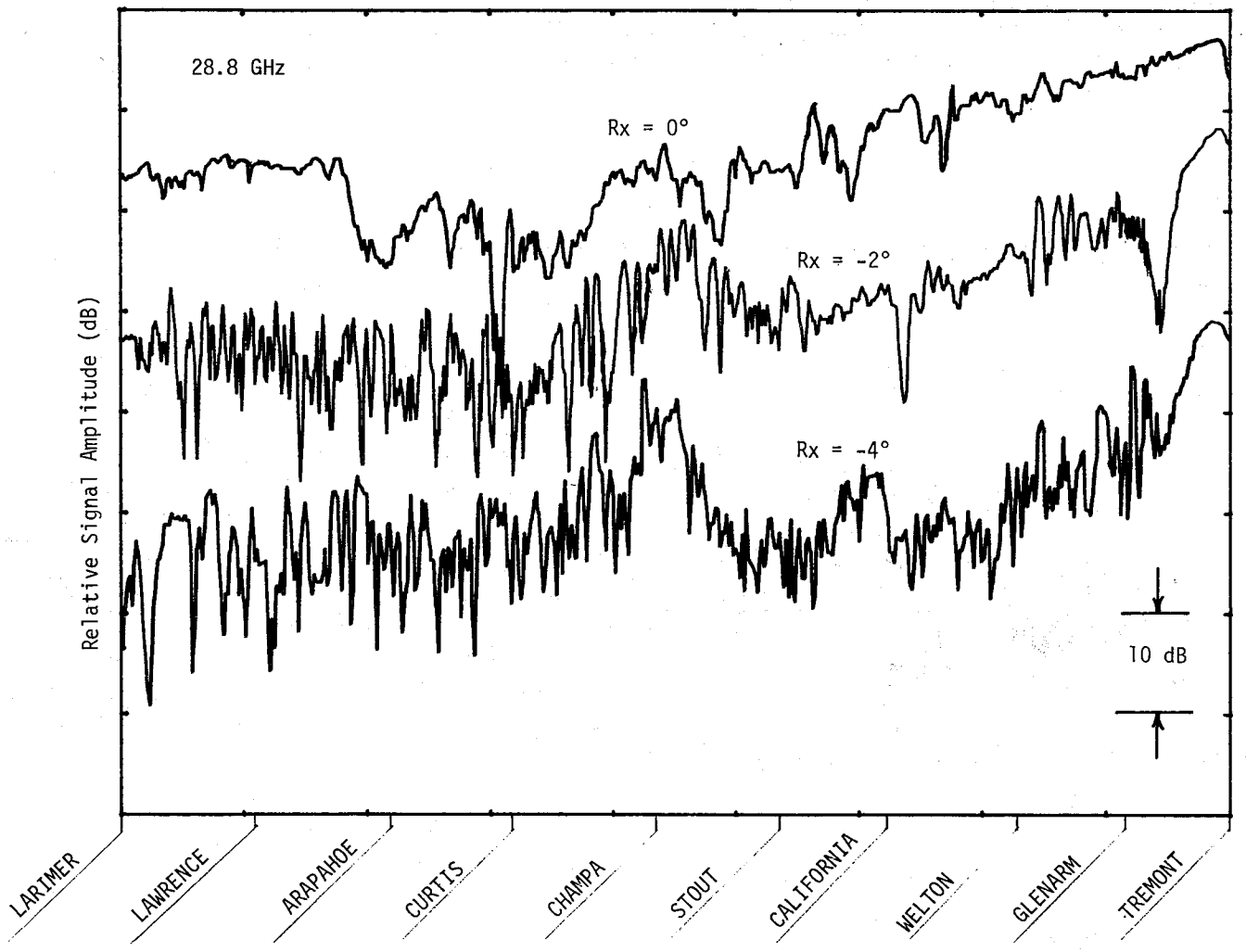

Figure 26. Signal amplitude at 28.8 GHz as a function of range measured along 17th Street in downtown Denver, CO. The transmitter is moved at a nearly constant velocity toward the receiver. Vertical antenna polarization. The receiving antenna is aligned as indicated for each run.

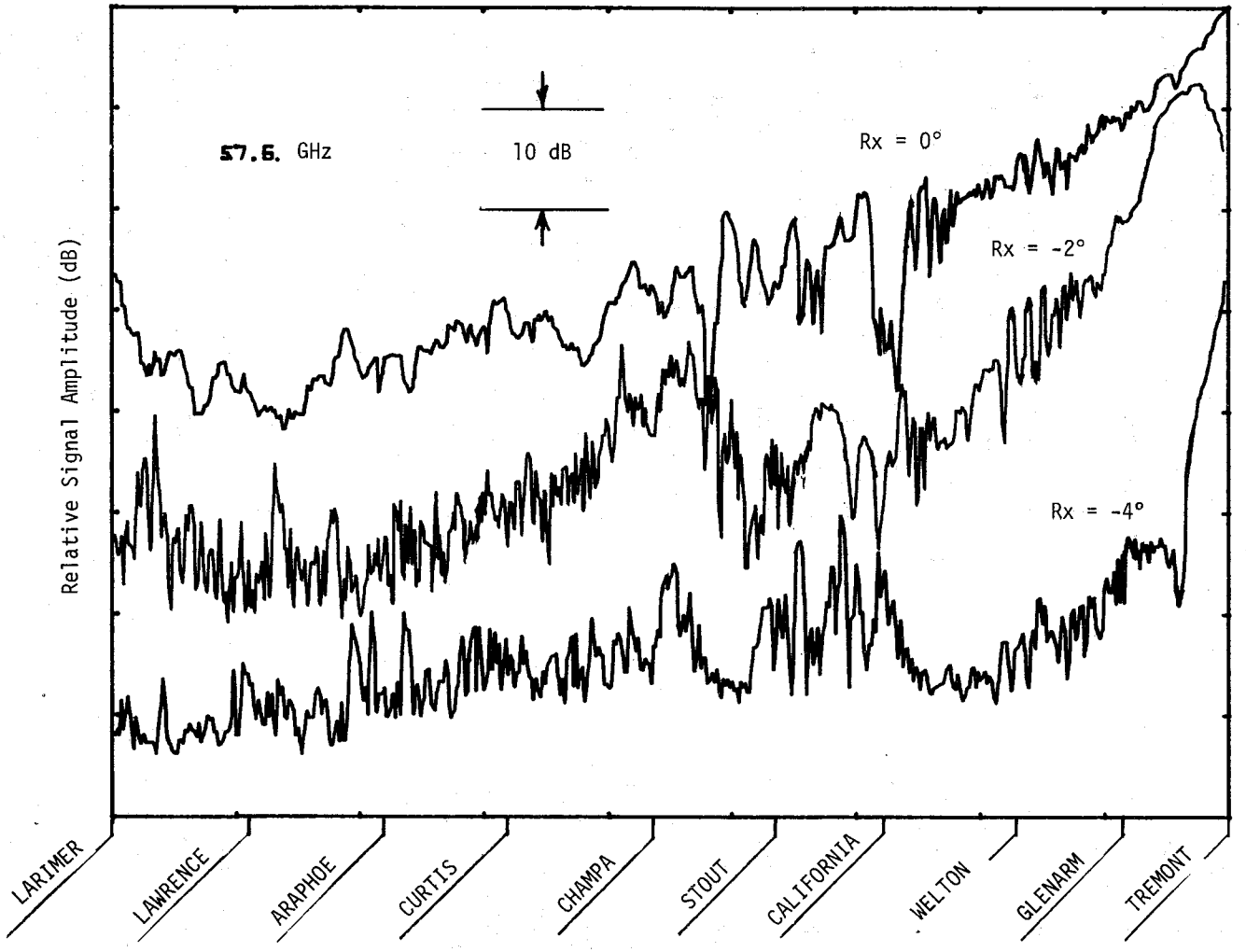

Figure 27. Signal amplitude at 57.6 GHz as a function of range measured along 17th Street in downtown Denver, CO. The transmitter is moved at a nearly constant velocity toward the receiver. Vertical antenna polarization. The receiving antenna is aligned as indicated for each run.

receiving antennas were scanned (±15°). Figure 28 shows a comparison of the "free space" antenna pattern (broken line) and the 17th Street azimuth scans with the transmitter pointing directly at the receiver (TX = 0°) for all three frequencies and both linear polarizations. From Figure 28 it is apparent that very little detailed information on reflected signals can be obtained with the 9.6-GHz scans because of the widebeam (4.8°) receiving antenna. However, scans for the higher two frequencies with 1.2°-beamwidth receiving antennas show multipath signals nicely separated. The resultant amplitude plots for the two higher frequencies with the transmitter off-pointed and for each receiving antenna polarization are shown in Figures 29 and 30.

These angle plots are the result of the unique geometry resulting from the particular transmitter and receiver locations. The amplitude of the reflected signal is determined by the angle of incidence and the properties of the surface at the location of reflection. Nevertheless, these measurements were primarily an effort to determine if a Brewster angle affect could be detected. For this situation the Brewster angle should occur between 5° to 15° (varies with surface conductivity and frequency) and appear in the horizontally polarized mode since a vertical wall is presumed the reflector instead of a horizontal surface. In comparing the patterns with building reflections for the two polarizations, taking account of the sidelobe patterns (Figure 28), there is not much evidence of a reduction in reflected signals for the horizontally polarized mode. Either the Brewster angle occurs at angles near or greater than 15° because of low surface conductivity, or the resolution of the measurements is not adequate for the amount of reduction in the reflection coefficient. Reflection angles of arrival larger than 15° are not likely for any normal urban street path geometry, however.

5.4 Diagnostic Measurements

At this point in the urban measurements, the instrumentation was improved to include the diagnostic capability of a wideband channel. This measurement system consists of narrow bandwidth channels at 11.4 and 28.8 GHz and a 1-GHz bandwidth channel at 30.3 GHz where all rf and modulation sources were fully coherent in all three channels. A complex propagation path can be analyzed in terms of resultant bit-error-rate and impulse response measurements with this system in addition to, and for comparison with, received signal characteristics as a function of antenna beamwidth and polarization.

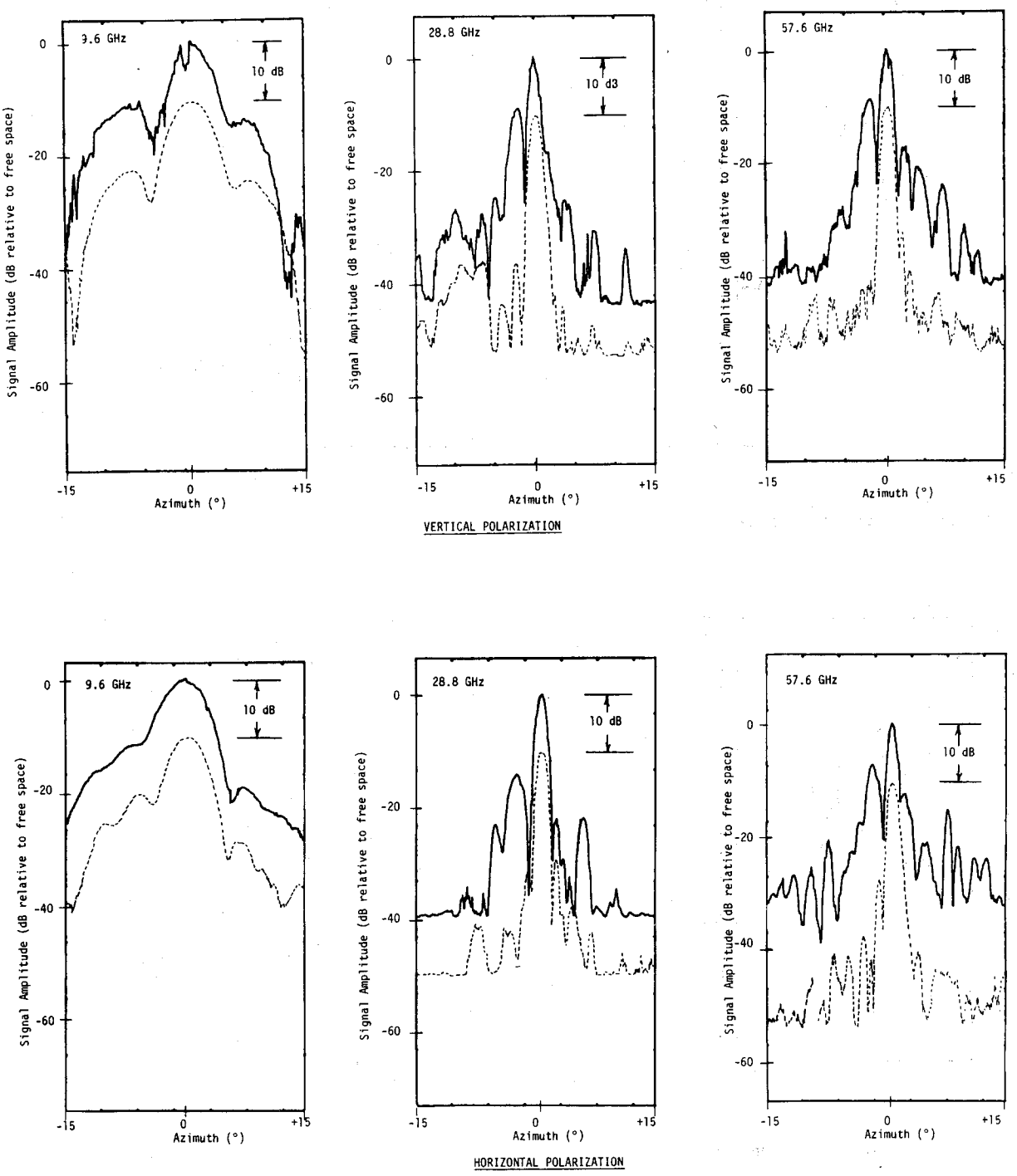

Figure 28. A comparison of measured signal levels for 0° transmitter antenna pointing to open field calibration levels. The calibration trace (broken line) is off set 10 dB at 0° azimuth.

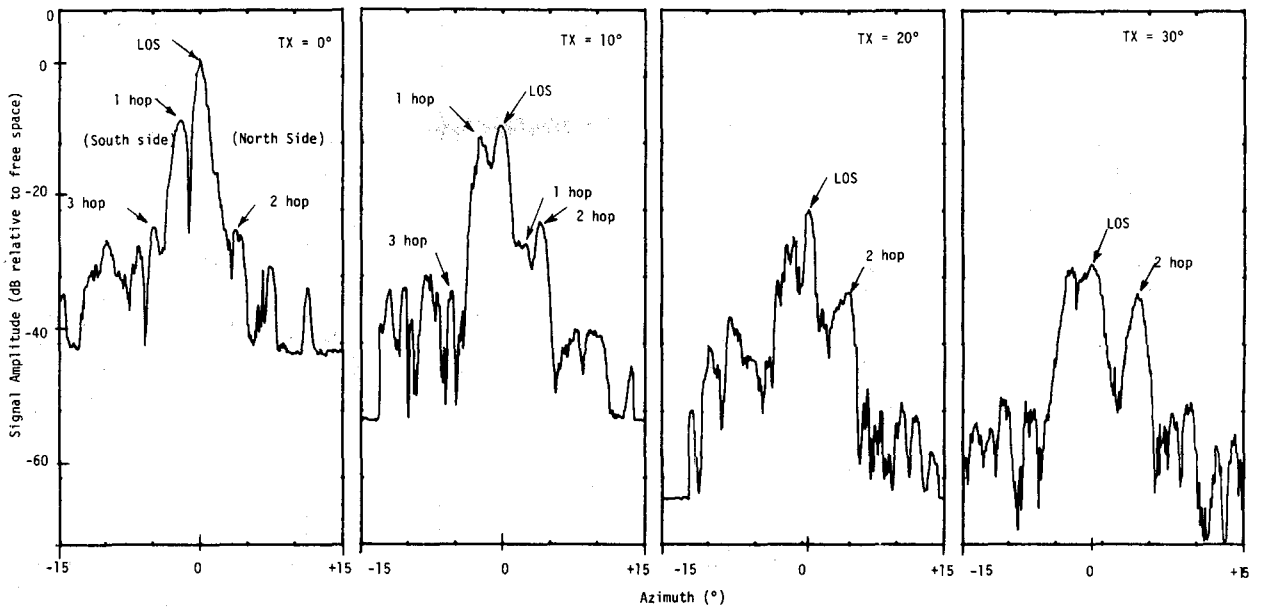

A) Vertical-vertical antenna polarization at 28.8 GHz

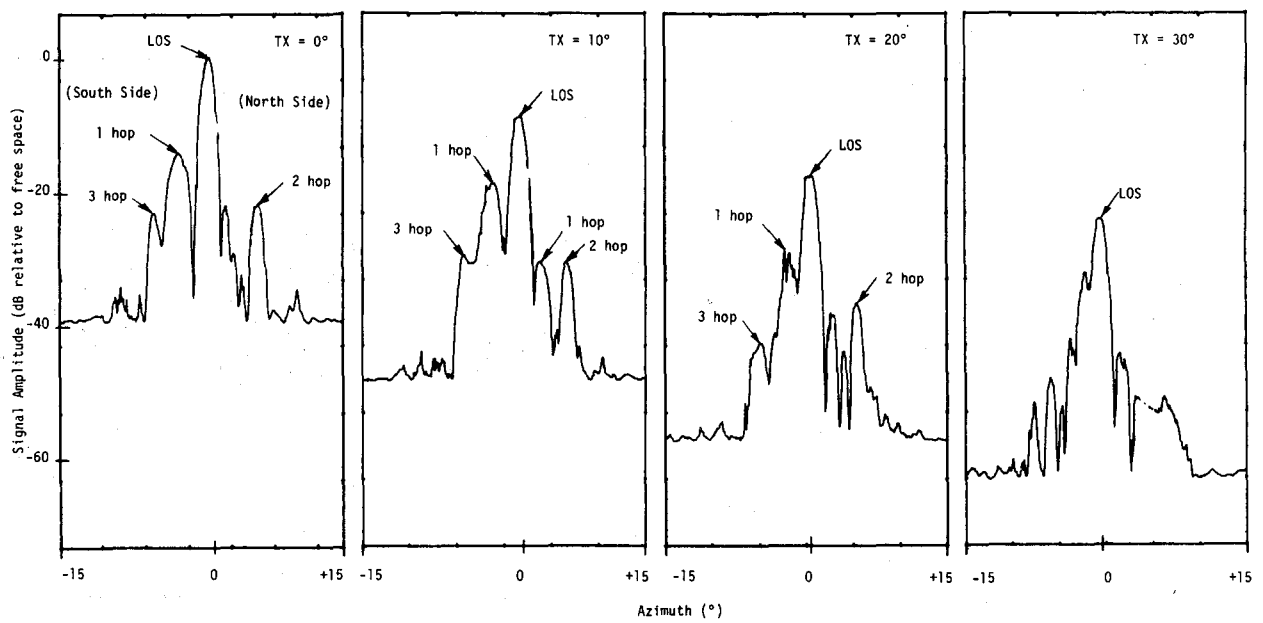

B) Horizontal-horizontal antenna polarization at 28.8 GHz

Figure 29. Measured signal levels at 28.8 GHz with off-angle transmitter antenna pointing of 0°, 10°, 20°, and 30°.

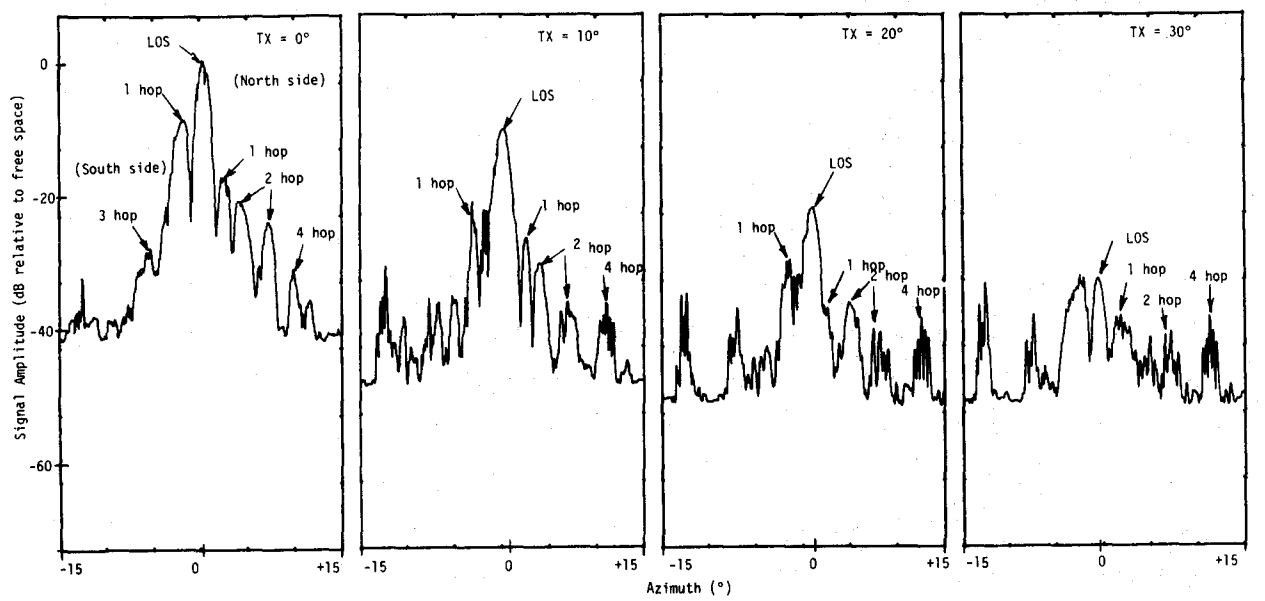

A) Vertical-vertical antenna polarization at 57.6 GHz

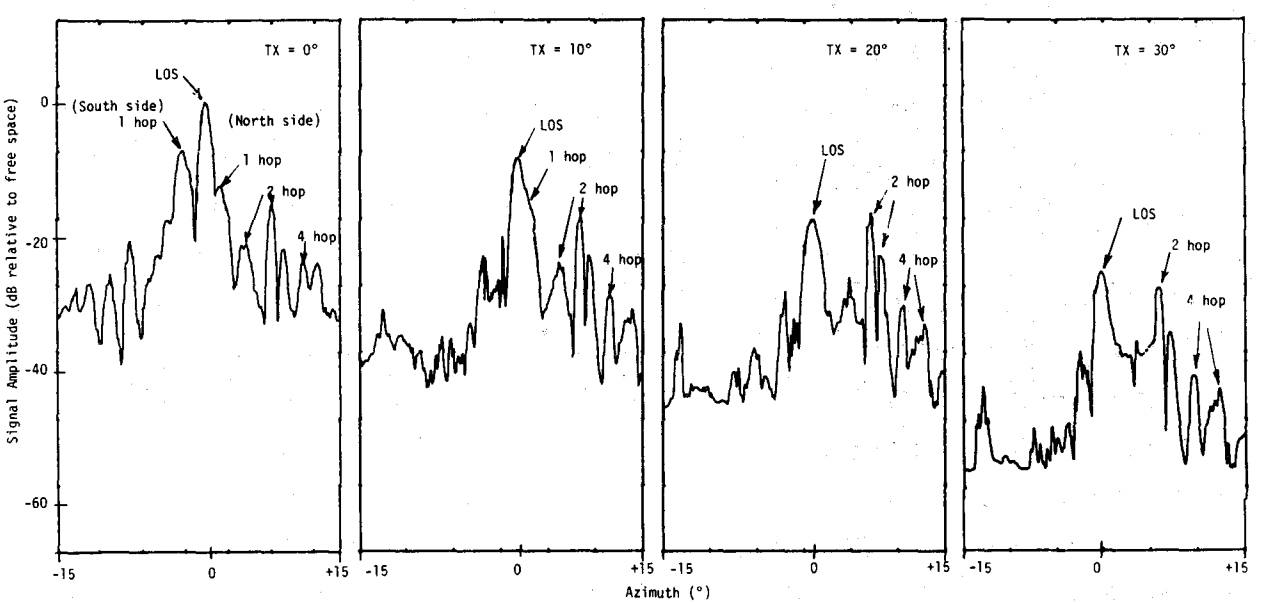

B) Horizontal-horizontal antenna polarization at 57.6 GHz

Figure 30. Measured signal levels at 57.6 GHz with off-angle transmitter antenna pointing of 0°, 10°, 20°, and 30°.

Multipath fading along 17th and Champa Streets is compared according to antenna polarization in Figures 31 and 32 by moving the transmitter terminal along the street toward a stationary receiver terminal, as described in the previous section. A single antenna is shared between the 28.8 and 30.3 GHz channels using an orthomode transducer, which allows a simultaneous dual linear output, one horizontally and one vertically polarized. When a transmitter and receiver channel is vertically polarized, the data are labeled "VV." For a channel where both antennas are horizontally polarized, the labeling is "HH." One reason for a difference between polarizations is a "Brewster" angle effect reducing the horizontally polarized reflected signal from the building walls. As discussed in the previous section it is believed that, for the frequency employed and the types of building surfaces involved, the Brewster angle would occur at an angle greater than 8°. For the street geometry shown in Figure 23, which is typical of most urban cases, the vertical building surfaces do not provide many reflection opportunities at angles steeper than 8°. In Figures 31 and 32 angles of reflections of 8° or more can only occur for straight-line geometry at a terminal separation of 100 m or less. Wide beamwidth antennas of 30° were used at both terminals for the two higher frequency channels so that reflection angles were not limited up to ±15° by the antenna beams. In examining the two figures at 100-m terminal separation and less, it appears the fade depths from "presumably" building wall surfaces were greater for the HH mode than the VV mode, which is contrary to what is expected from the presence of a Brewster angle affect. Six such comparisons were made for the two streets shown; two slightly favored a VV mode reflection enhancement and four favored HH mode enhancements. No conclusion can be drawn from these results. Possibly the Brewster angle exists at reflection angles greater than those attainable for the urban situations, or the conditions at the reflecting surface are not proper (very low conductivity) at millimeter wavelength. Testing for the occurrence of a phase reversal with grazing angle would be a more sensitive indication. Many linear polarization comparisons were made for the narrowbeam antennas (≅2.5°) along 17th as well as Champa, and the result showed a nearly identical fading pattern for each polarization. This seems consistent with what would be expected when using narrowbeam antennas.

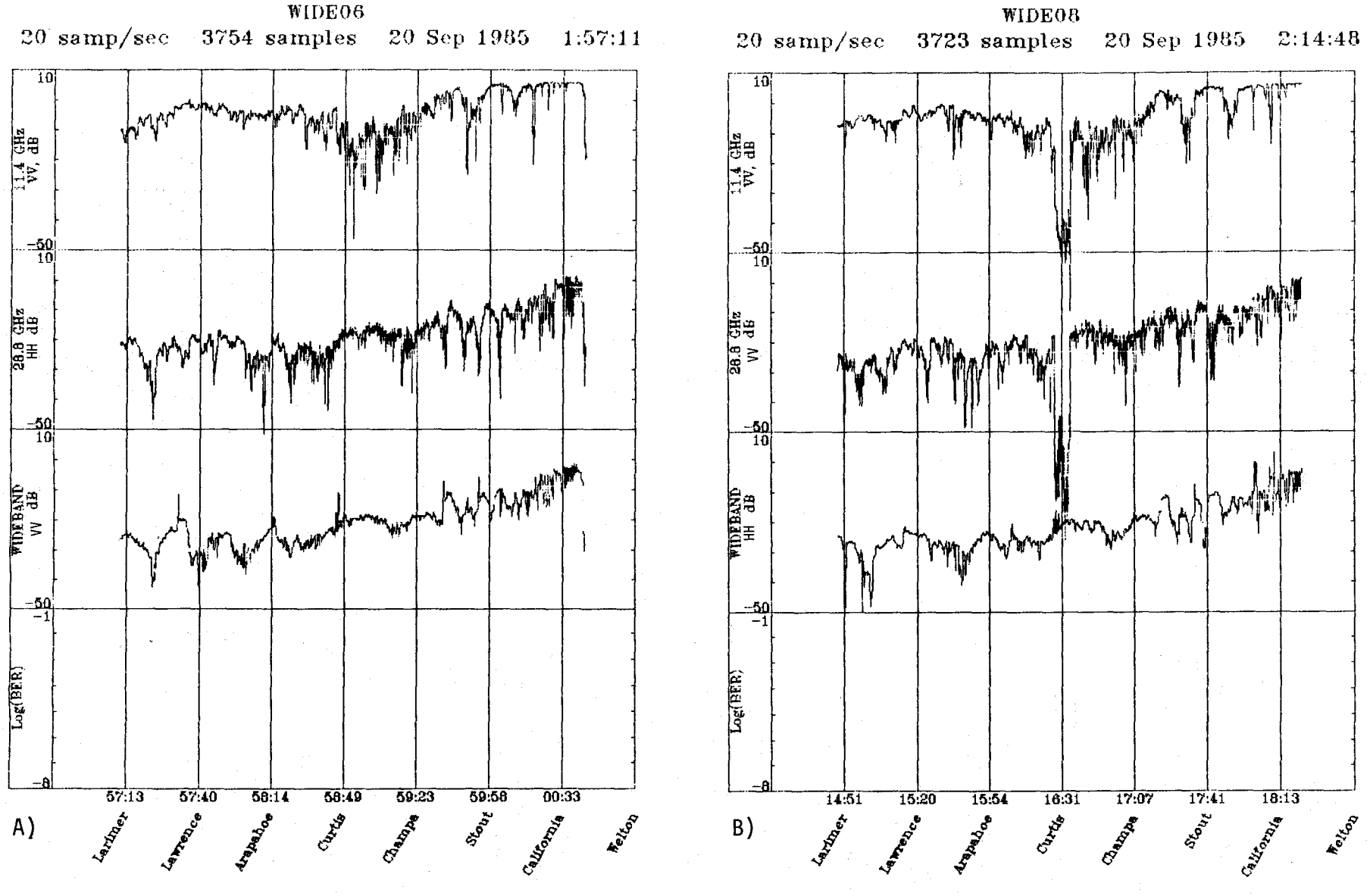

Figure 31. Signal amplitude as a function of range measured along 17th Street in downtown Denver, CO. The transmitter is moved at a nearly constant velocity toward the receiver. Antenna polarization as indicated.

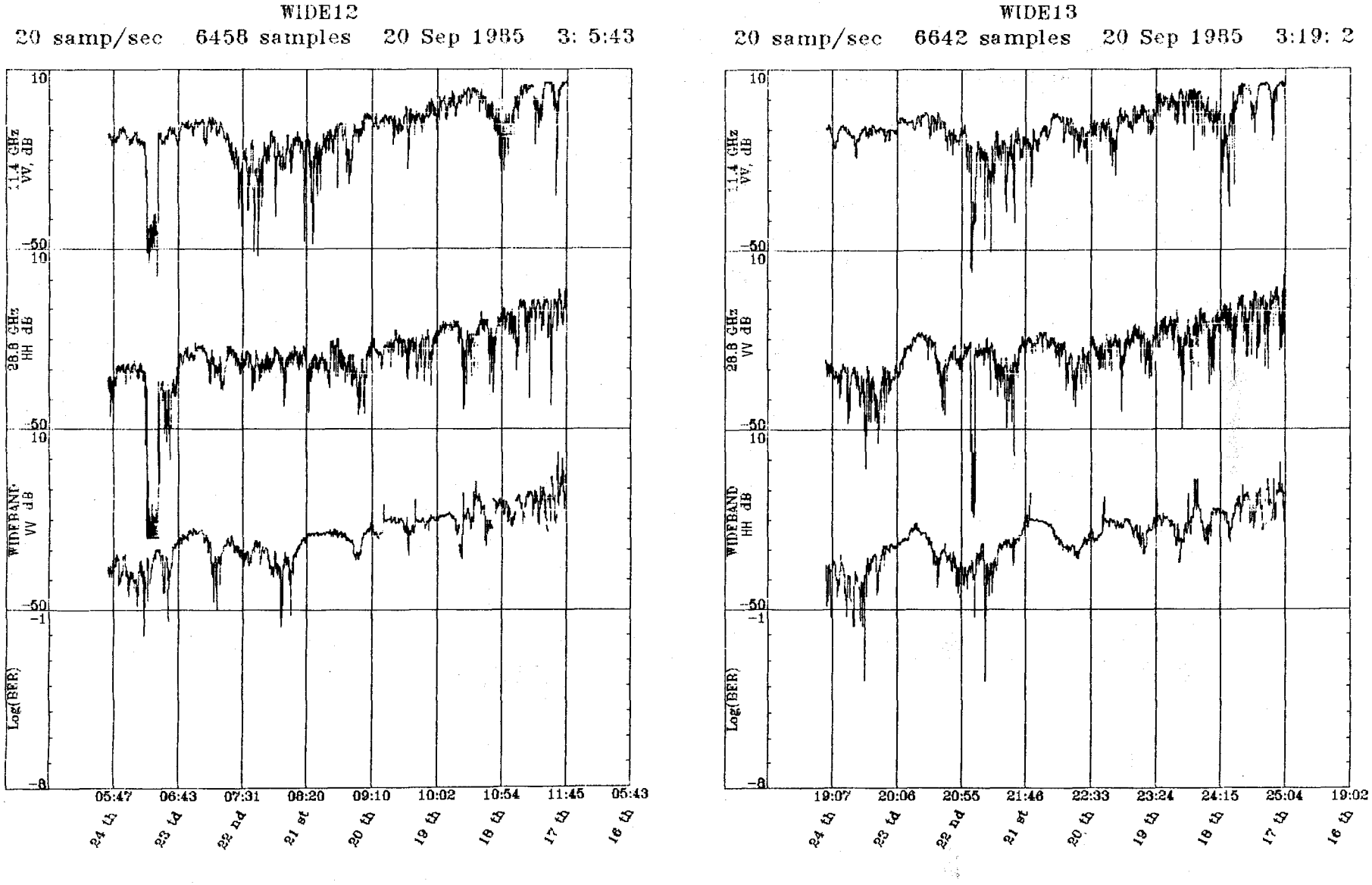

Figure 32. Signal amplitude as a function of range measured along Champa Street in downtown Denver, CO. The transmitter is moved at a nearly constant velocity toward the receiver. Antenna polarization as indicated.

Figure 33 shows a comparison of the RSL for a narrow beamwidth receiving antenna (2.5°) at 28.8 and 30.3 GHz and the RSL using a wide beamwidth antenna (30°) when the transmitter traveled the same path up 17th Street. It is logical that the wide beamwidth antennas will receive more multipath signals. With the widebeam antenna on the 28.8-GHz narrowband channel (Run 1), an increased number of strong, discrete multipath signals is suggested by increased occurrence of fades of 20 dB or greater, as compared to the data from the 28.8-GHz channel for Run 6. However, in the wideband channel (30.3 GHz), results show a greatly reduced RSL variation in Run 1 (widebeam antenna) as compared to Run 6 (narrowbeam antenna). The reason for this is that several fades and enhancements exist simultaneously within the wideband channel, greatly reducing the opportunities for deep fades that result only when two signals of near equal amplitude are present. The fact that many more strong multipath signals occur with the widebeam antenna is confirmed in the impulse response measurements recorded on these same paths and discussed in Section 5.5.

A set of measurements using a narrowbeam receiving antenna, but with the antennas off-pointed (horizontal plane) by 3° is shown in Figure 34. The resultant data (DEN07) has many similarities in signal fading characteristics to the data of Run 1 in Figure 33, which used the widebeam antennas. The reason for the similarity is that when the narrowbeam receiving antenna is off-pointed, reflected signal components become stronger relative to the line-of-sight component causing more and deeper fades in the narrowband 28.8-GHz channel, and the averaging of all fades within the wideband 30.3-GHz channel occurs as just described.

5.5 Impulse Response Measurements

One of the features of the diagnostic probe is the ability to measure the impulse response of the channel. This is accomplished by the phase modulation of a 30.3-GHz carrier with a pseudorandom binary sequence at a rate of 500 Mb/s. The 30.3-GHz signal is transmitted through the channel to a receiver where the signal is demodulated to reproduce the 500 Mb/s pseudorandom sequence degraded by any distortion that may have occurred in the propagation between transmitter and receiver. At the receiver terminal, a replica of the transmitted pseudorandom binary sequence is generated. A cross-correlation is performed between the received demodulated bit stream and the replica of the

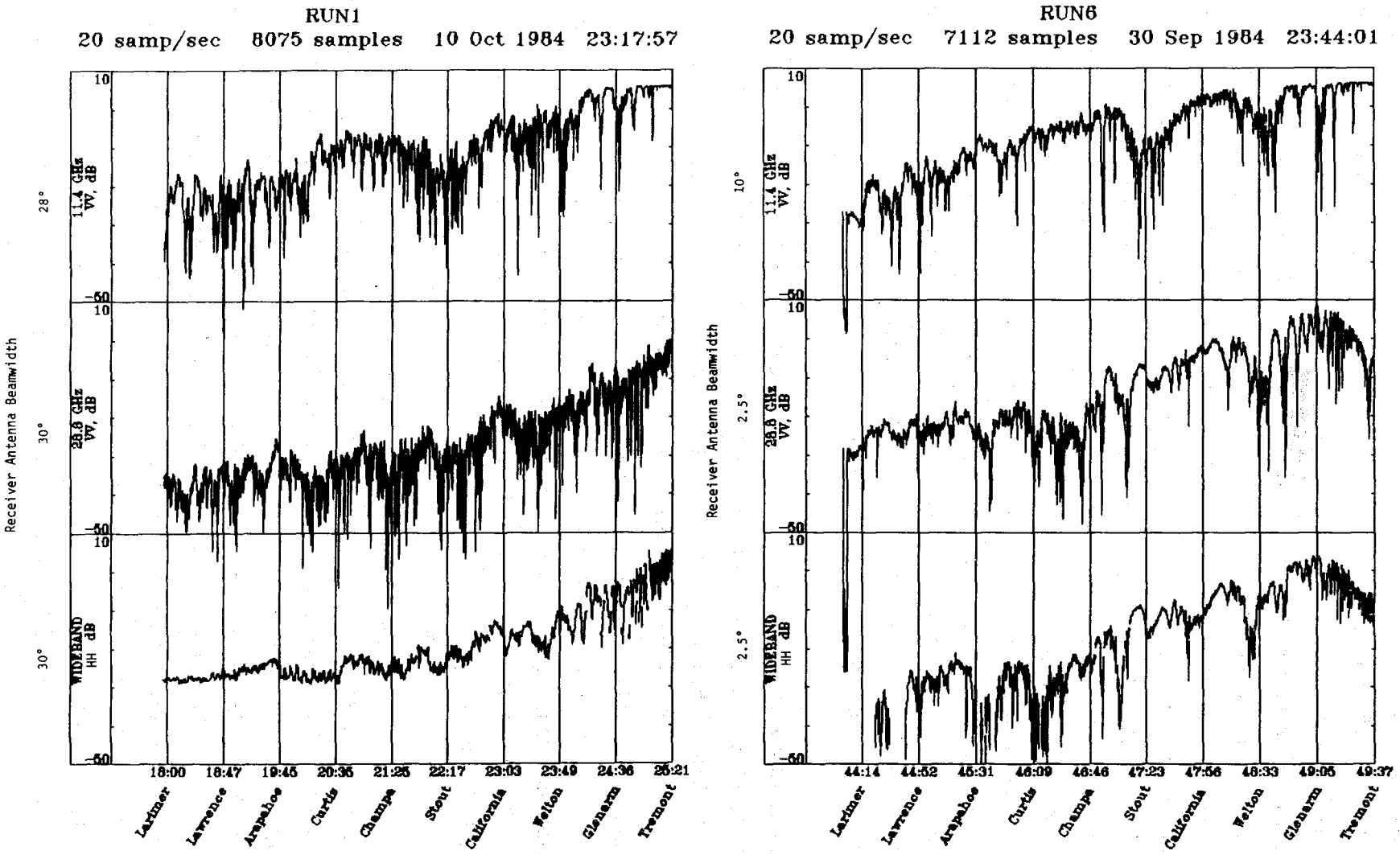

Figure 33. Received signal levels from run 1 (widebeam antennas) and run 6 (narrowbeam receiver antennas) along 17th Street (Larimer to Tremont) in Denver, CO.

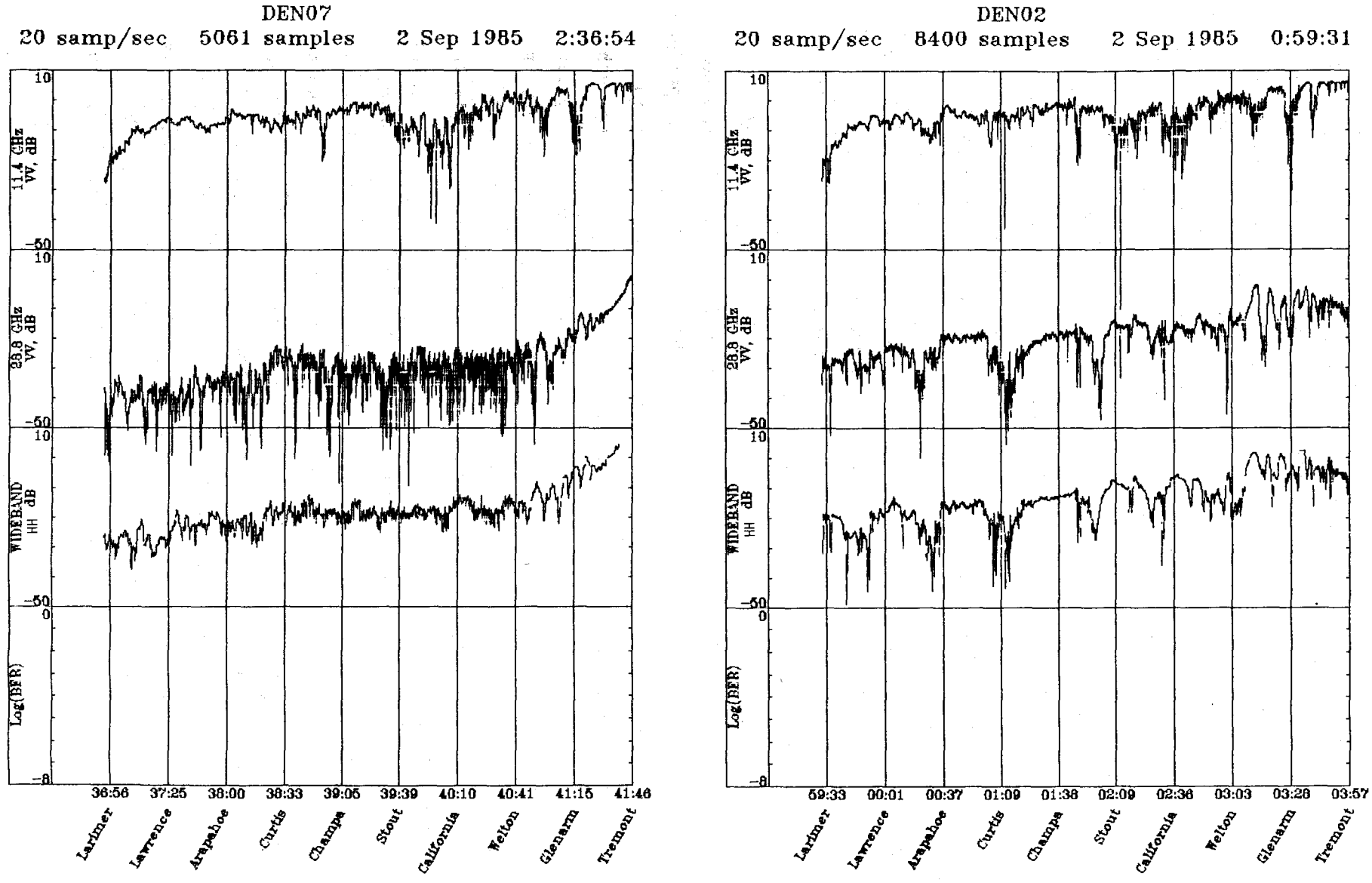

Figure 34. Received signal levels from runs DEN07 and DEN02 along 17th Street (Larimer to Tremont). Narrowbeam (2.5°) antennas were used on both runs. In DEN02 the antennas were adjusted for on-line pointing. In DEN07, the receiving antennas were pointed off-line by 3° for the 28.8 and 30.3 GHz channels.

transmitted bit stream by allowing one bit stream to slide by the other in time as a result of a slight offset in the bit-clock rate . At the point in time where the bit sequences are identically aligned, an impulse is generated with a base duration equal to two bit times. The impulse response measurement repeats at a rate corresponding to the number of bits in the sequence or word divided by the clock offset rate. Channel amplitude and phase dispersion during propagation of the signal appear as amplitude and time changes in the impulse shape. A channel is completely described by the channel impulse response or its Fourier transform, the transfer function of the channel. Thus, the diagnostic probe is a means of acquiring data to determine parameters in modeling channel characteristics and predicting performance for specific applications.

In order to assure that the impulse measurements accurately depict the response of the channel, a controlled test with known parameters was required. To accomplish this, physically measurable multipath signals for a realistic range of amplitudes and delay time were generated.

Figure 35 shows the test setup for the impulse circuitry calibration. All components, except the network between the dc to 18 GHz divider and combiner, are part of the channel probe system. The best method found to perform calibration measurements was to construct a set of coaxial cables cut in 1/4 ns steps to produce the actual propagation delays. The reason for such fine steps is that the summed output of the co- and quad-phase squaring circuits ($E_i^2 + E_j^2$, Figure 35) must be carefully balanced to produce an impulse curve that remains constant for all possible phase delays of the received carrier. Measuring a "direct" signal in the presence of delayed signals is the most critical test, because the phase of the 1.5 GHz reconstructed carrier is determined by the combined vector phase of all signals to be measured.

Several adjustments are required to obtain the best compromise in maintaining a proper power level ratio between the "direct" and delayed signals with phase shifts in the modulated carriers. Note that the combined sum-of-the-square signals ($E_i^2 + E_j^2$) is recorded in the impulse measurements and represents signal <u>power</u>. The phase of the reconstructed carrier injected into the co- and quad-phase demodulators must be finely adjusted to produce nulls in the quad-phase channel when the input carrier has a phase difference of 0° or 180° and nulls in the co-phase channel for phase difference of ±90°. To

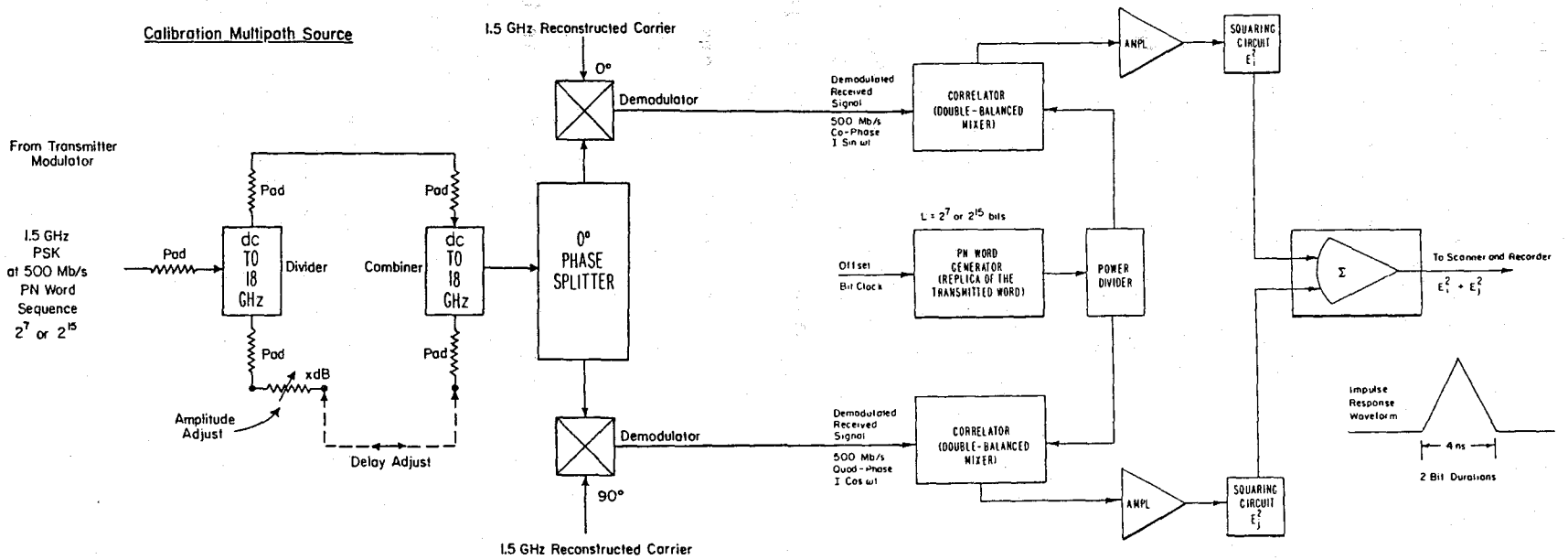

Figure 35. Test set up for the impulse circuitry calibration.

maintain these relationships, line lengths were adjusted to compensate for differences in time delays between the co- and quad-phase branches containing the demodulator, correlator, amplifier, and squaring circuits. By performing these adjustments carefully for all combinations of rf phase, agreement in power levels measured via the impulse response compared to within ±1 dB to the attenuator values for two signals delayed by more than 2 ns and for amplitude differences of less than 18 dB.

The data shown in Figure 36 are four sets of reference impulses plus multipath signal amplitudes with electrically delayed paths of approximately 0.9, 1.5, 3.0, and 4.5 ns as indicated on the figure. The reference impulse curve on each set marked reference is for a no multipath condition. In each set the multipath signal was delayed a fixed amount and then the combined amplitude levels were recorded for multipath signal-to-reference signal ratios of -3, -6, -10, and -13 dB. Each tracing is the resultant amplitude of a vector addition of the reference and multipath signals. For short delays, the presence of a multipath signal is manifest in the broadening of the trailing edge of the impulse response. As in 36(A), if the delay and amplitude values of the multipath were not known, one could conclude only that multipath signals were present, but could not predict the delay and amplitude values with any confidence. However, when the multipath delay values reach 3 ns and more, as shown in Figure 36(C) and (D), the multipath components become clearly separated from the reference impulse, and both delay and amplitude value can be assessed within the measurement accuracy.

Several sets of impulse response measurements were made along the same 17th Street path used for the received signal amplitude measurements in the previous section. In some cases, both amplitude and impulse measurements were recorded on the same run, with the amplitude being recorded continuously and the impulses sampled at 6- to 10-s intervals.

The impulse response curves from a calibration path are shown in Figure 37. These calibration data were recorded with the receiver located on 17th Street between Tremont and Court Place and the transmitter also on 17th Street between Welton and Glenarm. These positions can be located on the

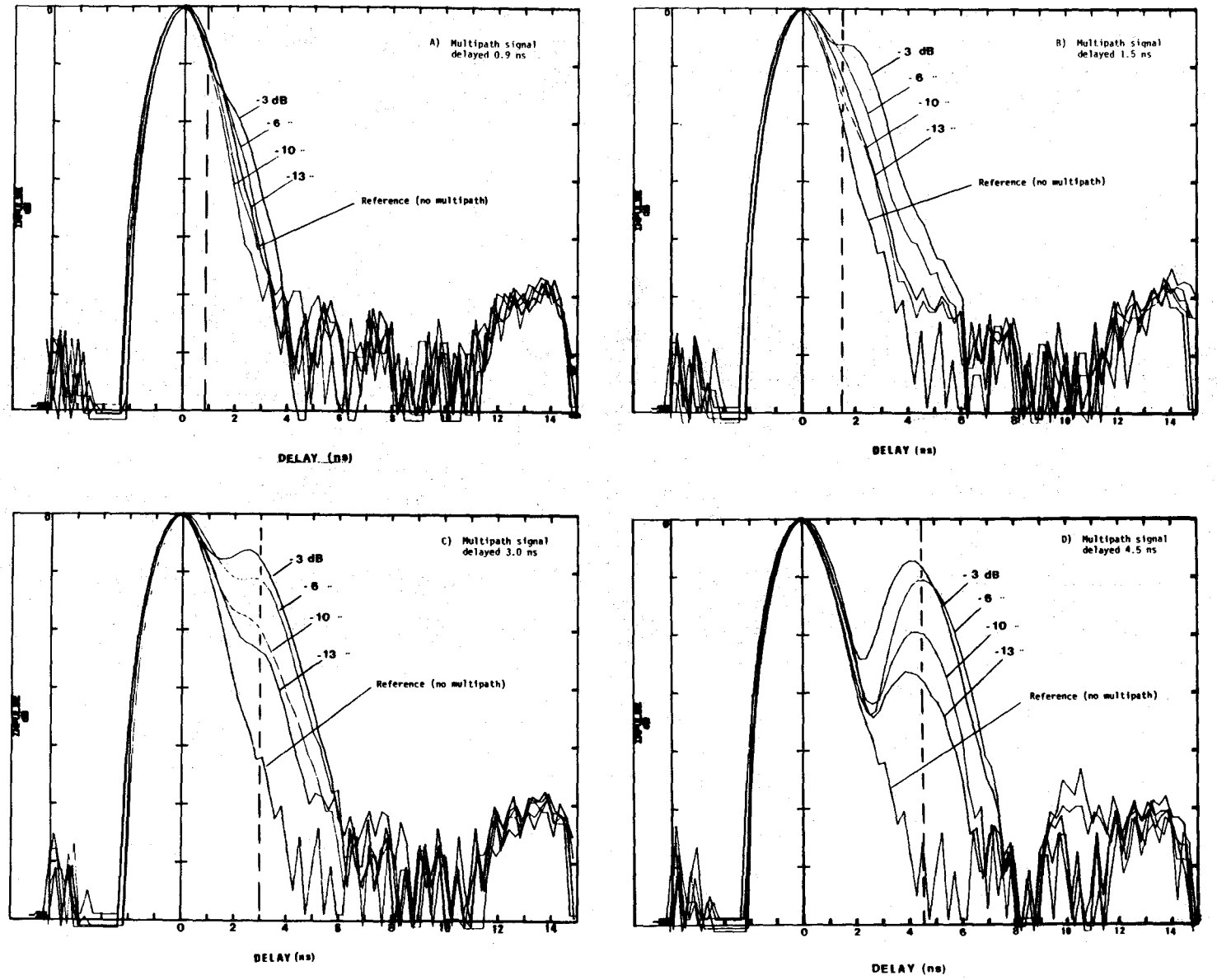

Figure 36. Sets of reference impulses plus multipath signal amplitudes for narrow multipath delay and amplitude values.

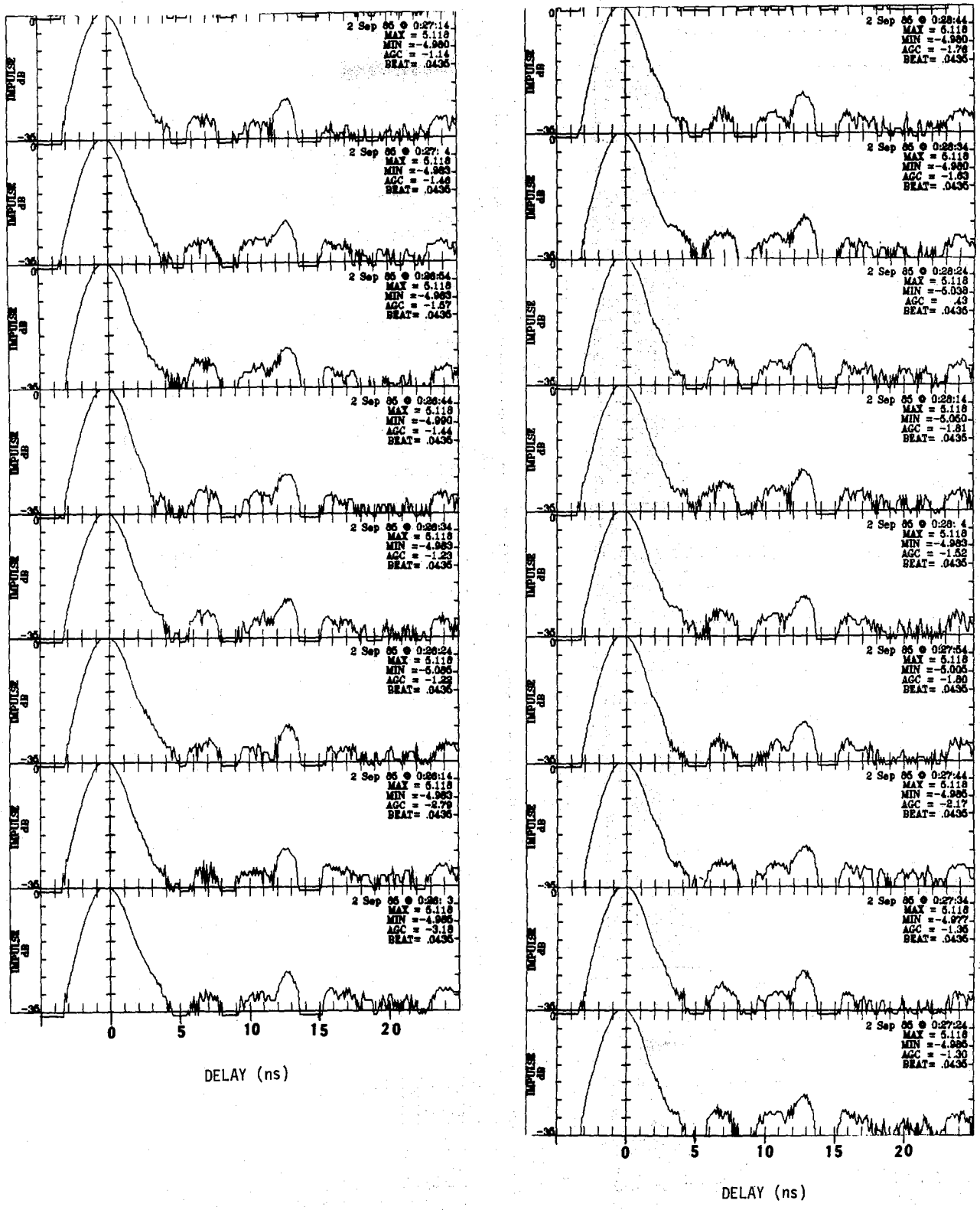

Figure 37. Impulse response curves recorded from a 225-m calibration path on 17th Street in Denver, CO.

street map of downtown Denver in Figure 38*. The 17 impulse response curves shown in Figure 37 were recorded on the 30.3-GHz channel with both the transmitter and receiver stationary at the locations indicated, using a 30° transmitting antenna and a 2.5° receiving antenna pointed on-line. These curves were recorded at 10-s intervals and as would be expected from a calibration run, each subsequent response curve is nearly an exact replica of the previous curve. Minor variations can be attributed to changes in street traffic during the 3-min test interval. The on-line path was clear of traffic during this test interval.

The curves in Figure 39 are the result of a run along 17th Street with the receiver stationary near the Tremont intersection and the transmitter moving slowly along 17th Street. A narrowbeam receiving antenna was used with on-line pointing. The curves were recorded in order starting at the bottom of the first column moving from bottom to top in each subsequent column. The impulse response curves recorded near the street intersections are indicated on the figure.

A cursory examination of the curves in Figure 39 shows the presence of some multipath signals. These multipath signals are evident in the broadening and reshaping of the trailing edge. Specific examples are the reshaping of the curves at Tremont and Glenarm and broadening of curves at Welton and Curtis. It is difficult to determine the delay and amplitude values of individual multipath signals with accuracy, but they can be estimated to fall in the 1- to 4-ns delay range and at -15 to -25 dB below the amplitude of the direct signal level at zero delay time.

At longer delay times, variations in patterns above the processing noise indicate additional multipath components at relative signal levels of 20 dB or more below the direct components. In Figure 39 these appear most frequently between 8 and 11 ns and occasionally between 14 and 18 ns. At the Tremont intersection, a multipath at about -24 dB is seen at about 20 ns. The fixed delay spurious signals appearing at about 7 and 13 ns at a level of around -24 dB mask delayed components below that level. Most delayed components occurring beyond about 2 ns in Figure 39 can be largely attributed to antenna sidelobe response as the direct signal experienced fading due to a short

*The 17th Street path between Larimer and Tremont is also identified in Figure 23 showing street intersections and an elevation profile.

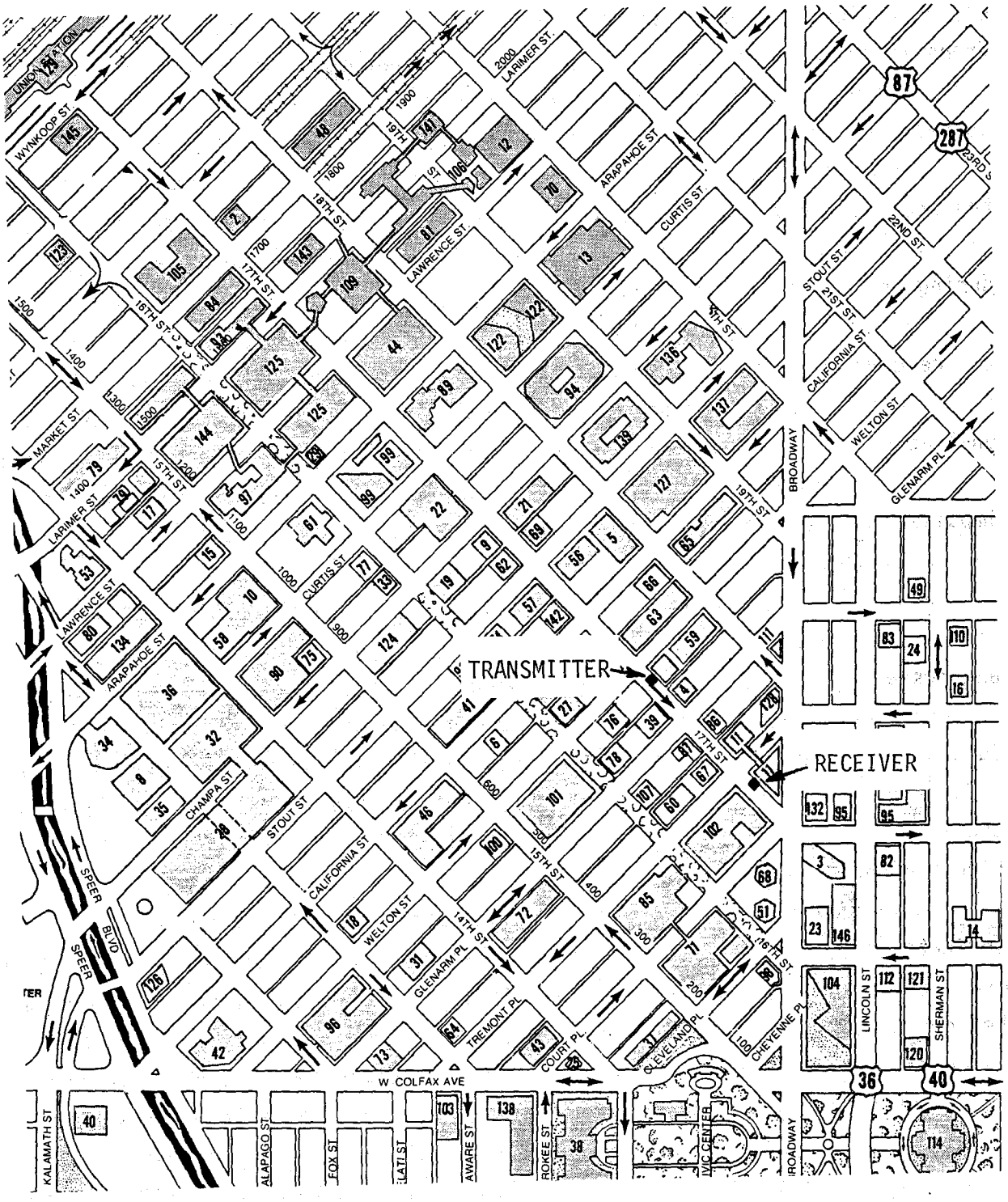

Figure 38. A map of the test areas in downtown Denver, CO.

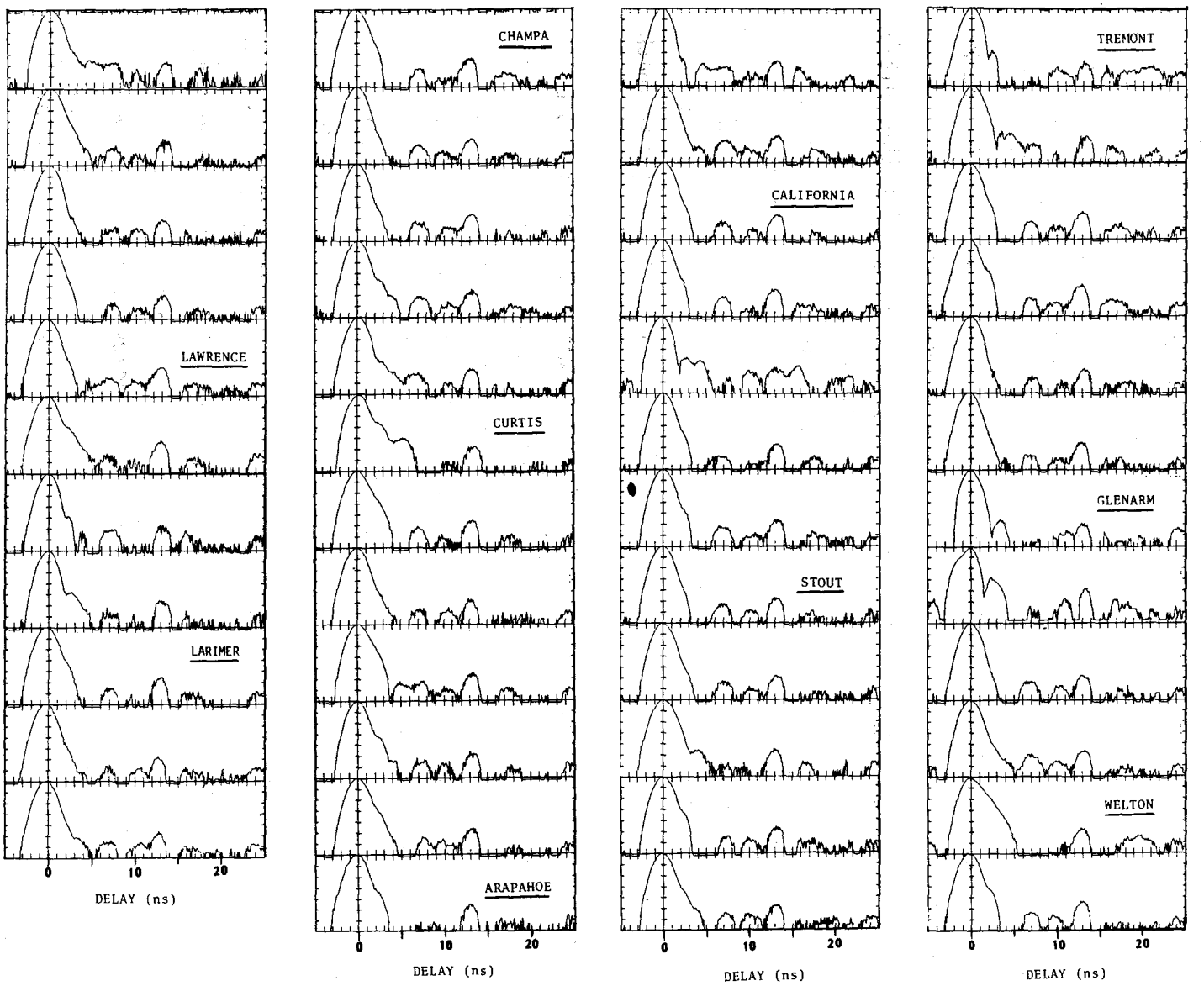

Figure 39. Impulse response curves recorded from the DEN02 run along 17th Street (Larimer to Tremont). A narrowbeam receiving antenna was used with the antenna adjusted for on-line pointing.

delayed (less the 1 ns) multipath component from the street surface.

The curves in Figure 40 are the result of a run along 17th Street with the receiver stationary near the Tremont intersection and the transmitter moving slowly along 17th Street. The test conditions were identical to those for Figure 39 with one exception. Instead of having the receiving antenna pointed on-line as in Figure 39, the receiving antenna was adjusted for 3° off-pointing to the left. This off-line pointing of the receiving antenna produced a dramatic change in the received multipath signals in Figure 40 as compared to Figure 39. There are many multipath signals with delays in the 8 to 10 ns range and amplitude ratios of -5 to -10 dB relative to the direct signal. With the receiving antenna off-pointed, it is possible for the multipath signal to be stronger in amplitude than the direct component. An example is shown at the Stout Street intersection impulse curve. The computer is programmed to position the signal with the greatest amplitude at 0 delay and for this case the direct signal, always the first to arrive, occurred at -3.3 ns. The impulse curves in Figure 40 are replotted in Figure 41, with reference impulse response curves that are cross-hatched so that the multipath segments can be more clearly identified.

In addition to the impulse response curves that were recorded using a narrowbeam receiving antenna (2.5°), several runs were made using a widebeam receiving antenna (30°). For these runs, on-line pointing was used. Two examples are shown in Figures 42 and 43. Many multipath signals are present in these data. This is not unexpected because the widebeam antenna would illuminate both sides of the street. The delay values of the individual multipath signals fall in the 1- to-10 ns range and the amplitude levels relative to the direct signal are in the range from -2 to -15 dB.

Up to this point all wideband measurements with the 30.3-GHz channel were performed along 17th Street. Two other streets were selected for measurements because each had differences but are very typical of an urban area. Champa Street between 24th and 14th Streets was selected because the building wall surfaces were much smoother and formed a more uniform line along the street than did those on 17th Street. Also Champa Street was nearly level in elevation and had fewer obstructions along the street, less road signs, trees, light poles, etc. The street width was the same as 17th Street (24 m) but the blocks were about 127 m long instead of the 100 m of 17th Street. Wall

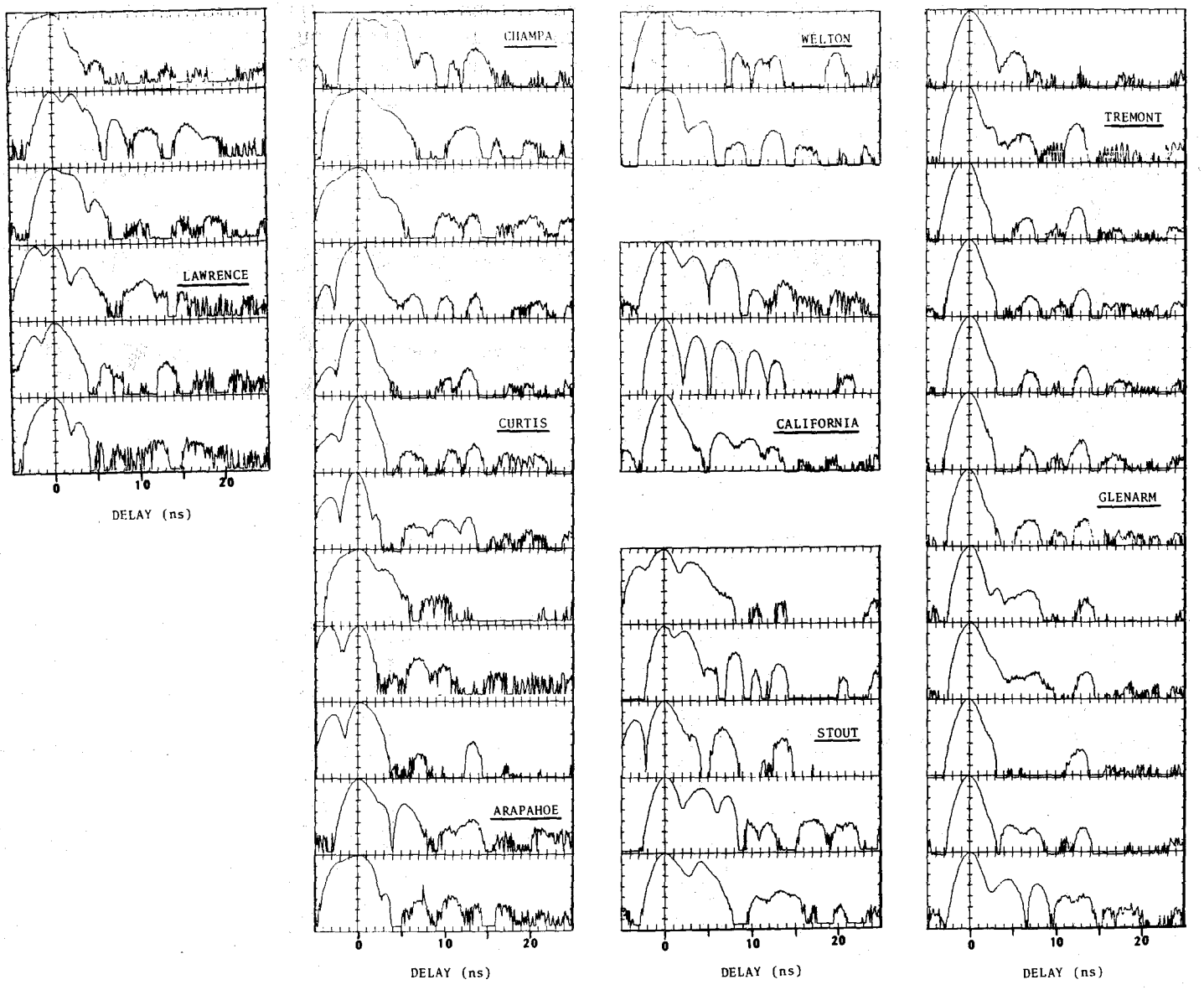

Figure 40. Impulse response curves recorded from the DEN07 run along 17th Street (Larimer to Tremont). A narrowbeam antenna was used with the antenna off-pointed at the receiver by 3° left.

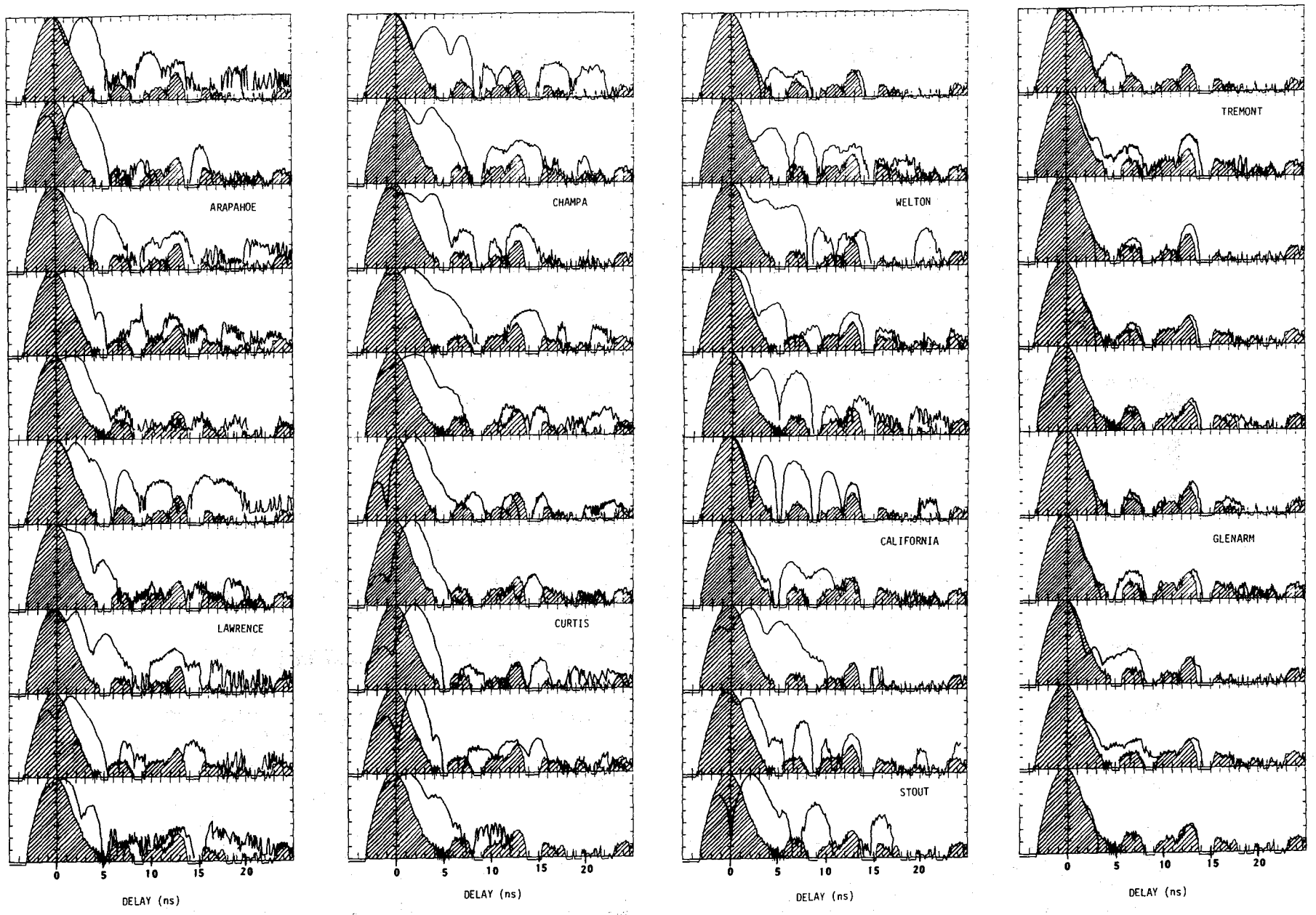

Figure 41. Impulse response curves recorded from a run along 17th Street (Larimer to Tremont). The impulse curves from the DEN07 run (3° off-pointing) are plotted against reference impulses that are "relatively" free of multipath signals.

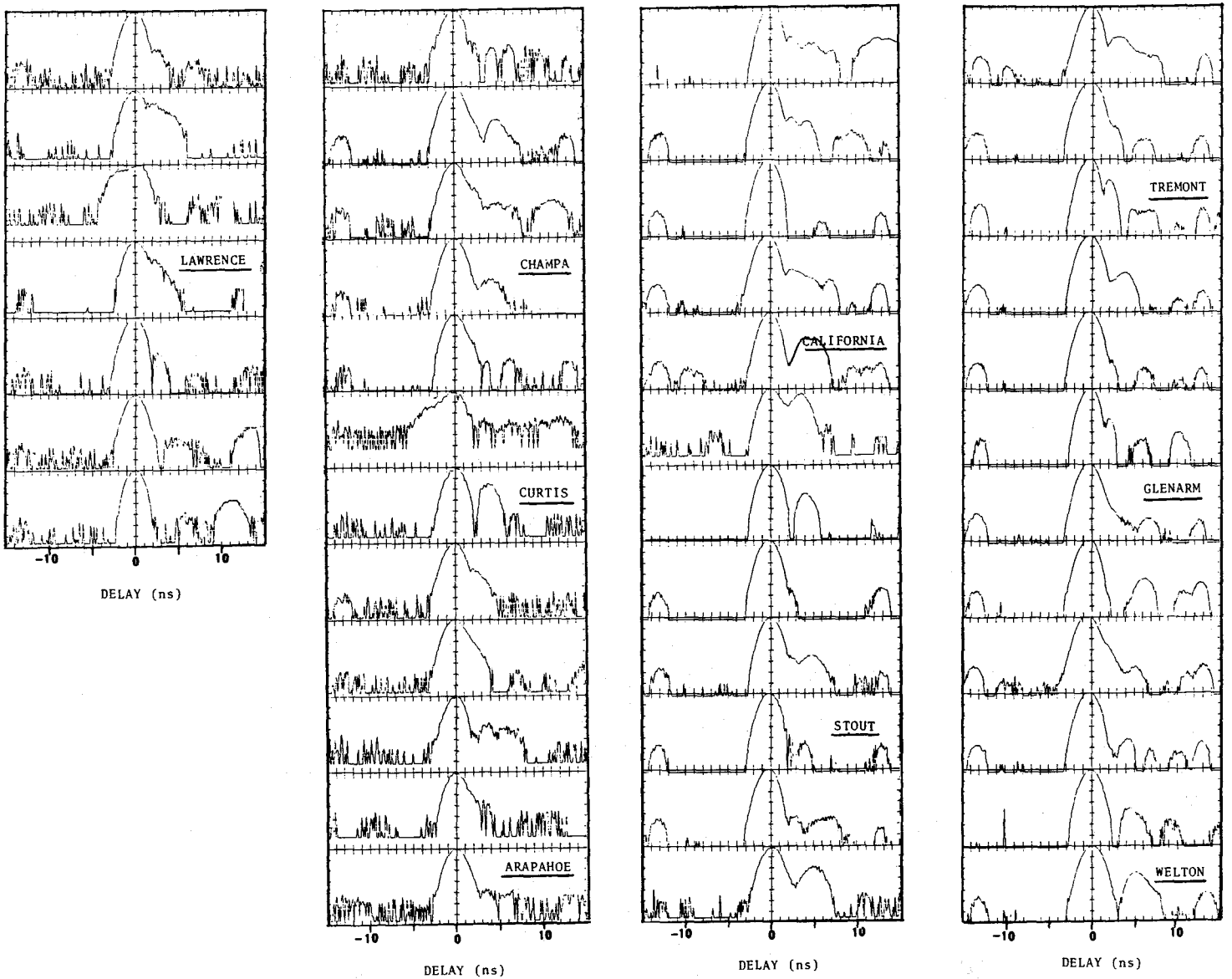

Figure 42. Impulse response curves recorded from the WIDE02 run along 17th Street (Lawrence to Tremont). Widebeam antennas were used with the antennas adjusted for on-line pointing.

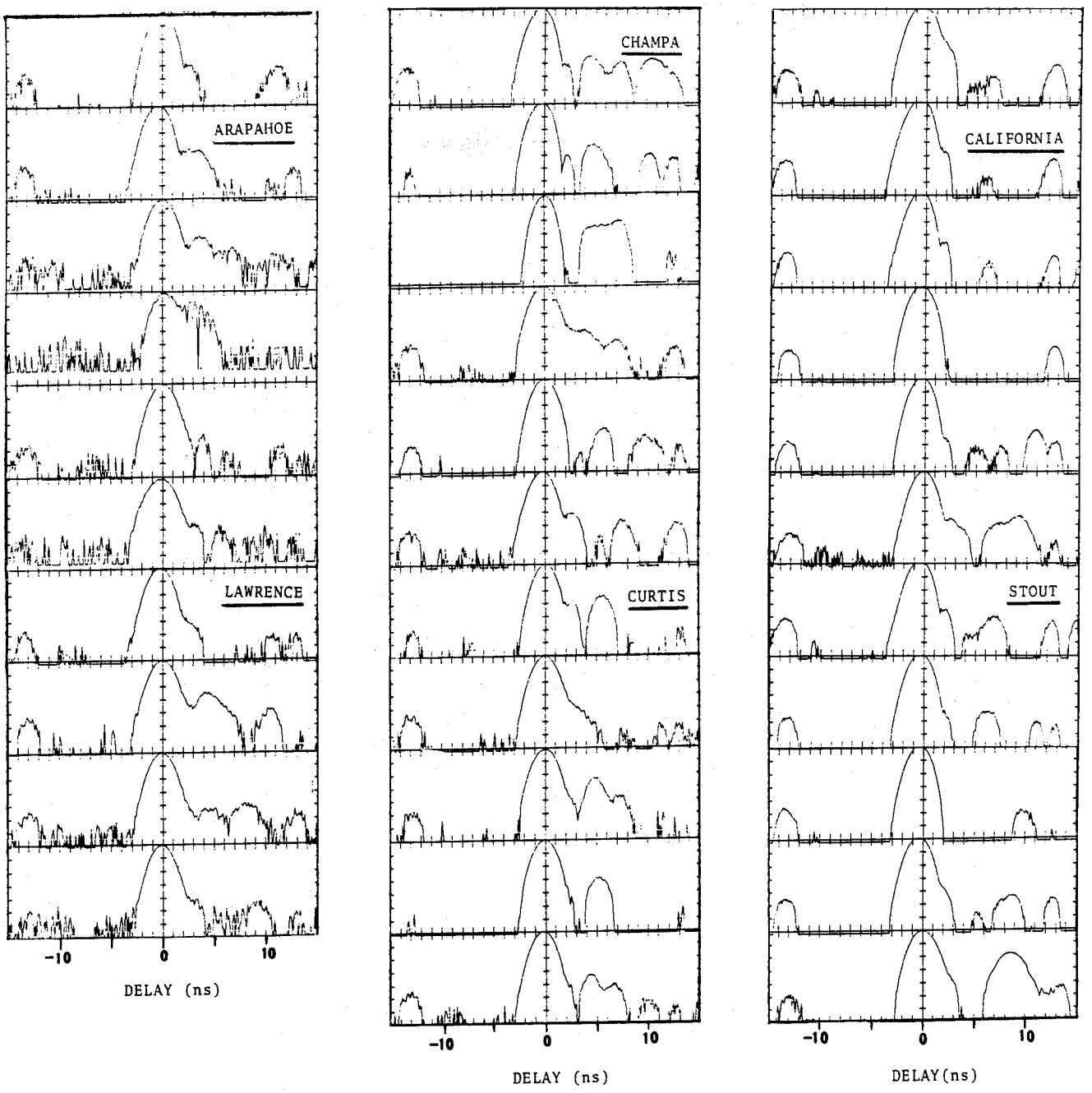

Figure 43. Impulse response curves recorded from the WIDE08 run along 17th Street (Arapahoe to California). Widebeam antennas were used with the antennas adjusted for on-line pointing.

surfaces are more completely filled on both sides of the street between 14th and 19th Streets; however, between 19th and 24th Streets, buildings were more sparse than any area previously measured in Denver. In Figure 44(A) is a photograph of Champa Street looking from 24th Street, and Figure 44(B) is a photograph from 16th Street toward 14th Street, where the receiver terminal was located.

Several runs were recorded with the transmitter terminal traveling down Champa Street toward the receiver terminal just beyond the 14th Street intersection. With the widebeam (30°) antennas on the 28.8- and 30.3-GHz channels, signal fading and fade depths were similar to the 17th Street data up to about 19th Street. Between 19th and 14th Streets the 28.8 GHz narrowband channel (as discussed in Section 5.4) appears to show more numerous and deeper fading. The best display of what happened over the channel as a result of multipath from building walls is provided by the history of impulse response curves shown in Figure 45. By comparing this figure with the 17th Street impulse curves in Figure 42, it is apparent that Champa Street produced more severe wall multipath because on several response curves, taken near the middle of the run, the multipath component equals or exceeds the direct signal. From these observations, the assumption is that the smoother, more uniform building wall surfaces between 19th and 14th on Champa provide more favorable conditions for generating larger multipath components. The results suggest that urban streets having these conditions will additionally diminish the performance of a millimeter-wave channel if wall reflections are involved.

The last series of measurements were made on Broadway, a main traffic route through Denver, and therefore a wider street measuring 31 m between buildings. Also, the distance between street intersections is 175 m as compared to 100 m and 127 m of the two previous streets measured. Buildings along the street are generally of the smaller (2 to 3 story) office and business types. Some open areas lie along the street, many of which are car or truck dealerships or for customer parking. There is very little elevation change over the approximately 16 blocks traveled for propagation measurements. Figure 46 show photographs of the sections near 12th Street (top) and near 6th Street looking south on Broadway. The received signal fading characteristics were quite similar to the other signal plots shown on 17th and Champa Streets, i.e., numerous fades with many exceeding 20 dB in

A)

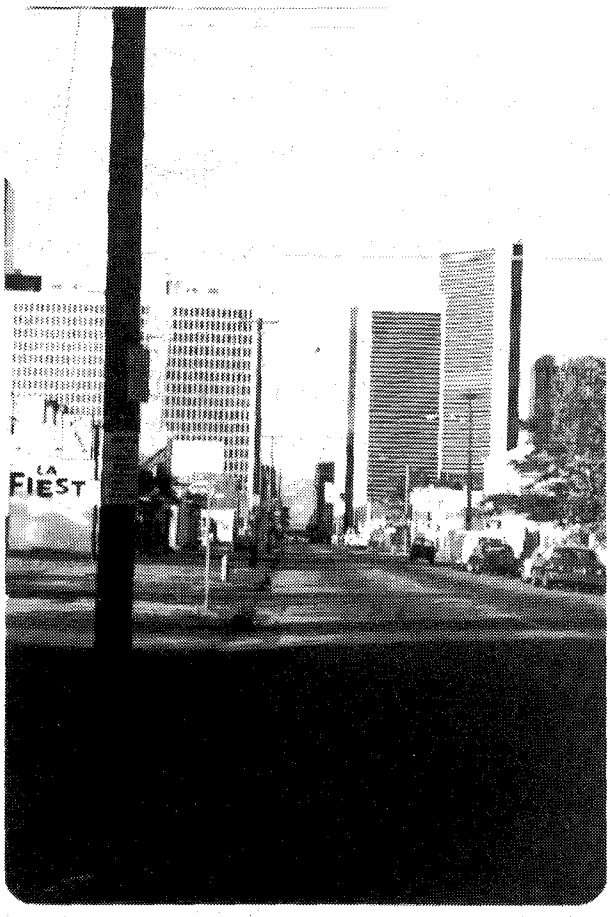

B)

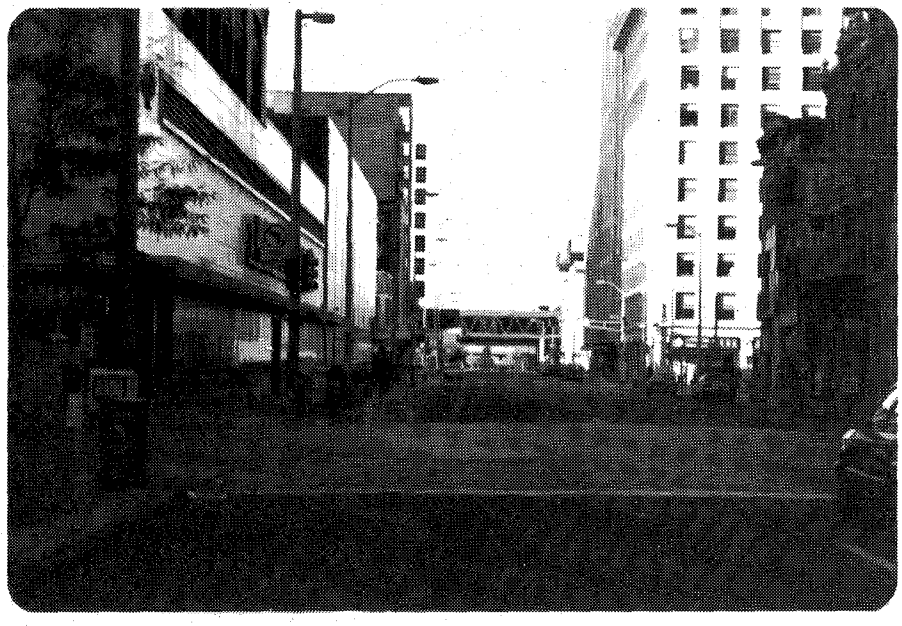

Figure 44. Photographs of Champa Street in Denver, CO.

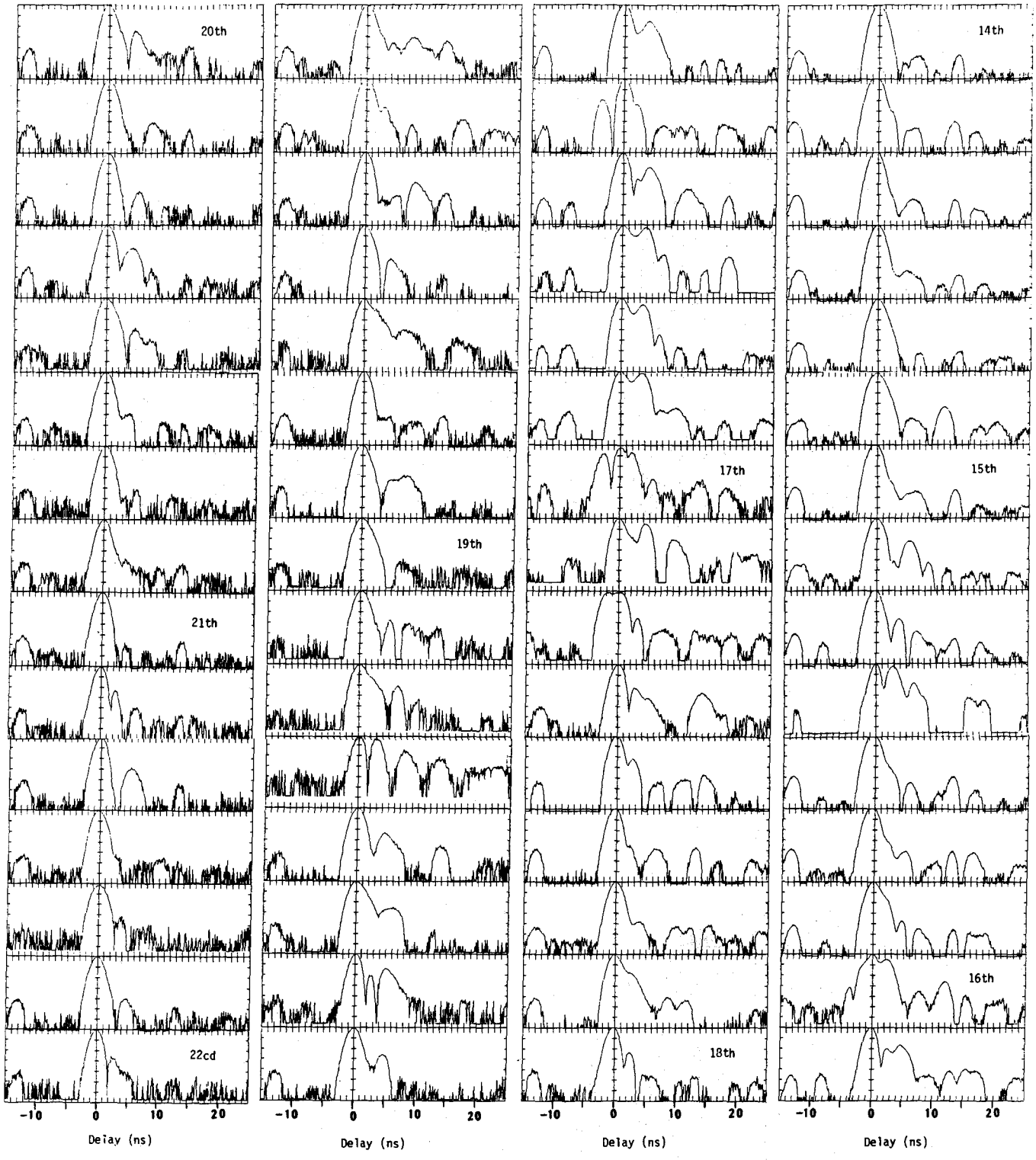

Figure 45. Impulse response curves recorded along Champa Street (22nd to 14th). Widebeam antennas were used with on-line pointing.

A)

B)

Figure 46. Photographs of Broadway Street in Denver, CO.

depth (from Section 5.4). Curves of the impulse response with the transmitter terminal traveling between 16th and 11th Streets and the receiving terminal using the widebeam antennas stationary just beyond 11th Street are shown in Figure 47. Amplitudes of the multipath signals seen in these impulse curves were stronger than expected over some portions of the run. However, there were even fewer obstructions along the street than in previous streets and some buildings certainly presented large smooth surfaces (see photographs) that are the conditions conducive to strong multipath generation. Another factor, which will be demonstrated more clearly by the model described in Section 6, is the distance between intersections. As can be imagined, many potential multipath reflections are diverted from the receiver at the street intersection. Thus, with all other conditions constant, if the ratio of building surface width to intersection width is increased, as is the case for Broadway, the number of multipath signals from building walls for a down-the-street run will also increase.

Because of the wider separations between buildings on Broadway, a longer multipath delay time relative to the direct signal might be expected especially as the path becomes short; i.e., the reflection angles are steeper. A study of the Broadway impulse curves does show numerous multipath components greater than -18 dB at delay times greater than 4 ns over the last half of the Broadway run. However, longer delayed signals are not an obvious feature in the Broadway impulse curves when compared to similar curves taken on the narrower streets.

The last set of data was taken on Broadway between 5th Street north and 2nd Street south. In this case both terminals were in motion with a separation of 3 blocks (525 m) maintained as accurately as possible for the approximately 7 block (1225 m) run. Widebeam antennas were used at both terminals producing the impulse curves shown in Figure 48. Again there were some very strong multipath components, at times exceeding the direct signal, and a considerable amount of variation over the run in multipath signal strength and delay times even though the terminals were always about the same distance apart. The reason for making a measurement with constant terminal spacing while traveling along the street was the expectation that more consistent propagation patterns would occur in both signal fading and impulse display of multipath signal delays and amplitude. No consistent patterns were evident and the signal characteristics were as random as for any run where the

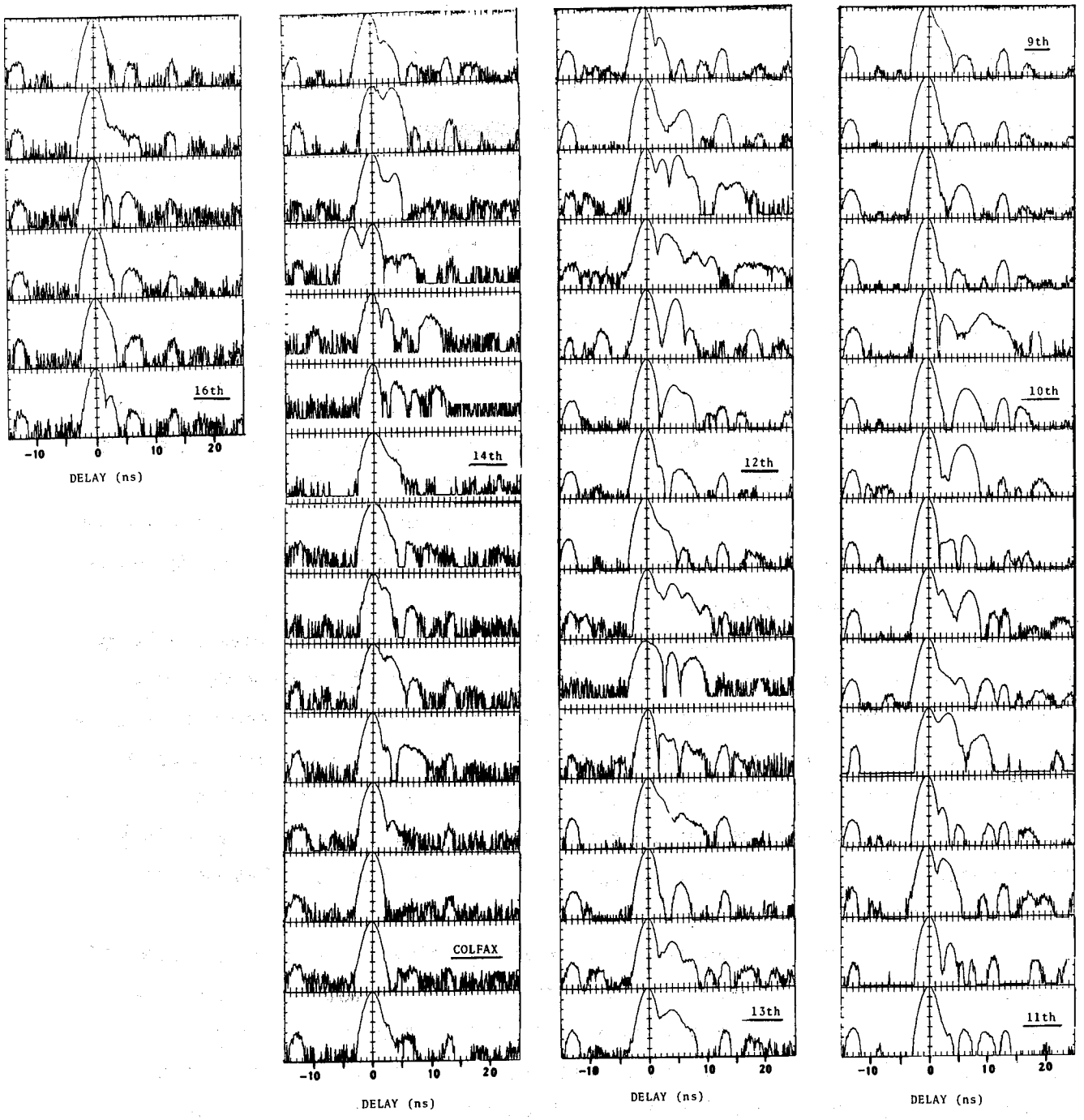

Figure 47. Impulse response curves recorded along Broadway (16th to 11th). Widebeam antennas were used with on-line pointing.

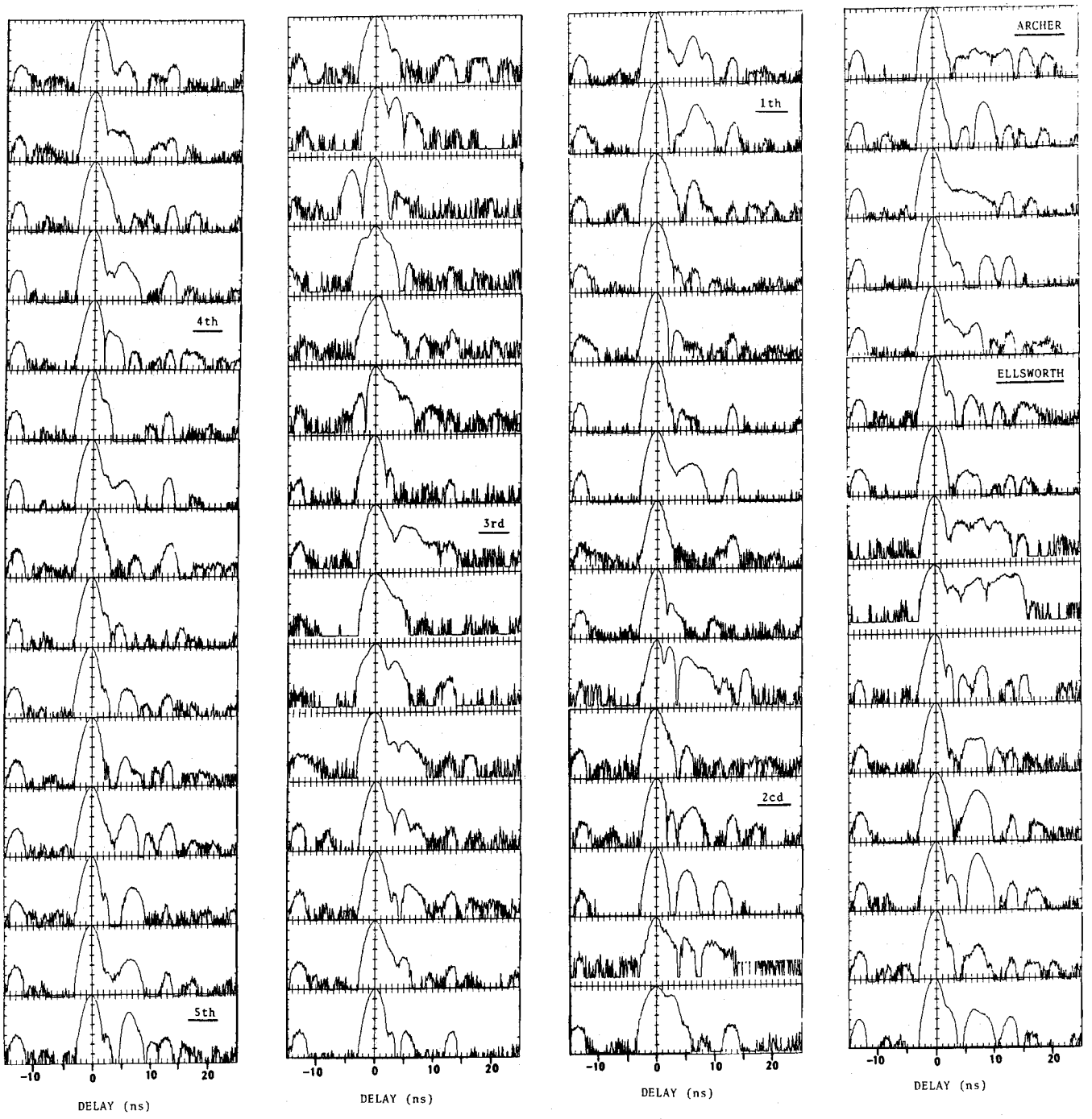

Figure 48. Impulse response curves recorded along Broadway with both terminals moving while maintaining a constant 3-block separation (525 m).

distance between terminals varied. This emphasizes the fact that the urban environment is very irregular and complex when a propagation path is examined at millimeter-wave frequencies.

5.6 Bit-Error-Rate Measurements

A common measure of performance of a digital modem is in terms of bit error rate (BER) for a given signal-to-noise ratio at the demodulator. By mixing very wideband noise with the signal at the demodulator input, accomplished by a link simulator developed for this purpose, a curve of BER versus signal-to-noise ratio (S/N) was drawn. This curve is typically compared to the theoretical or ideal performance curve, for coherent biphase shift keyed (BPSK) modulation in this case. The theoretical performance curve for a coherent BPSK, with additive Gaussian noise, is calculated from

$$BER = e^{-E_b/N_o} \Big/ 2\sqrt{\pi E_b/N_o} \qquad (2)$$

where E_b/N_o is defined as bit signal energy to one-sided noise spectral power density (Wozencraft and Jacobs, 1965). In terms of S/N, the ratio of signal power to noise power in the signal bandwidth is

$$E_b/N_o = S/N + 10 \log \frac{\text{Signal bandwidth (w)}}{\text{bit rate } (R_b)} \qquad (3)$$

For the 500 Mb/s, BPSK, BER measurements, the signal bandwidth is determined by a 1-GHz filter at the demodulator input. Figure 49 contains plots of the theoretical curve and measured values of some of the important stages within the system as well as through two rf links. The theoretical curve (#1) represents a distortion-free system. With the baseband generator and bit error receiver connected back-to-back, the E_b/N_o is within 1 dB of theoretical (curve not shown). With the 1.5-GHz PSK subcarrier modulator-demodulator connected back-to-back (curve #2 of Figure 49), the E_b/N_o departs by about 2 dB from theoretical at a BER of 10^{-8}, an excellent performance level. Matched filters are adjusted for optimum BER at an E_b/N_o of 6 dB for the curves shown, consistent with the probe's use as a diagnostic tool. When the filters are optimized at an E_b/N_o of 13 dB, the maximum departure from the theoretical curve for modulator-demodulator is about 1.5 dB.

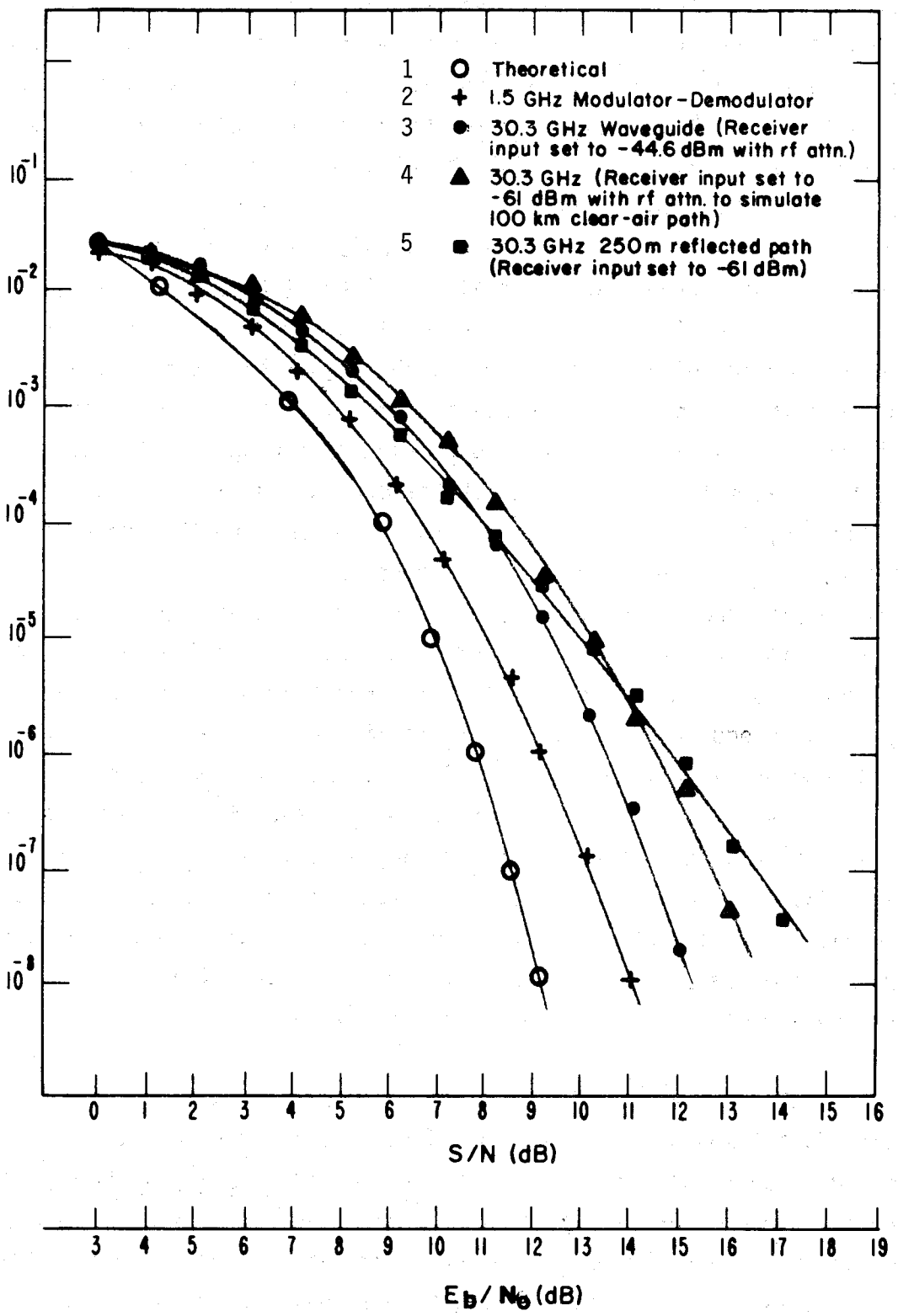

Figure 49. Plot of BER vs. E_b/N_o for several system configurations.

The third BER curve of Figure 49 indicates performance with the 30.3-GHz up converter, the wideband 30 GHz amplifier, and the receiver down converter connected through about 15 ft (4.5 m) of WR-28 waveguide. A departure of about 3 dB from the theoretical curve occurred, with the greatest contributor to increased errors being the dispersion in amplitude and phase of the 26- to 38-GHz power amplifier. The input level to the receiver down converter (balance strip-guide mixer) was -44.6 dBm for the plot shown in curve #3.

The local oscillator signal for the down converter is generated by a phase-locked, cavity-tuned multiplier and a low-noise, resistive-type waveguide tripler stage; even so, the local oscillator (LO) phase noise provides the noise figure limitation at the receiver. With the input level to the receiver reduced to -61 dBm, the LO phase noise just begins to cause an increase in the number of errors, as shown in curve #4, using the waveguide link. The LO phase noise was not included as part of the E_b/N_o in plotting this curve but it was measured as signal at the demodulator input at the subcarrier frequency of 1.5 GHz. The noise power to generate the curves of Figure 49 is injected at the demodulator input port.

Curve #5 results from a 250-m folded path through the atmosphere using 3-ft (91 cm) dishes for both transmitting and receiving, with a 56-cm trihedral (90° corner) reflector. Again, the input to the receiver up converter was set at -61 dBm, which is equivalent to the received level for a 100-km clear-air path assuming atmospheric absorption to be 0.12 dB/km. As seen by the small separation in curves #4 and #5, neither the antennas, the 250 m of atmosphere, nor the corner reflector produced appreciable degradation in the received signal. Curve #5, over the short atmospheric path, becomes the reference for relative S/N and/or distortion over a path under test. Long-term stability or the ability to reproduce the BER performance curve has been within the measurement accuracy of the power meter or about $\pm 1/4$ dB.

5.7 Effects of Multipath on Digital Link Performance

Multipath data taken on the 250-m folded path, using the 30.3 GHz, 500 Mb/s, coherent BPSK was compiled to give a view of multipath effects. To achieve a controlled multipath condition, a second trihedral reflector was mounted next to the main reflector. The second reflector, which provides the multipath signal, was attached to a milling head allowing adjustments to fractions of a wavelength (four crank turns per centimeter). Figure 50

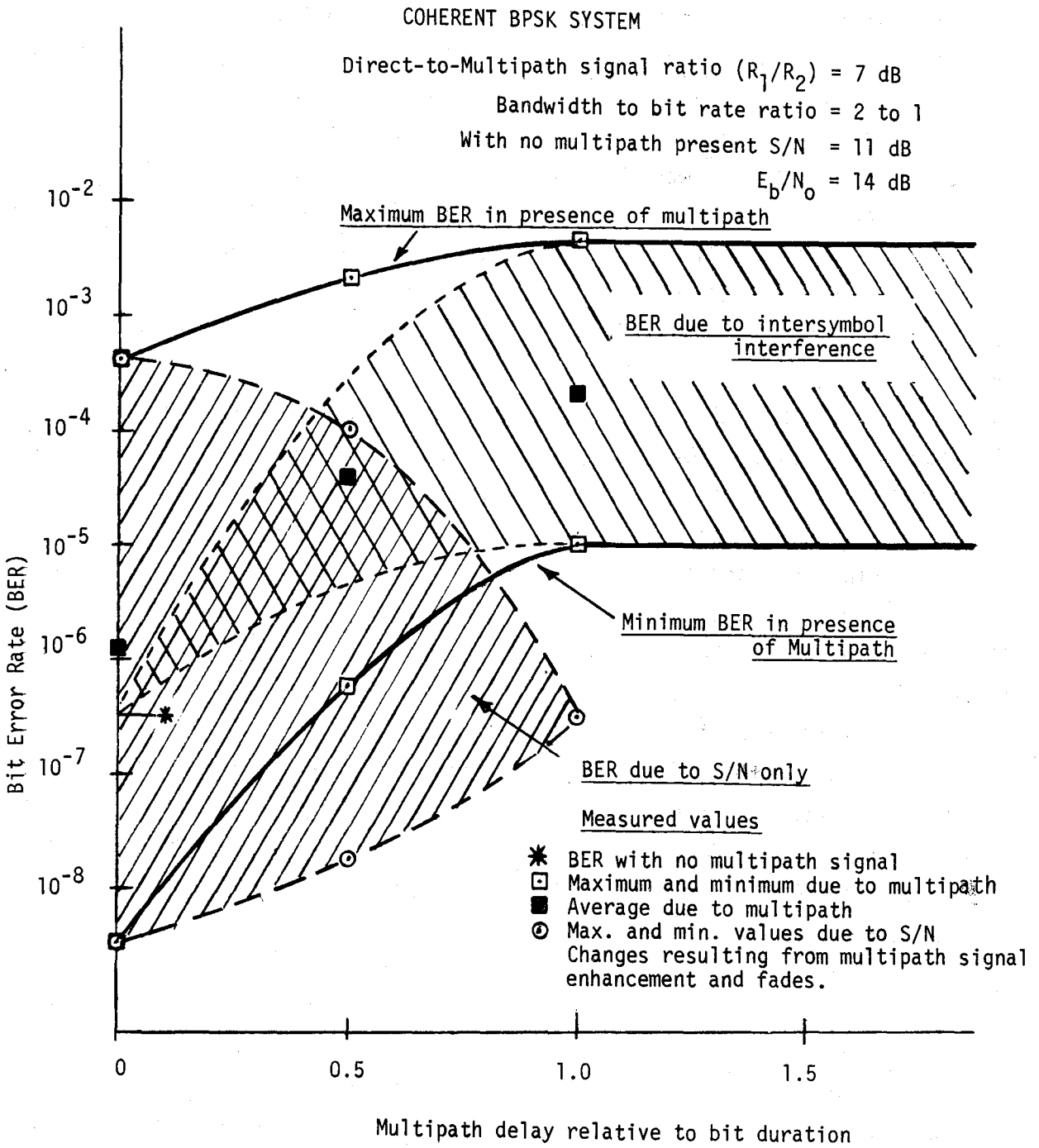

Figure 50. BER in the presence of multipath signals due to S/N and to intersymbol interference for a S/N of 11 dB and a direct-to-multipath signal ratio of 7 dB.

contains a plot of contributions to BER by S/N variations and intersymbol interference as a function of the time delay of a multipath signal relative to the direct signal normalized to bit duration. For this plot, the direct-to-multipath signal ratio (R_1/R_2) is 7 dB. With no multipath present and an 11-dB signal-to-noise ratio, set by injecting wideband noise at the demodulator input, a BER of 5×10^{-7} was measured. At zero multipath delay, the change in BER is due only to S/N changes with an average BER of about 1.5×10^{-6}. This average BER is greater than the no-multipath case because fades of 5.1 dB and enhancements of only 3.2 dB occur for a R_1/R_2 of 7 dB. Since a pseudorandom sequence bit generator is used to produce the data stream, the amplitude variations diminish as the multipath delay extends to 1-bit duration. Hence, the errors are due to S/N change as shown by the narrow hatched lines marked "BER due to S/N only." Amplitude variations as a result of multipath at delay times greater than one bit duration are small. Some additional amplitude variations in the system are due to cw components in the signal used for reconstructing the carrier.

Errors due to intersymbol interference for this multipath case (Figure 50) are shown to diverge from zero delay, beginning at the BER (5×10^{-7}) for a no-multipath state. This indicates that there is no intersymbol interference contribution at zero multipath delay relative to the direct signal. As the multipath delay increases, the maximum and minimum contribution from intersymbol interference is shown by the broad-spaced hatch lines extending to coincide with the total contribution of errors at a delay time equal to 1-bit duration. Part of the errors attributed to intersymbol interference are the result of the composite of the direct signal and multipath signal producing a phase shift in the reconstructed carrier. As shown in Figure 4, the reconstructed carrier is manually phase adjusted to provide a zero reference to the phase detector in the demodulator for recovery of the baseband signal. This composite signal phase shift is cyclic at the rf rate and the resultant phase error accounts for part of the maximum-minimum BER excursions. A similar process occurs with the reconstruction of the bit rate clock, which is also modulated at the rf rate by multipath signals.

The BER due to a multipath signal is dependent on the channel S/N and the strength of the multipath signal. For a direct-to-multipath signal ratio of 8 dB, Figure 51 shows measured and extrapolated values of BER as a function of S/N compared to a curve showing system performance without a multipath signal. All values plotted are for a case where the multipath signal delay is 1-bit duration or greater. The measured points using the passive reflectors to generate multipath are indicated by the small circles on the figure. These points include minimum, average, and maximum BER as a result of the multipath signal being continuously varied in delay time over several rf cycles.

Bit error rate versus S/N curves are extrapolated from measured data, for three different ratios of direct-to-multipath signal level in Figure 52. An estimated scale of R_1/R_2 starting at 7 dB and extending to ∞, which is the no-multipath state, is included for the case where the multipath delay time is 1-bit duration or greater.

Multipath signals in a high data rate channel have a serious effect on data transfer rates due to increased errors. This treatment of multipath involving a single discrete signal may not always be representative of an actual path. Several components of multipath may occur or numerous scatterers may exist such as those arising from reflections from irregular terrain. However, the measurements made for this report will provide a good reference of channel degradation for the conditions that may be encountered on LOS paths along city streets.

5.8 Bit-Error-Rate Measurements in Urban Environments

Several sets of bit-error-rate measurements were made along various Denver street paths. Generally, both received signal level and BER were recorded simultaneously. The measured range of BER is from a maximum of 5×10^{-1} to a minimum of 2×10^{-8}. A value of 5×10^{-1} means 50 percent errors occurred, or that the chance for a wrong decision is equal to the chance for a correct decision. A minimum resolution in BER of 2×10^{-8} means an error count period of 1 s was used. If a 10-s count period were used a minimum resolution of 2×10^{-9} would be available; a 100-s period gives 2×10^{-10} and so on. But for this experiment, samples at greater than 1-s intervals would omit too much detail and, therefore, were not used.

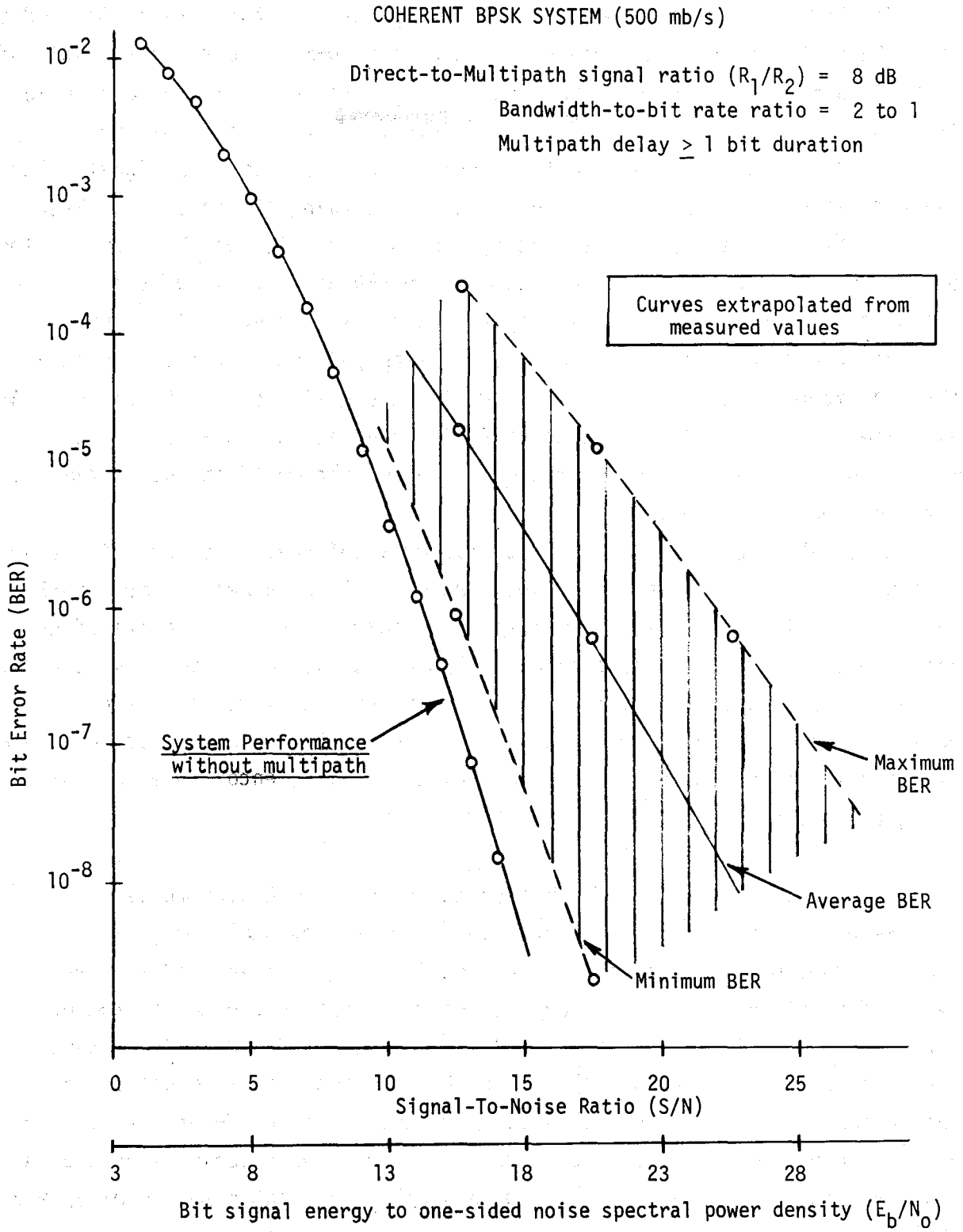

Figure 51. BER as a function of S/N for a direct-to-multipath signal ratio of 8 dB for multipath delays greater than 1 bit duration.

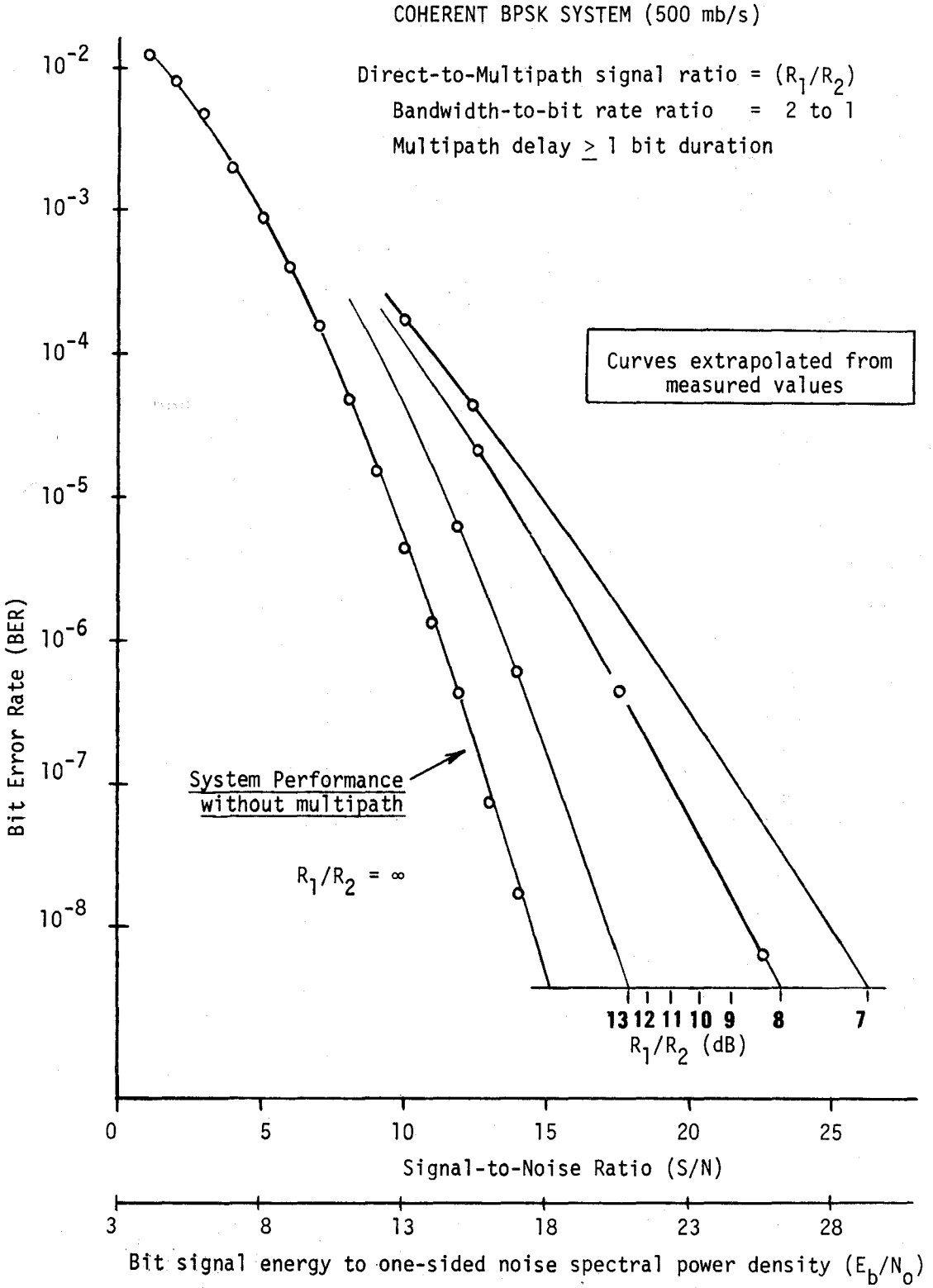

Figure 52. BER as a function of S/N for direct-to-multipath signal ratios (R_1/R_2) from 7 to 13 dB for multipath delays greater than 1 bit duration.

Received signal level and BER data were recorded along the 17th Street path using the narrowbeam antenna at the receiver, and the results are displayed in Figure 53. The BER data indicated that errors are a result of a combination of signal-to-noise ratio reduction and intersymbol interference from time-delayed multipath signals since the BER peaks do not exactly correlate with signal fades but they do occur when fading is active. Some of the high peak BER's near the end of the run suggest greater intersymbol interference effects. The impulse response characteristics showing samples of multipath components for the 17th Sreet path appear in Figure 40. As stated in the discussion of Figure 39, the multipath delay components occur betweeen 1 and 4 ns at an amplitude of 15 to 25 dB below the direct signal and are mainly a result of antenna sidelobe response. However, considering the high data rate (500 Mb/s), while using a 2.5° receiving antenna accurately pointed toward the transmitter, the channel performance was very good as indicated by the fact that the errors did not exceed the minimum detectable rate during most of the run.

A widebeam (30°) receiving antenna was installed for the 28.8 and the 30.3 GHz channels, and the BER experiment was repeated along 17th Street. In the change to the widebeam receiving antenna, the system gain was reduced by about 24 dB, which is directly reflected in the S/N of the channels. The result of this gain loss placed the BER at near 1×10^{-2}, with no fades present when the transmitter was located at the most distant point in the run. This condition of marginal S/N, in terms of BER performance, produced a high degree of sensitivity of the BER to signal fading as can be seen in Figure 54 where the transmitter traveled along 17th Street toward the receiver near Welton Street. In comparing the signal level and BER plots, almost a direct inverse correlation is seen up to approximately Champa Street where intersymbol interference begins to influence the BER as well. An example of the presence of intersymbol interference is most easily seen where the BER goes to a maximum (5×10^{-1}) at signal levels higher than points where BER's are less than 5×10^{-1} as indicated on Figure 54 (interval #1 compared to interval #2.) In interval #1, the BER varied from about 1×10^{-2} to 1×10^{-1} at signal levels up to 15 dB less than during interval #2 where the data were totally random (BER at 5×10^{-1}).

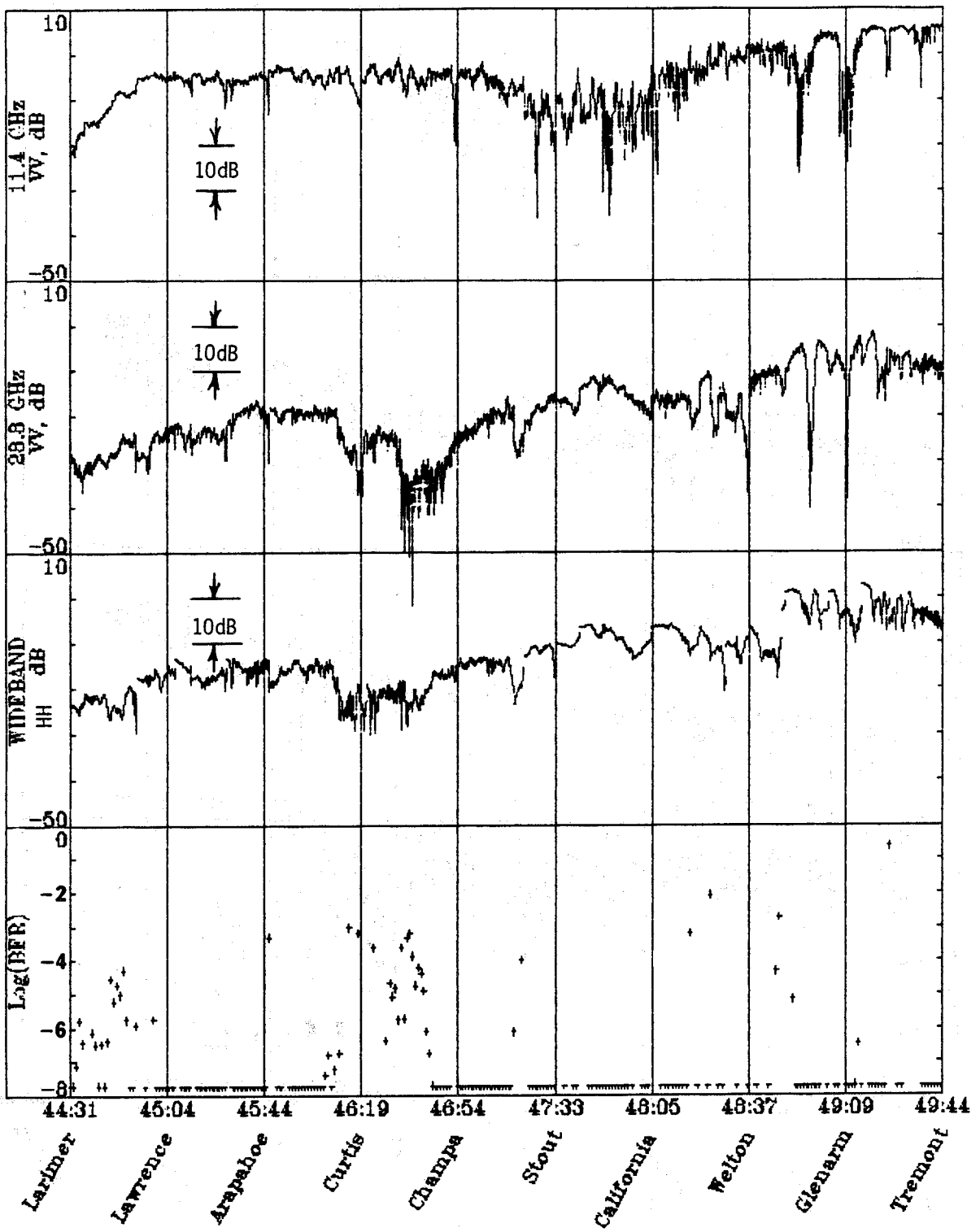

Figure 53. Received signal levels and BER from 17th Street (DEN01) using a narrowbeam antenna.

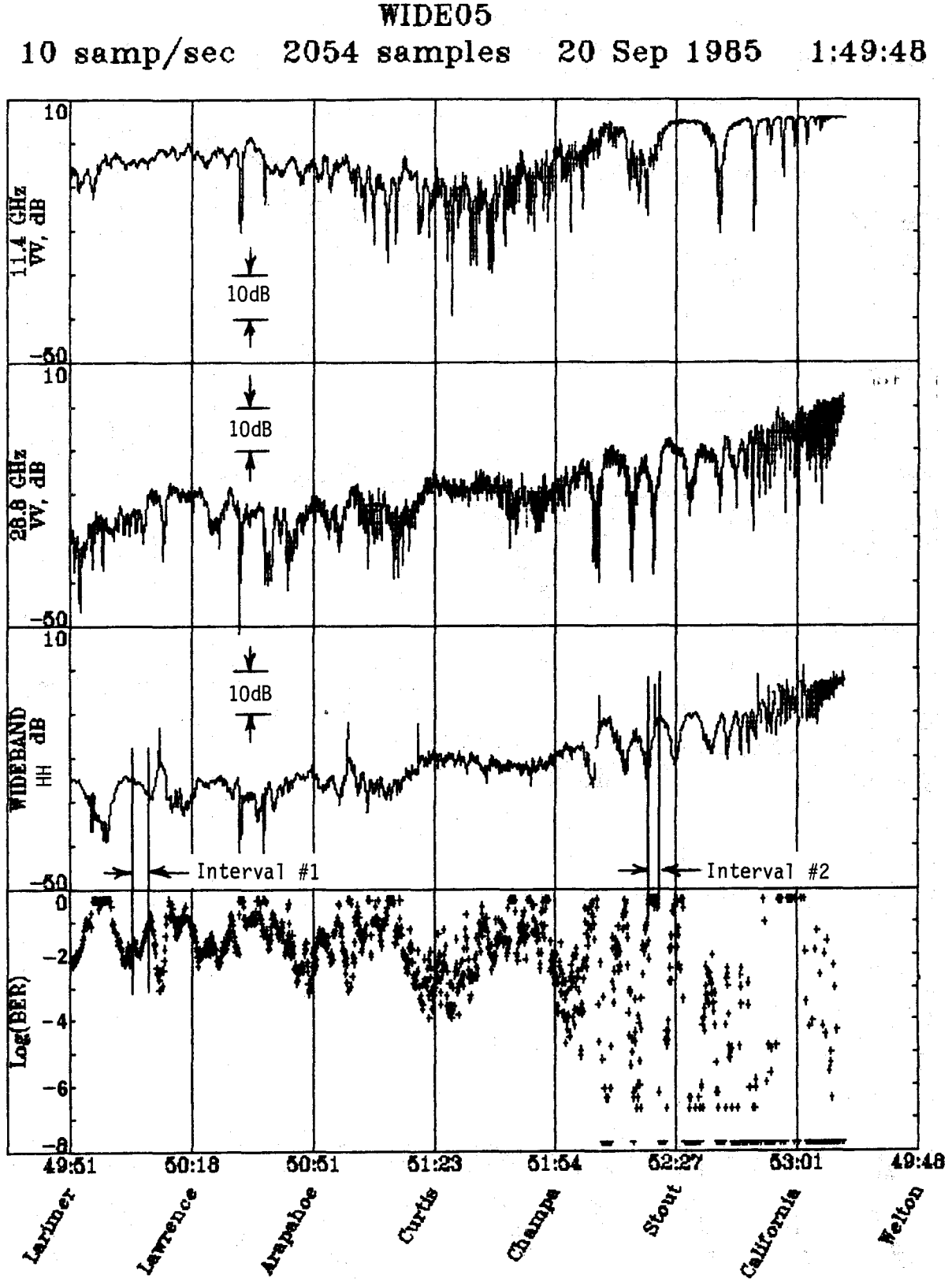

Figure 54. Received signal levels and BER from 17th Street (WIDE05) using a widebeam antenna.

A second BER plot, where the transmitter traveled along Champa Street, is shown in Figure 55. The results for Champa Street are very similar to 17th Street, except for the much larger excursions in BER on Champa Street over the last two blocks. Referring to the impulse curves for Champa Street (Figure 45) we find the longer delayed multipath components to be very strong over the same two-block area (19th through 17th Streets), which is consistent with the high BER observed.

6. URBAN MILLIMETER-WAVE PROPAGATION COMPUTER MODEL

The urban-propagation computer model was developed to predict major propagation modes and effects of LOS paths at street level in an urban environment and to compare the results to measured data. Our objective was to have the predictions display the same characteristics and have the same statistics as the measured data. The comparison of the model predictions to measured data would then serve several purposes. First, it helps to identify propagation effects that cause features observed in the data, i.e., the measured data are better understood. Secondly, it shows how the model can be improved to better account for the propagation effects actually observed, i.e., the limits of the model are better understood. After this is accomplished, the model can be used to predict the propagation effects of different scenarios. This is, of course, the real value of the model--the ability to predict results without having to measure them.

Measurements reported from the 1983 studies (Violette et al., 1983a) show that the received signal was dominated by a LOS ray and a street reflected ray and that additional rays reflected from the walls of the buildings along the street were important. The model was developed to account for these propagation modes.

6.1 Description of the Model

In order to make the model mathematically tractable and not more complex than necessary, an idealized physical model of the urban environment is used.

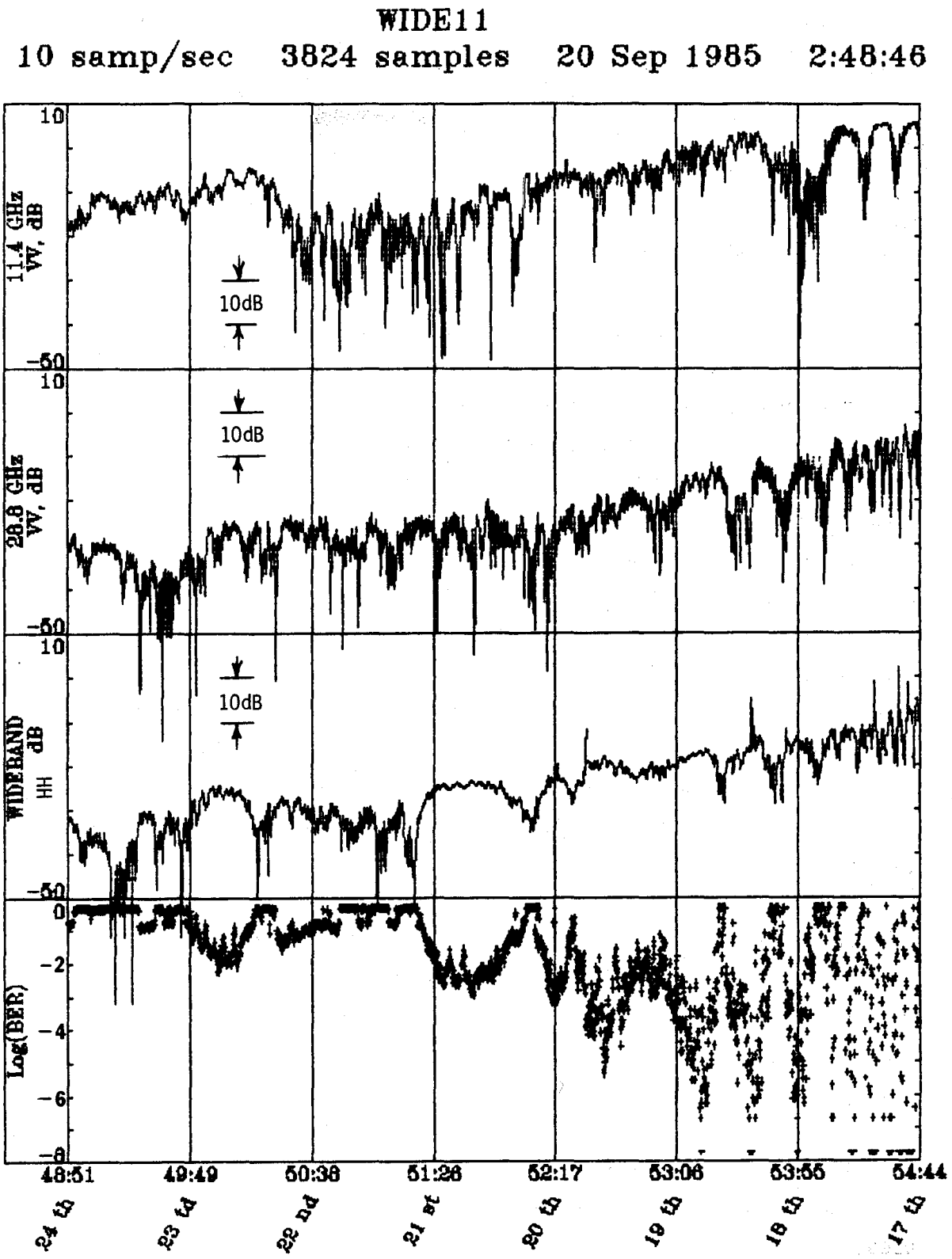

Figure 55. Received signal levels and BER from Champa Street (WIDE11) using a widebeam antenna.

6.1.1 Physical Model

In the idealized model, the street is assumed to be perfectly flat. The building walls are also assumed to be perfectly flat and the width of the street, i.e., the distance between building walls, is constant. Figure 56 depicts the idealized environment. Thus, we end up with a waveguide that is open on one side. Figure 57 shows several streets used for experimental measurements.

This idealized physical model simplifies a complex environment but preserves the basic elements that have the greatest effect on propagation. The shallow reflection angles involved in the geometry make this possible. The effects of variations in building distance from the street center, cross streets, and scattering from objects are discussed later.

6.1.2 Mathematical Model

To develop the mathematical model, geometrical optics or ray theory is used. The received signal is assumed to consist of the sum of a number of rays. These rays arrive at the antenna either directly from the transmitter or after reflection from the street and walls. Specular reflection is assumed with a single coefficient of reflection for all wall surfaces and the same or a different value used for the street surface.

Cross streets were accounted for by letting rays go down the cross street (lost power) rather than be reflected to the receiver. In general, this resulted in model predictions that did not match the measured data as well as when no cross streets were assumed in the model. This weakness in the model can be easily understood and is discussed later.

The idealized physical model makes the accounting of all the possible rays from the transmitter to the receiver simple. The reflections from the street and walls are dealt with by using the image space. Multiple images of the receiver rather than of the transmitter are used here. That is, a ray reflected from a wall appears to be arriving at an image of the receiver beyond the wall.

Ray Geometry

The coordinate system convention is shown in Figure 58(A). In Figure 58(B) and 58(C), the locations of the receiver images are shown along with the ray paths. Each receiver image in Figure 58(B) corresponds to one ray path to the real receiver. Each image is given a double index. The first

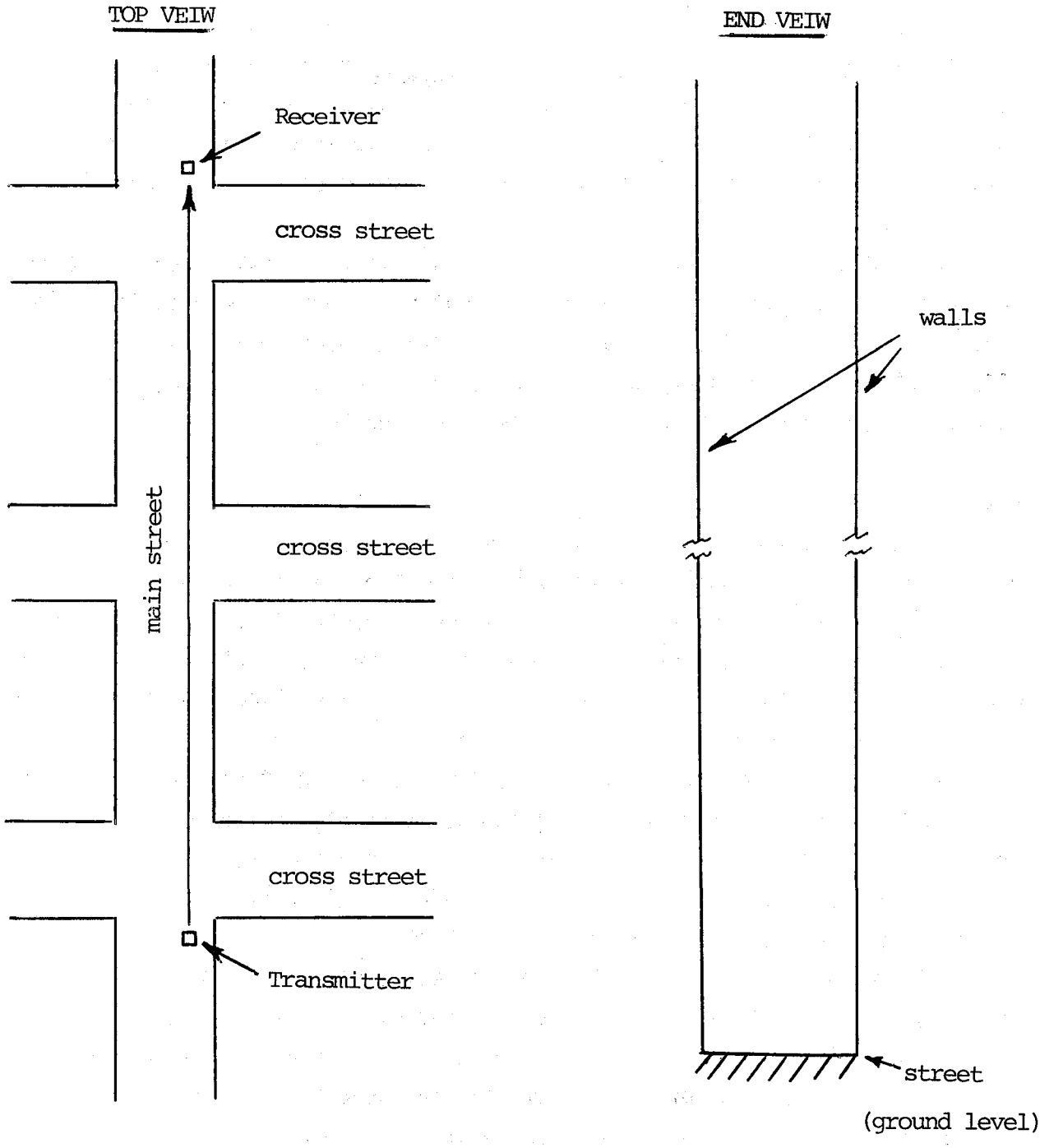

Figure 56. Top and side views of idealized street environment.

A)

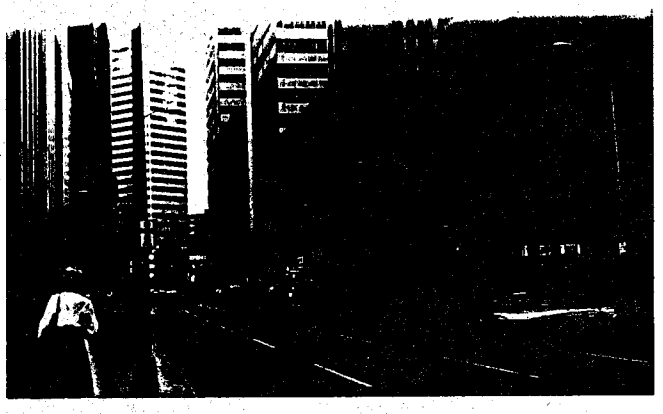

B)

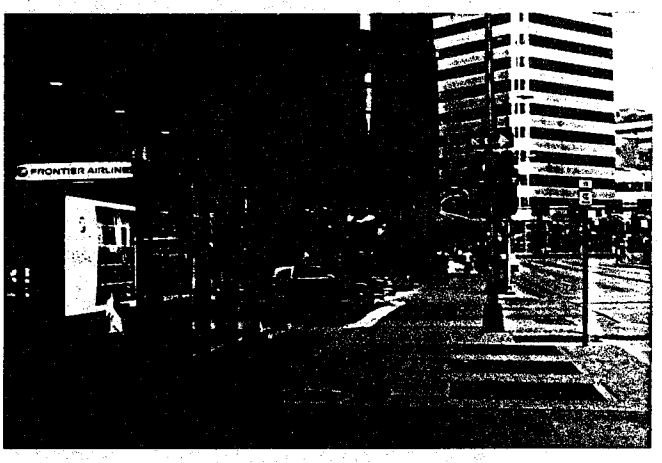

C)

Figure 57. Photographs of street fronts along 17th Street in Denver, CO.

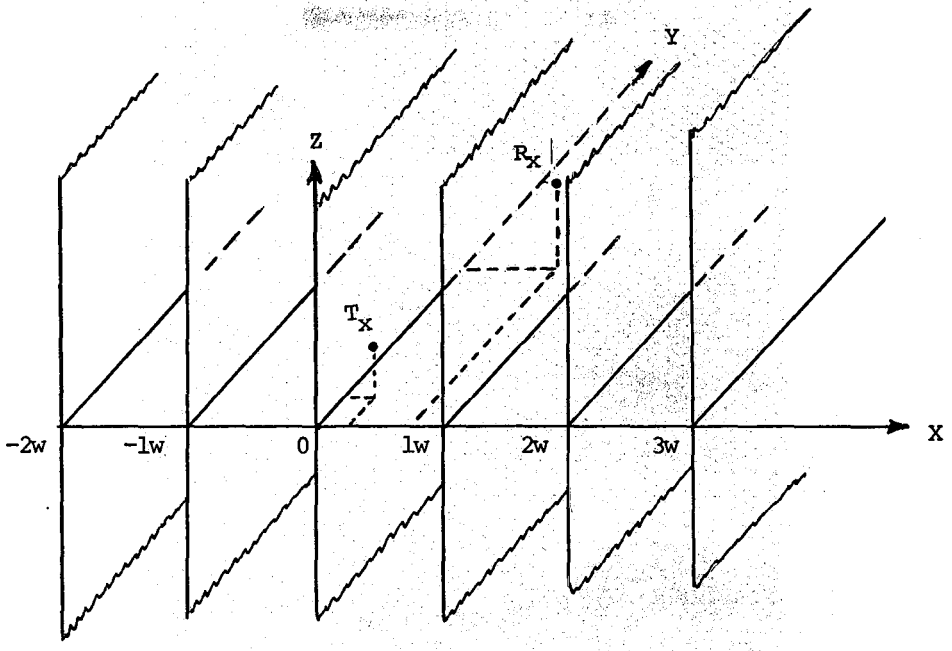

A Image streets created to each side.

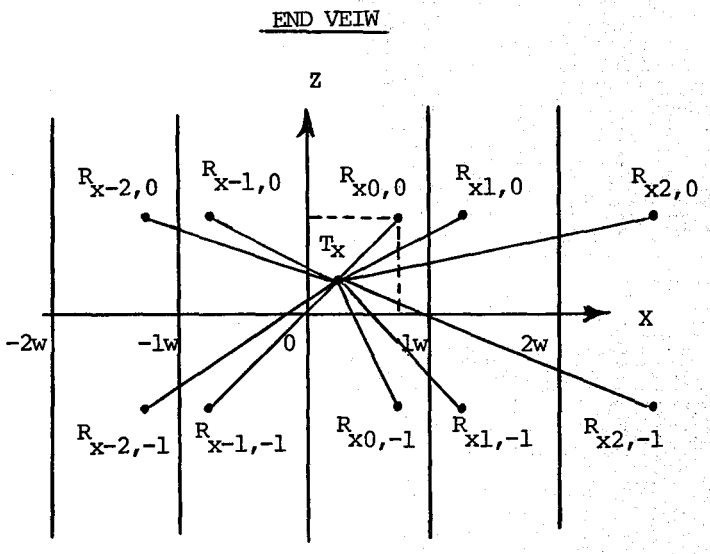

B Imaging for street and wall reflected rays.

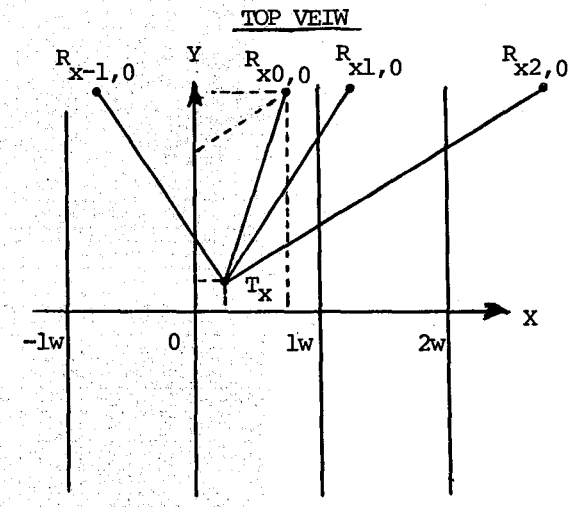

C Above ground wall reflection imaging.

Figure 58. Illustrations of the ray path imaging technique.

index, N, gives the number of wall reflections. A negative or positive sign corresponds to the first reflection being to the left or right of the transmitter, respectively, when looking toward the receiver. Thus, all the images for which this index is negative are to the left of the transmitter and all to the right are positive. The second index, M, indicates whether or not the ray has reflected from the street. A value of positive one means the ray is not reflected from the street and the image is above ground level. A value of negative one indicates the ray is reflected from the street and the image is below ground level. The index (0,1) corresponds to the real receiver location and the direct line-of-sight ray.

The geometry of each ray is easily computed from the location of each receiver image and the sum of the rays is found by looping through the double index of the images.

The location of the transmitter is $(X_t,0,Z_t)$ as shown in Figure 58. The location of the receiver shown in the same figure is (X_r, Y_r, Z_r) and the street width is W. The receiver is a distance Y_r down the street from the transmitter. The location of each receiver image is given by

$$X(N,M) = W(N + (1 - (-1)^N)/2) + X_r(-1)^N \quad (4)$$

$$Y(N,M) = Y_r \quad (5)$$

$$Z(N,M) = MZ_r \quad (6)$$

where N and M are the first and second indexes of the image, respectively, as defined above.

The length of each ray is given by

$$L = \sqrt{(X-X_t)^2 + Y^2 + (Z-Z_t)^2}\ , \quad (7)$$

where the index arguments have been dropped from the coordinate locations of the receiver image. The horizontal length of each ray, i.e., the length of the ray projected onto the x-z plane is

$$L_h = \sqrt{(X-X_t)^2 + (Y-Y_t)^2}\ . \quad (8)$$

The azimuthal angle (in the x-y plane) of the ray from the transmitter to the receiver is

$$\alpha_t = \text{arctangent}((X-X_t)/(Y-Y_t)) \quad (9)$$

where a negative angle is to the left and a positive angle is to the right. The azimuthal angle from the receiver to the transmitter is

$$\alpha_r = \alpha_t(-1)^N \tag{10}$$

where the N dependence accounts for the change in direction of each reflection from the walls. A negative angle is to the left and a positive angle is to the right again when looking toward the other terminal.

The elevation angle from the transmitter to the receiver is

$$\beta_t = \text{arctangent}((Z-Z_t)/L_h) \tag{11}$$

and the elevation angle from the receiver to the transmitter is

$$\beta_r = -M\beta_t. \tag{12}$$

The elevation angles are measured with respect to the horizontal, with a positive angle being above horizontal and a negative angle below horizontal.

The formula for the true angle between two intersecting lines in three dimensional space,

$$T = \text{arccosine}\left[\frac{A1*A2 + B1*B2 + C1*C2}{\sqrt{A1^2+B1^2+C1^2}\cdot\sqrt{A2^2+B2^2+C2^2}},\right] \tag{13}$$

is very useful here. The variables A1, B1, and C1 are the direction ratios of the first line and A2, B2, and C2 are the direction ratios of the second line. The direction ratios can be thought of as the change in each of the linear geometric coordinates when moving from one end to the other of an arbitrarily fixed length of the line. The set of direction ratios for each line can be multiplied by arbitrary constants with no effect on the true angle given by (13). This formula is easily derived from the dot product of the two line segments.

Using (13), the angle of reflection from the street with respect to the normal to the street is found to be

$$\alpha_s = \text{arccosine}((Z-Z_t)/L). \tag{14}$$

The angles of reflection from the walls with respect to the normal to the walls are all equal, as can be seen in Figure 58, and again are found from (13) to be

$$\alpha_w = \text{arccosine}((X-X_t)/L). \tag{15}$$

A ray to the receiver image with first index N has a total number of reflections from the walls equal to the absolute value of N. These reflections alternate between the left and right walls so that the x-coordinate, X_w,

equals 0 or W. If N>0, the images are to the right so that the first reflection is from the right wall. The x-coordinate of the I^{th} reflection point is then given by

$$X_w = W(I - (1)^I)/2), \qquad \text{for } N>0. \tag{16}$$

The other coordinates are given by

$$Y_w = Y_t + (IW-X_t)(Y-Y_t)/(X-X_t), \qquad \text{for } N>0, \tag{17}$$

and

$$Z_w = |Zt + (IW-X_t)(Z-Z_t)/(X-X_t)|, \qquad \text{for } N>0. \tag{18}$$

When N<0, the images are to the left and the first reflection is from the left wall. The x-coordinate of the I^{th} reflection is then given by

$$X_w = W(1 + (-1)^I)/2), \qquad \text{for } N<0. \tag{19}$$

The other coordinates are given by

$$Y_w = Y_t + ((1-I)W-X_t)(Y-Y_t)/(X-X_t), \qquad \text{for } N<0, \tag{20}$$

and

$$Z_w = |Z_t + ((1-I)W-X_t)(Z-Z_t)/(X-X_t)|, \qquad \text{for } N<0. \tag{21}$$

For the street (ground) reflection (M = -1), the z-coordinate is, of course, zero, $Z_s = 0$. The y-coordinate is given by

$$Y_s = Y_t - Z_t(Y-Y_t)/(Z-Z_t). \tag{22}$$

The derivation of the real x-coordinate of the ground reflection is somewhat more complex because of the folding in the image space along the x-axis. In the image space, the x-coordinate of the ground reflection in the image space is given by

$$\hat{X_s} = X_t - Z_t(X-X_t)/(Z-Z_t). \tag{23}$$

Another useful variable is given by

$$I_s = Int(\hat{X_s}/W) - u(-N), \tag{24}$$

where u(x) denotes the unit-step function operating on x, i.e., u(x) = 0 if x <= 0 and u(x) = 1 if x > 0. Int denotes the integer function. This variable is the index of the image of the street in which the ground reflection occurs and is zero for the real street. If I_s is odd, the street image is reversed, i.e., a mirror image. If I_s is even, the image has the same left and right directions as the real street. See Figure 58(C). The x-coordinate location of the ground reflection in the real street is given by

$$X_s = X_s - I_s W, \qquad \text{for even } I_s, \tag{25}$$

and

$$X_s = W - (X_s - I_s W), \qquad \text{for odd } I_s. \tag{26}$$

Ray Amplitude

In the model developed here for the idealized environment, the ray amplitude is determined by a number of factors: the transmitter power, P_t, the transmitter and receiver antenna gains, G_t and G_r, the losses due to reflection from the walls and street, L_r, the absorption due to water vapor and dry air, L_a, and, of course, the free-space loss, L_f. The ray amplitude, A, at the receiver is therefore given by

$$A = P_t + G_t + G_r + L_f + L_r + L_a, \tag{27}$$

where all the quantities are in dB (A and P_t in dBm).

The free-space loss is

$$L_f = 20 \log(4\pi L/\lambda) = 32.45 + 20 \log(FL) \tag{28}$$

where λ is the wavelength, L is in meters and the radio frequency, F, is in gigzhertz.

Assuming parabolic dish antennas, the antenna gains for the ray depend on the antenna patterns and the angles between the ray and the boresights of the antennas. Real antenna patterns could, of course, be used, but for simplicity, the antenna patterns are approximated by sinc functions of the true angles between the ray and the boresights (sinc(x) = sin(x)/x). Then, only a boresight gain and beamwidth are necessary to define each antenna pattern. The antenna patterns are approximated by

$$G(\alpha_b) = G + 10\log(\text{sinc}^2(K\alpha_b)) \tag{29}$$

where G is the gain of the antenna along the boresight, α_b is the true angle between the boresight and the ray, and K is a constant determining the beamwidth of the antenna. Suppose the antenna pattern to be approximated has a 3 dB beamwidth of B_w. Then because 20log(sinc(v)) = -3 dB when v = 1.39, $KB_w/2$ must equal 1.39, so that

$$K = 2.78/B_w. \tag{30}$$

The true angle, α_b between the antenna boresight, having an azimuthal angle of B_a and elevation angle of B_e, and the ray, is found from (13) using the appropriate direction ratios. For the transmitter, the direction ratios are

$$A1 = \cos(B_a)\cos(B_e) \tag{31a}$$
$$B1 = \sin(B_a)\cos(B_e) \tag{31b}$$
$$C1 = \sin(B_e) \tag{31c}$$

$$A2 = \cos(\alpha_t)\cos(\beta_t), \tag{32a}$$
$$B2 = \sin(\alpha_t)\cos(\beta_t), \tag{32b}$$

and

$$C2 = \sin(\beta_t). \tag{32c}$$

For the receiver, the first three direction ratios are given by (31) where Ba and Be are now the azimuthal and elevation angles of the boresight of the receiving antenna. The last three direction ratios for the receiver are given by

$$A2 = \cos(\alpha_r)\cos(\beta_r), \tag{33a}$$
$$B2 = \sin(\alpha_r), \cos(\beta_r), \tag{33b}$$

and

$$C2 = \sin(\beta_r). \tag{33c}$$

For the idealized physical model, separate but constant coefficients of reflection are used for the walls and street. The phase of the reflection coefficients is assumed to be 180°. The magnitude is treated as a loss given in decibels. The total loss in decibels due to reflections is then given by the wall reflection loss multiplied by the number of wall reflections plus the

street reflection loss, if there is a street reflection. With the wall and street reflection losses given in decibels by C_W and C_S, respectively, the loss due to reflection is

$$L_r = |N| \cdot C_W + u(-M) \cdot C_S. \tag{34}$$

where again u(-) is the unit step function as defined above.

The clear-air absorption loss is

$$L_a = \alpha_a \cdot L, \tag{35}$$

where L is the length of the ray and α_a is the attenuation rate in decibels per kilometer as computed based on the model of Liebe (1985).

Ray Phase

The phase of each ray is determined by its length and its reflection from the walls and street. The ray phase at the receiver is given by

$$\theta = 2\pi L/\lambda + \pi(|N| + u(-M)) \tag{36}$$

where a phase shift of π has been assumed for each reflection.

Received Signal Level

The signal at the receiver is modeled as consisting of the sum of all the possible rays from the transmitter to the receiver. In (27), the ray amplitude is given in dBm (at the output of the receiving antenna). In order to sum the rays, the amplitude, a, of each ray in arbitrary linear units is needed. These two measures of ray amplitude are related by

$$A = 20\log(a) \tag{37}$$

and

$$a = 10^{A/20}. \tag{38}$$

Using (27), (36), and (38) the rays may be summed as

$$S = \quad a_{N,M}\exp(-j\theta_{N,M}). \tag{39}$$

The received signal amplitude in dBm is then

$$A_S = 20\log(|S|). \tag{40}$$

Effect of Variations in Building Walls

Variations in the building walls such as differences in building materials, surface roughness, windows and doors, etc., will in the real world cause the reflection coefficient for the walls to vary along the street. This variation is not accounted for in the above model for the ray amplitude. These same features will also cause scattering and diffraction of the millimeter waves into the receiving antenna as will other objects in the vicinity. These effects are not included in the specular reflection model, but more will be said about them below.

In Figure 57, it can be seen that the variation in the distance of the buildings from the street center becomes geometrically insignificant after a few blocks' distance. A Fresnel zone of reflection several blocks away would have a large horizontal extent encompassing a great deal of surface roughness. The surface variation within the Fresnel zone can be thought of as effecting the phase and amplitude of the reflected ray but not significantly altering the geometry of its reflection. That is, the phase and amplitude of a ray will in reality depend on the point of reflection. The gaps in the walls due to cross streets can also be considered to modulate the phase and amplitude of the reflected ray since the horizontal extent of the reflection Fresnel zone is greater than the cross street width for paths longer than about 300 m.

6.1.3 Cumulative Distribution of the Received Signal Amplitude

The model, as it has been developed above, predicts a single value for received signal amplitude based on the summation of a number of ray paths between the transmitter and receiver as determined by the link geometry. Of course, as discussed above, the variations in the walls of a real street would result in ray phases and amplitudes that would cause the received signal level to deviate significantly from that predicted by the idealized model. The signal level predicted from the idealized model is not even the expected value of the received signal level. It is a unique value determined by the particular phases and amplitudes of the summed rays. At best, it could be hoped that the signal level would behave similarly in a qualitative sense to real received signal levels as a function of receiver location, frequency, etc.

Because the propagation situation of a real street would be so complex that it would not be practical to predict an exact received signal level for arbitrary locations of the transmitter and receiver, it is desirable to predict the cumulative distribution of the signal level for an ensemble of real streets. That is, for all streets of a particular approximate width, what would be the distribution of the received signal level as the transmitter and receiver are moved from street to street maintaining the same link geometry within the streets? Equivalently, what would be the distribution of the received signal level if the transmitter and receiver were kept in the same relative position to each other and to the sides of the street, but were moving down the street? This sort of statistical estimate of the received signal level can be made using the idealized model.

Some information about the relative phase of the rays can be retained and therefore improve the estimate of the signal level. In particular, since the surface of the street is rather uniform and in many places approximately flat, the prediction from the idealized model of the relative amplitude and phase of the direct line-of-sight ray and street reflected ray is probably close to what would be measured on a real street. Therefore, the sum of these two rays is treated as a known component of the received signal.

Next, it is assumed that the relative phase of the wall-reflected rays is uniformly distributed from 0 to 2π because of the random deviation of real building walls from the idealized geometry. In addition, it is assumed that the summation of these rays is not dominated by any one ray. That is, although the amplitudes of the rays are random, no one ray has an amplitude so large that it unduly influences the sum. Then the magnitude or amplitude of the sum of the wall-reflected rays has a Rayleigh distribution.

The Rayleigh distribution is named after Lord Rayleigh (1894) who first derived it for the sum of a number of waves with independent uniformly distributed phase. The Rayleigh distribution is given by

$$p(|S_w|<z) = 1 - \exp(-z^2/\bar{a}_w^2), \qquad z > 0 \qquad (41)$$

where $|Sw|$ is the amplitude and $\bar{a}_w^2$ is the average power of the sum of the wall-reflected rays. The average power of the sum is the sum of the powers of the wall-reflected rays given by

$$\bar{a}_w^2 = \sum_{M,N\neq 0} a_{M,N}^2. \qquad (42)$$

Converting to decibels by using

$$A_w = 20\log(|S_w|) \qquad (43)$$

to substitute for the amplitude in the complement of (41) gives the complementary Rayleigh decibel distribution,

$$p(A_w>Z) = \exp(-10^{Z/10}/\bar{a}_w^2), \qquad (44)$$

which gives the probability that the received signal amplitude in dB will be greater than Z. It is convenient to solve (44) for Z in terms of p giving the quantile

$$Z(p) = 10\log(-\ln(p)) + 10\log(\bar{a}_w^2) \qquad (45)$$

so that the signal level exceeded p fraction of the time can be determined. This equation is especially convenient for computing mean and median signal levels and confidence intervals. The second term on the right-hand side of (45) is the average power in dBm and is exceeded 1/e (≈0.368) fraction of the time. The median signal level is exceeded one-half the time by definition and from (45) is found to be 1.59 dB less than the average signal level.

Now, the received signal can be estimated as the sum of a known or constant component (direct plus street-reflected ray) and a Rayleigh distributed component (wall-reflected rays). The distribution of a constant plus a Rayleigh distributed component is known as the Nakagami-Rice or Ricean distribution (Nakagami, 1940; Rice, 1945). There is one parameter, C, for the Nakagami-Rice distribution. This parameter is the ratio in dB of the power in the constant component to the average power in the Rayleigh component. When $C = -\infty$, the distribution is Rayleigh. When $C = +\infty$, the received signal is a constant. The Nakagami-Rice distribution normalized to the median is shown plotted on "Rayleigh paper" in Figure 59.

The power in the known component (direct and street-reflected ray) of the signal is

$$a_c^2 = |a_{0,1}\exp(-j\theta_{0,1}) + a_{0,-1}\exp(-j\theta_{0,-1}|^2. \qquad (46)$$

The parameter C is then given by

$$C = 20\log(a_c/\bar{a}_w). \qquad (47)$$

Because the computation of the Nakagami-Rice distribution involves the evaluation of Bessel functions and it depends on the parameter C in a non-trivial way, a convenient approximation is desirable. As can be seen in Figure 59, the Nakagami-Rice distribution is approximately a straight line on Rayleigh paper with its slope depending on the parameter C. The Weibull distribution (Weibull, 1951) plots as a straight line on Rayleigh paper with an arbitrary slope equal to $-\alpha$, where α is a parameter of the distribution. Therefore the Weibull distribution can be used to approximate the Nakagami-Rice distribution (at least over the range of probabilities from 0.001 to 0.999).

Because on Rayleigh paper, the Rayleigh distribution is a straight line with a slope of -1 and the Weibull distribution is a straight line with slope $-\alpha$, the quantiles of the Weibull decibel distribution are easily found from (45) to be

$$Z(p) = \alpha 10\log(-\ln(p)) + 10\log(\bar{a}_w^2). \qquad (48)$$

Notice that the median signal level is now 1.59α dB less than the average.

To approximate the distribution of the signal level by the Weibull distribution, the nontrivial relationship between α and C must be known. Although, the relationship between α and C could be derived by matching the standard deviation or variance of the Weibull and Nakagami-Rice distributions, the interdecile range is used here. The interdecile range, ΔZ, is the difference between the signal levels exceeded 0.1 and 0.9 fractions of the time. The interdecile range of the Weibull distribution is easily found from (48) to be

$$\Delta Z_W = 13.3954\alpha. \qquad (49)$$

The interdecile range for the Nakagami-Rice distribution has been given by (Hufford and Ebaugh, 1985) as shown in Figure 60. The values of the interdecile range for the Nakagami-Rice distribution have been given by (Rice, et al., 1967) and are presented in the table following.

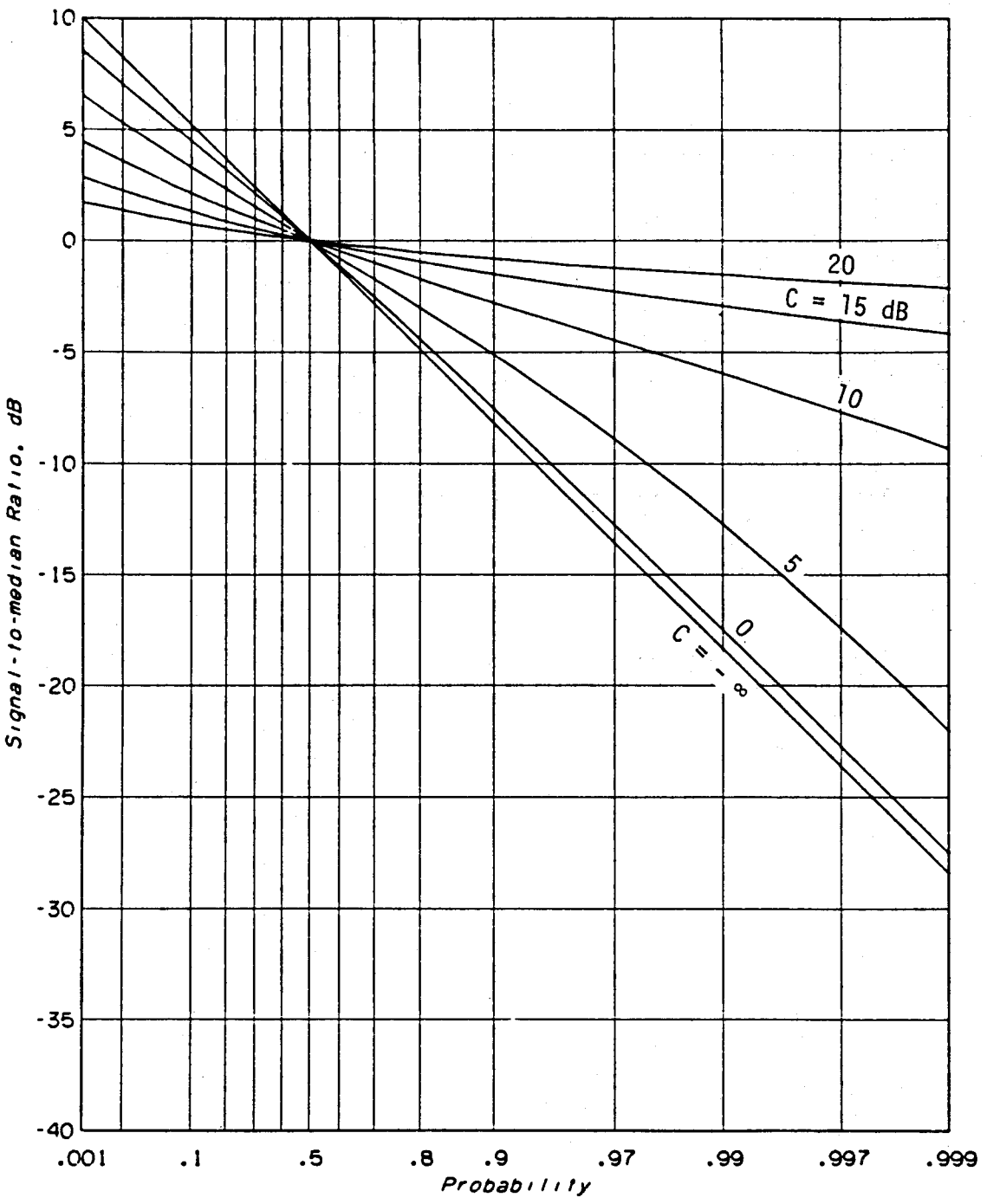

Figure 59. Nakagami-Rice distributions drawn on Rayleigh paper. The parameter C is the constant-to-scattered ratio in decibels.

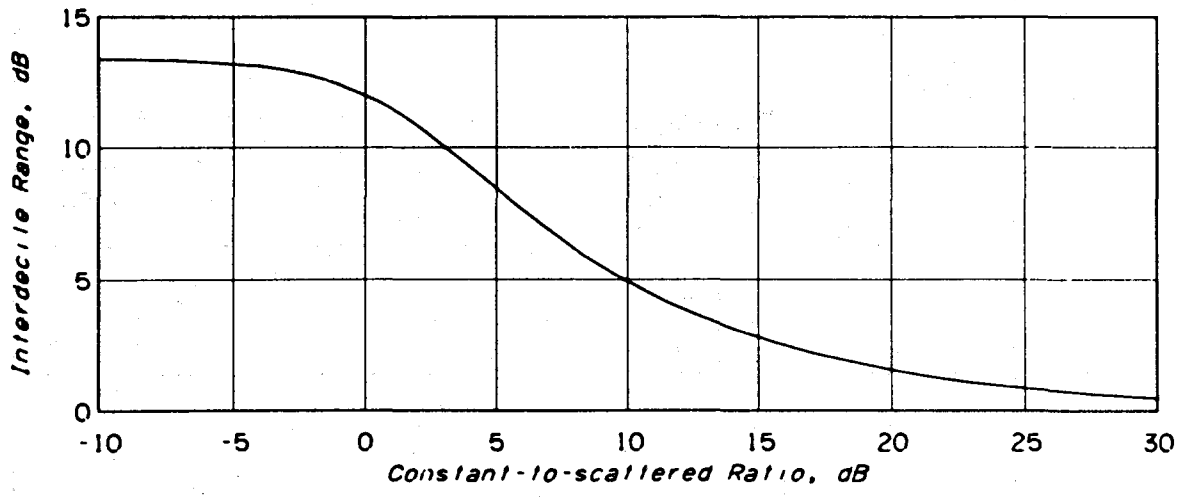

Figure 60. The interdecile range of the Nakagami-Rice distribution.

TABLE 8

The Interdecile Range of the Nakagami-Rice Distribution and the Parameter C

C	ΔZ_N
$-\infty$	13.3954
-10	13.3729
- 6	13.2619
0	12.0049
6	7.6021
10	4.9193
16	2.4884
20	1.5726
25	0.8850
30	0.4978
$+\infty$	0

A function fitting the table above giving ΔZ as a function of C is needed. It is convenient to choose the function

$$\Delta Z_N = 13.3954/(t + 1) \tag{50}$$

since it approaches 13.4 as t goes to zero and 0 as t goes to $+\infty$. Now, t needs to be a function of C such that it goes to zero as C goes to $-\infty$ and to $+\infty$ as C goes to $+\infty$. The function $t = \exp(C)$ satisfies this requirement but a more complicated dependence on C can be achieved if $t = \exp(g(C))$ is used where g is a function such that as C goes to $+\infty$ or $-\infty$, g also goes to $+\infty$ or $-\infty$, respectively. A polynomial of odd order with a positive coefficient for the highest power term satisfies this requirement. The value of the constant term of the polynomial is found to be -2.15565 from (50) using the value of ΔZ_N at C= 0. A third order polynomial such that

$$t = \exp(g_0 + g_1C + g_2C^2 + g_3C^3) \tag{51a}$$

was used to fit (50) to the data in Table 8 with a resultant root-mean-square error of about 0.002 dB for the interdecile range with the coefficient values

$$g_0 = -2.1556515, \tag{51b}$$

$$g_1 = 0.3801766, \tag{51c}$$

$$g_2 = -0.01295302, \tag{51d}$$

and

$$g_3 = 2.145651 \times 10^{-4}. \tag{51e}$$

Using (46) and (47) then gives

$$\alpha = 1/(t + 1) \tag{52}$$

where t(C) is defined by (51), completing the information necessary to use the Weibull distribution to estimate the statistics of the received signal amplitude for an ensemble of streets.

It is important to note that the average power in (42) is computed for the idealized model in which the loss due to a wall reflection is constant for each reflection. This is not the case in the real world; the question arises immediately of how to estimate the power in the Rayleigh component when the reflection loss varies from reflection to reflection in the real world. It is the average power of the sum of the rays reflected from the real walls that is needed to compute C and predict the statistics of a signal in the real world. Fortunately, it can be assumed that the reflection losses are statistically independent because of the surface irregularities. Then, it is simple to show that if the constant reflection loss, C_w, equals the average reflection loss of the real street, the average power computed in (42) equals the average power of the sum of the wall-reflected waves in the real street. In this case, the distribution as derived should give a good estimate of the expected signal level and confidence intervals when one knows beforehand the width of the street and the locations of the end terminals with respect to the building walls and each other.

6.2 Computer Model Capabilities

The model developed in the previous section was encoded in Fortran to run on an HP 1000 computer and later on an IBM PC. The program begins with a menu that allows the user to select the particular output he would like calculated. The user then enters the parameter values needed for the chosen output that describe the street environment and equipment specifications.

Because each reflection decreases the amplitude of the ray, rays with many reflections can be neglected. The user chooses the maximum number of wall reflections for which ray paths should be computed. This maximum is the upper limit on the index N in the summation in (39). This maximum is limited

to 10 by the computer program. If 3 reflections were chosen as the maximum, then 14 rays would be used. They are the direct line-of-sight ray, the ground reflected ray, three rays without a ground reflection that are reflected from the right wall first (1, 2, and 3 reflections), three more rays to the right with ground reflections, and finally the rays reflected first from the left wall that correspond to the previous six rays reflected first from the right.

Although all six outputs of the program are described below, only three of these output types (range scan, angle scan, and impulse response) are used for direct comparison between the measured and predicted (model data) in Section 6.4.

Ray Table

The ray table output provides useful information about the characteristics of each ray that enters into the calculation of the received signal level. Figure 61 is an example ray table output. The rays each have an index (M, N). The first index, M, describes whether or not the ray is reflected from the ground before reaching the receiver. If M is -1, the ray is reflected from the ground. If M is 1, the ray is not reflected from the ground. The second index, N, is the number of reflections from the walls. If N is negative, the ray is reflected first from the left wall. Otherwise, the ray is reflected first from the right wall. The program uses this same index system for all calculations involving the path of the rays.

The ray table describes each ray that arrives at the receiver. The first piece of information listed is the ray length, which determines the free space and absorption losses as well as the delay time to the receiver. The table also describes the angles of departure and arrival at the respective antennas. These angles determine the antenna gain factor for the amplitude of the ray. The table also lists the angle of reflection from the street and from the buildings as well as the geometric coordinates of each reflection location. The effect of cross streets is approximated by assuming that when a wall reflection is located at a cross street, there is no reflection and the ray is lost (goes down the cross street). In other words, if a y-coordinate of the wall reflection is greater than the beginning y-coordinate and less than the ending y-coordinate of a cross street, it is lost and not included in the computation of the received signal amplitude. In Figure 61, two rays are identified as having gone "down a cross street." In practice this method of

SUMMARY OF PARAMETERS

Index	Description	Value
1.	Maximum number of wall reflections (integer)	2.000
2.	Distance between building walls (m)	24.000
3.	TX distance from left wall (m)	5.000
5.	TX height from street (m)	2.150
6.	RX distance from right wall (m)	5.000
7.	RX distance from TX (m)	100.000
11.	RX height from street (m)	1.800
43.	Are cross streets to be used (1=yes,0=no)	1.000
44.	Distance from TX to first cross street (m)	10.000
45.	Distance between cross streets (m)	76.000
46.	Width of cross street (m)	24.000
47.	Plot distribution: (0=no, 1=yes)	0.000
48.	Plot distribution separately: (0=no, 1=yes)	1.000
49.	Plot actual value: (0=no, 1=yes)	1.000
50.	Confidence interval (decimal)	0.900

TABLE OF RAY PATHS

RAY INDEX: -1,-2 Ray Length: 110.994
Transmitter: Azimuth= -25.641 Elevation= -2.039
Receiver : Azimuth= -25.641 Elevation= -2.039
Angle of reflection from buildings= 25.623
Angle of reflection from street= 2.039
Locations of reflection points:

X	Y	Z
0.00	10.42	1.74
24.00	60.42	0.24
21.13	54.43	0.00

THIS RAY WENT DOWN A CROSS STREET.

RAY INDEX: -1,-1 Ray Length: 100.576
Transmitter: Azimuth= -5.711 Elevation= -2.251
Receiver : Azimuth= 5.711 Elevation= -2.251
Angle of reflection from buildings= 5.706
Angle of reflection from street= 2.251
Locations of reflection points:

X	Y	Z
0.00	50.00	0.18
0.44	54.43	0.00

RAY INDEX: -1, 0 Ray Length: 100.078
Transmitter: Azimuth= 0.000 Elevation= -2.262
Receiver : Azimuth= 0.000 Elevation= -2.262
Angle of reflection from street= 2.262
Locations of reflection points:

X	Y	Z
5.00	54.43	0.00

RAY INDEX: -1, 1 Ray Length: 107.050
Transmitter: Azimuth= 20.807 Elevation= -2.115
Receiver : Azimuth= -20.807 Elevation= -2.115
Angle of reflection from buildings= 20.792
Angle of reflection from street= 2.114
Locations of reflection points:

X	Y	Z
24.00	50.00	0.18
22.32	54.43	0.00

RAY INDEX: -1, 2 Ray Length: 110.994
Transmitter: Azimuth= 25.641 Elevation= -2.039
Receiver : Azimuth= 25.641 Elevation= -2.039
Angle of reflection from buildings= 25.624
Angle of reflection from street= 2.039
Locations of reflection points:

X	Y	Z
24.00	39.58	0.59
0.00	89.58	1.39
16.87	54.43	0.00

RAY INDEX: 1,-2 Ray Length: 110.924
Transmitter: Azimuth= -25.641 Elevation= -0.181
Receiver : Azimuth= -25.641 Elevation= 0.181
Angle of reflection from buildings= 25.641
Locations of reflection points:

X	Y	Z
0.00	10.42	2.11
24.00	60.42	1.94

THIS RAY WENT DOWN A CROSS STREET.

RAY INDEX: 1,-1 Ray Length: 100.499
Transmitter: Azimuth= -5.711 Elevation= -0.200
Receiver : Azimuth= 5.711 Elevation= 0.200
Angle of reflection from buildings= 5.710
Locations of reflection points:

X	Y	Z
0.00	50.00	1.98

RAY INDEX: 1, 0 Ray Length: 100.001
Transmitter: Azimuth= 0.000 Elevation= -0.201
Receiver : Azimuth= 0.000 Elevation= 0.201
LINE OF SIGHT RAY

RAY INDEX: 1, 1 Ray Length: 106.977
Transmitter: Azimuth= 20.807 Elevation= -0.187
Receiver : Azimuth= -20.807 Elevation= 0.187
Angle of reflection from buildings= 20.807
Locations of reflection points:

X	Y	Z
24.00	50.00	1.98

RAY INDEX: 1, 2 Ray Length: 110.924
Transmitter: Azimuth= 25.641 Elevation= -0.181
Receiver : Azimuth= 25.641 Elevation= 0.181
Angle of reflection from buildings= 25.641
Locations of reflection points:

X	Y	Z
24.00	39.58	2.01
0.00	89.58	1.84

Figure 61. An example of ray table output with input parameter listing.

accounting for the effects of cross streets results in discontinuities in the received signal level. Ignoring the cross streets gives outputs that look more like measured data.

Range Scan

The range scan output mode predicts the distance dependence of the received signal level. The receiver is moved back from the transmitter along the y-axis while the transmitter remains fixed. For each receiver location the computer calculates the path of the rays between the transmitter and receiver. The computer plots received signal level in dBm vs. distance in meters. Figure 62 is an example range scan output. Expected signal level and confidence intervals are also available.

Frequency Scan

The frequency scan mode predicts the received signal level as a function of the frequency. Both the receiver and the transmitter remain in fixed positions. The computer calculates the signal level over a user-defined frequency interval. Zero bandwidth is assumed. Because the relative phase of the rays depends on the frequency, the signal level varies with frequency. A plot of signal level versus frequency is shown in Figure 63. Again, expected signal level and confidence intervals are available.

Angle Scan

The signal level as a function of either the azimuth or elevation angle of the receiving antenna is estimated. Like the frequency scan mode, the receiver and the transmitter locations remain fixed. The user defines the azimuth or elevation angle interval. The antenna gain for each ray changes as a function of the antenna angle. The output is a plot of the received signal level as a function of azimuth or elevation angle. Figure 64 depicts an azimuth angle scan output. Again, expected signal level and confidence intervals are available also.

Angles of Arrival

The angle-of-arrival mode shows the angles of arrival at the receiver and the relative strengths of the rays. The transmitter and the receiver remain fixed. The output consists of dots on the azimuth-elevation plane representing the rays. The relative size of the dots gives the relative amplitude of the rays. The computer can calculate the ray amplitude with or without considering the antenna gains. Figure 65 shows angles-of-arrival plots with antenna gains considered. The plot shows the effects of the antenna pointing.

SUMMARY OF PARAMETERS

Index	Description	Value
1.	Maximum number of wall reflections (integer)	4.000
2.	Distance between building walls (m)	24.000
3.	TX distance from left wall (m)	5.000
5.	TX height from street (m)	2.150
6.	RX distance from right wall (m)	5.000
8.	Minimum distance from TX to RX (m)	50.000
9.	Maximum distance from TX to RX (m)	950.000
10.	Step size in distance from TX to RX (m)	1.000
11.	RX height from street (m)	1.800
12.	Radio Frequency (GHz)	28.800
16.	TX ant. beamwidth (degrees)	30.000
17.	TX antenna gain (dB)	17.000
18.	TX ant. elevation angle (degrees)	0.000
22.	TX ant. azmuthal angle (left-neg., degrees)	0.000
26.	RX ant. beamwidth (degrees)	2.400
27.	RX antenna gain (dB)	17.000
28.	RX ant. elevation angle (degrees)	0.000
32.	RX ant. azmuthal angle (left-neg., degrees)	0.000
36.	Transmitter power (dBm)	18.500
38.	Loss for street reflection (dB)	1.000
39.	Loss for wall reflection (dB)	1.000
40.	Atmospheric Pressure (kPa)	83.000
41.	Relative Humidity (Percent)	50.000
42.	Temperature (Celsius)	20.000
43.	Are cross streets to be used (1=yes,0=no)	0.000
44.	Distance from TX to first cross street (m)	10.000
45.	Distance between cross streets (m)	76.000
46.	Width of cross street (m)	24.000
47.	Plot distribution: (0=no, 1=yes)	0.000
48.	Plot distribution separately: (0=no, 1=yes)	1.000
49.	Plot actual value: (0=no, 1=yes)	1.000
50.	Confidence interval (decimal)	0.900

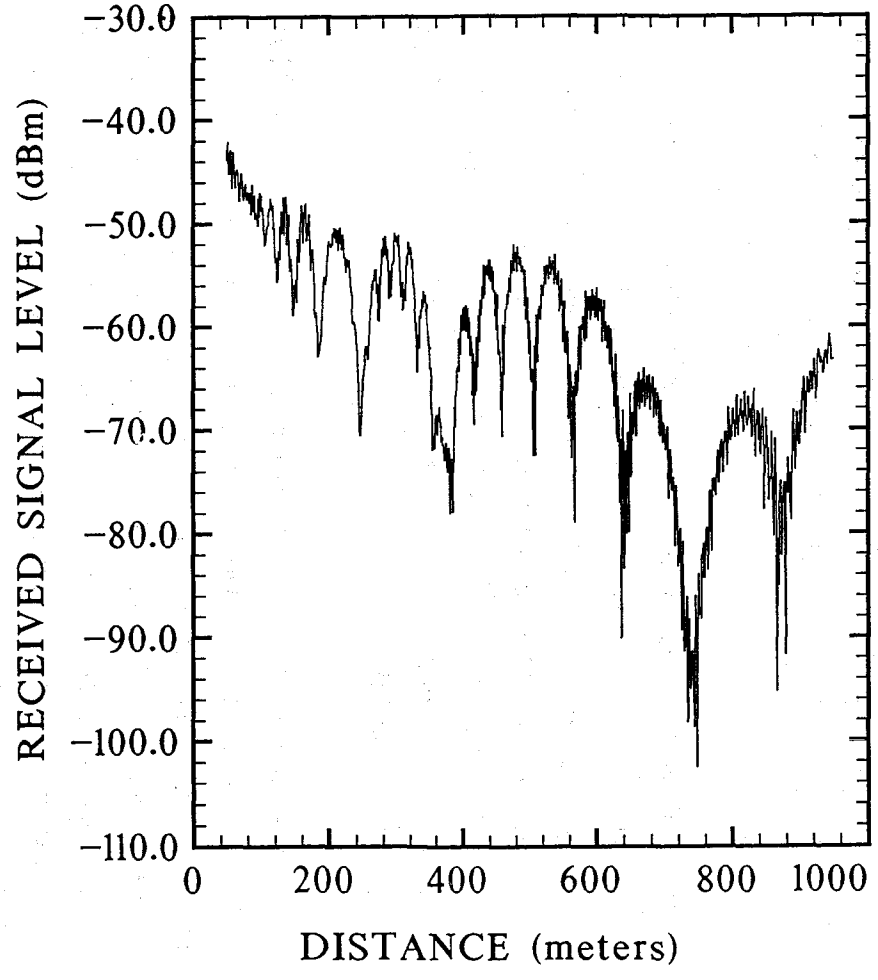

Figure 62. An example of range scan output with input parameter listing.

SUMMARY OF PARAMETERS

Index	Description	Value
1.	Maximum number of wall reflections (integer)	4.000
2.	Distance between building walls (m)	24.000
3.	TX distance from left wall (m)	5.000
5.	TX height from street (m)	2.150
6.	RX distance from right wall (m)	5.000
7.	RX distance from TX (m)	500.000
11.	RX height from street (m)	1.800
13.	Minimum radio frequency (GHz)	10.000
14.	Maximum radio frequency (GHz)	60.000
15.	Step in radio frequency (GHz)	0.100
16.	TX ant. beamwidth (degrees)	30.000
17.	TX antenna gain (dB)	17.000
18.	TX ant. elevation angle (degrees)	0.000
22.	TX ant. azmuthal angle (left-neg., degrees)	0.000
26.	RX ant. beamwidth (degrees)	2.400
27.	RX antenna gain (dB)	17.000
28.	RX ant. elevation angle (degrees)	0.000
32.	RX ant. azmuthal angle (left-neg., degrees)	0.000
36.	Transmitter power (dBm)	18.500
38.	Loss for street reflection (dB)	1.000
39.	Loss for wall reflection (dB)	1.000
40.	Atmospheric Pressure (kPa)	83.000
41.	Relative Humidity (Percent)	50.000
42.	Temperature (Celsius)	20.000
43.	Are cross streets to be used (1=yes,0=no)	0.000
44.	Distance from TX to first cross street (m)	10.000
45.	Distance between cross streets (m)	76.000
46.	Width of cross street (m)	24.000
47.	Plot distribution: (0=no, 1=yes)	0.000
48.	Plot distribution separately: (0=no, 1=yes)	1.000
49.	Plot actual value: (0=no, 1=yes)	1.000
50.	Confidence interval (decimal)	0.900

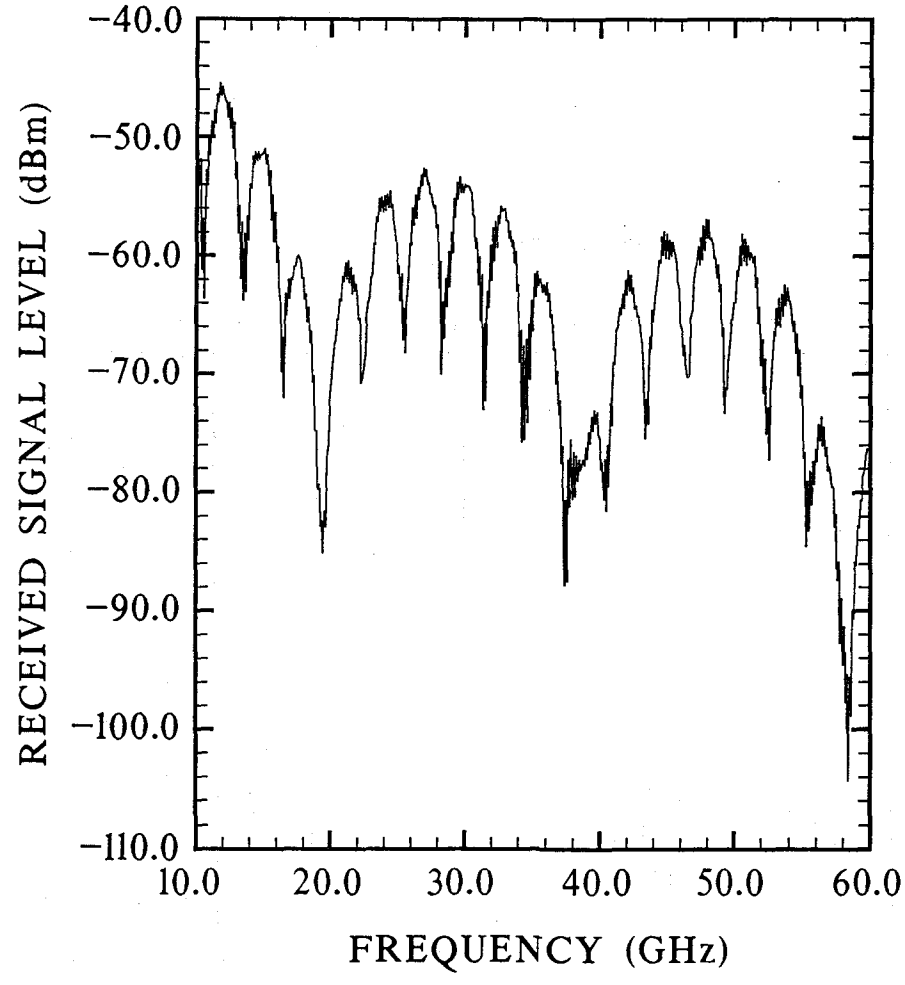

Figure 63. A plot of signal level vs. frequency and input parameter listing.

SUMMARY OF PARAMETERS

Index	Description	Value
1.	Maximum number of wall reflections (integer)	4.000
2.	Distance between building walls (m)	24.000
3.	TX distance from left wall (m)	5.000
5.	TX height from street (m)	2.150
6.	RX distance from right wall (m)	5.000
7.	RX distance from TX (m)	200.000
11.	RX height from street (m)	1.800
12.	Radio Frequency (GHz)	28.800
16.	TX ant. beamwidth (degrees)	30.000
17.	TX antenna gain (dB)	17.000
22.	TX ant. azmuthal angle (left-neg., degrees)	0.000
26.	RX ant. beamwidth (degrees)	2.400
27.	RX antenna gain (dB)	17.000
28.	RX ant. elevation angle (degrees)	0.000
29.	Minimum RX elevation angle (degrees)	-5.000
30.	Maximum RX elevation angle (degrees)	5.000
31.	Step size in RX elevation angle (degrees)	0.010
32.	RX ant. azmuthal angle (left-neg., degrees)	0.000
33.	Minimum RX azmuthal angle (degrees)	-30.000
34.	Maximum RX azmuthal angle (degrees)	30.000
35.	Step size in RX azmuthal angle (degrees)	0.100
36.	Transmitter power (dBm)	18.500
37.	Receiver noise figure (dB)	6.000
38.	Loss for street reflection (dB)	1.000
39.	Loss for wall reflection (dB)	1.000
40.	Atmospheric Pressure (kPa)	83.000
41.	Relative Humidity (Percent)	50.000
42.	Temperature (Celsius)	20.000
43.	Are cross streets to be used (1=yes,0=no)	0.000
44.	Distance from TX to first cross street (m)	10.000
45.	Distance between cross streets (m)	76.000
46.	Width of cross street (m)	24.000
47.	Plot distribution: (0=no, 1=yes)	0.000
48.	Plot distribution separately: (0=no, 1=yes)	0.000
49.	Plot actual value: (0=no, 1=yes)	1.000
50.	Confidence interval (decimal)	0.900

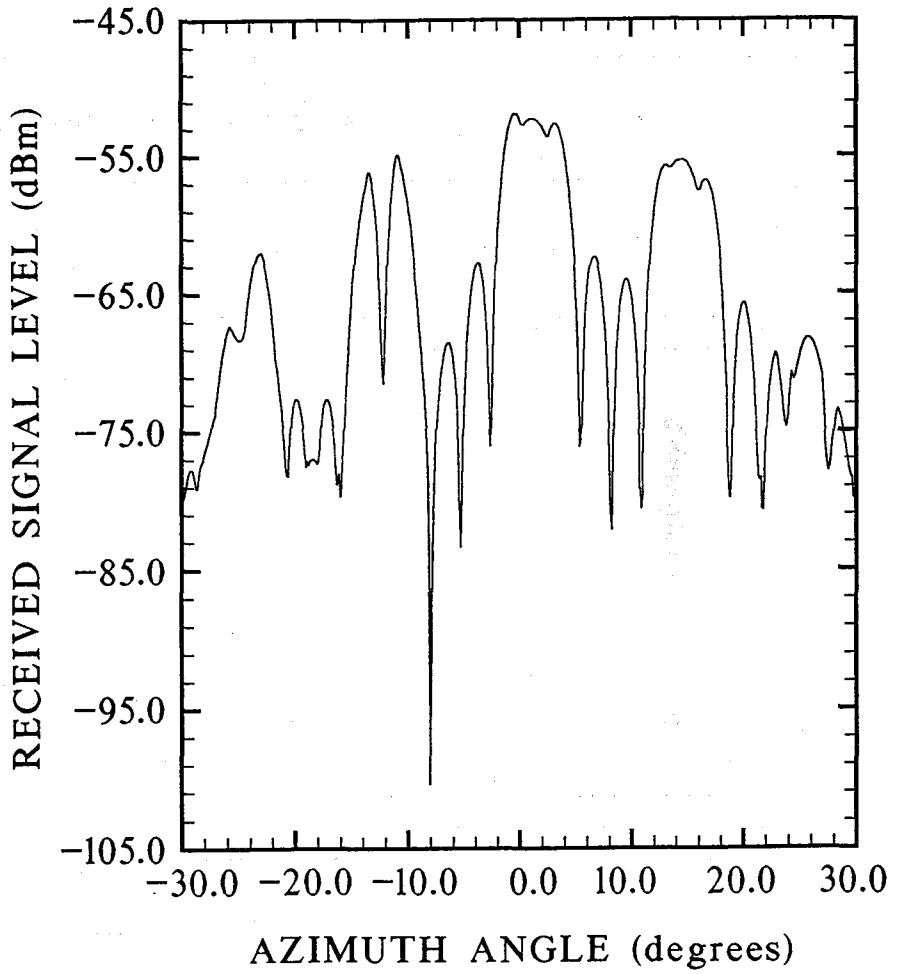

Figure 64. A plot of signal level vs. azimuth angle and input parameter listing.

SUMMARY OF PARAMETERS

Index	Description	Value
1.	Maximum number of wall reflections (integer)	4.000
2.	Distance between building walls (m)	24.000
3.	TX distance from left wall (m)	5.000
5.	TX height from street (m)	2.150
6.	RX distance from right wall (m)	5.000
7.	RX distance from TX (m)	200.000
11.	RX height from street (m)	1.800
12.	Radio Frequency (GHz)	28.800
16.	TX ant. beamwidth (degrees)	30.000
17.	TX antenna gain (dB)	17.000
22.	TX ant. azmuthal angle (left-neg., degrees)	0.000
26.	RX ant. beamwidth (degrees)	2.400
27.	RX antenna gain (dB)	17.000
28.	RX ant. elevation angle (degrees)	0.000
29.	Minimum RX elevation angle (degrees)	-5.000
30.	Maximum RX elevation angle (degrees)	5.000
31.	Step size in RX elevation angle (degrees)	0.010
32.	RX ant. azmuthal angle (left-neg., degrees)	0.000
33.	Minimum RX azmuthal angle (degrees)	-30.000
34.	Maximum RX azmuthal angle (degrees)	30.000
35.	Step size in RX azmuthal angle (degrees)	0.100
36.	Transmitter power (dBm)	18.500
37.	Receiver noise figure (dB)	6.000
38.	Loss for street reflection (dB)	1.000
39.	Loss for wall reflection (dB)	1.000
40.	Atmospheric Pressure (kPa)	83.000
41.	Relative Humidity (Percent)	50.000
42.	Temperature (Celsius)	20.000
43.	Are cross streets to be used (1=yes,0=no)	0.000
44.	Distance from TX to first cross street (m)	10.000
45.	Distance between cross streets (m)	100.000
46.	Width of cross street (m)	10.000
47.	Plot distribution: (0=no, 1=yes)	1.000
48.	Plot distribution separately: (0=no, 1=yes)	1.000
49.	Plot actual value: (0=no, 1=yes)	1.000
50.	Confidence interval (decimal)	0.900

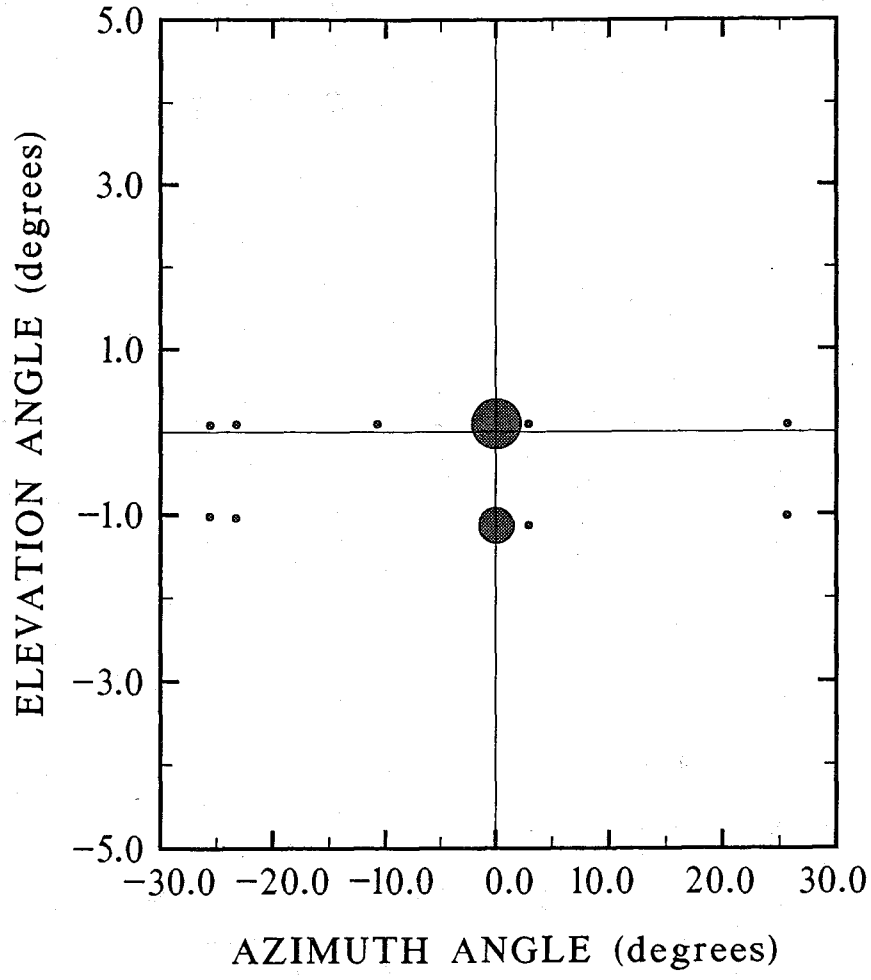

Figure 65. A plot showing angles of arrival data and the input parameter listing.

The angle-of-arrival plot can be used to improve antenna pointing. The plot indicates where to look for possible rays. Especially in the case of narrowbeam antennas, this information makes maximization of the received signal level possible as well as aiding in the avoidance of undesired delayed components. For example, if the ground-reflected ray destructively interferes with the line-of-sight ray, the plot provides information that helps align the antenna on a possibly stronger building-reflected ray.

Impulse Response

The impulse response mode plots the amplitude and delay time of the rays. The delay time of each ray is determined from the path length of the ray. The ray that arrives first appears at time zero. All other rays appear at the difference between its delay time and the delay time of the first ray (the line-of-sight ray). The computer plots the signal level relative to the strongest ray (the line-of-sight ray). The strongest ray has a signal level of 0 dB. Figure 66 shows an impulse response plot.

6.3 Parameter Dependence

As discussed in Section 6.2, for each of the six types of computer outputs, a set of parameter values must be specified. In this section, the outputs of the computer program model are examined for their dependence on some of the input parameters such as frequency, antenna beamwidth, etc. The selected outputs demonstrate the propagation effects of these parameters and a possible means to improve performance of a communication link in an urban environment.

6.3.1 Effect of Losses at Reflecting Surfaces

To demonstrate the effect of reflection losses, four range scans were chosen. In these scans, shown in Figure 67, the received signal level is plotted as a function of distance. The only values changed in this figure were the loss for street reflection (Index 38) and loss for wall reflection (Index 39). The summary of parameters for Figure 67(A) is shown in Figure 68. In Figure 68, the reflection loss values for both the street and the walls were set at 50 dB in order to effectively eliminate all reflection components from the street and the walls. With no reflections, only the direct component contributes to the received signal level displayed in Figure 67(A). The decreasing level with increasing distance results from free-space loss.

SUMMARY OF PARAMETERS

Index	Description	Value
1.	Maximum number of wall reflections (integer)	4.000
2.	Distance between building walls (m)	24.000
3.	TX distance from left wall (m)	5.000
5.	TX height from street (m)	2.150
6.	RX distance from right wall (m)	5.000
7.	RX distance from TX (m)	300.000
11.	RX height from street (m)	1.800
12.	Radio Frequency (GHz)	30.300
16.	TX ant. beamwidth (degrees)	30.000
17.	TX antenna gain (dB)	17.000
18.	TX ant. elevation angle (degrees)	0.000
22.	TX ant. azmuthal angle (left-neg., degrees)	0.000
26.	RX ant. beamwidth (degrees)	30.000
27.	RX antenna gain (dB)	17.000
28.	RX ant. elevation angle (degrees)	0.000
32.	RX ant. azmuthal angle (left-neg., degrees)	0.000
36.	Transmitter power (dBm)	18.500
37.	Receiver noise figure (dB)	6.000
38.	Loss for street reflection (dB)	1.000
39.	Loss for wall reflection (dB)	1.000
40.	Atmospheric Pressure (kPa)	83.000
41.	Relative Humidity (Percent)	50.000
42.	Temperature (Celsius)	20.000
43.	Are cross streets to be used (1=yes,0=no)	0.000
44.	Distance from TX to first cross street (m)	10.000
45.	Distance between cross streets (m)	76.000
46.	Width of cross street (m)	24.000

The line of sight ray is **** dBm.

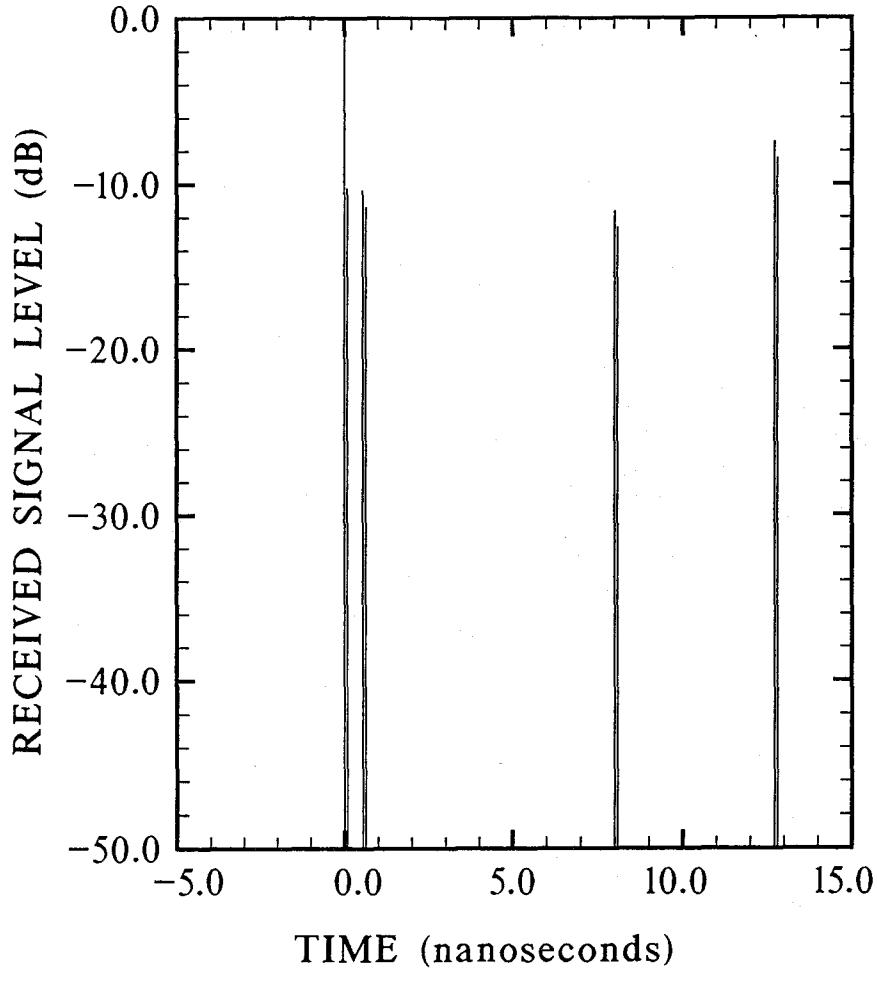

Figure 66. An impulse response plot and input parameter listing.

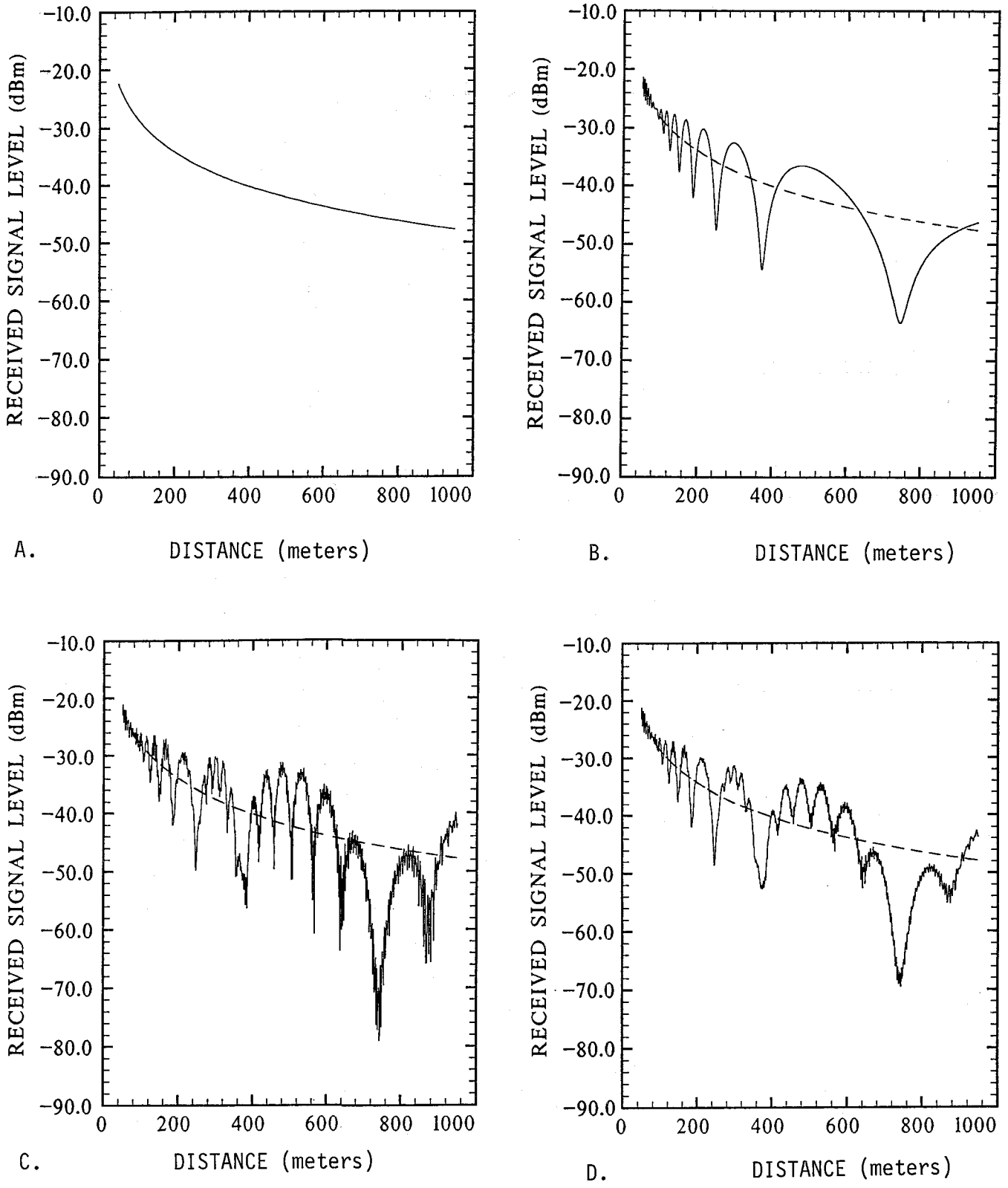

Figure 67. A set of four range scans showing received signal level as a function of distance.

SUMMARY OF PARAMETERS

Index	Description	Value
1.	Maximum number of wall reflections (integer)	3.000
2.	Distance between building walls (m)	24.000
3.	TX distance from left wall (m)	5.000
5.	TX height from street (m)	2.150
6.	RX distance from right wall (m)	5.000
8.	Minimum distance from TX to RX (m)	50.000
9.	Maximum distance from TX to RX (m)	950.000
10.	Step size in distance from TX to RX (m)	1.000
11.	RX height from street (m)	1.800
12.	Radio Frequency (GHz)	28.800
16.	TX ant. beamwidth (degrees)	30.000
17.	TX antenna gain (dB)	17.000
18.	TX ant. elevation angle (degrees)	0.000
22.	TX ant. azmuthal angle (left-neg., degrees)	0.000
26.	RX ant. beamwidth (degrees)	2.400
27.	RX antenna gain (dB)	38.000
28.	RX ant. elevation angle (degrees)	0.000
32.	RX ant. azmuthal angle (left-neg., degrees)	0.000
36.	Transmitter power (dBm)	18.500
38.	Loss for street reflection (dB)	50.000
39.	Loss for wall reflection (dB)	50.000
40.	Atmospheric Pressure (kPa)	83.000
41.	Relative Humidity (Percent)	50.000
42.	Temperature (Celsius)	20.000
43.	Are cross streets to be used (1=yes,0=no)	0.000
44.	Distance from TX to first cross street (m)	10.000
45.	Distance between cross streets (m)	76.000
46.	Width of cross street (m)	24.000
47.	Plot distribution: (0=no, 1=yes)	0.000
48.	Plot distribution separately: (0=no, 1=yes)	1.000
49.	Plot actual value: (0=no, 1=yes)	1.000
50.	Confidence interval (decimal)	0.900

Figure 68. The input parameter list for Figure 67A.

In Figure 67(B), Index 38 (loss for street reflection) was changed from 50 dB to 1 dB. This produced a strong street- (ground-) reflected component, which when mixed with the direct component shows a destructive/constructive interference pattern. The dashed line shows the superimposed direct component.

In Figure 67(C), Index 39 (loss for wall reflection) was also changed from 50 dB to 1 dB and the loss for street reflection remained at 1 dB. Now the received signal level is the combination of the direct component, the ground-reflected component, and several wall-reflected components resulting in even more rapid fading. The final pattern in this set, Figure 67(D), resulted from an increase in the wall-reflection loss to 6 dB. Realistic values for the street reflections are estimated to be between 0.5 and 3 dB and between 0.5 and 6 dB for wall reflections as judged from the measured data. Comparisons of measured data and model predicted ouptuts are presented in Section 6.4. As observed in Figure 68, the maximum number of wall reflections for these plots was set at three (Index 1).

6.3.2 Frequency Dependence

The received signal level as a function of frequency shown in Figure 69 was produced using the parameter values indicated in the summary. The losses for street reflection and wall reflection were both set at 50 dB. With these high reflection losses, only the direct component is received. The displayed curve between (5 and 80 GHz) results from the free-space loss factor (20 log ft). The additional signal loss centered at 60 GHz, which reaches a maximum of 6 dB for a 500 m path, is due to the oxygen absorption line. Perhaps a more realistic example of how signal level may depend on frequency is shown in Figure 70, where losses of 1 and 3 dB are used for street and wall reflections, respectively.

A second set of data is shown in Figure 71, also to emphasize the frequency dependence on the received signal. These displays are received signal level as a function of distance (range scans) at three discrete frequencies. These frequencies, 9.6, 28.8, and 57.6 GHz, were used in the measurements program and were also used in the comparison of measured versus model data in Section 6.4.

SUMMARY OF PARAMETERS

Index	Description	Value
1.	Maximum number of wall reflections (integer)	4.000
2.	Distance between building walls (m)	24.000
3.	TX distance from left wall (m)	5.000
5.	TX height from street (m)	2.150
6.	RX distance from right wall (m)	5.000
7.	RX distance from TX (m)	500.000
11.	RX height from street (m)	1.800
13.	Minimum radio frequency (GHz)	5.000
14.	Maximum radio frequency (GHz)	80.000
15.	Step in radio frequency (GHz)	0.100
16.	TX ant. beamwidth (degrees)	30.000
17.	TX antenna gain (dB)	17.000
18.	TX ant. elevation angle (degrees)	0.000
22.	TX ant. azmuthal angle (left-neg., degrees)	0.000
26.	RX ant. beamwidth (degrees)	2.400
27.	RX antenna gain (dB)	38.000
28.	RX ant. elevation angle (degrees)	0.000
32.	RX ant. azmuthal angle (left-neg., degrees)	0.000
36.	Transmitter power (dBm)	18.500
38.	Loss for street reflection (dB)	50.000
39.	Loss for wall reflection (dB)	50.000
40.	Atmospheric Pressure (kPa)	83.000
41.	Relative Humidity (Percent)	50.000
42.	Temperature (Celsius)	20.000
43.	Are cross streets to be used (1=yes,0=no)	0.000
44.	Distance from TX to first cross street (m)	10.000
45.	Distance between cross streets (m)	76.000
46.	Width of cross street (m)	24.000
47.	Plot distribution: (0=no, 1=yes)	0.000
48.	Plot distribution separately: (0=no, 1=yes)	1.000
49.	Plot actual value: (0=no, 1=yes)	1.000
50.	Confidence interval (decimal)	0.900

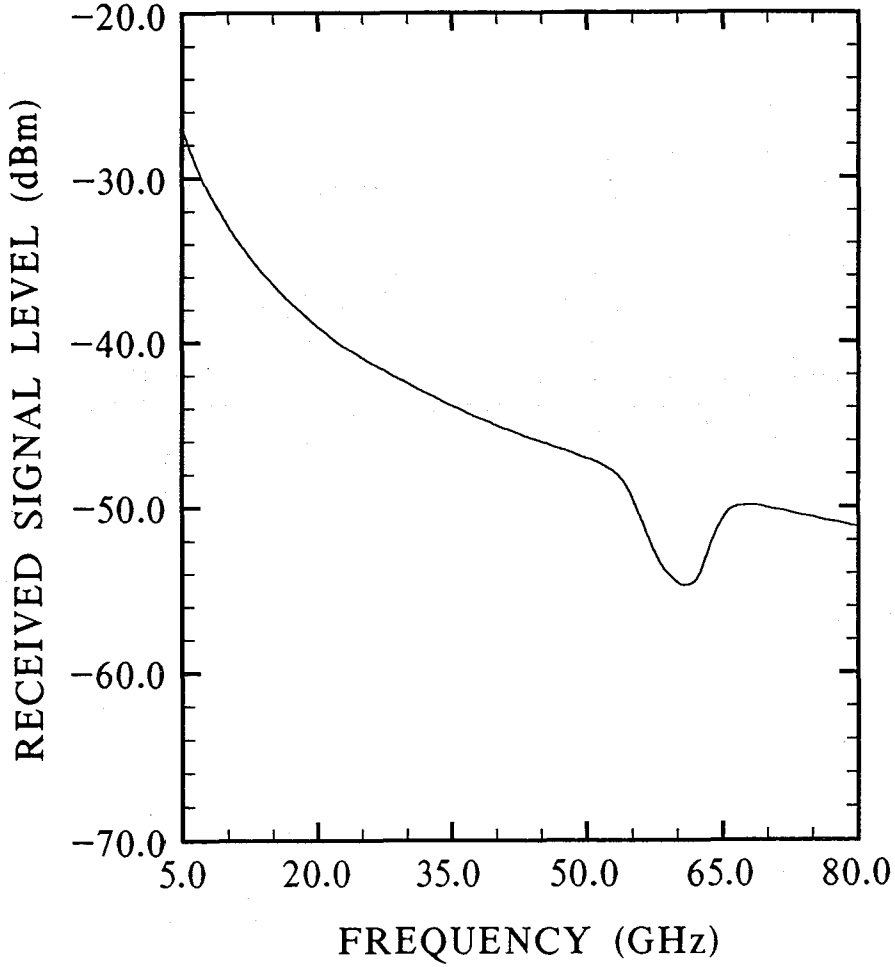

Figure 69. Received signal level as a function of frequency and the input parameter list.

SUMMARY OF PARAMETERS

Index	Description	Value
1.	Maximum number of wall reflections (integer)	4.000
2.	Distance between building walls (m)	24.000
3.	TX distance from left wall (m)	5.000
5.	TX height from street (m)	2.150
6.	RX distance from right wall (m)	5.000
7.	RX distance from TX (m)	500.000
11.	RX height from street (m)	1.800
13.	Minimum radio frequency (GHz)	10.000
14.	Maximum radio frequency (GHz)	60.000
15.	Step in radio frequency (GHz)	0.100
16.	TX ant. beamwidth (degrees)	30.000
17.	TX antenna gain (dB)	17.000
18.	TX ant. elevation angle (degrees)	0.000
22.	TX ant. azmuthal angle (left-neg., degrees)	0.000
26.	RX ant. beamwidth (degrees)	2.400
27.	RX antenna gain (dB)	38.000
28.	RX ant. elevation angle (degrees)	0.000
32.	RX ant. azmuthal angle (left-neg., degrees)	0.000
36.	Transmitter power (dBm)	18.500
38.	Loss for street reflection (dB)	1.000
39.	Loss for wall reflection (dB)	3.000
40.	Atmospheric Pressure (kPa)	83.000
41.	Relative Humidity (Percent)	50.000
42.	Temperature (Celsius)	20.000
43.	Are cross streets to be used (1=yes,0=no)	0.000
44.	Distance from TX to first cross street (m)	10.000
45.	Distance between cross streets (m)	76.000
46.	Width of cross street (m)	24.000
47.	Plot distribution: (0=no, 1=yes)	0.000
48.	Plot distribution separately: (0=no, 1=yes)	1.000
49.	Plot actual value: (0=no, 1=yes)	1.000
50.	Confidence interval (decimal)	0.900

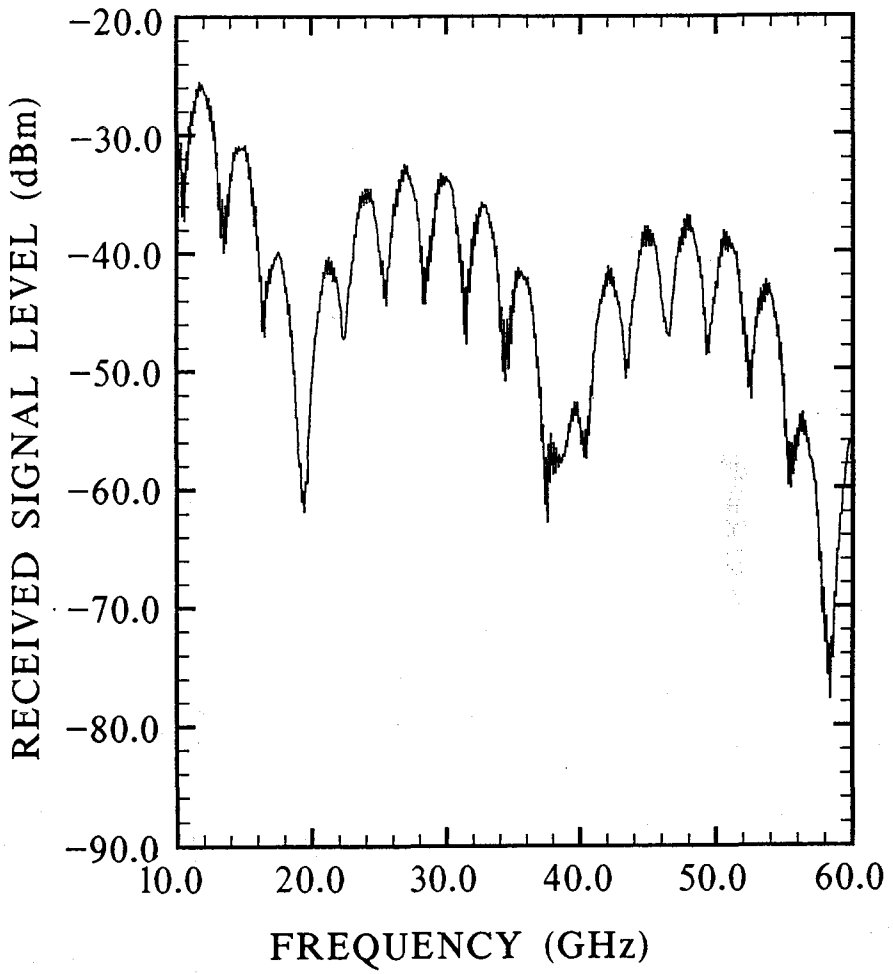

Figure 70. A second data set showing received signal level as a function of frequency and input parameter list.

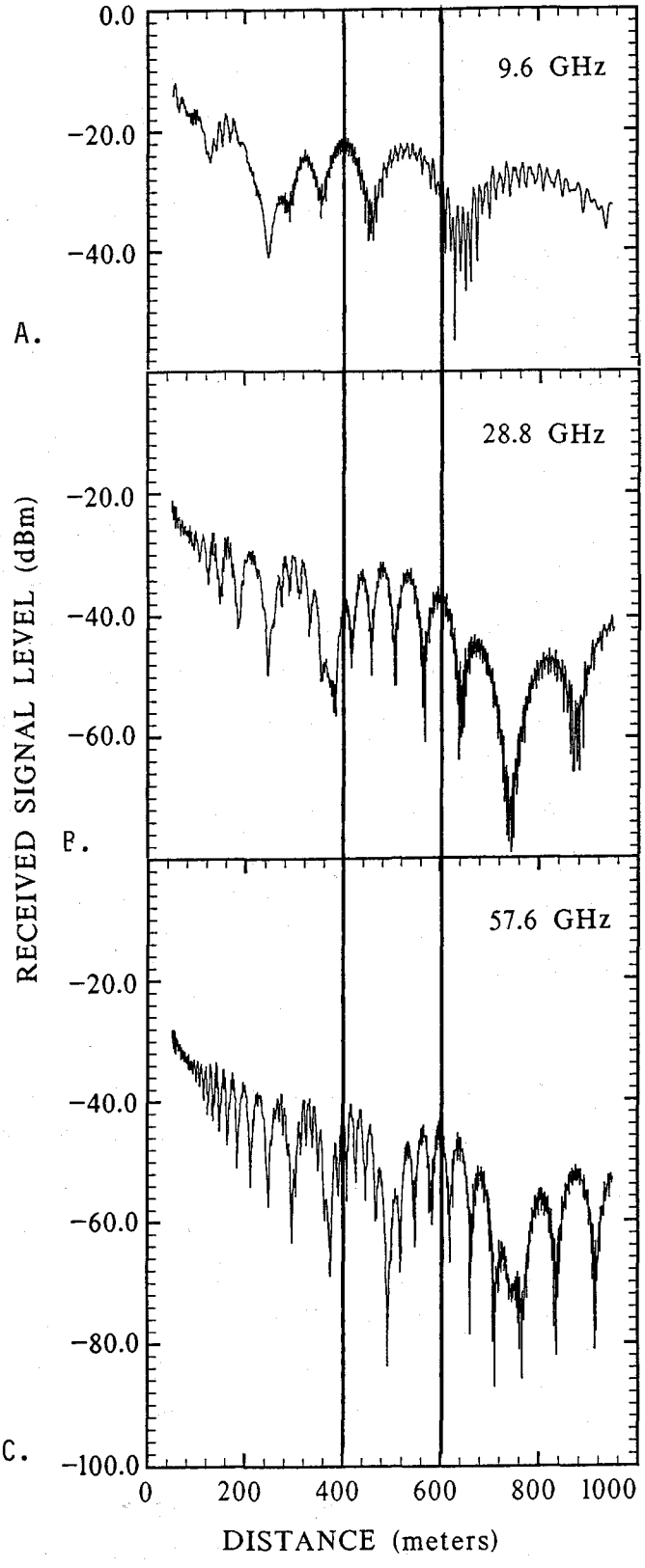

Figure 71. Received signal levels as a function of distance.

A first observation is that the number of fades per unit length of path increases with frequency. This is understandable since the rate of change of the relative phases of the different rays is proportional to frequency (inversely proportional to wavelength).

A summary of the input parameter values used for Figure 71(A) is given in Figure 72. Only the operating frequency was changed for Figures 71(B) and 71(C).

6.3.3 Beamwidth Dependence

The beamwidth affects the signal by determining the antenna illumination at the transmitter and receiver.

Outputs produced to demonstrate the effect of antenna beamwidth are shown in Figure 73. For comparison, to emphasize the effect of antenna beamwidth, the data in Figure 73(B) were produced by changing only the receiving antenna beamwidth from 2.4° to 30° and the receiving antenna gain from 38 dB to 17 dB. Two effects are observed from these figures. The first is the change in received signal level because of the 21-dB gain difference. The second effect is the increased number of wall reflected components in Figure 73(B) as indicated by the rapid signal changes along with deep fades and strong enhancements. The ground reflected component is essentially unchanged by the change in receiving antenna beamwidth.

6.3.4 Path Geometries

The parameters that affect path geometries are street width, street intersections, the position of the transmitter and receiver in the street, and the height of the antennas above ground. The data in Figure 74 demonstrate the effect of the relative positions of the transmitter and receiver in the street as indicated in the adjacent drawings. The summary of parameter values for Figure 74(A) is given in Figure 75. The signal in Figure 74(A) is a composite of the direct component, the ground-reflected component, and wall-reflected components from the near side of the street. In Figure 74(B) the wall reflected components are decreased because of the very narrowbeam antenna used at the receiver. The signal in Figure 74(C) is a combination of ground-reflected and wall-reflected components, plus an attenuated direct component because of the of misalignment of the antennas. As indicated in the drawings, the antennas are pointed parallel to the street.

SUMMARY OF PARAMETERS

Index	Description	Value
1.	Maximum number of wall reflections (integer)	3.000
2.	Distance between building walls (m)	24.000
3.	TX distance from left wall (m)	5.000
5.	TX height from street (m)	2.150
6.	RX distance from right wall (m)	5.000
8.	Minimum distance from TX to RX (m)	50.000
9.	Maximum distance from TX to RX (m)	950.000
10.	Step size in distance from TX to RX (m)	1.000
11.	RX height from street (m)	1.800
12.	Radio Frequency (GHz)	9.600
16.	TX ant. beamwidth (degrees)	30.000
17.	TX antenna gain (dB)	17.000
18.	TX ant. elevation angle (degrees)	0.000
22.	TX ant. azmuthal angle (left-neg., degrees)	0.000
26.	RX ant. beamwidth (degrees)	2.400
27.	RX antenna gain (dB)	38.000
28.	RX ant. elevation angle (degrees)	0.000
32.	RX ant. azmuthal angle (left-neg., degrees)	0.000
36.	Transmitter power (dBm)	18.500
38.	Loss for street reflection (dB)	1.000
39.	Loss for wall reflection (dB)	1.000
40.	Atmospheric Pressure (kPa)	83.000
41.	Relative Humidity (Percent)	50.000
42.	Temperature (Celsius)	20.000
43.	Are cross streets to be used (1=yes,0=no)	0.000
44.	Distance from TX to first cross street (m)	10.000
45.	Distance between cross streets (m)	76.000
46.	Width of cross street (m)	24.000
47.	Plot distribution: (0=no, 1=yes)	0.000
48.	Plot distribution separately: (0=no, 1=yes)	1.000
49.	Plot actual value: (0=no, 1=yes)	1.000
50.	Confidence interval (decimal)	0.900

Figure 72. Computer input parameter list for Figure 71A.

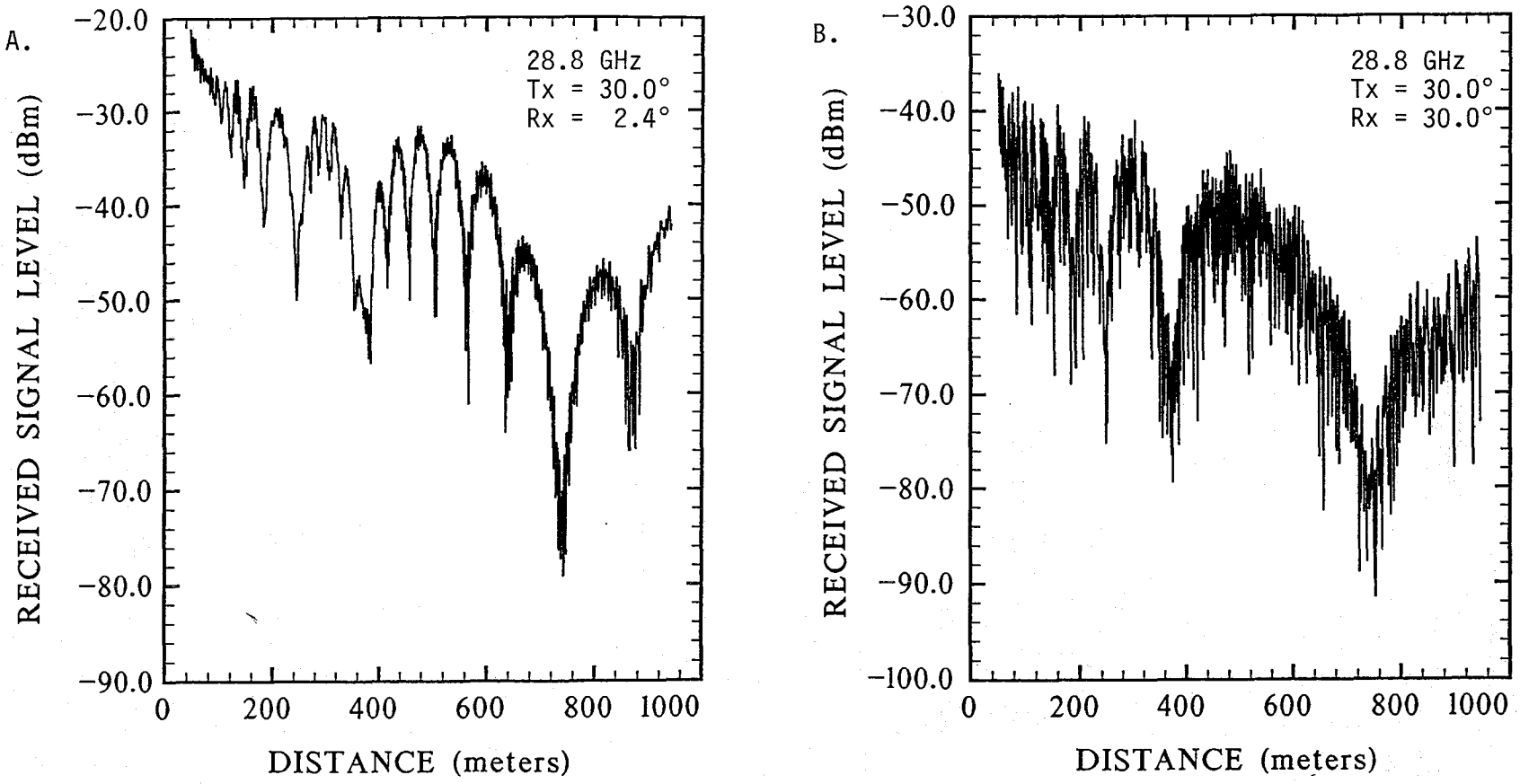

Figure 73. Range scan data to show the effect of antenna beamwidth.

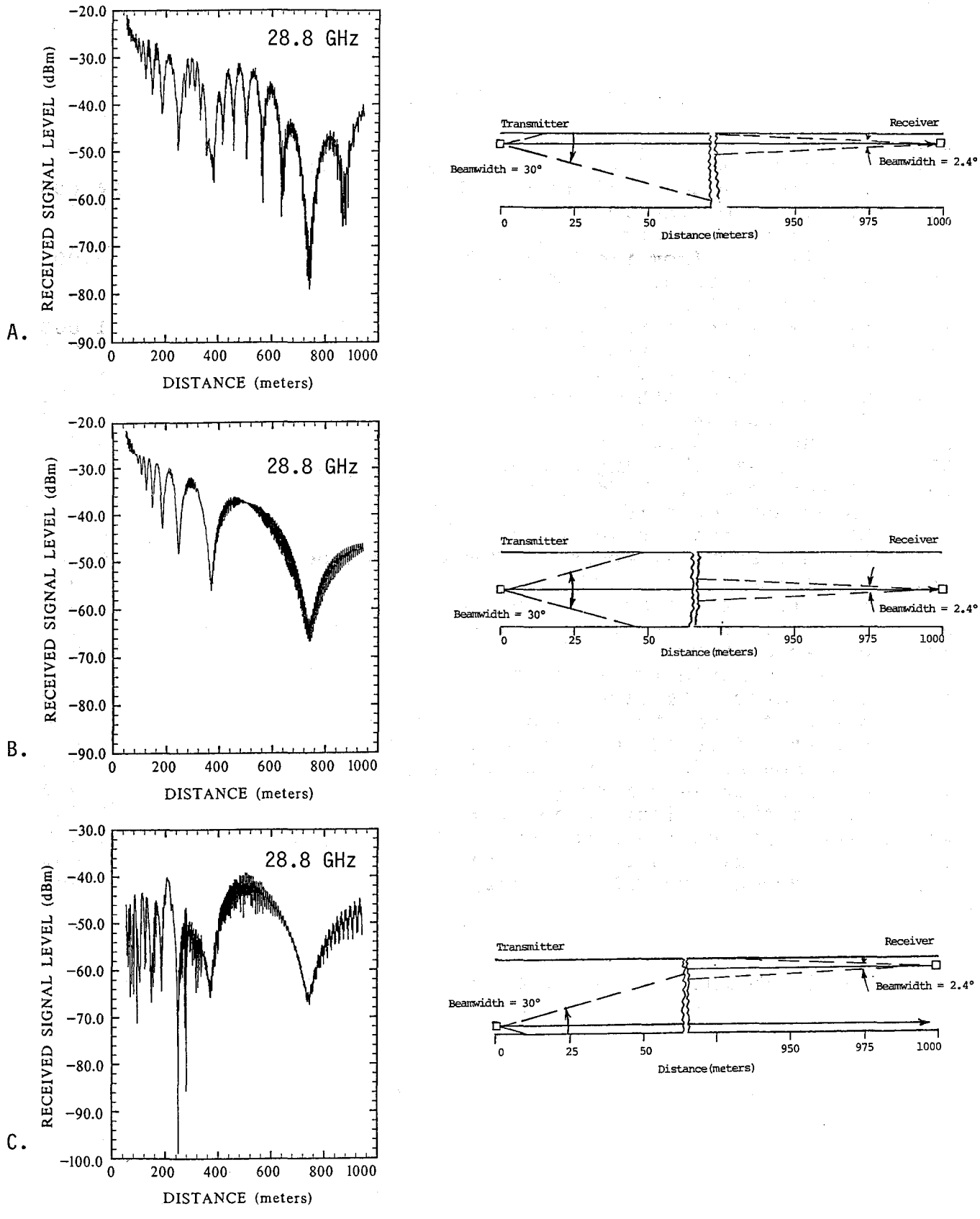

Figure 74. Range scans to demonstrate the effect of the relative position of the transmitter and receiver in the street (transmitter beamwidth is 30°, receiver beamwidth is 2.4°).

SUMMARY OF PARAMETERS

Index	Description	Value
1.	Maximum number of wall reflections (integer)	3.000
2.	Distance between building walls (m)	24.000
3.	TX distance from left wall (m)	5.000
5.	TX height from street (m)	2.150
6.	RX distance from right wall (m)	5.000
8.	Minimum distance from TX to RX (m)	50.000
9.	Maximum distance from TX to RX (m)	950.000
10.	Step size in distance from TX to RX (m)	1.000
11.	RX height from street (m)	1.800
12.	Radio Frequency (GHz)	28.800
16.	TX ant. beamwidth (degrees)	30.000
17.	TX antenna gain (dB)	17.000
18.	TX ant. elevation angle (degrees)	0.000
22.	TX ant. azmuthal angle (left-neg., degrees)	0.000
26.	RX ant. beamwidth (degrees)	30.000
27.	RX antenna gain (dB)	17.000
28.	RX ant. elevation angle (degrees)	0.000
32.	RX ant. azmuthal angle (left-neg., degrees)	0.000
36.	Transmitter power (dBm)	18.500
38.	Loss for street reflection (dB)	1.000
39.	Loss for wall reflection (dB)	1.000
40.	Atmospheric Pressure (kPa)	83.000
41.	Relative Humidity (Percent)	50.000
42.	Temperature (Celsius)	20.000
43.	Are cross streets to be used (1=yes,0=no)	0.000
44.	Distance from TX to first cross street (m)	10.000
45.	Distance between cross streets (m)	76.000
46.	Width of cross street (m)	24.000
47.	Plot distribution: (0=no, 1=yes)	0.000
48.	Plot distribution separately: (0=no, 1=yes)	1.000
49.	Plot actual value: (0=no, 1=yes)	1.000
50.	Confidence interval (decimal)	0.900

Figure 75. Computer program parameter values used to generate Figure 74A.

The parameter values in Figures 76(A), (B), and (C) are identical to Figures 74(A), (B), and (C), with the exception of the receiver beamwidth. For these figures, the receiver beamwidth is increased to 6°. The signal levels in Figure 76 are similar to the signal levels for corresponding terminal positions in Figure 74, except that the reflected components are stronger. Again in Figure 77, the only parameter change is to increase the receiver beamwidth from 6° to 30°. Now the strong, wall-reflected components are very numerous. The effect of terminal positions is still evident in these figures.

The traces in Figures 74, 76, and 77 were all run with no cross streets included. The data in Figure 78 are presented to show the effect of cross streets on the received signal level as a function of path distance. Figures 78(A) and (C) are duplicates of Figures 77(A) and (B). Figures 78(B) and (D) are the same as Figures 78(A) and (C) except that cross streets are present (Index 43). A point to remember is that only the wall-reflected components are affected by the presence of cross streets. Only slight differences are observed between the two fading patterns in Figure 78(A) (without cross streets) and Figure 78(B) (with cross streets). This result is due to the non-symmetry of the terminals relative to the side of the street. Contrasting results are seen in Figures 78(C) and (D), where perfect street symmetry exists by placing the terminals in the middle of the street. Comparing Figure 78(D) to 78(C) shows that for several distance intervals all wall-reflected components are lost at the cross street intersections. Figure 78d is an example of how the loss of rays down side streets gives unrealistic results.

6.4 Measured Results vs. Model Predictions

Extensive measurements of propagated millimeter-wave signals in urban and rural areas are reported in the earlier sections of this report. In this section, for line-of-sight paths, comparisons are made between the measured results and model predictions where the model parameters are chosen to best match the actual measurement conditions. These data are presented as sets for comparison.

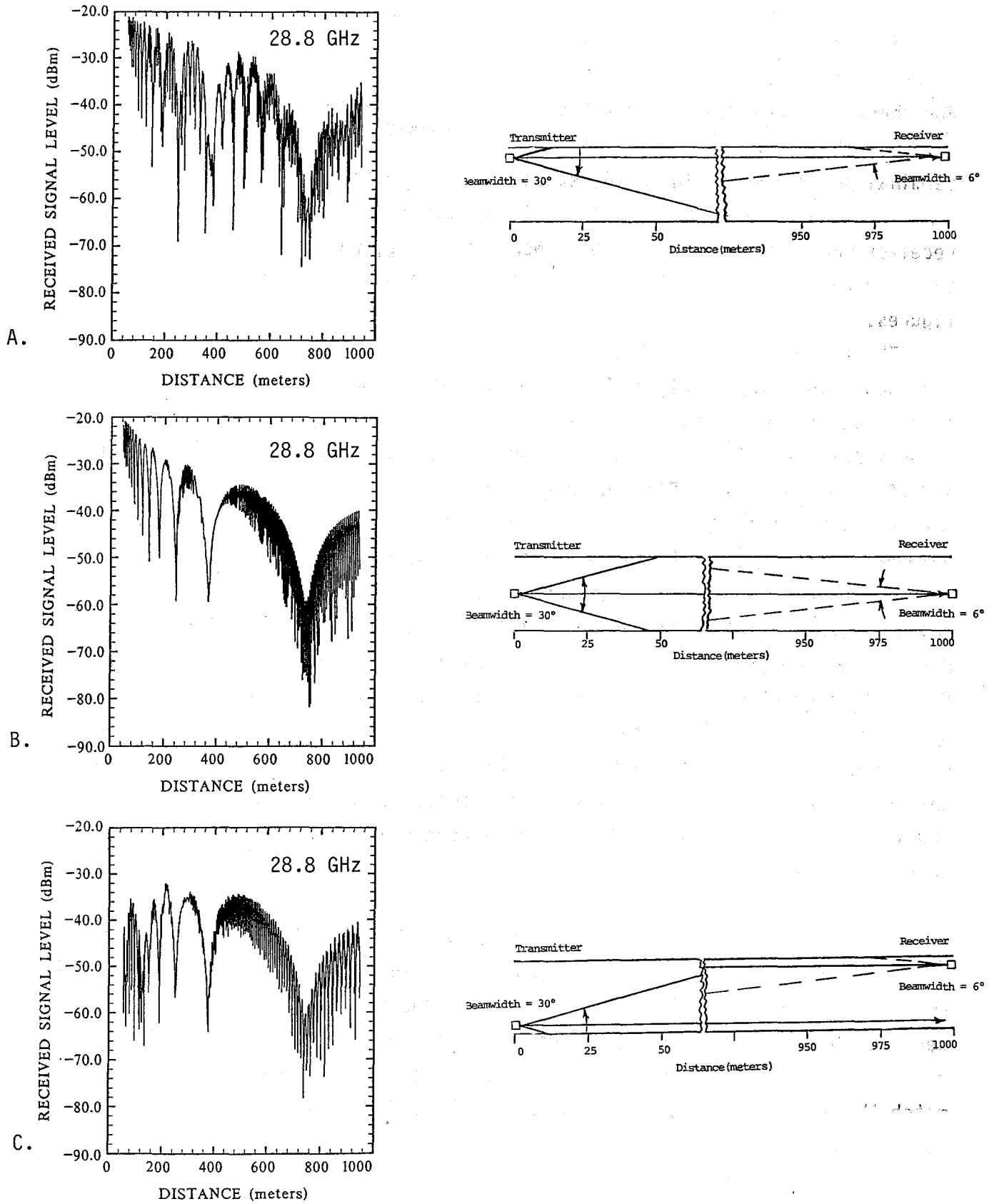

Figure 76. Range scans to demonstrate the effect of the relative position of the transmitter and receiver in the street (transmitter beamwidth is 30°, receiver beamwidth is 6°).

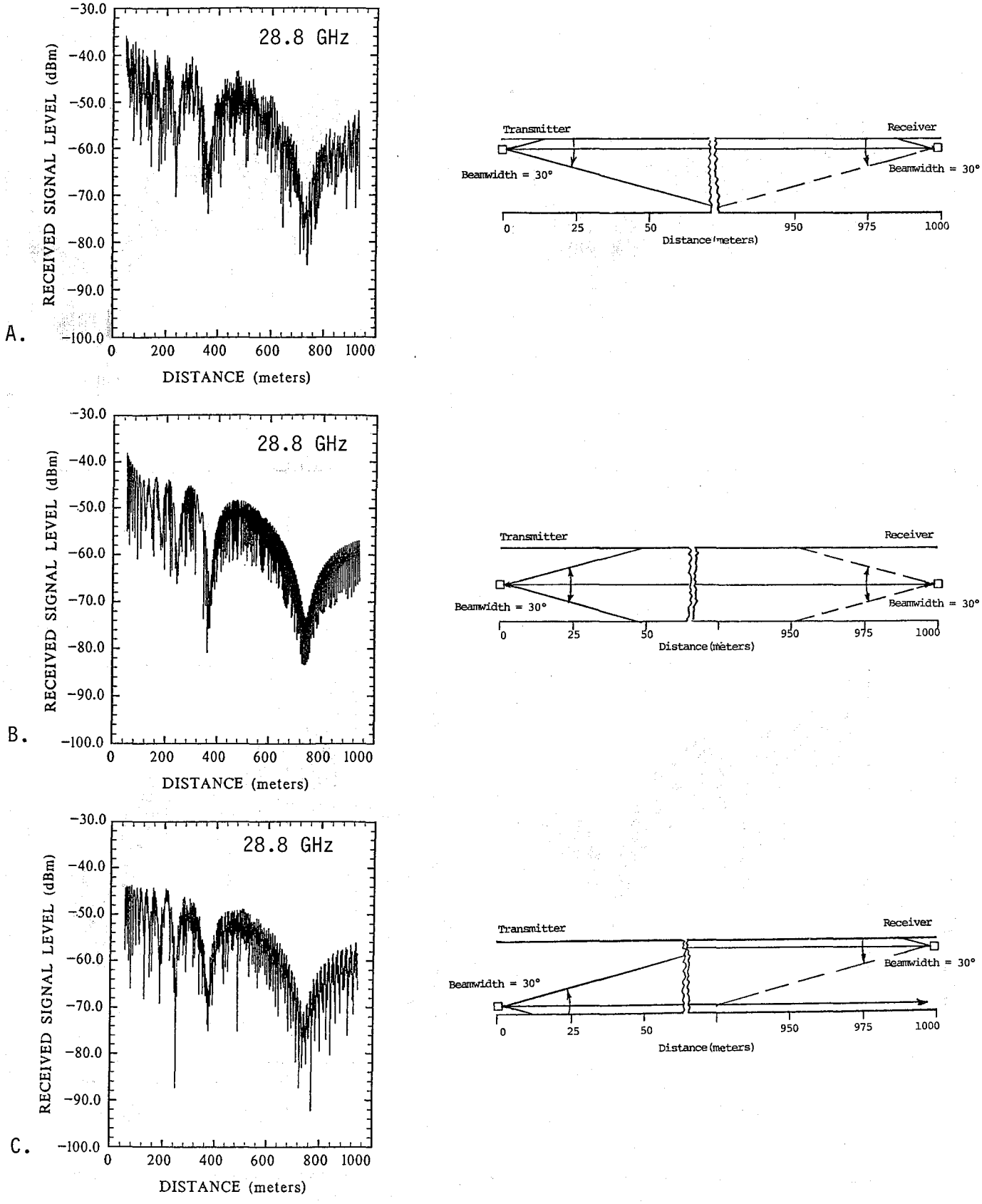

Figure 77. Range scans to demonstrate the effect of the relative position of the transmitter and receiver in the street (transmitter beamwidth = 30°, receiver beamwidth = 30°).

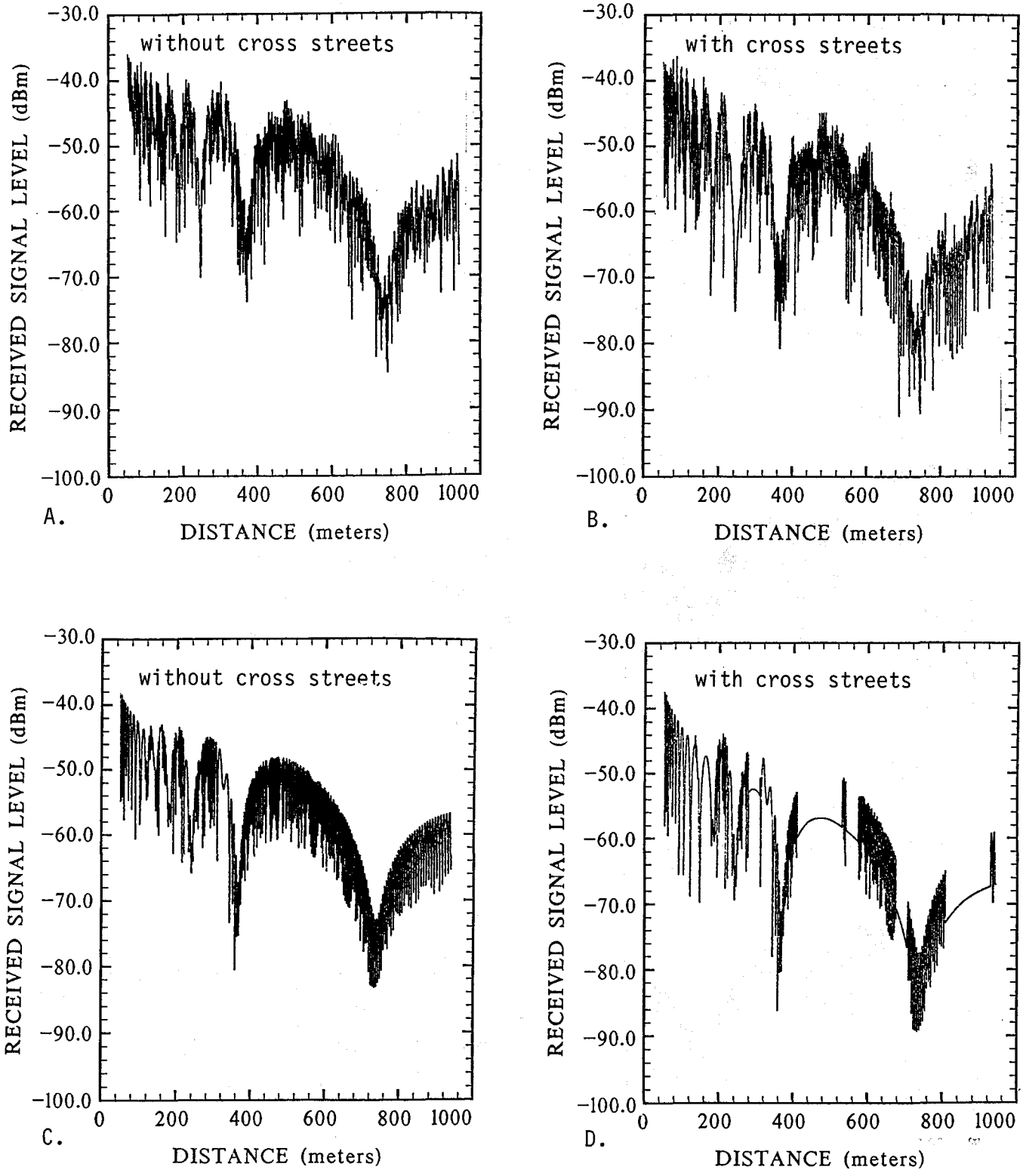

Figure 78. Range scans to show the effect of cross streets on the received signal as a function of distance (28.8 GHz).

6.4.1 Range Scans

The data set on the left side in Figure 79 shows measured results recorded at 9.6, 28.8, and 57.6 GHz on a nearly flat asphalt road in a rural area. The transmitting antennas had a 10° beamwidth and were 2.15 m above the road surface and the receiver antennas were 4.8°, 1.2°, and 1.2° respectively at 9.6, 28.8, and 57.6 GHz and were 3.25 m above the road surface. The data on the right side are predicted results for each frequency and were obtained by selecting model parameters to match the operating conditions for the measured data. The table of parameter values used for the three frequencies are listed in Figure 80. To simulate an open road with no structures at the sides of the road, the loss for wall reflections was set at 50 dB (Index 39) and there are no cross streets (Index 43).

In general, the measured and predicted data compare quite well at each frequency, remembering that the model assumes a perfectly flat, uniform, reflecting road surface and that the antennas are always aligned parallel to the road at their respective heights, whereas for the measurements, the road was not perfectly flat nor was the reflecting surface necessarily uniform. The signal roll-off on the 28.8-GHz and 57.6-GHz traces at short distances occurs because with antennas at different heights and receiving antenna beamwidths of only 1.2° the on-line pointing is not maintained as the vehicles separation is shortened.

The second set of rural area data is shown in Figure 81. The measurement conditions for this set were identical to the set in Figure 79, except that the receiving antennas were 1.00 m above ground instead of 3.25 m. Again, the general shape of the traces agree, but there are fewer fades in Figure 81.

The measured results in Figure 82 are from runs along 17th Street in Denver (urban area) using a medium beamwidth antenna (10°) at the transmitters and a narrow beamwidth (4.8°) receiving antenna at 9.6 GHz. The operating conditions were similar (antenna beamwidth and antenna heights) to those in Figure 81. The actual difference was the presence of the buildings and cross streets in Denver as opposed to the open fields of the rural area. To model an urban street setting, the parameter values for the three runs in Figure 82 were chosen as indicated in Figure 83. The street dimensions were selected to match the physical size of 17th Street and the cross streets. The loss for wall reflection was set at 6 dB to produce a match with the measured data. The measured and predicted data are paired in Figure 82. The set at the top

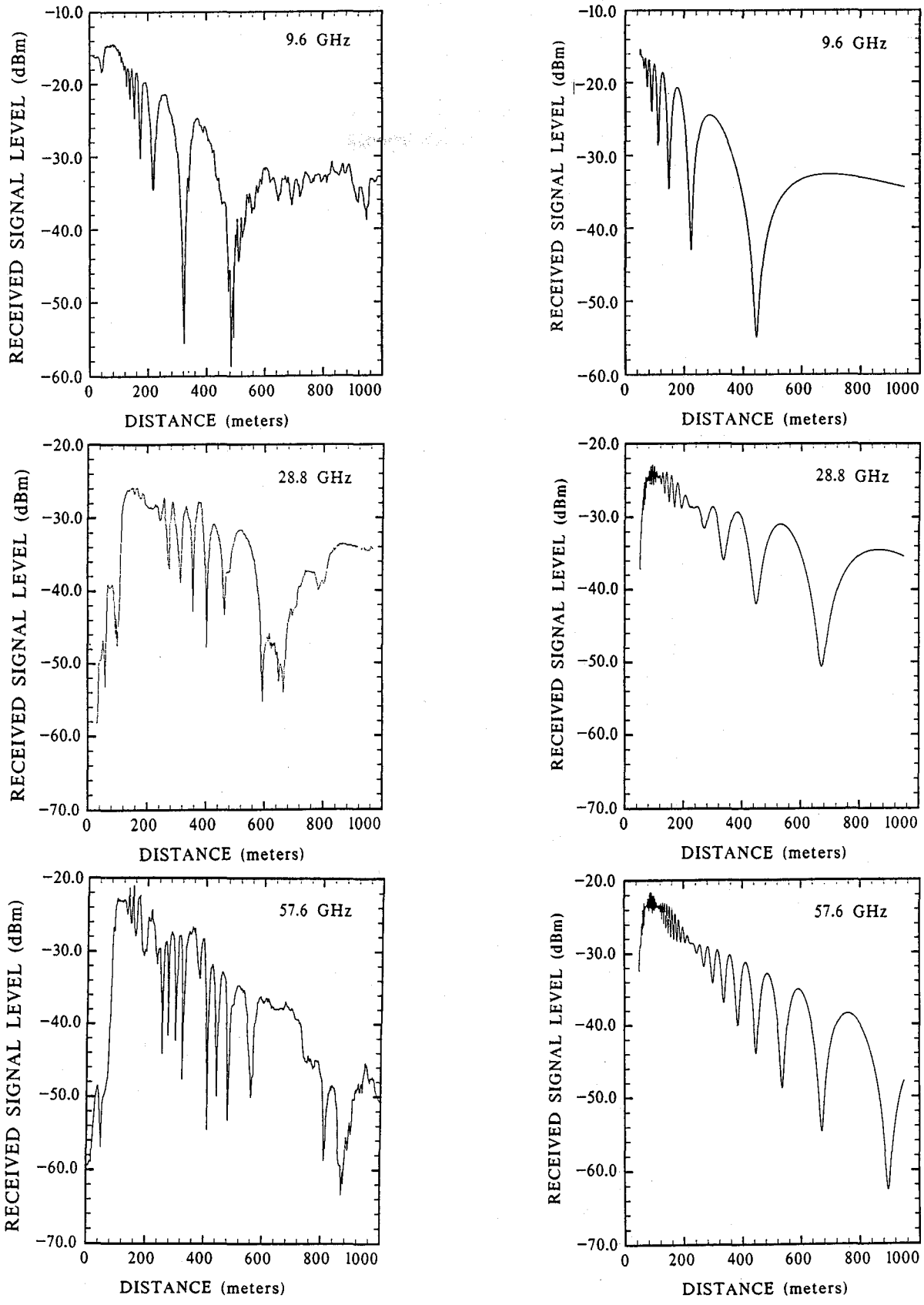

Figure 79. Range scan data sets to compare measured results (left side) with the computer model predictions (right side). Rural area (transmitter height = 2.15 m, receiver height = 3.25 m).

SUMMARY OF PARAMETERS

Index	Description	Value	Value	Value
1.	Maximum number of wall reflections (integer)	4.000	4.000	4.000
2.	Distance between building walls (m)	24.000	24.000	24.000
3.	TX distance from left wall (m)	12.000	12.000	12.000
5.	TX height from street (m)	2.150	2.150	2.150
6.	RX distance from right wall (m)	12.000	12.000	12.000
8.	Minimum distance from TX to RX (m)	50.000	50.000	50.000
9.	Maximum distance from TX to RX (m)	950.000	950.000	950.000
10.	Step size in distance from TX to RX (m)	1.000	1.000	1.000
11.	RX height from street (m)	3.250	3.250	3.250
12.	Radio Frequency (GHz)	9.600	28.800	57.600
16.	TX ant. beamwidth (degrees)	10.000	10.000	10.000
17.	TX antenna gain (dB)	25.000	25.000	25.000
18.	TX ant. elevation angle (degrees)	0.000	0.000	0.000
22.	TX ant. azmuthal angle (left-neg., degrees)	0.000	0.000	0.000
26.	RX ant. beamwidth (degrees)	4.800	1.200	1.200
27.	RX antenna gain (dB)	31.000	42.800	43.100
28.	RX ant. elevation angle (degrees)	0.000	0.000	0.000
32.	RX ant. azmuthal angle (left-neg., degrees)	0.000	0.000	0.000
36.	Transmitter power (dBm)	15.500	13.000	20.800
38.	Loss for street reflection (dB)	0.500	0.500	0.500
39.	Loss for wall reflection (dB)	50.000	50.000	50.000
40.	Atmospheric Pressure (kPa)	83.000	83.000	83.000
41.	Relative Humidity (Percent)	50.000	50.000	50.000
42.	Temperature (Celsius)	20.000	20.000	20.000
43.	Are cross streets to be used (1=yes,0=no)	0.000	0.000	0.000
44.	Distance from TX to first cross street (m)	10.000	10.000	10.000
45.	Distance between cross streets (m)	76.000	76.000	76.000
46.	Width of cross street (m)	24.000	24.000	24.000
47.	Plot distribution: (0=no, 1=yes)	0.000	0.000	0.000
48.	Plot distribution separately: (0=no, 1=yes)	1.000	1.000	1.000
49.	Plot actual value: (0=no, 1=yes)	1.000	1.000	1.000
50.	Confidence interval (decimal)	0.900	0.900	0.900

Figure 80. Computer model parameter values for the three frequencies used in Figure 79.

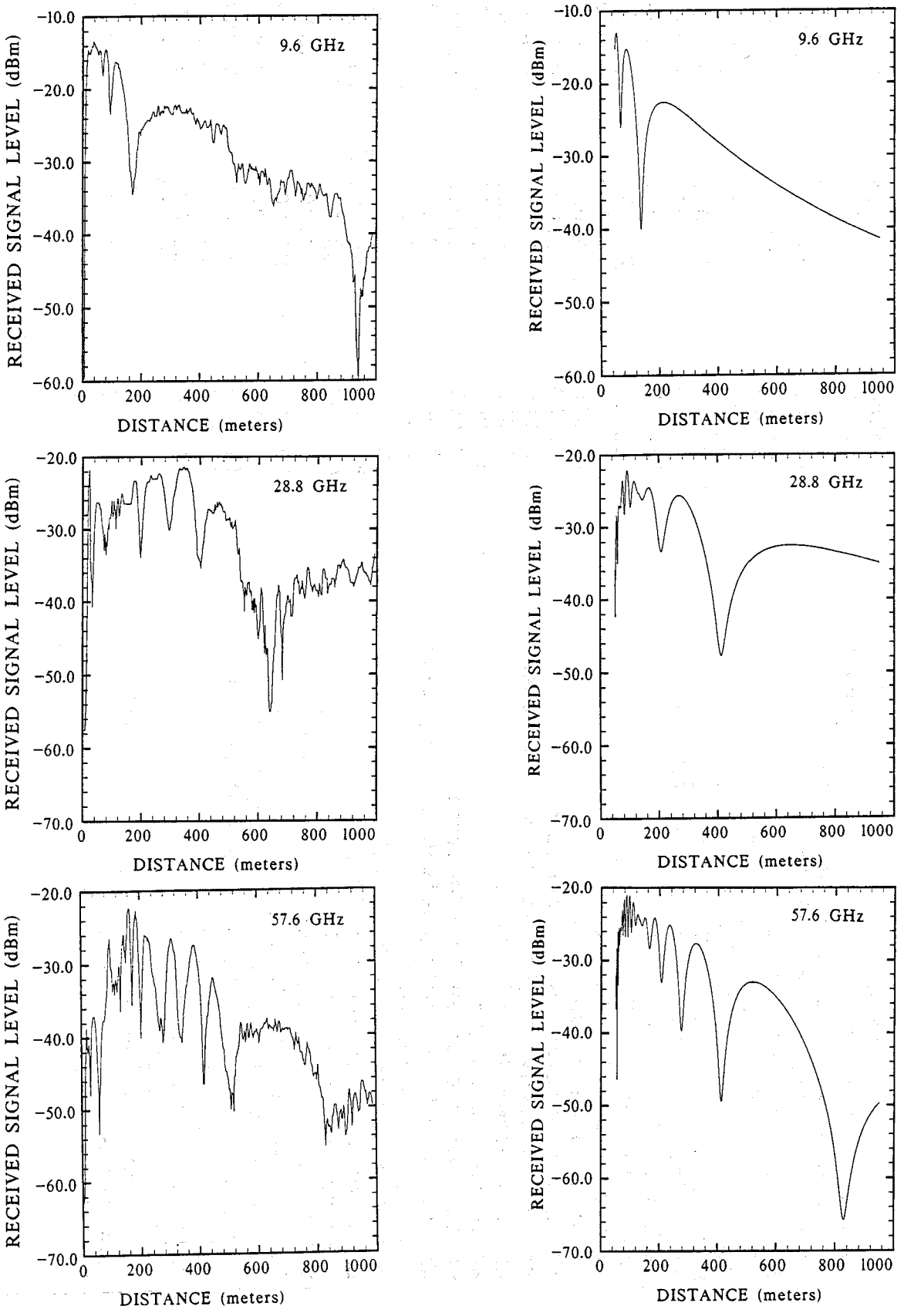

Figure 81. Range scan data sets to compare measured results (left side) with the computer model predictions (right side). Rural area (transmitter height = 2.15 m, receiver height = 1.00 m).

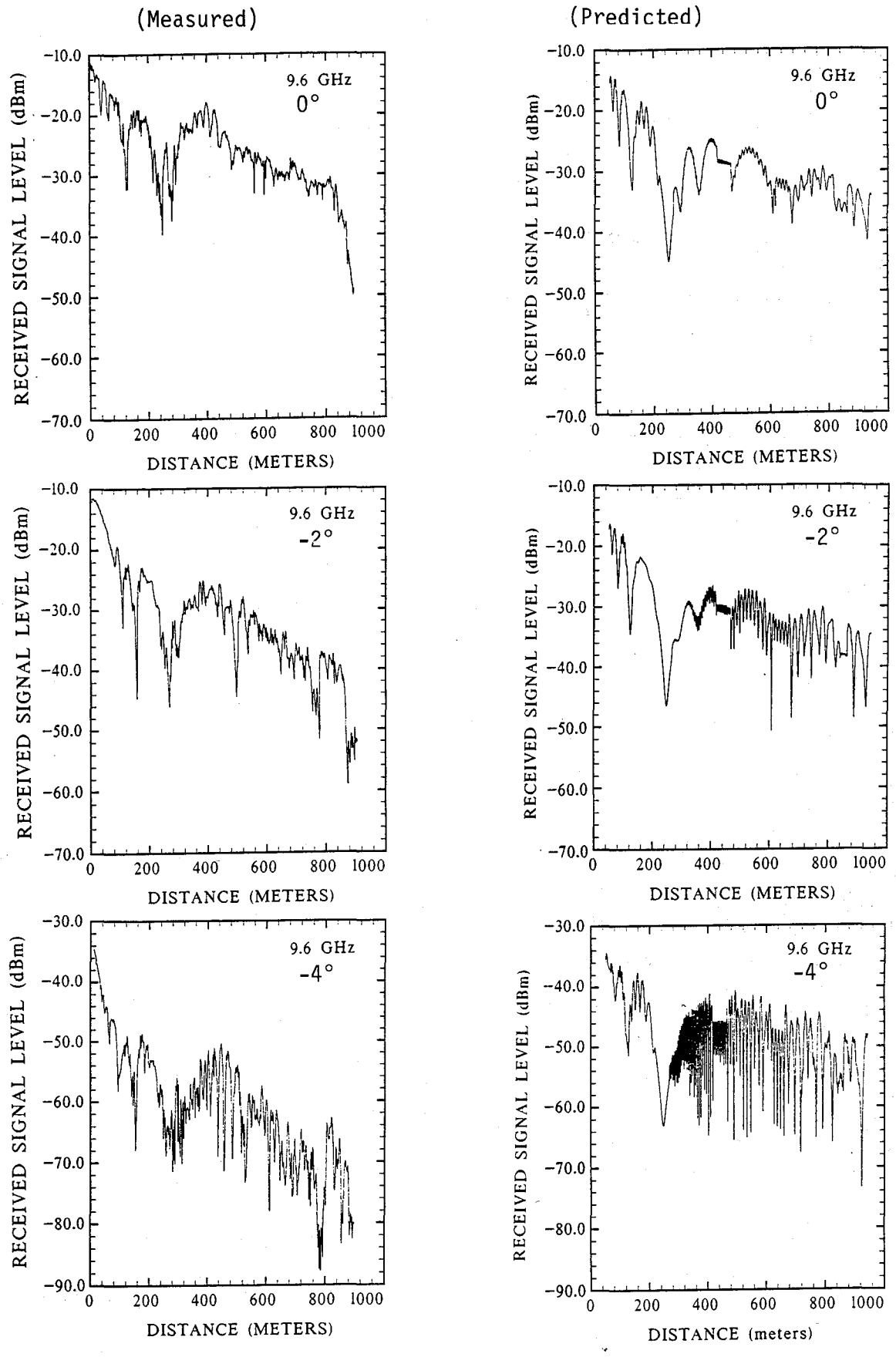

Figure 82. Range scan data sets to compare measured results (left side) with the computer model predictions (right side). Urban area (transmitter height = 2.15 m, receiver height = 1.8 m, 9.6 GHz).

SUMMARY OF PARAMETERS

Index	Description	Value	Value	Value
1.	Maximum number of wall reflections (integer)	4.000	4.000	4.000
2.	Distance between building walls (m)	24.000	24.000	24.000
3.	TX distance from left wall (m)	5.000	5.000	5.000
5.	TX height from street (m)	2.150	2.150	2.150
6.	RX distance from right wall (m)	5.000	5.000	5.000
8.	Minimum distance from TX to RX (m)	50.000	50.000	50.000
9.	Maximum distance from TX to RX (m)	950.000	950.000	950.000
10.	Step size in distance from TX to RX (m)	1.000	1.000	1.000
11.	RX height from street (m)	1.800	1.800	1.800
12.	Radio Frequency (GHz)	9.600	9.600	9.600
16.	TX ant. beamwidth (degrees)	10.000	10.000	10.000
17.	TX antenna gain (dB)	25.000	25.000	25.000
18.	TX ant. elevation angle (degrees)	0.000	0.000	0.000
22.	TX ant. azmuthal angle (left-neg., degrees)	0.000	-2.000	-4.000
26.	RX ant. beamwidth (degrees)	4.800	4.800	4.800
27.	RX antenna gain (dB)	31.000	31.000	31.000
28.	RX ant. elevation angle (degrees)	0.000	0.000	0.000
32.	RX ant. azmuthal angle (left-neg., degrees)	0.000	0.000	0.000
36.	Transmitter power (dBm)	15.500	15.500	15.500
38.	Loss for street reflection (dB)	1.000	1.000	1.000
39.	Loss for wall reflection (dB)	6.000	6.000	6.000
40.	Atmospheric Pressure (kPa)	83.000	83.000	83.000
41.	Relative Humidity (Percent)	50.000	50.000	50.000
42.	Temperature (Celsius)	20.000	20.000	20.000
43.	Are cross streets to be used (1=yes,0=no)	1.000	1.000	1.000
44.	Distance from TX to first cross street (m)	10.000	10.000	10.000
45.	Distance between cross streets (m)	76.000	76.000	76.000
46.	Width of cross street (m)	24.000	24.000	24.000
47.	Plot distribution: (0=no, 1=yes)	0.000	0.000	0.000
48.	Plot distribution separately: (0=no, 1=yes)	1.000	1.000	1.000
49.	Plot actual value: (0=no, 1=yes)	1.000	1.000	1.000
50.	Confidence interval (decimal)	0.900	0.900	0.900

Figure 83. Computer model parameter values used for the 9.6 GHz data in Figure 82 with (0°), (-2°), and (-4°) pointing.

is with the antennas adjusted for on-line pointing. The middle and bottom set show results when the receiving antenna off-pointed at 2° and 4°, respectively, to the left (toward the far-side of the street). The off-pointing of the receiving antenna enhances the wall-reflected components. As with the rural data, again the pattern agreement is good. The major differences appear in a more uniform display of multipath in the predicted data and an overemphasis of the effect of cross streets as seen between 420 m and 460 m. The data in Figures 84 and 85 are similar to Figure 82. The principal differences are operating frequency and receiving antenna beamwidth. The measured and predicted results in Figure 84 are for 28.8 GHz using a 1.2° receiving antenna, and the results in Figure 85 are for 57.6 GHz, also using a 1.2° receiving antenna.

The final sets of measured and predicted range scan data at 28.8 GHz are shown in Figure 86, which compares the narrowbeam (2.4°) and the widebeam (30°) receiving antenna results.

The important features of these data are the increase in number and depth of fades due to wall reflections associated with the wider beam antennas.

6.4.2 Azimuth Scans

The data set in Figure 87 compares measured and predicted receiver azimuthal scan results at 9.6, 28.8, and 57.6 GHz for a path length of 485 m. The model parameter values for the predicted data are given in Figure 88. These are the same parameters as used for the on-line pointing in Figures 82, 84, and 85. For the measured and predicted data in Figure 87, the receiver was 5 m from the right-hand street wall (positive angle values) and 19 m from the left-hand wall (negative angle values). In each azimuth scan the multipath signal levels are larger on the left side of the scan. These data sets show good agreement considering the idealized model geometry and the non ideal characteristics of the measurement scenario. Even better agreement would be expected had the computer model antenna side lobes been more representative of the measurement antenna pattterns. The data set in Figure 89 compares the measured and computed patterns. Observe that in the computed patterns, the side lobes are symmetrical and well-defined, whereas the side lobes of the measured patterns are neither symmetrical nor well-defined and are much lower relative to the main lobe, particularly for the 28.8 and 57.6 GHz channels. A better representation of the antenna pattern might greatly improve the comparison of the azimuth scan predicted data and the measured

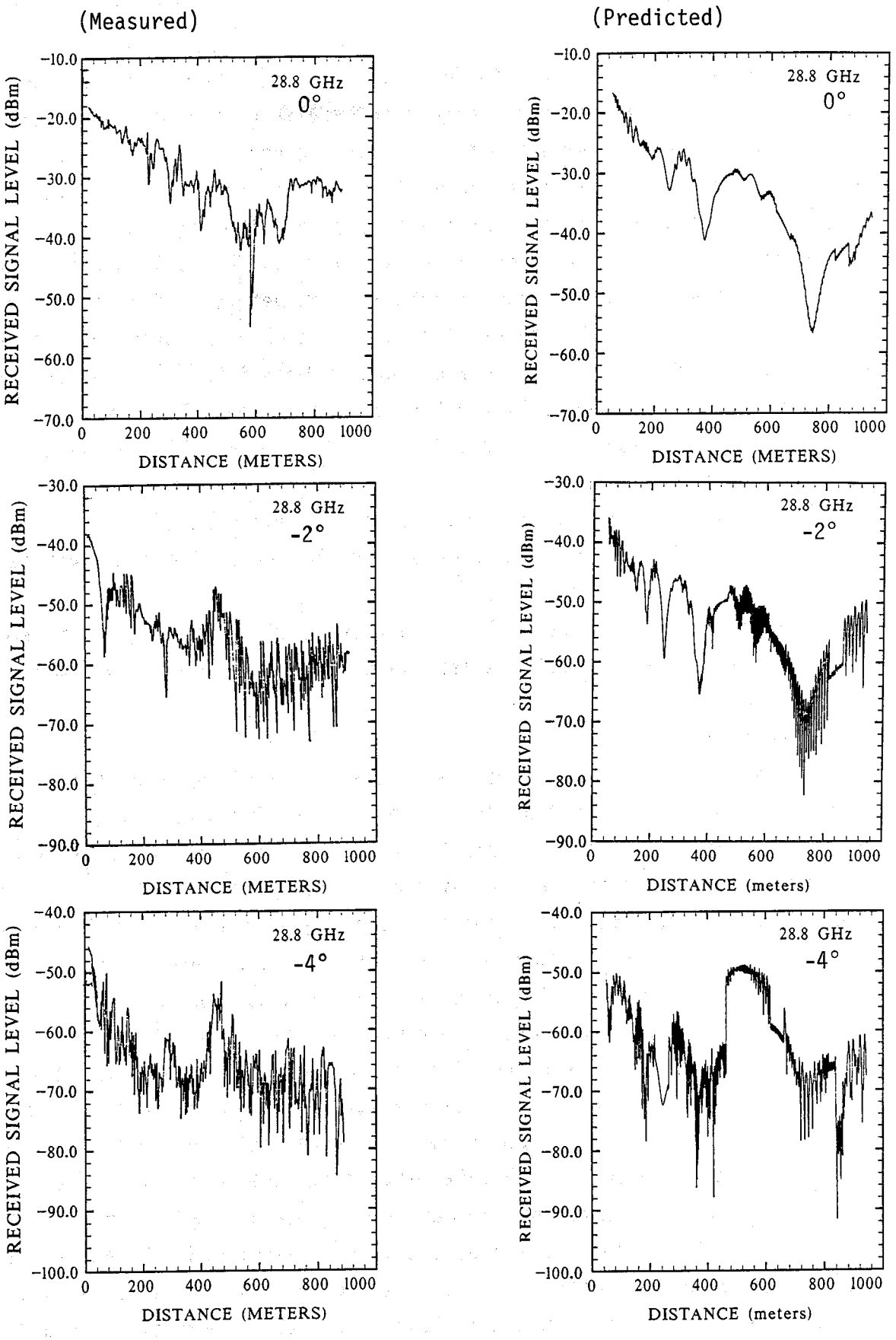

Figure 84. Range scan data sets to compare measured results (left side) with the computer model predictions (right side). Urban area (transmitter height = 2.15 m, receiver height = 1.8 m, 28.8 GHz).

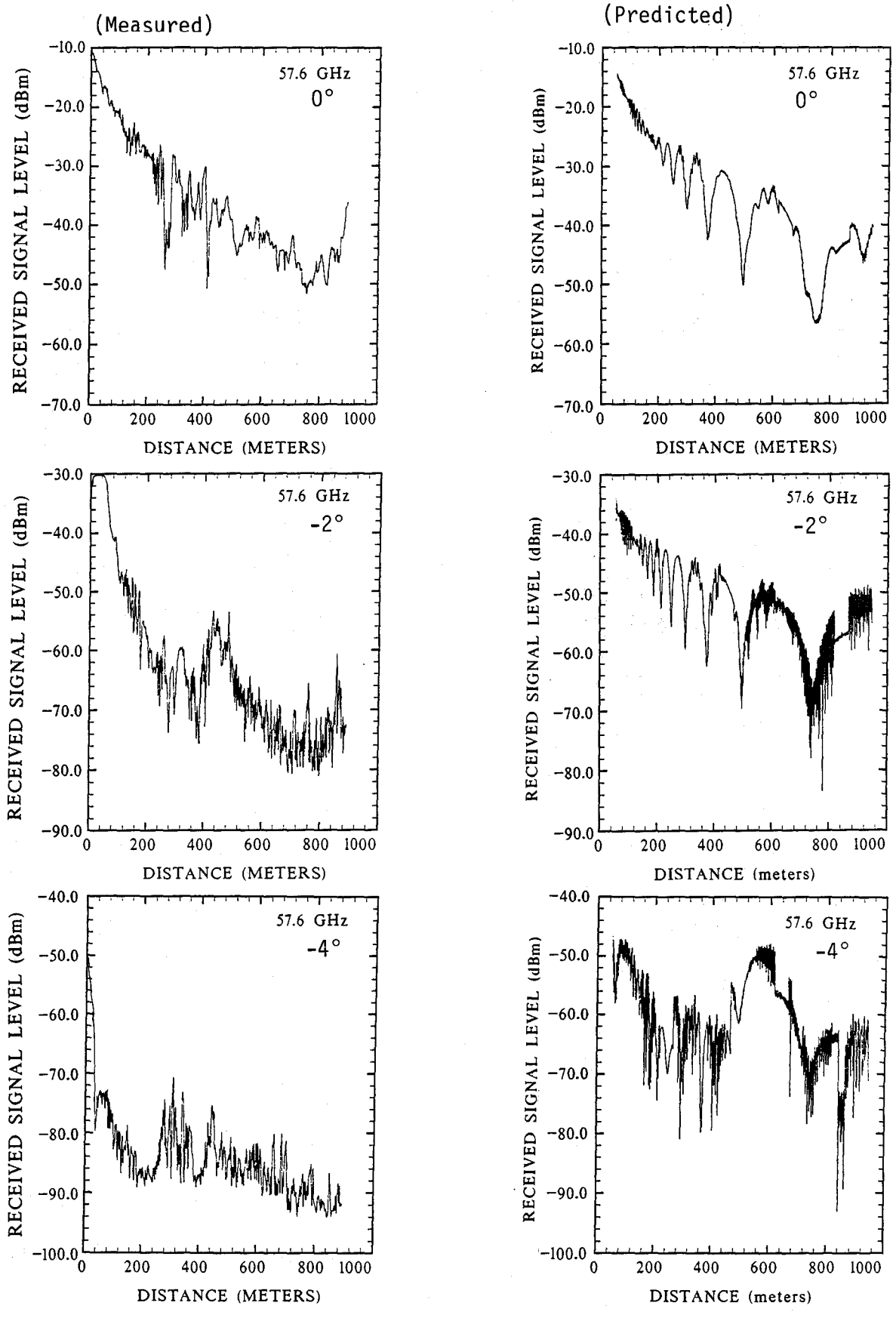

Figure 85. Range scan data sets to compare measured results (left side) with the computer model predictions (right side). Urban area (transmitter height = 2.15 m, receiver height = 1.8 m, 57.6 GHz).

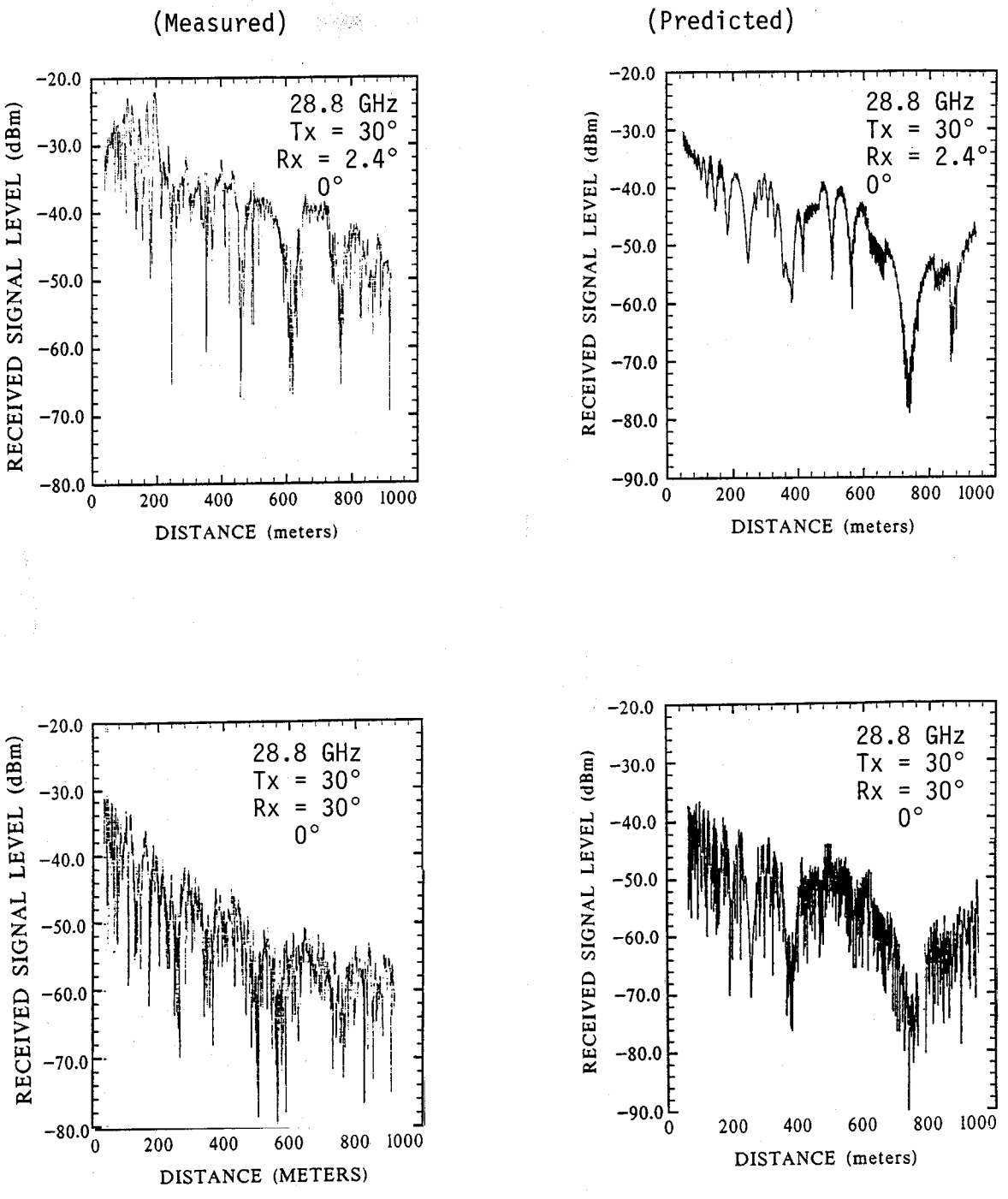

Figure 86. Range scan data sets to compare measured results (left side) with the computer model predictions (right side). Urban area (transmitter height = 2.15 m, receiver height = 1.80 m, 28.8 GHz and 30° transmitter antenna beamwidth.

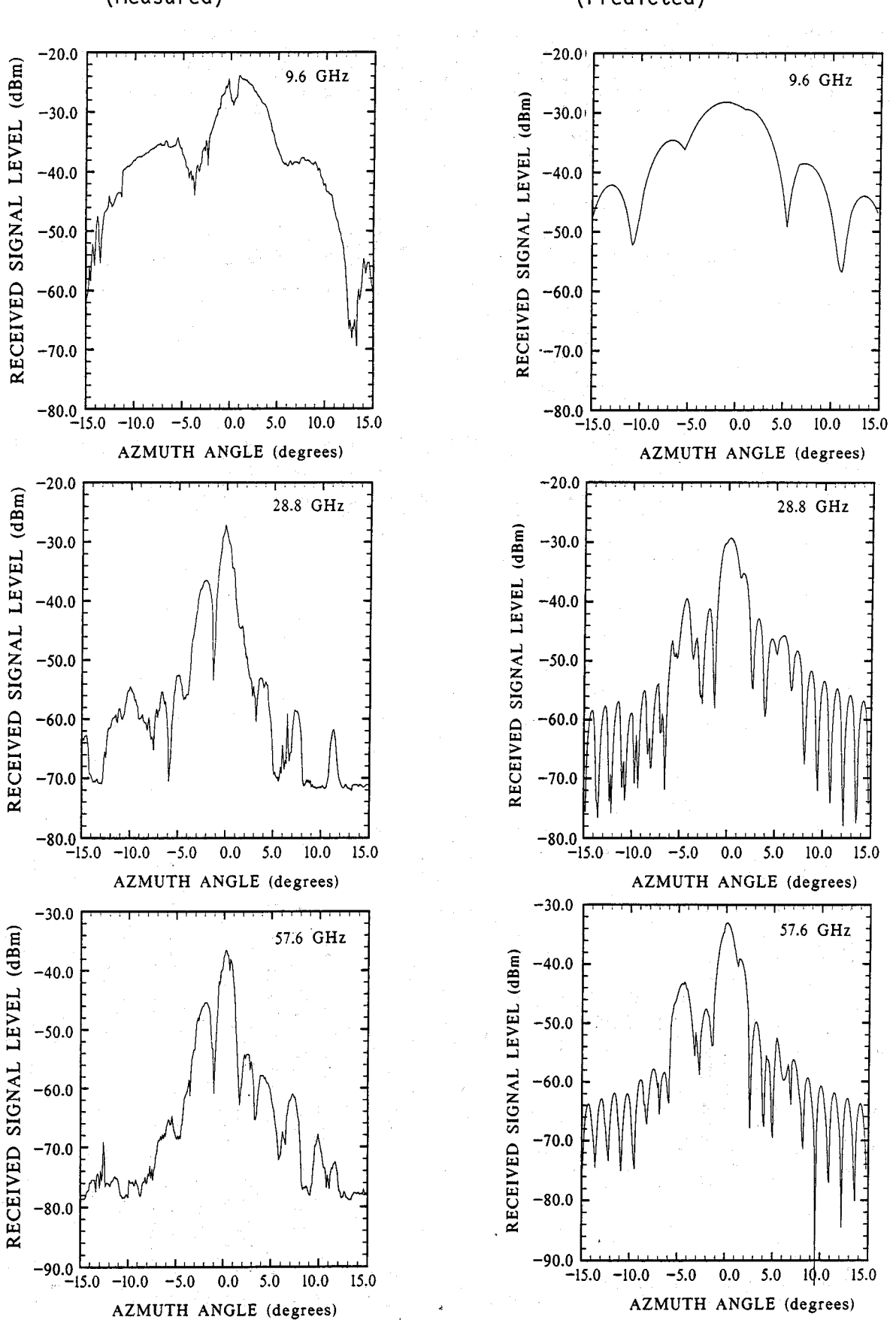

Figure 87. Azimuth scan data sets to compare measured results (left side) with the computer model predictions (right side). Urban data (transmitter height = 2.15 m, receiver height = 1.8 m, 485 m path).

SUMMARY OF PARAMETERS

Index	Description	Value	Value	Value
1.	Maximum number of wall reflections (integer)	4.000	4.000	4.000
2.	Distance between building walls (m)	24.000	24.000	24.000
3.	TX distance from left wall (m)	5.000	5.000	5.000
5.	TX height from street (m)	2.150	2.150	2.150
6.	RX distance from right wall (m)	5.000	5.000	5.000
7.	RX distance from TX (m)	485.000	485.000	485.000
11.	RX height from street (m)	1.800	1.800	1.800
12.	Radio Frequency (GHz)	9.600	28.800	57.600
16.	TX ant. beamwidth (degrees)	10.000	10.000	10.000
17.	TX antenna gain (dB)	25.000	25.000	25.000
22.	TX ant. azmuthal angle (left-neg., degrees)	0.000	0.000	0.000
26.	RX ant. beamwidth (degrees)	4.800	1.200	1.200
27.	RX antenna gain (dB)	31.000	42.800	43.100
28.	RX ant. elevation angle (degrees)	0.000	0.000	0.000
29.	Minimum RX elevation angle (degrees)	-5.000	-5.000	-5.000
30.	Maximum RX elevation angle (degrees)	5.000	5.000	5.000
31.	Step size in RX elevation angle (degrees)	0.010	0.010	0.010
32.	RX ant. azmuthal angle (left-neg., degrees)	0.000	0.000	0.000
33.	Minimum RX azmuthal angle (degrees)	-15.000	-15.000	-15.000
34.	Maximum RX azmuthal angle (degrees)	15.000	15.000	15.000
35.	Step size in RX azmuthal angle (degrees)	0.100	0.100	0.100
36.	Transmitter power (dBm)	15.500	13.000	20.800
37.	Receiver noise figure (dB)	6.000	6.000	6.000
38.	Loss for street reflection (dB)	1.000	1.000	1.000
39.	Loss for wall reflection (dB)	6.000	6.000	6.000
40.	Atmospheric Pressure (kPa)	83.000	83.000	83.000
41.	Relative Humidity (Percent)	50.000	50.000	50.000
42.	Temperature (Celsius)	20.000	20.000	20.000
43.	Are cross streets to be used (1=yes,0=no)	1.000	1.000	1.000
44.	Distance from TX to first cross street (m)	10.000	10.000	10.000
45.	Distance between cross streets (m)	76.000	76.000	76.000
46.	Width of cross street (m)	24.000	24.000	24.000
47.	Plot distribution: (0=no, 1=yes)	0.000	0.000	0.000
48.	Plot distribution separately: (0=no, 1=yes)	1.000	1.000	1.000
49.	Plot actual value: (0=no, 1=yes)	1.000	1.000	1.000
50.	Confidence interval (decimal)	0.900	0.900	0.900

Figure 88. Computer model parameter values used for the three frequencies in Figure 87.

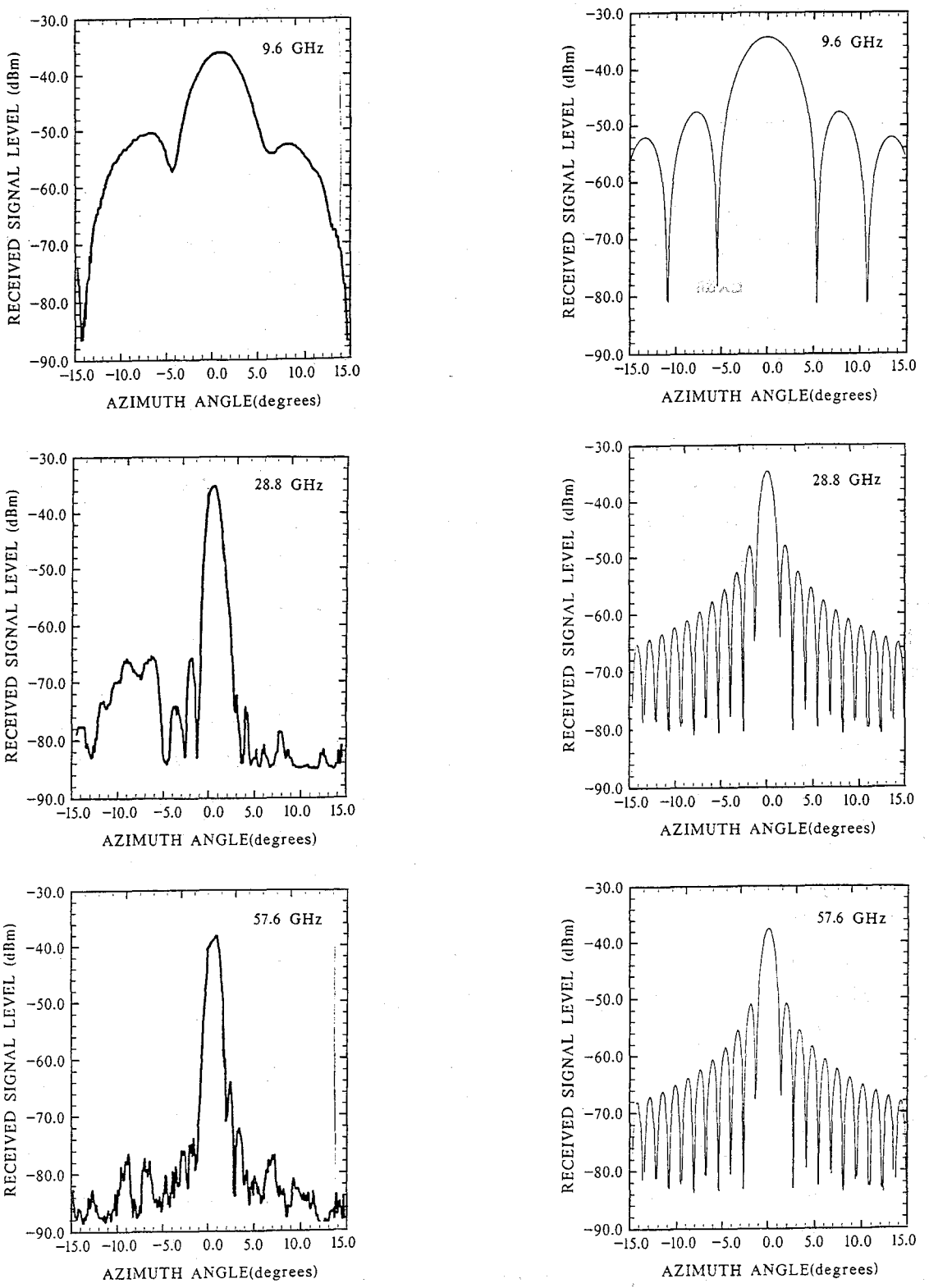

Figure 89. Azimuth scan data to compare measured results (left side) with computer model antenna patterns (right side).

data and also provide better agreement in the range scan and impulse response areas.

6.4.3 Impulse Response

The last of the comparisons between measured results and model predictions is with the impulse response data. These comparisons are not as easy to make as were the range scans and the azimuthal scans because of the differences in display. Examples of measured data are discussed in detail in Section 5 of this report and are shown in Figure 36. The impulses in Figure 36 are the result of a controlled experiment, where the delay value and amplitude of the multipath components are preset. The cross-correlation technique used in the measured data process broadens the impulse response according to the limits imposed by the data rate and processing bandwidth. The response at zero is the direct or reference signal, and the multipath impulse response delay is measured relative to reference (center-to-center). The amplitude of the multipath impulse response is also measured relative to the reference (peak-to-peak).

The data in Figure 90 are impulse response data generated by the computer model. In this display, the computer plots the line-of-sight ray with an amplitude of zero dB at zero time (which is the reference for all other rays). All multipath rays are shown as a line indicating relative amplitude and delay. The identification of the rays (lines) in Figure 90 was made from a ray table.

The data in Figure 91 are a sampling of model predicted outputs. The summary of parameters is shown in Figure 92. The transmitter-receiver separation is 300 m. The transmitter antenna beamwidth is 30° and the receiver beamwidth is 1.2°. The antennas are arranged for on-line pointing (zero degrees in Index 22 and 32) and the model is set for solid walls (no cross streets, Index 43). In Figure 91(A), all the multipath rays (except the ground-reflected direct and the 1-hop, left components) are more than 30 dB below the reference. By comparison, in Figure 91(B), where the receiving antenna has been broadened to 30°; all the multipath rays are well above 30 dB. The list of summary parameters for Figure 91(B) is in Figure 92(B). A second comparison is between Figures 91(A) and 91(C). In Figure 91(A), the azimuthal angle was 0° and in 91(C) the azimuthal angle was -3°. This receiver antenna pointing change caused an increase in the multipath rays of

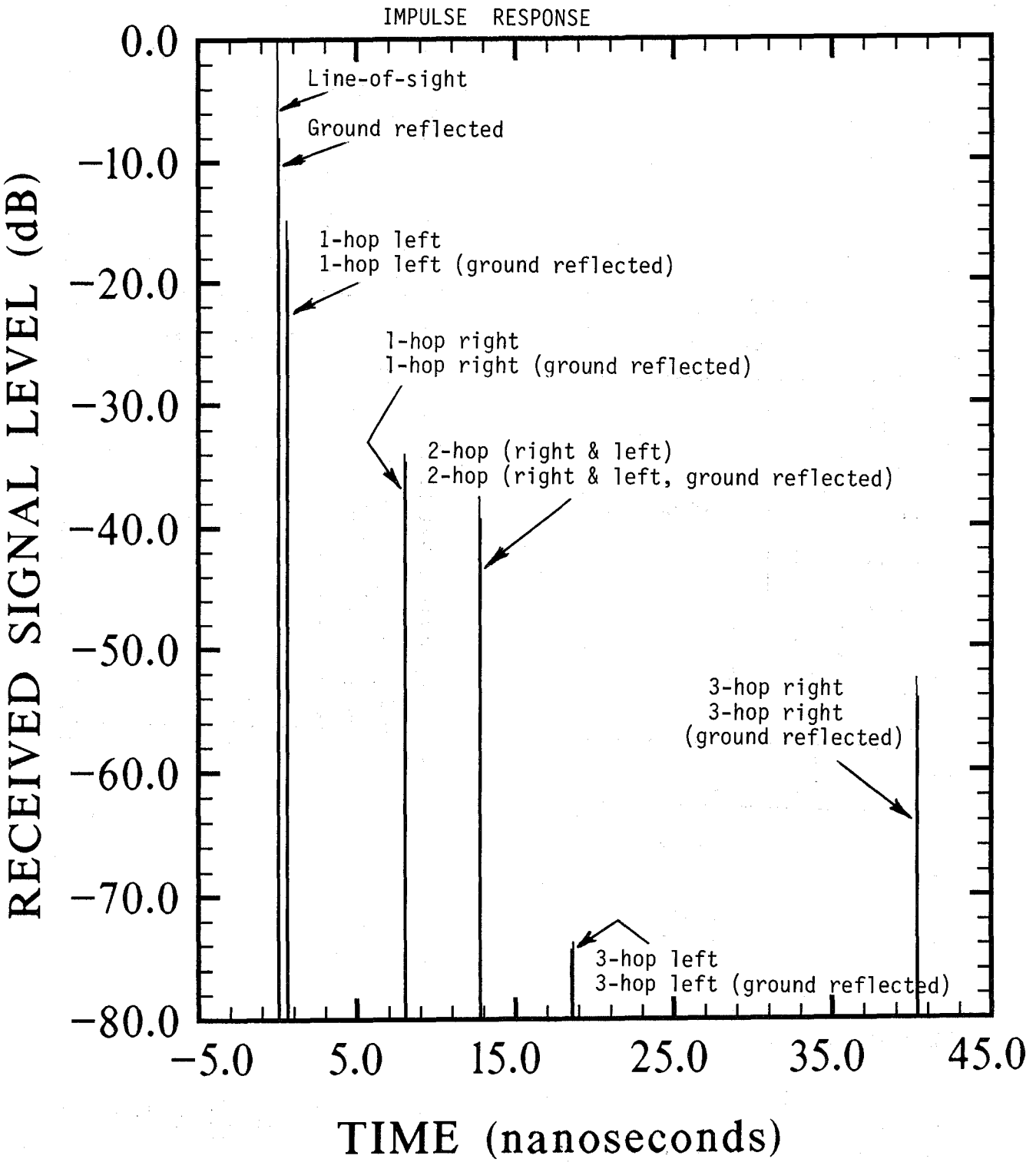

Figure 90. Impulse response data generated by the computer prediction model.

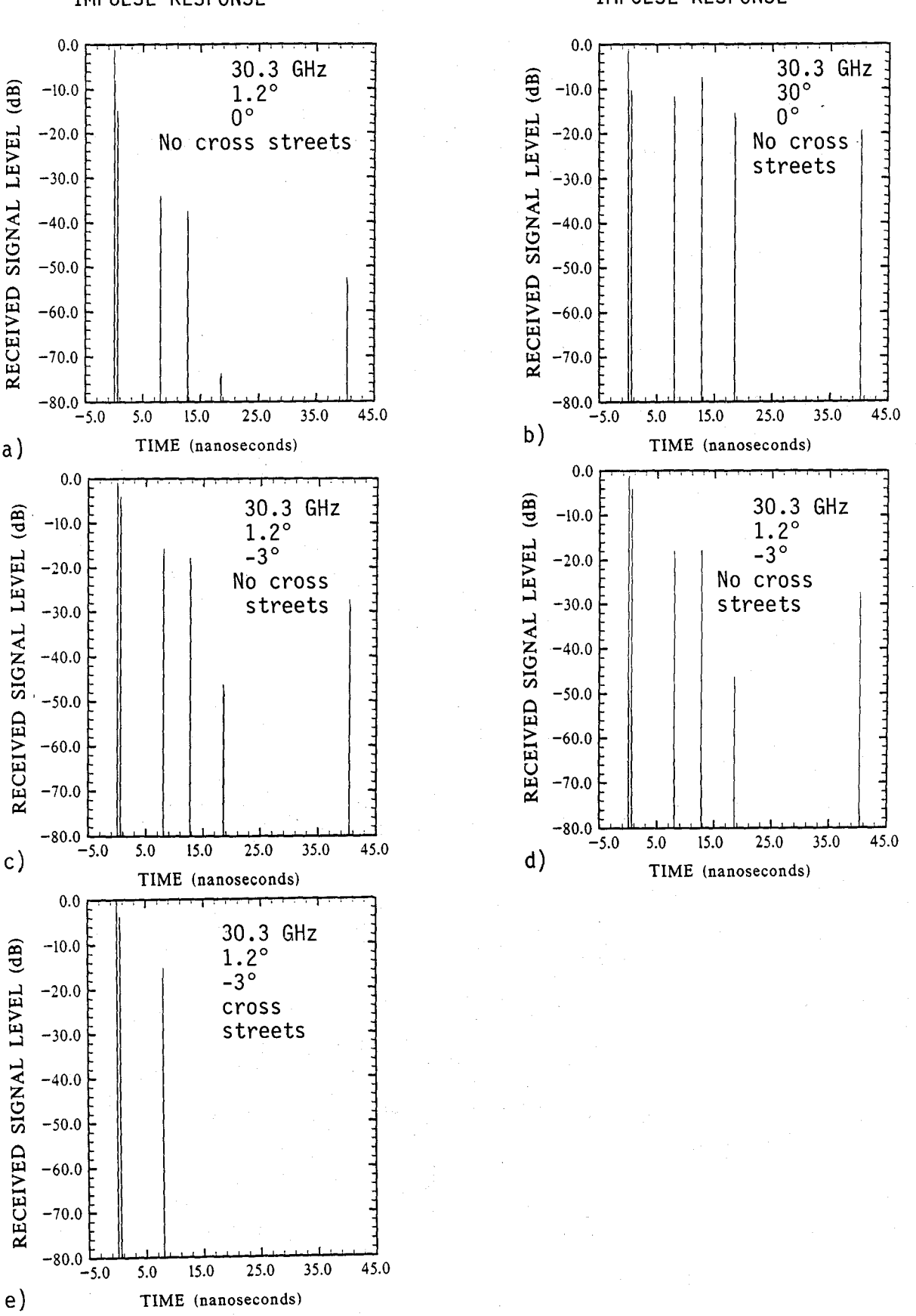

Figure 91. A set of model predicted impulse response data, with parameter values as indicated. Variations in cross-street geometry and off-angle pointing.

SUMMARY OF PARAMETERS

Index	Description	(a) Value	(b) Value
1.	Maximum number of wall reflections (integer)	4.000	4.000
2.	Distance between building walls (m)	24.000	24.000
3.	TX distance from left wall (m)	5.000	5.000
5.	TX height from street (m)	2.000	2.150
6.	RX distance from right wall (m)	5.000	5.000
7.	RX distance from TX (m)	300.000	300.000
11.	RX height from street (m)	2.500	1.800
12.	Radio Frequency (GHz)	30.300	30.300
16.	TX ant. beamwidth (degrees)	10.000	30.000
17.	TX antenna gain (dB)	25.000	17.000
18.	TX ant. elevation angle (degrees)	0.000	0.000
22.	TX ant. azmuthal angle (left-neg., degrees)	0.000	0.000
26.	RX ant. beamwidth (degrees)	1.200	30.000
27.	RX antenna gain (dB)	42.800	17.000
28.	RX ant. elevation angle (degrees)	0.000	0.000
32.	RX ant. azmuthal angle (left-neg., degrees)	0.000	0.000
36.	Transmitter power (dBm)	13.000	18.500
37.	Receiver noise figure (dB)	6.000	6.000
38.	Loss for street reflection (dB)	1.000	1.000
39.	Loss for wall reflection (dB)	1.000	1.000
40.	Atmospheric Pressure (kPa)	83.000	83.000
41.	Relative Humidity (Percent)	50.000	50.000
42.	Temperature (Celsius)	20.000	20.000
43.	Are cross streets to be used (1=yes,0=no)	0.000	0.000
44.	Distance from TX to first cross street (m)	10.000	10.000
45.	Distance between cross streets (m)	76.000	76.000
46.	Width of cross street (m)	24.000	24.000

Figure 92. Summaries of computer parameter values. Summary (a) is used for Figures 90 and 91 A and Summary (b) is used for Figure 91 B.

about 20 dB relative to the direct signal.

As observed in Figure 90, the multipath rays (impulses) occur in pairs. The first ray is the line-of-sight ray or the direct multipath ray and the second (slightly delayed) ray in each pair is the ground-reflected component. In Figure 91(D), the loss for street reflection (Index 38) was increased to 50 dB from 1 dB in Figure 91(C). This parameter change identifies the ground reflected components in Figure 91(D), which are reduced by 49 dB. The parameter values for Figure 91(E) are the same as for Figure 91(C), except that cross streets (Index 43) are used in Figure 91(E) and not used in 91(C). For this particular path length and street geometry, the components between 10 and 45 ns are lost at the cross streets. In reality, the model output probably more severely crops the multipath ray response at street crossings than what happens at a street crossing for an actual path, as indicated in the measured data. This is because in the geometrical ray model used here, a ray can be completely lost down a side street while in the physical case the cross street probably only reduces the energy reflected from the Fresnel zone straddling the cross street.

The comparisons between the measured impulse response data and the model impulse response outputs are of three types. These are: (a) widebeam transmitter antenna and narrowbeam receiver antenna with on-line (0°) pointing, (b) widebeam transmitter antenna and narrowbeam receiver antenna with off-line (-3°) receiver antenna pointing, and (c) widebeam transmitter antenna and widebeam receiver antenna with on-line (0°) pointing. Because of the lack of resolution in the measured data, particularly for short delays and for closely spaced delays, the measured data and predicted data must be compared with these features in mind.

The impulse data in Figures 93 and 94 were recorded using a widebeam transmitting antenna and a narrowbeam receiving antenna with on-line (0°) pointing. The path length for each impulse response is indicated on the right. For comparison, the model predicted rays for corresponding conditions are superimposed on the 100-m, 120-m, and 140-m responses of Figure 93 and on the 300-m, 320-m, and 340-m responses of Figure 94. As observed in Figure 93, the model predicted rays are of short delay and low amplitude, and would contribute very little to the overall shaping of the direct ray component of the impulse responses. In Figure 94, the predicted rays are significantly increased in amplitude but of even shorter delay and these rays also

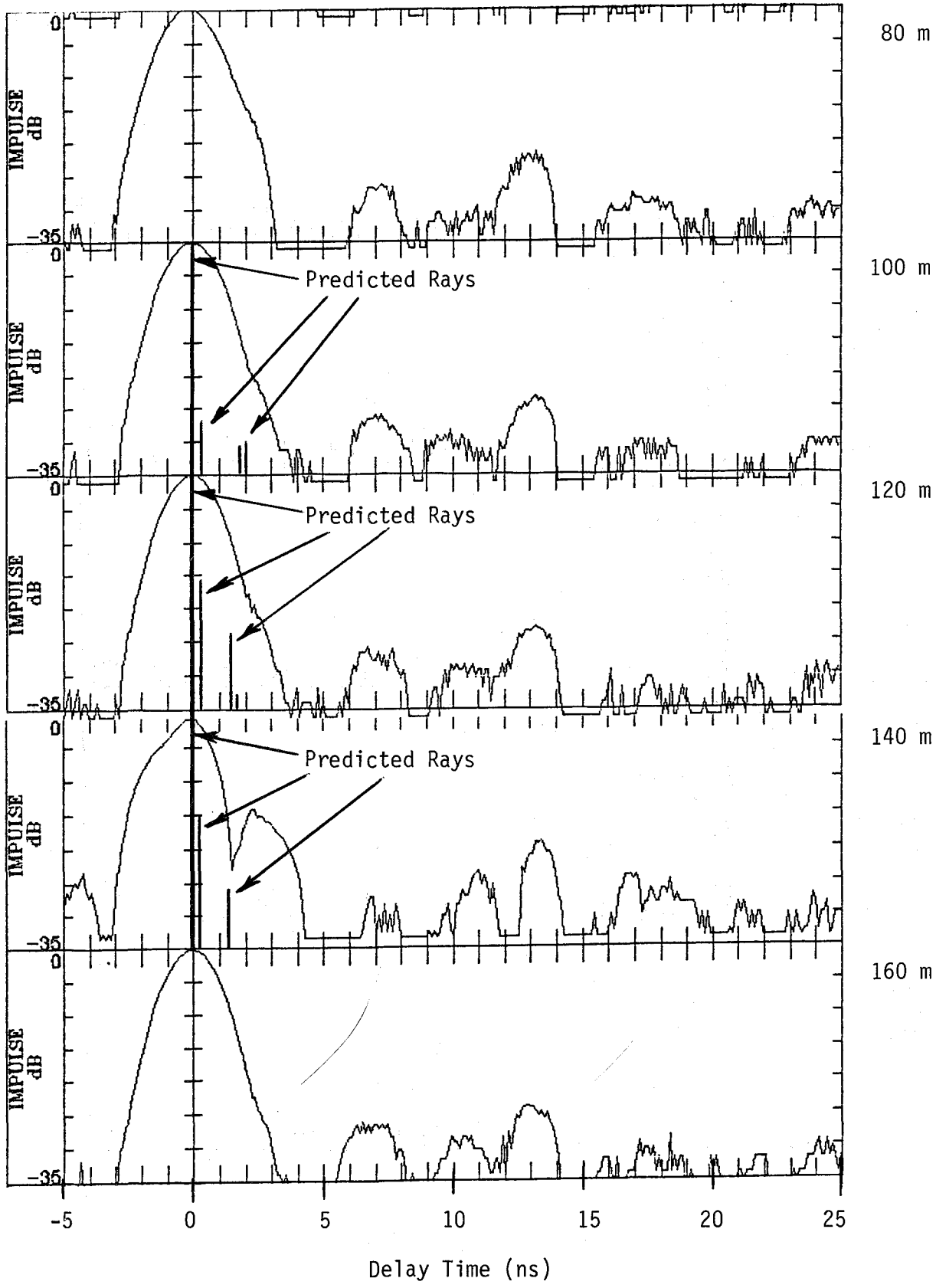

Figure 93. A set of measured path impulse response data, centered on a 120-m path, with model predicted rays as indicated.

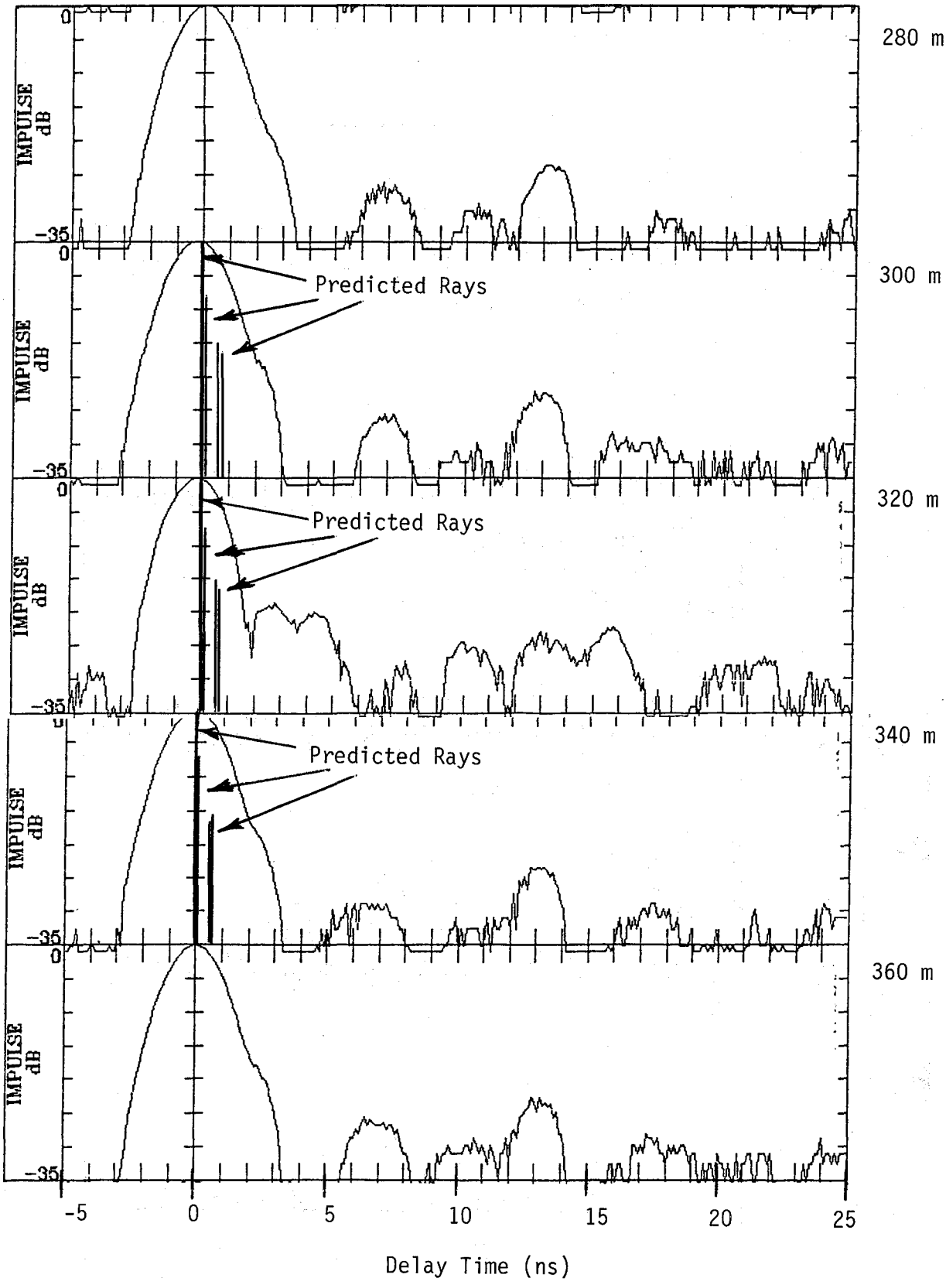

Figure 94. A set of measured impulse response data, centered on a 320 m path, with model predicted rays as indicated.

contribute very little to the shaping of the direct ray component of the impulse response.

The second set of measured and predicted data are shown in Figures 95 and 96. The measured impulse response data in these figures are displayed as a direct ray (shaded portion) and a composite direct ray and multipath components (contour is defined by a solid line). System parameters and path geometry were the same as in Figures 93 and 94, except that the receiving antenna was off-pointed by 3°. By off-pointing the receiving antenna, reception of the wall-reflected rays was enhanced. This reshaped the direct ray impulse response and created additional impulses in the 5- to 15-ns region. Again, in this set of data, there is a general correspondence between the measured and predicted results.

The final set of measured and predicted data are in Figures 97 and 98. For this set, both antennas were widebeam (30°) and were pointed on-line. In this set, as in the other two, there is a general correspondence between the measured and predicted results.

7. SUMMARY AND CONCLUSION

Two basic types of measurements were made. The first type of measurement involved non-line-of-sight paths and the characterization of reflection/transmission properties of selected building materials. The second type of measurement involved line-of-sight paths for which multipath from various urban structures was examined. The two sets of measurements are summarized separately below.

7.1 Non-Line-of-Sight Paths

Three CW signal probes, at 9.6, 28.8, and 57.6 GHz, were used to evaluate propagation characteristics of non-line-of-sight paths. In suburban areas, with residential homes, trees, and shrubs obscuring the direct paths, very high attenuations were experienced and tended to increase as a function of frequency. At the upper two probe frequencies, the added path loss for these types of obstructions were often greater than 60 dB above what the loss would have been were the path line of sight. Elevating one terminal clearly reduced the loss even though the path still contained a large number of obstructions. The primary difference in the elevated terminal path was that there were opportunities for common illumination of edges, mainly trees or rooftops, by

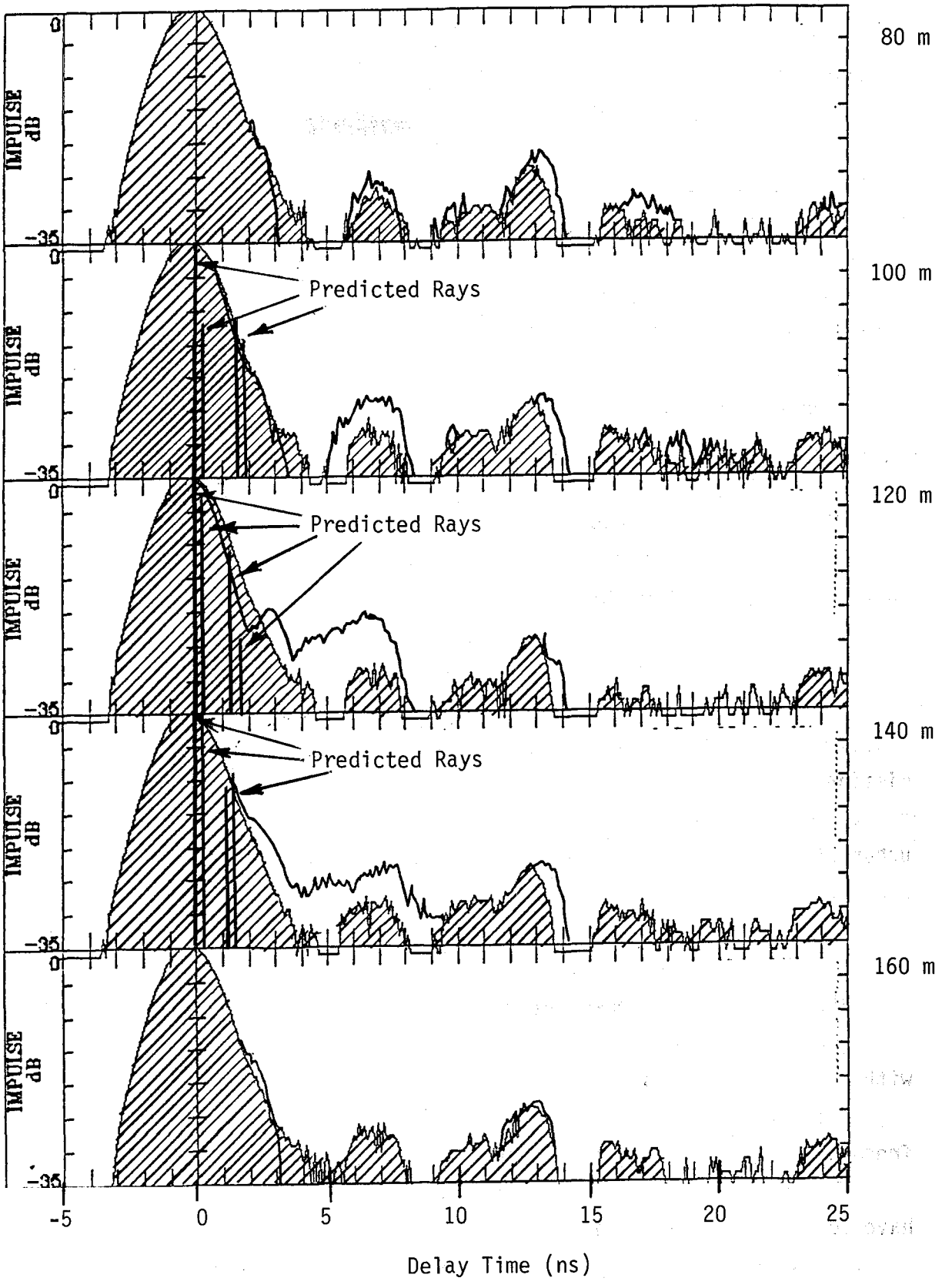

Figure 95. A set of measured impulse response data centered on a 120-m path with 3° receiving antenna off-pointing. The model predicted rays are superimposed on the 100-, 120-, and 140-m paths.

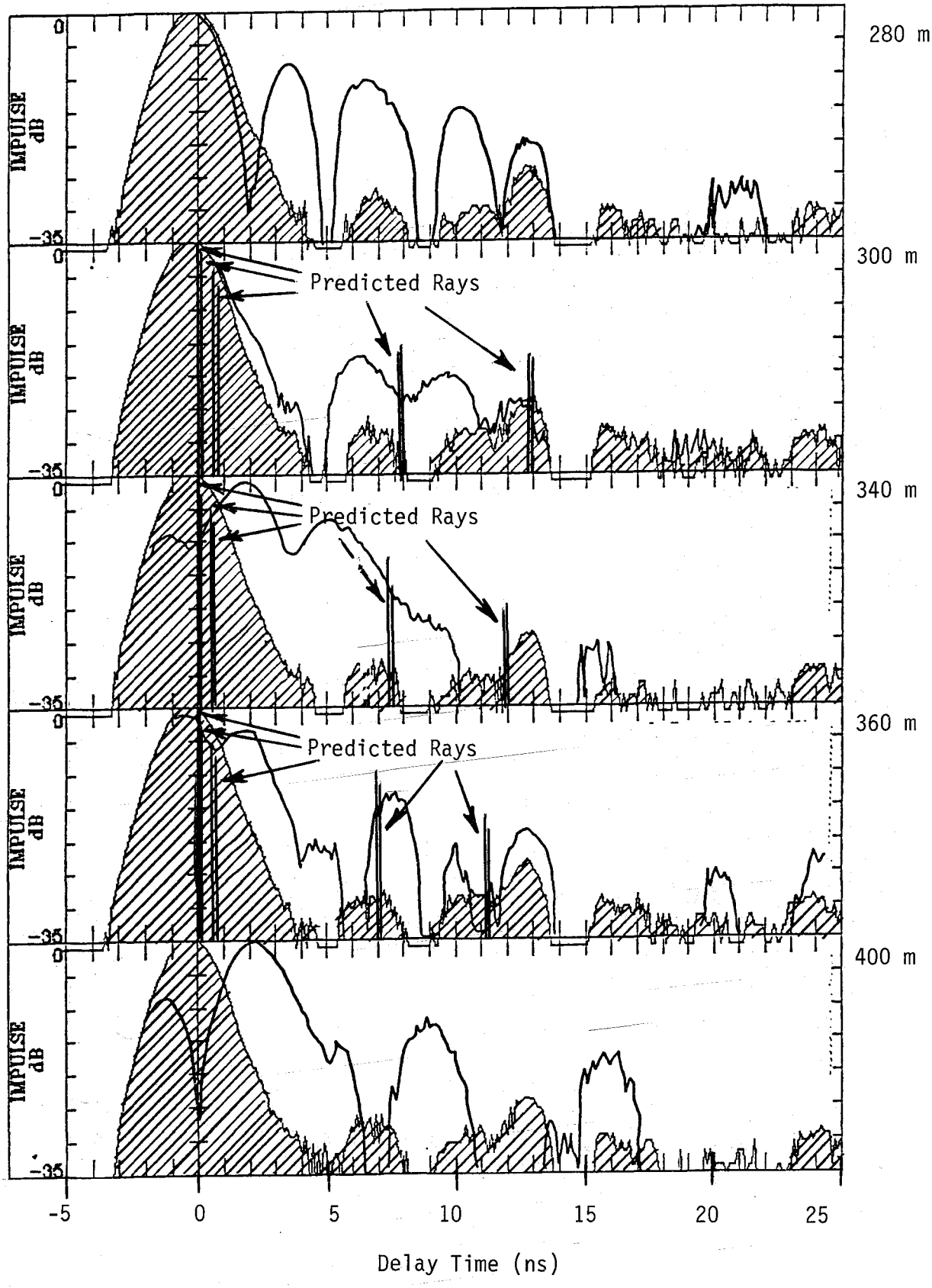

Figure 96. A set of measured impulse response data centered on a 340-m path with 3° receiving antenna off-pointing. The model predicted rays are superimposed on the 300-, 320-, and 340-m paths.

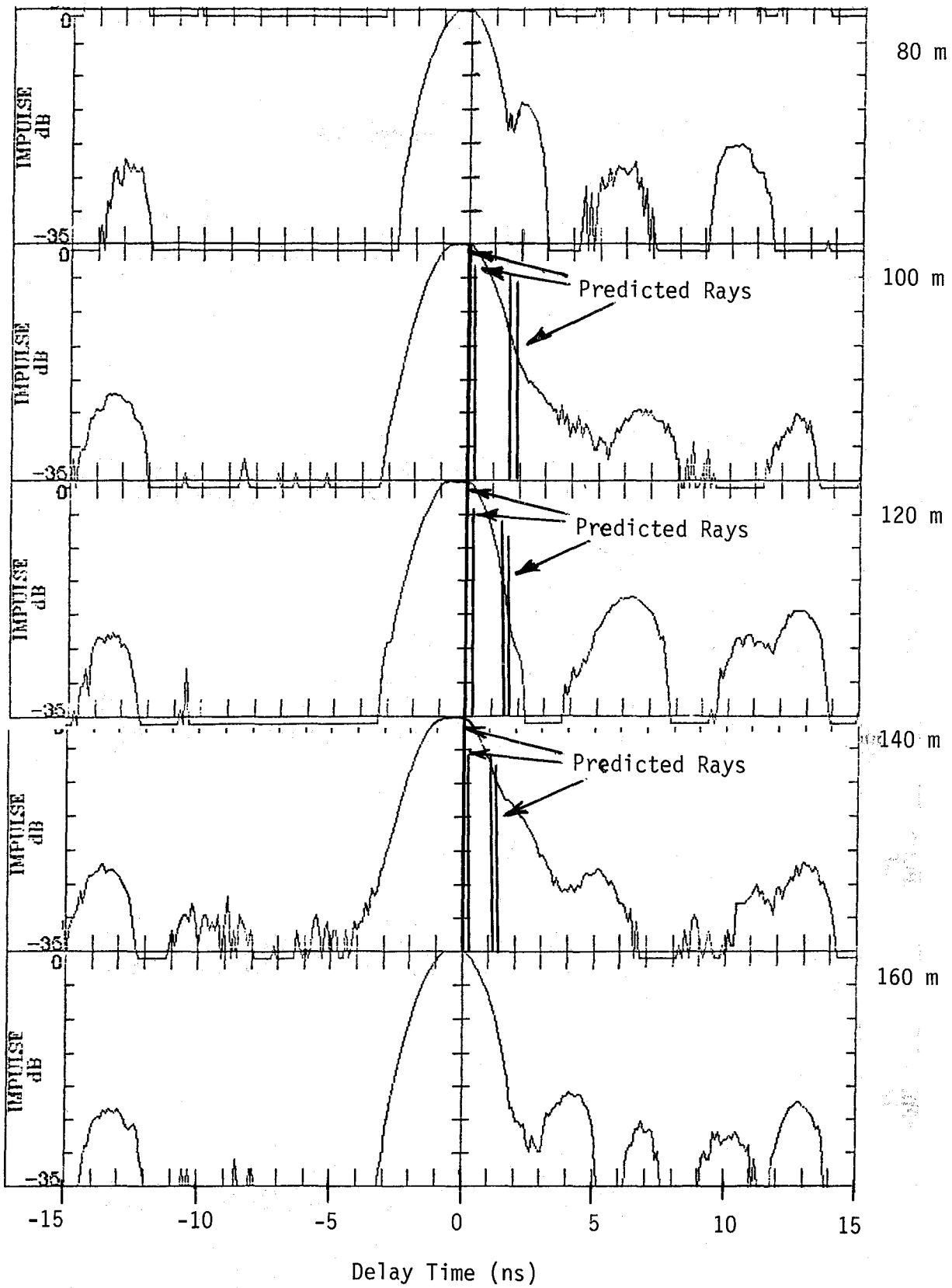

Figure 97. A set of measured impulse response data centered on a 120-m path with a 30° receiving antenna beamwidth. The model predicted rays are superimposed on the 100-, 120-, and 140-m paths.

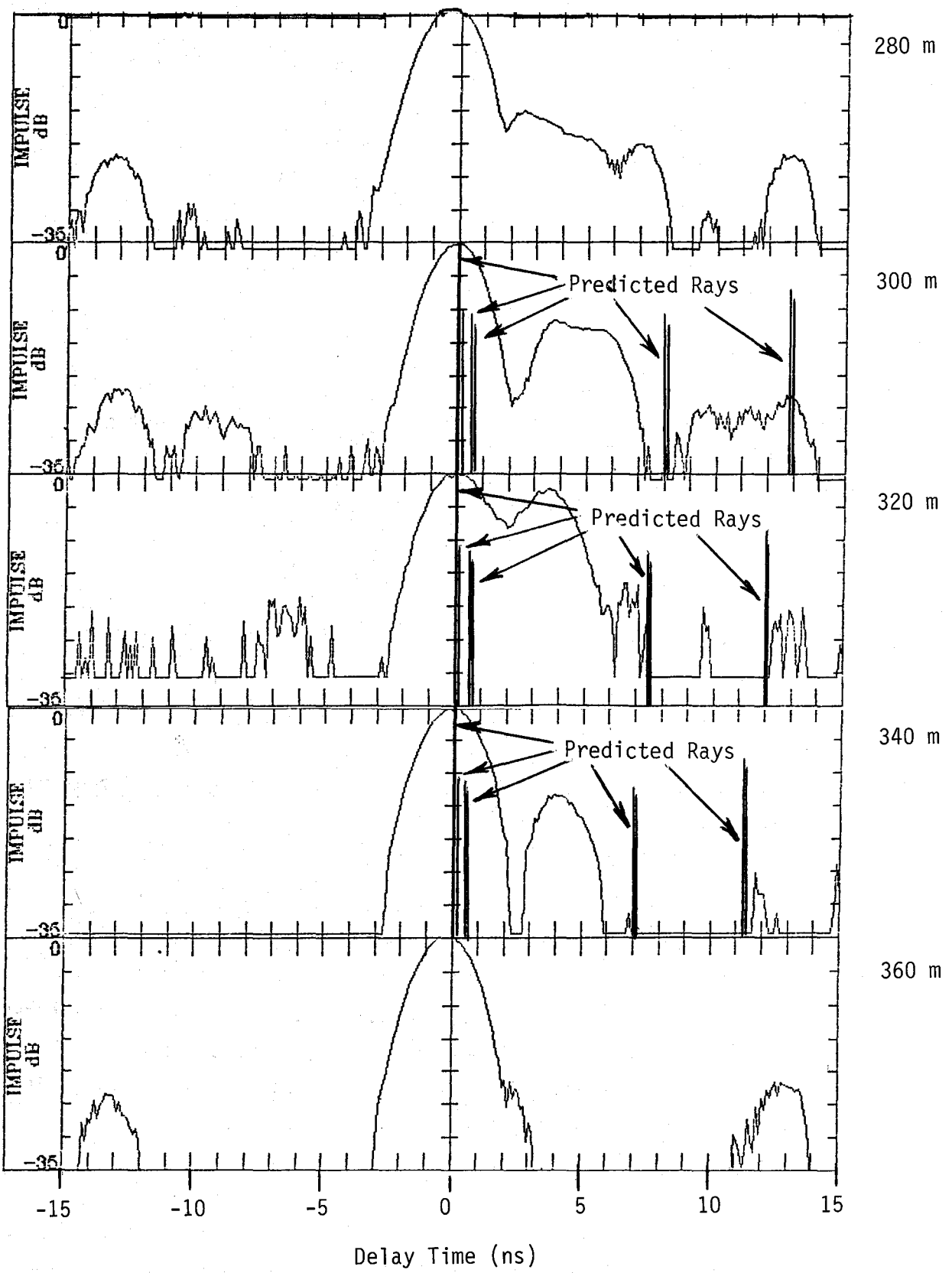

Figure 98. A set of measured impulse response data centered on a 320-m path with a 30° receiving antenna beamwidth. The model predicted rays are superimposed on the 300-, 320-, and 340-m paths.

the antennas of each terminal. For this condition, most of the signals were propagated by the edge diffraction and/or scattering mode, which is characterized by a considerable amount of signal scintillation, especially if trees are the diffractor and a wind is present. But the time delay spread from the edge contribution would only be expected to be a few nanoseconds, so a coherent bandwidth of perhaps up to 100 MHz could be sustained if a sufficient signal level was present.

Measurements were also conducted using the same frequency probes with large office buildings obstructing the path. Similar results were found as those described above. Attenuation through most structures was very large, showing increased attenuation with increasing frequencies. In most cases no signal could be detected through steel-reinforced concrete or brick-type buildings indicating a signal attenuation in excess of 90 dB. Again, if an edge diffraction mode from a roof or even a double-edge diffraction mode were used, detectable signal levels could be achieved. The coherent bandwidth for an edge diffraction channel of this type would probably be in tens of megahertz. Both coherent bandwidth and system gain improve as the antenna beamwidths are narrowed; however, illuminating a common volume becomes increasingly difficult so a practical trade-off is necessary if such an application is to be used.

Buildings that have large areas of window glass have lower attenuation and a detectable signal appears on paths directly through the building. An exception to this is when ultraviolet and infrared reflecting glass is used, which have metalized coatings. In this case, the signal attenuation increases from 25 to 50 dB for each metalized glass layer in the path.

The conclusion from the non-line-of-sight measurements conducted in this report is that the amount of signal penetrating typical obstructions in urban and suburban areas would be too small to provide a communication link without elaborate hardware to increase sensitivity. But if the highest point between two terminals were illuminated by each antenna, a usable link might be possible by edge diffraction or even multiedge diffraction propagation modes.

7.2 Line-of Sight Paths

Because of the confined surroundings in an urban/suburban environment and the existence of many flat surfaces, such as building walls, roadways, signs,

cars, trucks, etc., reflected signals play a major part in propagation characteristics of a line-of-sight communication channel.

Measurements were conducted to learn more about the properties of such reflecting surfaces at millimeter-wave frequencies.

Data were recorded to determine the reflection coefficient of building walls at normal incidence. As would be expected, the reflection coefficients were a direct function of the conductivity and smoothness factors of the reflecting surface. Not only does the smoothness criterion apply for small-scale roughness (relative to the wavelength of the measuring probe), but also the larger surface illuminated by the antenna beams may not be flat and the effective reflector gain is reduced relative to a flat-plate type reflector. It was found that if a transmitter moved parallel to a building surface, the returned signal level varied by as much as 15 to 20 dB from the gain pattern determined by the same procedure using a known flat-plate reflector. Therefore, the effective reflection coefficient for large building surfaces is very much a function of terminal position because of the large-scale irregularities. It was not unusual for the magnitude of the effective coefficient of reflection to vary from 1 to 1/10 for only a meter or two shift in terminal positions in the normal incidence mode.

In the case of a real link application along a street lined with buildings, the angle of incidence ($\emptyset$) on the reflecting surface approaches 90° (near grazing angles.) The criterium for surface smoothness includes the functions $1/\cos \emptyset$, and, therefore, as the angle of incidence becomes larger, the surface as seen by the radio wave appears smoother and the reflection coefficient becomes larger. This fact was supported by the data as reflections from street and building surfaces at very shallow angles along the path produced reflection coefficients of nearly -1.

Even with relatively narrowbeam antennas (2.5°), at heights above the street of 2 to 3 m, multipath signals from the street surface produced fades in excess of 30 dB. Because of the small angle between the direct path and the street at midpath, the delay time difference was likewise small. As the terminal distance is closed from a 1-km separation, only a few fades of this magnitude occur (the number is proportional to frequency, but two or three were observed for a 30-GHz carrier). With these small delay times (much less than 1 ns) for multipath from the street, the channel distortion is low, or conversely, the available bandwidth is large, in excess of 500 MHz or a data

rate of around 250 Mb/s using PSK modulation. Multipath reflection from building walls and other reflecting surfaces along the side of the street, with narrowbeam antennas in the system, generally had amplitudes that were 15 dB or more below the direct signal at delay times not greater than 10 ns. These low level multipath signals will cause some channel degradation at bandwidths above 100 MHz or about a 50 Mb/s data rate. The worst-case distortion will occur when the interference between the direct signal and the street reflection produces a deep fade allowing the longer delay multipath signal to approach the amplitude of the direct signal.

From the measurements performed, our findings indicate that for a line-of-sight millimeter-wave link up to 1 km in length along an urban street using accurately pointed narrowbeam antennas ($\cong 2.5°$), a nearly 100 percent reliable channel would be available for bandwidths up to 100 MHz if a 30 dB fade margin were provided. If the terminals are mobile, maintaining accurate coupling between terminals may be difficult. An antenna misalignment of 1° or 2° would cause degradation of the channel, but a reduction in the system bandwidth requirement may permit satisfactory performance for this condition. For near optimum channel performance of a communication link propagating along an urban street, the data taken in Denver suggests, as a rule of thumb, that the antenna beamwidth be twice the expected antenna pointing error.

For situations where the locations of other terminals are not known (such as in mobile units) or if several separate terminals are employed and require simultaneous reception, widebeam antenna coverage is needed. In order to examine channel performance for such conditions, antennas with 30° beamwidth were used in measurements on the along-the-street path and multipath signal amplitudes and delay times were recorded. For these antenna beamwidths, multipath signals equal to the amplitude of the composite direct plus street-reflected signal often occurred with a delay time of 10 ns relative to the direct signal. Consequently, a link using a 30° beamwidth antenna can support a bandwidth of about 10 MHz or a data rate of about 5 Mb/s with a BER less than 1×10^{-7} on a line-of-sight urban street path if a 30 dB fade margin were provided.

Additional information on channel performance was obtained from an experimental diagnostic probe operating at 30.3 GHz with a PSK modulation of 500 Mb/s. This probe was applied to street paths in Denver, CO, and BER estimates were extrapolated from the data. Also, using the same probe

channel, impulse responses were measured, which provide the actual multipath amplitudes and time delay data.

With this probe, linear antenna polarizations were compared to determine if millimeter-wave propagation in an urban environment shows any dependence on polarization. In particular, the Brewsters angle effect for shallow angle reflections was examined to determine if reflected signal levels could be reduced by selecting an appropriate polarization. The conclusion is that for the condition found in the Denver streets on LOS paths, reflected signal power was not a function of antenna polarization at grazing angles up to 8°.

A propagation model was developed for the urban street path. Values of coefficient of reflection and multipath amplitudes and delay times were derived from the measured data and incorporated into the model to adjust path parameters. The model was given the geometry of the street and the rf parameters of the link and the results were compared to the measured data. The fit to the measured data was very good, and it is felt that a good estimate of channel characteristics and performance can be obtained when these basic parameters are used. Plots or tabulations of multipath amplitudes and delay times, channel fading, and impulse response characteristics can be computed as a function of distance between terminals. This report contains several examples of the measured data versus model comparisons.

8. ACKNOWLEDGMENTS

The authors wish to acknowledge help from Greg Hand, Robert DeBolt, and Richard Chavez in the measurements phases of this program. Scott Hector, Tracey Brown, Robert DeBolt, and Andrew Katz are likewise acknowledged for their work with the development of the computer model and data processing. Finally, a thank you to Sharon Kirby who typed the manuscript.

9. REFERENCES

Beckman, P., and A. Spizzichino (1963), "The Scattering of Electromagnetic Waves from Rough Surfaces," Macmillan Co., NY.

Espeland, R.H., E.J. Violette, and K.C. Allen (1984), Atmospheric channel performance measurements at 10 to 100 GHz, NTIA Report 84-149, April (NTIS* Order No. PB 84-211325).

* National Technical Information Service, 5285 Port Royal Road, Springfield, VA 22161.

Hufford, G.A., and D.R. Ebaugh, Jr. (1985), A study of interference fields in a ducting environment, NTIA Report 85-177 (NTIS* Order No. PB 85-242998), June.

Jenkins, F.A., and H.E. White (1957), Fundamentals of Optics, 3rd ed., (McGraw Hill, New York).

Keller, J.B. (1962), Geometrical theory of diffraction, J. Optical Soc. Am., 52, No. 2, pp. 116-130, February.

Liebe, H.J. (1985), An updated model for millimeter wave propagation in moist air, Radio Sci., 20, No. 5, pp. 1069-1089, September - October.

Nakagami, M. (1940), Study on the resultant amplitude of many vibrations whose phase and amplitudes are random, Nippon Elec. Comm. Eng. 22, pp. 69-92, October.

Rice, P.L., A.G. Longley, K.A. Norton, and A.P. Barsis (1967), Transmission loss predictions for tropospheric communications circuits, NBS Technical Note 101 (revised), (NTIS* Order No. AD 687-820, Vol. I; AD 687-821, Vol. II.)

Rice, S.O. (1945), Mathematical analysis of random noise, Bell Sys. Tech. J. 33, pp. 417-504, January.

Violette, E.J., R.H. Espeland, and K.C. Allen (1983a), A diagnostic probe to investigate propagation at millimeter wavelengths, NTIA Report 83-128, (NTIS* Order No. PB 84-104223), August.

Violette, E.J., R.H. Espeland, K.C. Allen, and F. Schwering (1983b), Urban millimeter wave propagation studies, Research and Development Technical Report, CECOM-83-3, U.S. Army Communications-Electronics Command, Fort Monmouth, NJ 07703, April.

Violette, E.J., R.H. Espeland, and G.R. Hand (1985), Millimeter-wave urban and suburban propagation measurements using narrow and wide bandwidth channel probes, NTIA Report 85-184 (NTIS* Order No. PB 86-147741), November.

Weibull, W. (1951), A statistical distribution function of wide applicability, J. Appl. Mech. 18, pp. 203-297.

Wozencraft, J.M., and I.M. Jacobs (1965), Principles of Communications Engineering (John Wiley and Sons, Inc.

FORM **NTIA-29**
(4-80)

U.S. DEPARTMENT OF COMMERCE
NAT'L. TELECOMMUNICATIONS AND INFORMATION ADMINISTRATION

BIBLIOGRAPHIC DATA SHEET

	1. PUBLICATION NO.	2. Gov't Accession No.	3. Recipient's Accession No.
	NTIA Report 88-239		

4. TITLE AND SUBTITLE

Millimeter Wave Propagation Characteristics and Channel Performance for Urban-Suburban Environments

5. Publication Date
December 1988

6. Performing Organization Code
NTIA/ITS.S3

7. AUTHOR(S)
Edmond Violette, Richard Espeland and Kenneth C. Allen

9. Project/Task/Work Unit No.
910 8108

8. PERFORMING ORGANIZATION NAME AND ADDRESS

National Telecommunications & Information Administration
Institute for Telecommunication Sciences
325 Broadway
Boulder, CO 80303 3328

10. Contract/Grant No.

11. Sponsoring Organization Name and Address

National Telecommunications & Information Administation
Herbert C. Hoover Building
14th & Constitution Avenue, N.W.
Washington, D.C. 20203

12. Type of Report and Period Covered

13.

14. SUPPLEMENTARY NOTES

15. ABSTRACT *(A 200-word or less factual summary of most significant information. If document includes a significant bibliography or literature survey, mention it here.)*

Measurements were performed in an urban-suburban environment with narrow and wideband rf probes, which include millimeter wave frequencies, in order to study propagation characteristics for street level paths. The primary objective of this report is to evaluate the performance of the rf channels in these environments for both line-of-sight and non line-of-sight paths and to compare a model developed for line-of-sight paths to measurements taken in Denver, CO.

16. Key Words *(Alphabetical order, separated by semicolons)*

urban-suburban, millimeter wave, propagation, performance, model

17. AVAILABILITY STATEMENT

☒ UNLIMITED.

☐ FOR OFFICIAL DISTRIBUTION.

18. Security Class. *(This report)*
Unclassified

20. Number of pages
178

19. Security Class. *(This page)*
Unclassified

21. Price:

GPO 673-002/92021